Distances and Ages of Galactic Globular Clusters via Infrared Photometry

David R.V. Buckley

Ph. D. Thesis

University of Edinburgh

1993

This thesis has been composed of my own work, except where specifically noted in the text

David R.V. Buckley

September 1993

Acknowledgements

This thesis would not have been possible without all the help and encouragement I have received from my supervisor, Andy Longmore, over the last four years, for which I am grateful.

Many other people have contributed to the scientific content of this thesis. In particular, I should like to acknowledge useful scientific and technical discussions with Russell Cannon, Phil Blanco, Richard Dixon, Lance Gardiner and Hugh Jones. Correspondence with R. Kurucz, R. Bell, S. Jeffreys, and K. Jones on the subject of model atmospheres, and how to run them, was very useful. R. Bell, D. VandenBerg and P. Bergbusch provided the V, (V-K) isochrones in advance of publication, while J. Hesser sent me the 47 Tuc field F3 data in machine-readable form within one day of my asking for them, thus saving me a *very* long session at the keyboard typing them all in.

At the Royal Observatory, special mention must go to the STARLINK system manager John Barrow, who was always willing to up my disk or other quotas and didn't complain about my ability to crash any of the computers seemingly at will. Thanks must also go to the librarians: Angus, Shona, Sally and Sarah. Angus knew where *everything* was in the library no matter how obscure, while Shona gave me many lifts up Blackford Hill. Dorothy and Maureen always had time for a chat.

Late night data reduction at the observatory would have been considerably less fun without the other members of the 'night shift' - Penny, Brian, Richard, and Phil - who provided friendship and company.

At various times over the past four years I have been privileged to share an office with Philippe, Suzie, Lance, Pippa, Ruth, Hugh [and not forgetting Edgar the plant], and not one of them complained about all the cartoons I stuck to the door.

Outside the observatory thanks go to fellow trekkies Penny - for company at the cinema and over the odd pizza - and Rachel - for the excellent music.

Financial support for the first three years came from a Science and Engineering Research Council studentship.

Finally, my biggest thank-you goes to my Mum and Dad, for their love and support (and computer equipment!). This thesis is dedicated to them, with love.

Abstract

One of the most promising routes to the formation of a quantitative model of the processes and timescales involved in transforming primordial, pre-galactic material into the galaxy as we know it today is the study of the 'fossil record', one important component of which is the galactic globular-cluster system. It is therefore vital to have information of the basic parameters - reddening, chemical composition, distance, age and internal and orbital dynamics - of many globular clusters.

This thesis is concerned with the derivation of the distances and ages of the four galactic globular clusters M13 (NGC6205), M30 (NGC7099), NGC6752 and 47 Tuc (NGC104). To this end we have obtained infrared photometry of respectively 21, 344, 123 and 688 stars in these clusters. We have matched this photometry with existing optical photometry to form the optical-infrared colour magnitude diagrams which are the basic tool for this study. These colour-magnitude diagrams are to the best of our knowledge the deepest of their kind in existence, and in NGC6752 and 47 Tuc reach to some five V magnitudes below the main-sequence turn-off.

The distances are derived using a sample of six metal-poor field subdwarf stars with accurate trigonometric parallax measurements, and a discussion is given of the sensitivity of these distances to various sources of error. We find that distances derived using the optical-infrared colour-magnitude planes are less sensitive to some systematic errors in the photometry than purely optical colour-magnitude diagrams, while distances determined in K, (B-V) are least sensitive to errors in the adopted ratio of total-to-selective extinction. Other sources of error considered are small photometric errors and errors in the adopted values of E[B-V] and [Fe/H]. For M13, M30, NGC6752 and 47 Tuc we derive distances of 7.1, 8.1, 4.0 and 4.4 kpc without Lutz-Kelker corrections. Distances derived applying full Lutz-Kelker corrections to the subdwarf magnitudes are also given.

Ages are derived for each cluster both directly from the Bergbusch & VandenBerg isochrones and also from the distance and reddening independent (V-K) and (B-V) colour differences between the main-sequence turn-off and the subgiant branch, calibrated against age using the isochrones. The results from both of these methods are compared, and ages of respectively 14.1±1.4, 14.9±2.3, 13.6±1.1 and 14.6±1.5 Gyr for M13, M30, NGC6752 and 47 Tuc are adopted. Since the foreground reddening to one of our clusters - M30 - is controversial, the colours of the subgiant branches are also used to check for internal consistency among the adopted cluster reddenings. We find good internal consistency among all the reddenings, although there is marginal evidence that the value adopted for M30 {E[B-V]=0.07} is too high by 0.01 to 0.02 magnitudes.

New Kurucz ATLAS9 model atmosphere results are used to derive colour to effective temperature relations and bolometric corrections, and these are applied to transform the Bergbusch & VandenBerg theoretical isochrones to the V, (B-V) and V, (V-K) planes for comparison with the data. The rationale behind this transformation was to use the very latest model atmospheres to produce isochrones in the observational planes which are independent of colour-shift problems found particularly in V, (V-K).

The cluster distances and ages are re-examined in the light of these 'new' models. The adopted ages are found to agree within the errors with those derived from the 'original' models.

Finally, we examine the consequences of these cluster ages in the context of the currently favoured galactic formation scenario. We find that recognisable structure must have existed within the inner halo at least as long ago as (14.1±1.4) Gyr. From the age and chemical composition of 47 Tuc, we conclude that protostellar material significantly enriched in heavy elements either co-existed with metal-poor protostellar material, or that the enrichment occurred over a period of ~2 Gyr. Since 47 Tuc has disk kinematics, we also conclude that the galactic disk began to form within ~2 Gyr of the inner halo.

We also conclude that if, as has been suggested, such very metal-poor clusters as M30 formed in outlying proto-galactic fragments that subsequently merged into the main body of the galaxy, then recognisable structure had formed within these 'ancestral objects' within ~2 Gyr of the formation of structure within the halo and disk.

Table of Contents

In addition to the numbered sections, each chapter contains an abstract at the beginning and references at the end

Introduction 1

1 Why study globular clusters? 2
2 Why study globular clusters in the infrared? 4
2.1 Ages 4
2.2 Distances 6
2.3 Reddening 9
2.4 Chemical composition 9
2.4.1 Oxygen and α-element enhancements 9
2.4.2 Star-to-star variations in chemical composition 10
3 Thesis Plan 10

Chapter 1: Observations and data reduction 14

1 NGC6752 observations and data reduction 15
1.1 Observations 15
1.2 Data reduction 17
1.2.1 The NGC6752 observations 17
1.2.2 The standard stars 21
1.2.3 The absolute calibration of the mosaics 23
1.2.4 A brief summary of IRIS data reduction procedures 33
2 47 Tucana observations 34
2.1 Field 3 34
2.2 Field 1 35
3 M13 observations 60
3.1 Standard stars 60
3.2 Deep M13 observations 61
4 M30 observations 64
4.1 Standard stars 65
4.2 Data reduction 65
5 Completeness and bias in the 47 Tuc & M30 main-sequence data 66

5.1 M30 artificial star experiments 70
5.2 47 Tuc artificial star experiments 74

Chapter 2: Globular cluster distances and ages 80

1 Bergbusch & VandenBerg model isochrones 83
1.1 Bolometric corrections and (B-V) transformations 83
1.2 The transformation to V, (V-K) by Bell (1992) 85
2 Basic cluster parameters 85
2.1 The metallicity of NGC6752 86
2.2 The reddening of NGC6752 88
2.3 The metallicity of M13 89
2.4 The reddening of M13 89
2.5 The metallicity of M30 90
2.6 The reddening of M30 91
2.7 The metallicity of 47 Tuc 92
2.8 The reddening of 47 Tuc 95
3 Cluster distances from subdwarfs 95
3.1 Pros and cons of subdwarf derived distances 95
3.2 Basic subdwarf data 97
3.3 Sensitivity of the subdwarf fits to various sources of error 100
3.3.1 Sensitivity to systematic shifts 100
3.3.2 Sensitivity to small photometric errors 101
3.3.3 Sensitivity to errors in adopted cluster reddening 103
3.3.4 Sensitivity to metallicity errors 106
3.4 The distance to M13 107
3.5 The distance to NGC6752 109
3.6 The distances to 47 Tuc and M30 109
4 Distance and reddening independent age estimates 111
5 Do the adopted reddenings form a consistent picture? 117
6 Absolute age estimates from the isochrones 121
6.1 Are the isochrone absolute magnitudes correct? 122
6.2 Comparison of isochrones and NGC6752 & M13 colour-magnitude data 124
6.3 Comparison of isochrones and 47 Tuc colour-magnitude data 130
6.4 Comparison of isochrones and M30 colour-magnitude data 136
7 Comparison of distance and reddening independent age estimates with those from the isochrones 136
7.1 The best overall ages for each cluster 140
8 Conclusions 141

Chapter 3: New colours from ATLAS9 model atmospheres 147

1 Introduction 147
2 Filter profiles and the terrestrial atmospheric transmission 149
3 Calibration of the model colours 152
4 Bolometric corrections 157
5 Temperature normalisation 157
6 Comparison with other colour-temperature relations 164
7 Conclusion 167

Chapter 4: A re-evaluation of cluster ages in the light of "new" models 172

1 New models 173
2 Comparison of the original and new isochrones 176
3 Distances and ages revisited 181
3.1 Distance estimates using subdwarfs 181
3.2 Absolute ages from the isochrones 182
3.2.1 Comparison of isochrones and M13 colour-magnitude data 184
3.2.2 Comparison of isochrones and NGC6752 colour-magnitude data 188
3.2.3 Comparison of isochrones and 47 Tuc colour-magnitude data 188
3.2.4 Comparison of isochrones and M30 colour-magnitude data 195
3.3 Distance and reddening independent age estimates 200
4 Two colour information 203
5 Conclusions 206

Conclusion: The age and formation of the galaxy 208

1 The cluster-galaxy connection 208
1.1 The current picture 209
1.2 The classification of M13, M30, NGC6752 and 47 Tuc 211
1.3 Constraints on the galactic age 212
1.4 A potential 'fly in the ointment' ? 215
1.5 Consequences of coevolution for the M_V(HB) versus [Fe/H] relation 218
1.6 Further constraints on the M13 distance via the horizontal branch - the RR Lyrae $\log_{10}$(period) versus mean K magnitude relation .. 221
2 Suggestions for future work 226
2.1 Serendipitous discoveries 226

2.2 Other suggestions 227
2.3 Whither now? 229

Appendix A: Finding charts 232

Appendix B: Publications list 254

Appendix C: A query 255

Introduction

" 'The time has come,' the Walrus said,
'to talk of many things...' "
- Lewis Carroll, Through the Looking-Glass.

This thesis is concerned with the derivation of the distances and ages of the four galactic globular clusters M13, M30, NGC6752 and 47 Tuc. To this end infrared photometry of stars in each cluster, with published complementary optical photometry, has been obtained. The resulting optical-infrared colour-magnitude diagrams, which form the basic tool for this study, are to the best of our knowledge the deepest yet presented for any globular cluster. In particular, those for NGC6752 and 47 Tuc reach to some five V magnitudes below the main-sequence turn-off.

Cluster name		Constellation	Coordinates[a] (1950)	
Messier	NGC		right ascension	declination
M13	NGC6205	Hercules	$16^h39.9^m$	+36°33'
M30	NGC7099	Capricornus (the goat)	$21^h37.5^m$	-23°25'
-	NGC6752	Pavo (the peacock)	$19^h06.4^m$	-60°04'
47 Tuc	NGC104	Tucana (the toucan)	$00^h21.9^m$	-72°21'

[a]From Sawyer-Hogg (1973)

This thesis is a continuation and extension of the pioneering work carried out by Dixon (1992), who used optical-infrared colour-magnitude data in his studies of globular clusters M71 (NGC6838) and M4 (NGC6121). However, the clusters studied here all have low, and excepting M30, uncontroversial foreground reddening. They thus form an ideal sample for the extension of these studies to clusters with higher and less secure reddening,

which are often not amenable to purely optical colour-magnitude studies.

Dixon has already given, in his introduction, an in-depth review of why the study of globular clusters is important, and how infrared observations can aid this study - together with the associated literature survey. A brief résumé of these points is given here.

1 WHY STUDY GLOBULAR CLUSTERS?

As some of the oldest structures within our galaxy, the globular cluster system is an important part of the 'fossil record', offering a route to the quantitative understanding of the processes and timescales involved in galaxy formation. Just as the geologist and geophysicist, by studying the terrestrial 'fossil record', can determine the age of the Earth [from the oldest rocks] or the chronology and duration of formation of geological features [by the widths and compositions of rock beds] or gain an idea how the chemical makeup of the atmosphere has changed over geological timescales [from analysis of the chemicals locked within antarctic ice], so the astronomer and astrophysicist can do likewise for the galaxy, as follows.

☞ The age of the oldest cluster sets the time at which recognisable structure first formed, giving in effect, the age of the galaxy. This age can also be used to set a lower limit to the age of the universe, placing constraints on cosmological models. See, for example, Catelan & de Freitas Pacheco (1992) and references therein.

☞ Age determinations for globular clusters can be used to trace the chronology of formation not just of the spherical components of the galaxy such as the halo and the bulge [for photometry of bulge-cluster stars see Friel & Geisler (1990) and Ortolani, Barbuy & Bica (1990)], but also of the disk, since many clusters with [Fe/H]>-0.8 such as 47 Tuc, have disk kinematics [Armandroff (1989) and references therein]. Furthermore, the age spread among the clusters associated with any component of the galaxy will show how long that component took to form.

☞ A determination of the chemical composition of globular cluster stars allows the chemical evolution of protostellar material in the early galaxy to be traced, and working backwards, allows limits to be placed on the composition of the primordial material from which the galaxy formed.

☞ The luminosity functions of globular clusters provide information on star formation in the early galaxy, provided the dynamical processes which act to change the initial mass function into the presently observed mass function are understood [Elson, Hut & Inagaki (1987)]. There is also the possibility that observations of main-sequence luminosity

functions can be used as a further check of the stellar evolution models - when coupled with an accurate cluster distance - since a steep rise in the luminosity function is predicted at M_V~9.6 as a consequence of the change in the structure of the stellar interior from convective-radiative to fully convective. The magnitude of this turn-up is virtually independent of evolutionary effects [VandenBerg (1986)]. The infrared is an ideal waveband to study deep main-sequence luminosity functions, although until recently this has been precluded by the small sizes of infrared arrays.

☞ The globular cluster system is distributed spherically about, and strongly concentrated on the galactic centre. An analysis of the spatial distribution and distances gives a method of determining the distance to the galactic centre. The concentration of the globular cluster system towards the direction of Sagittarius has been known since the time of the Hershels, and was used by Shapley to determine the solar galactocentric distance [see for example Shapley (1918) or Trumpler (1930)]. This same method was recently used by Racine & Harris (1989), although with some 70 years of added refinement, to determine a solar galactocentric distance of (7.5±0.9) kpc, assuming the absolute magnitude of the horizontal branch varies with abundance as $M_V(HB) = 0.84 + 0.15[m/H]$.

☞ An examination of cluster orbits allows conclusions to be drawn about the bulk dynamics of the gas from which the clusters formed. For example, van den Bergh (1993a) discriminates between those clusters with prograde or retrograde orbits - concluding that the outer part of the globular cluster system formed from one or more ancestral objects which were in retrograde motion while the inner part formed from ancestral objects in prograde motion - and between those clusters with plunging or circular orbits - concluding that one or more ancestral objects with the correct age and composition to form Oosterhoff I clusters merged with the main body of the proto-galaxy. See also van den Bergh (1993b). Care must be taken, however, because this involves extrapolating back over the entire lifetime of the galaxy, to when dynamical conditions were likely to have been very different from those in effect today. For example Aguilar, Hut & Ostriker (1988) conclude that bulge shocking was the most important mechanism acting to destroy clusters early in the history of the galaxy, while evaporation is currently the most important, followed by dynamical friction and disk shocking. And since Hut & Djorgovski (1992) have determined a destruction rate of (5±3) clusters Gyr^{-1}, suggesting that the current globular cluster system is a mere shadow of the original system, care must also be taken when drawing conclusions from statistical work, lest bias be introduced by preferential destruction of one class of clusters - for example, those with orbits which passed too close to the bulge - relative to other classes. As an introduction to the paper by Hut & Djorgovski, see the excellent summary by Heggie (1992).

☞ Globular clusters offer a laboratory within which theoretical models of stellar structure can be tested, and the predictions of the various branches of the theory can be compared.

For examples of such comparisons see many of the papers in the proceedings of the two most recent *Confrontation Between Stellar Pulsation and Evolution* conferences [Astronomical Society of the Pacific Conference Series volumes 11 (C. Cacciari & G. Clementini, editors) and in press]. See also Renzini *et al.* (1991) and references therein.

2 WHY STUDY GLOBULAR CLUSTERS IN THE INFRARED?

By now the reader is hopefully convinced that determinations of the basic parameters of globular clusters - age, distance, reddening, chemical compositions, orbital parameters and internal dynamics - can yield important science. In this section we briefly outline how infrared observations of globular clusters can be used in the determination of some of the above parameters, paying particular attention to those methods which may offer an improvement in accuracy over previous determinations.

2.1 Ages

The single most basic tool for those seeking to derive globular-cluster ages is probably the Hertzsprung-Russell diagram, both observational and theoretical. Observationally, this is a plot of the apparent brightness of clusters stars in some passband versus colour. Examples of colour-magnitude diagrams include Hesser *et al.* (1987) [V, (B-V)], Alcaino & Liller (1987) [various combinations of B, V, R & I], Guarnieri *et al.* (1990), Longmore, Dixon & Guarnieri (1990) and Buckley & Longmore (1992) [V, (V-K) diagrams of M3, M71 and M13 respectively]. The theoretician produces stellar evolution model results on the luminosity versus effective temperature plane, and herein lies a major problem - that of transforming one plane into the other. The parameters necessary for this transformation are:

The bolometric correction: The bolometric correction relates the total energy output (luminosity) to that observed in a particular passband, and has to be calculated from model stellar atmospheres as a function of temperature, chemical composition and surface gravity [see, for example, Kurucz (1991)].

The effective-temperature to colour transformation: These transformations are also calculated from model atmospheres, again as a function of chemical composition and surface gravity. It is here that coupling optical and infrared observations to use a colour such as (V-K) has the potential to offer many advantages. The long wavelength baseline between the V(0.55μm) and K(2.2μm) filters makes (V-K) a much more sensitive function of temperature than, say, (B-V) where the baseline only spans $0.43<\lambda/\mu m<0.55$. This long baseline ensures that the temperatures derived from (V-K) are less sensitive to

photometric errors than temperatures derived from (B-V) [see Persson & Frogel (1980)]. This is shown illustratively in figures 2 and 3 of the introduction of Dixon (1992). The reduced line blocking in the K band over, say, the B band makes (V-K) less sensitive to errors in the adopted cluster abundance than (B-V) [see Carney (1983), in particular figure 4].

Ages may then be derived in a variety of ways, some of which are listed below. All of these rely on the models - and thus a knowledge of the chemical abundance of the cluster stars - for their absolute calibration, and also on knowledge of the cluster distance, the foreground reddening, or both.

☞ **The magnitude of the main-sequence turn-off:** The main sequence brightward and blueward of the turn-off is not populated in globular clusters, simply because stars on that section have lifetimes which are shorter than the age of the cluster. Thus cluster ages can be determined from the luminosity of stars which are at the turn-off. The distance of the cluster is needed to turn the apparent magnitude of the turn-off stars into the absolute magnitude for comparison with the models. Indeed, as VandenBerg (1991) points out "...the turn-off *luminosity* must continue to be regarded as the prime age indicator, which then demands accurate distances." He makes this comment because he considers that the matching of predicted and observed colours should not be given high weight due to current uncertainties in opacity data, convection theory and stellar atmosphere models. Unfortunately, because the turn-off region is vertical in the colour-magnitude plane, it is difficult to determine the precise turn-off magnitude to better than 0.1 magnitudes, which means the age has an error of ~10% already, *before* uncertainties in the distance are taken into account.

☞ **The horizontal-branch to turn-off magnitude difference:** Determining cluster ages from the V magnitude difference between the main-sequence turn-off and the horizontal branch at the colour of the turn-off is a variation of the above method. It has the advantage that, once calibrated, it is independent of the distance and reddening of the cluster. The disadvantages of the method are threefold, however. First, as mentioned above, it is difficult to determine the turn-off magnitude to better than 0.1 magnitudes. Second, the horizontal branches of many clusters are just not populated at the colour of the turn-off. Assumptions then have to be made about what the magnitudes *would be* if the horizontal branches *were* populated at that colour. The associated errors in the estimates of the horizontal branch magnitude may therefore be greater than ~0.1 magnitudes [Buonanno, Corsi & Fusi Pecci (1989)]. Third, the use of this parameter requires knowledge of how the absolute magnitude of the horizontal branch varies with chemical composition, which is probably the most controversial function in the subject of globular cluster studies today. See Buonanno *et al.* and also the conclusion to this thesis for more discussion.

☞ **Δ(V-K) and Δ(B-V):** VandenBerg, Bolte & Stetson (1990) used the (B-V) colour difference between the main-sequence turn-off and the subgiant branch to derive relative ages between clusters of similar chemical composition. Expressing reservations similar to those of VandenBerg (1991), which were discussed above in the context of the main-sequence turn-off, they warn that absolute ages determined from Δ(B-V) calibrated by stellar evolution results should not be relied upon. Since more discussion of these points is given in Chapters 2 and 4, we simply note here that since this method relies on relative colours, it is independent of cluster distance, reddening and photometric zero-point errors, and also that the larger colour difference between the turn-off and the subgiant branch in (V-K) as opposed to (B-V) offers the potential to determine more accurate ages given equivalent photometric errors.

☞ **Matching the isochrones over the whole colour-magnitude diagram:** Given the possibility of errors in the adopted cluster distance, reddening and chemical composition, it seems sensible to use all the colour-magnitude information at one's disposal to match the theoretical results to the observations over the entire colour-magnitude diagram of the cluster - main-sequence, turn-off, giant branch and horizontal branch. Then errors in, for example, adopted chemical abundance would show up as a mismatch between the slope of the observed and theoretical giant branches, while errors in the reddening would appear as a mismatch between the near-vertical observed and theoretical subgiant branches, or errors in the distance would be evident from mismatches between the observed and theoretical main-sequences or horizontal-branches. Furthermore, if the models fit over the whole colour-magnitude plane for the canonical values of distance, abundance and reddening - or at least within the errors on these - then one might feel more confident about the age derived from the turn-off region. To be sure, the uncertainties in bolometric corrections, colour-temperature equations and convective theory can introduce changes in the shapes of the theoretical colour-magnitude diagram which mimic errors in distance, reddening, chemical composition and so forth, but it is still worth using all of the information at one's disposal in deriving an age.

2.2 Distances

An accurate distance is one of the most fundamental and important parameters one can determine for any astronomical object; it is also one of the most difficult.

The only direct method of determining distances to objects outwith the solar system is that of annual parallax. This method was first developed by Aristarchus of Samos (~310 to 230 B.C.) - who was also responsible for the heliocentric hypothesis 'rediscoverd' by Copernicus some 2000 years later - and relies on measuring the change in apparent position of a star relative to more distant background stars as the Earth moves in orbit

from one side of the sun to the other. After removing the abberation effects caused by the motion of the Earth, simple trigonometry yields the distance. Unfortunately for Aristarchus, the annual parallaxes of even the closest stars are very small - α Centauri has the largest known parallax of 0.75 arcseconds - and far beyond the limit of the technology available to him. Indeed, it was to be 1837 before a parallax was determined - a value of 0.3 arcseconds was measured for 61 Cygni by Bessel.

Unfortunately, the small angles involved, coupled with the effects of atmospheric seeing limit the viability of this method to distances of a few tens of parsecs. For example, the parallax of a star at a distance of 25 pc is 0.04 arcseconds. Even with measurements made using a large number of photographic plates, the error on this parallax determination is ±0.004 arcseconds, or 10% [from The Astronomy Encyclopaedia, P. Moore, general editor. Mitchell Beazley Publishers, 1987]. Results from the HIPPARCOS - **HI** Precision **PAR**allax **CO**llecting **S**atellite - mission are eagerly awaited! Further details of HIPPARCOS can be found in Kovalevsky (1990).

To determine the distances to more remote objects, including all galactic globular clusters, it is necessary to use other methods such as standard candles. By standard candles we mean easily distinguishable objects which have some distance-independent property that can be related to the intrinsic luminosity. Some of the methods used to determine globular cluster distances are listed below. A snapshot of the current state-of-the-art regarding standard candles can be found in the proceedings of the workshop on *New Results on Standard Candles* [*Mem. Soc. Astron. Ital.* **63** (1992)].

☞ **Main-sequence fitting:** For this method, a fiducial main-sequence is defined in the colour-absolute-magnitude plane from observations of metal-poor field dwarf stars with absolute magnitudes determined from parallax measurements. Once the cluster reddening is known, the distance can be calculated from the shift required to overlay the cluster main-sequence onto the fiducial. The main drawbacks are that there are very few significantly metal-poor field dwarfs with accurate parallax determinations, and that the statistical procedures to correct biases in the parallax-determined absolute magnitudes, more commonly known as Lutz-Kelker corrections [Lutz & Kelker (1973)], are controversial. More discussion of this method, and the sensitivity of the subdwarf-determined distances to various sources of error, is given in Chapter 2.

☞ **RR Lyrae $\log_{10}$(period) versus mean K magnitude relation:** RR Lyrae stars are the dominant type of Population II variable, and many globular clusters contain this type of variable star in copious abundance. For example, Table 1 of Sawyer-Hogg (1973) lists the following clusters with over 100 RR Lyrae variables: M3 (212), M15 (111), ω Cen (179) and IC4499 (129).

There exists a tight correlation between the logarithm of the fundamental pulsation period of an RR Lyrae star and the mean K(2.2μm) magnitude, which was discovered by Longmore *et al.* (1986), and subsequently used to derive distances to eight clusters by Longmore *et al.* (1990). The fact that one of the relations exhibiting the least scatter is that derived for the variables of ω Cen, which display a large range in chemical composition, suggests that distances can be derived from this relation which are insensitive to metallicity errors. The relation also offers distances which are almost independent of foreground extinction, which is much lower at infrared wavelengths compared to the optical extinction.

The four clusters with which this thesis are concerned contain few RR Lyrae stars. NGC6752 is not known to contain any, while 47 Tuc probably contains only one which is truly a cluster member [Carney, Storm & Williams (1993)]. M13 and M30 contain three each. More discussion of the RR Lyrae $\log_{10}$(period) versus mean K magnitude relation and the M13 variables can be found in the conclusion.

☞ **The horizontal branch:** The horizontal branch has been widely used to set globular cluster distances, because of it's relative brightness. However, before distances can be determined, the variation of the horizontal-branch magnitude with chemical composition must also be known. As we have already mentioned, this is a controversial parameter [see the discussion in Buonanno, Corsi & Fusi Pecci (1989) and the summary in Table 3 of Renzini *et al.* (1991). More discussion is also given in the conclusion.].

☞ **The brightest red giants:** Recently, VandenBerg & Durrell (1990) have used the brightest red giants to remove distance variations from the colour-magnitude diagrams of several clusters in an attempt to determine if age variations are to blame for differences in horizontal-branch morphology between clusters whose stars have ostensibly the same chemical composition. They discuss the observational and theoretical support for the idea that the brightest red giant in a typical globular cluster will be located within ~0.1 magnitudes of the theoretical helium-flash luminosity. Provided one has photometry for a large enough sample of red giants in each cluster to be sure that the brightest is representative of the limit attained by the whole red giant population, and provided one is sure that the brightest red giant really is a first-ascent red giant and not an asymptotic red giant, for instance, then this method obviously has the potential to determine cluster distances with accuracies of 10%. Green & Norris (1990) have criticised the results of VandenBerg & Durrell on both of the above points.

2.3 Reddening

A full presentation of the techniques used to determine the foreground reddening to globular clusters is beyond the scope of this introduction, although many techniques are discussed in Chapter 2 when literature values of the reddening to the four program clusters are presented. We simply note here that because E[V-K]~2.7E[B-V], if reddening can be determined in a plane such as V, (V-K) - for example, from the colour of the near-vertical subgiant branch - then an increase in the accuracy of E[B-V] can be achieved, all else being equal.

2.4 Chemical composition

One of the input parameters of the stellar evolution and atmosphere models is chemical composition, and therefore an *a priori* knowledge of the abundances of globular cluster stars is necessary before observational colour-magnitude and theoretical temperature-luminosity results can be meaningfully compared. A discussion of the techniques used to determine chemical abundances in globular cluster stars can be found in Bell (1987), and further discussion of the metallicities of our program clusters is given in Chapter 2.

2.4.1 Oxygen and α-element enhancements

Until recently, stellar evolution models, and the resulting isochrones, and indeed model atmospheres, all assumed a scaled-solar mixture of chemical elements. See, for example, Table 1 of Gustafsson et al. (1975).

However, current evidence suggests that the mix of elements in globular cluster stars is *not* scaled solar. This can be seen, for example, in Table 1 of Wheeler, Sneden & Truran (1989). Of particular importance is the enhancement of oxygen and other α-elements (magnesium, silicon, calcium, titanium are specifically mentioned in the table) with respect to iron. Since the inclusion of oxygen enhancements, in particular, into the isochrones can have a large effect on the derived ages of globular clusters [VandenBerg (1985)], it is important that these be taken into account properly.

The recent Bergbusch & VandenBerg (1992) isochrones are the first to include an oxygen enhancement, and we discuss these further in Chapter 2 before using them to derive the ages of our four program clusters. The size of the oxygen enhancement included in the models by Bergbusch & VandenBerg was based primarily on observations of metal-poor field stars, and is still a controversial subject [VandenBerg (1992) and references therein; also references in Chapter 2]. It is also not clear that the size of the oxygen enhancements

derived from field stars should apply to cluster stars [Wheeler *et al.*]. And although VandenBerg (1992) notes that there is generally good agreement between globular cluster oxygen abundances and those of field giants, he does warn of the possibility that the abundances in upper red-giant branch stars have been altered by mixing of CNO processed material.

2.4.2 Star-to-star variations in chemical composition

ω Cen is a well-studied example of a globular cluster which exhibits large star-to-star variations in chemical composition; a range of ~1 dex in [Fe/H] is observed among the evolved cluster stars. The broad main-sequence found in photometric studies of this cluster [Noble *et al.* (1991) and Alcaino & Liller (1987)] is indicative that the unevolved stars also have a large range of chemical composition. One possible explanation is that this cluster has been able to retain chemically enriched material ejected when the more massive cluster stars became supernovae soon after the cluster formed [Freeman & Rodgers (1975) and Smith (1986)].

M22 is the only other cluster known to exhibit star-to-star variations in [Fe/H] {Pilachowski *et al* (1982)}. The suggestion by Alcaino *et al.* (1990) that NGC1851 has a very broad main-sequence, reminiscent of that of ω Cen, possibly indicating a similar range of [Fe/H] among the unevolved stars, has been refuted by the more recent work of Walker (1992).

For other clusters, the possible range in [Fe/H] is constrained to be very small by the thinness of the main sequence and giant branch in the colour-magnitude plane. For example, from the width of the 47 Tuc main-sequence, Hesser *et al.* (1987) find that the star-to-star abundance variations in that cluster are constrianed to be less than ~0.04 dex.

There are, however, variations in lighter metals such as cyanogen (CN) abundances observed in many clusters, including 47 Tuc. For a summary and further references, see Chun (1991).

3 THESIS PLAN

The remainder of this thesis consists of five chapters.

In Chapter 1 we present the infrared observations of stars in the four globular clusters and discuss the data reduction.

In Chapter 2 we discuss the Bergbusch & VandenBerg isochrones, summarise and discuss the literature values of foreground reddening and abundance for the four clusters, discuss the sensitivity of distances derived from subdwarfs to various sources of error and derive the distance to each cluster. We derive ages for each cluster both directly from the Bergbusch & VandenBerg isochrones and also from the (V-K) and (B-V) colour difference between the turn-off and the subgiant branch; the colours of the subgiant branches are also used to check for internal consistency among the cluster reddenings. Finally the ages derived from these two methods are compared and an age is adopted for each cluster.

Chapter 3 is concerned with the derivation of a grid of bolometric corrections and (V-K) & (B-V) colours from spectral energy distributions resulting from the latest Kurucz model atmospheres.

In Chapter 4 the distances and ages of the clusters are discussed again in the light of isochrones formed by converting the Bergbusch & VandenBerg theoretical isochrones to the observational planes using the Kurucz model atmosphere results discussed in Chapter 3.

A conclusion is presented wherein the consequences of the cluster ages for the galactic formation scenario and chronology are discussed.

Finding charts and a publications list can be found in appendices.

REFERENCES

Aguilar, L., Hut, P. & Ostriker, J.P., 1988. *Astrophys. J.* **335,** 720.

Alcaino, G. & Liller, W., 1987. *Astron. J.* **94,** 1585.

Alcaino, G., Liller, W., Alvarado, F. & Wenderoth, E., 1990. Astron. J. **99,** 817.

Armandroff, T.E., 1989. Astron. J. **97,** 375.

Bell, R.A., 1987. In *The Harlow Shapley Symposium on Globular Cluster Systems in the Galaxy.* J.E. Grindlay and Philip, A.G.D., editors. Kluwer Academic Publishers. Page 79.

Bergbusch, P.A. & VandenBerg, D.A., 1992. *Astrophys. J. Suppl.* **81,** 163.

Buckley, D.R.V. & Longmore, A.J., 1992. *Mon. Not. Roy. astr. Soc.* **257,** 731.

Buonanno, R., Corsi, C.E. & Fusi Pecci, F., 1989. *Astron. Astrophys.* **216,** 80.

Carney, B.W., 1983. *Astron. J.* **88,** 623.

Carney, B.W., Storm, J. & Williams, C., 1993. *Publs astr. Soc. Pacif.* **105,** 294.

Catelan, M. & de Freitas Pecheco, J.A., 1992. *Astron. Astrophys.* **258,** 5.

Chun, M-S., 1991. P*roc. astr. Soc. Australia* **9,** 37.

Dixon, R.I., 1992. Ph.D. thesis, University of Edinburgh.

Elson, R., Hut, P. & Inagaki, S., 1987. *Ann. Rev. Astron. Astrophys.* **25,** 565.

Freeman, K.C. & Rodgers, A.W., 1975. *Astrophys. J.* **201,** L71.

Friel, E.D. & Geisler, D., 1990. In *Proceedings of the ESO/CTIO Workshop on Bulges of Galaxies.* ESO Conference and Workshop Proceedings Number 35. B.J. Jarvis and D.M. Terndrup, editors. Page 153.

Green, E.M. & Norris, E., 1990. *Astrophys. J. Lett.* **353,** L17.

Guarnieri, M.D., Longmore, A.J., Fusi Pecci, F. & Dixon, R.I., 1990. Mem. Soc. Astron. Ital. **61,** 143.

Gustafsson, B., Bell, R.A., Eriksson, K. & Nordlund, Å., 1975. *Astron. Astrophys.* **42,** 407.

Heggie, D.C., 1992. *Nature* **359,** 772.

Hesser, J.E., Harris, W.E., VandenBerg, D.A., Allwright, J.W.B., Shott, P. & Stetson, P.B., 1987. *Publs astr. Soc. Pacif.* **99,** 739.

Hut, P. & Djorgovski, S., 1992. *Nature* **359,** 806.

Kovalevsky, J., 1990. *Sky & Telescope* **79,** (May) 493.

Kurucz, R.L., 1991. in *Precision Photometry,* A.G. Davis Philip, A.R. Upgren & K.A. Janes, editors. L. Davis Press. Page 27.

Longmore, A.J., Dixon, R.I. & Guarnieri, M.D., 1990. In *Astrophysics with Infrared Arrays.* Astronomical Society of the Pacific Conference Series, volume 14. R. Elston, editor. Page 121.

Longmore, A.J., Dixon, R.I., Skillen, I., Jameson, R.F. & Fernley, J.A., 1990. *Mon. Not. Roy. astr. Soc.* **247,** 684.

Longmore, A.J., Fernley, J.A. & Jameson, R.F., 1986. *Mon. Not. Roy. astr. Soc.* **220,** 279.

Lutz, T.E. & Kelker, D.H., 1973. *Publs astr. Soc. Pacif.* **85,** 573.

Noble, R.G., Dickens, R.J., Buttress, J., Griffiths, W.K. & Penny, A.J., 1991. *Mon. Not. Roy. astr. Soc.* **250,** 314.

Ortolani, S., Barbuy, B. & Bica, E., 1990. In *Proceedings of the ESO/CTIO Workshop on Bulges of Galaxies.* ESO Conference and Workshop Proceedings Number 35. B.J. Jarvis and D.M. Terndrup, editors. Page 153.

Persson, S.E. & Frogel, J.A., 1980. In *Globular Clusters.* D. Hanes and B. Madore, editors. Cambridge University Press. Page 21.

Pilachowski, C., Wallerstein, G., Leep, E.M. & Peterson, R.C., 1982. *Astrophys. J.* **263,** 187.

Racine, R. & Harris, W.E., 1989. *Astron. J.* **98,** 1609.

Renzini, A., Rowan-Robinson, M., Demarque, P., Penny, A.J. & Hoyle, F., 1991. In *Observational Tests of Cosmological Inflation*, volume 348, chapter 58. T. Shanks, A.J. Banday, R.S. Ellis, C.S. Frenk, A.W. Wolfendale, editors. Kluwer Academic Publishers. Page 131. (only preprint seen).

Sawyer-Hogg, H., 1973. The Third Catalogue of Variable Stars in Globular Clusters. *Publs David Dunlop Obs.* **3,** number 6.

Shapley, H., 1918. *Publs astr. Soc Pacif.* **30,** 42.

Smith, G.H., 1986. *Astrophys. J.* **306,** 565.

Trumpler, R.J., 1930. *Lick Obs. Bull.* number 420.

VandenBerg, D.A., 1985. In *ESO Workshop on the Production and Distribution of CNO Elements.* I.J. Danziger, F. Matteucci and K. Kjär, editors. Page 73.

VandenBerg, D.A., 1986. *Mem. Soc. Astron. Ital.* **57,** 373.

VandenBerg, D.A., 1991. In *The Formation and Evolution of Star Clusters.* Astronomical Society of the Pacific Conference Series, volume 13. K.A. Janes, editor. Page 183.

VandenBerg, D.A., 1992. *Astrophys. J.* **391,** 685.

VandenBerg, D.A., Bolte, M. & Stetson, P.B., 1990. *Astron. J.* **100,** 445.

VandenBerg, D.A. & Durrell, P.R., 1990. *Astron. J.* **99,** 221.

van den Bergh, S., 1993a. *Astrophys. J.* **411,** 178.

van den Bergh, S., 1993b. *Astron. J.* **105,** 971.

Walker, A.R., 1992. *Publs astr. Soc Pacif.* **104,** 1063.

Wheeler, J.C., Sneden, C. & Truran, J.W., 1989. *Ann. Rev. Astron. Astrophys.* **27,** 279.

Chapter 1

Observations and Data Reduction

" Make things as simple as possible, but no simpler. " - Albert Einstein

ABSTRACT

In this chapter we present new infrared photometry for stars in the four globular clusters M13 (NGC6205), M30 (NGC7099), NGC6752 and 47 Tuc (NGC104), as outlined in Table 1. The M13 and M30 data were obtained using IRCAM, while the 47 Tuc and NGC6752 data were obtained using IRIS, which are common-user array cameras mounted respectively on the United Kingdom Infrared Telescope and the Anglo-Australian Observatory Telescope.

A full and detailed discussion of the data reduction procedures used on the NGC6752 data is given, since no discussion of the reduction of IRIS photometric data appears outwith the (unpublished) IRIS User Guide, and because some intriguing problems were encountered with some of the data. For the other clusters, we limit our discussion to instrument

Table 1: A brief summary of the observations outlined in this chapter.

Cluster	Stars photometered	Passband(s)	Source of optical photometry	Approximate V limit below turn-off	quality of colour-magnitude diagram
M13	21	K	Richer & Fahlman (1986)	2	sparse but good
NGC6752	123	K & K'	Penny & Dickens (1986)	5	very good
47 Tuc	688	K' & J	Hesser *et al.* (1987)	5	very good
M30	344	K	Richer *et al.* (1988)	3.5	fair to poor

configurations, weather conditions on the nights in question and a presentation of the photometry of the standards and cluster observations.

1 NGC6752 OBSERVATIONS AND DATA REDUCTION

1.1 Observations

The observations of NGC6752 were carried out on the nights of 4/5 & 5/6 May 1991 and 16/17, 17/18 & 19/20 April 1992 with the common user 128x128 HgCdTe array IRIS mounted at the F36 focal station of the 3.8m Anglo-Australian Telescope. This configuration gave a plate scale of 0.79 arcseconds $pixel^{-1}$.

Weather conditions during the 1991 run were fully photometric with ~1 arcsecond seeing. However, while all the 1992 observations were made during extended photometric periods, only the night of 19/20 April was uninterrupted by non-photometric weather. Most of the night of 16/17 April was lost to thick cloud, while the night of 17/18 April was interrupted by ridge cloud and fog. The seeing was > ~2 arcseconds on all three of these nights, as can be seen from column 8 of Table 2, but particularly variable on the night of 19/20 April, where minimum and maximum recorded optical seeing values were 1.5 and 4.0 arcseconds respectively.

Regions were selected from fields 3, 5 and 8 of the Penny & Dickens (1986) photometric study, to ensure that the turn-off region would be well defined and also to delineate the main-sequence as deep as possible. Observations were made of the field centres and in spiral jitter patterns around them with offsets of typically ±10 arcseconds in each coordinate. More details of the observations are given in Table 2. Columns 1 and 2 give the date of the observation and the field being observed. Column 3 gives the total number of frames observed in each field on each night, while columns 4 and 5 give the number of coadds and on-chip integration time of a single frame. Columns 7 and 8 detail the filter used for the observations and an estimate of the full-width half-maximum of the seeing disk, determined from the DAOPHOT point spread function. Blank, or at least less crowded, sky frames were taken immediately before and after each set of nine jittered frames.

The rationale behind our use of the K' filter on the nights of 17/18 and 19/20 April 1992 is discussed in section 1.2.2.

Table 2: Details of the observations of NGC6752.

Date (UT)	Field	N	Coadds	t_{int}/s	N_{final}	Filter	Seeing (FWHM/ arcsecs)	cutoff/ optical pixels
4/5 May 1991	5	18	30	3	18	K	1.2	2.7
	8	9	20	5	9	K	1.2	1.6
5/6 May 1991	5	9	20	5	9	K	1.1	2.7
	8	31	20	5	23	K	1.0	1.5
16/17 April 1992	5	9	30	5	8	K	2.0	2.5
	8	19	30	5	15	K	2.2	1.8
17/18 April 1992	5	18	10	15	18	K′	2.1	2.8
19/20 April 1992	3				11		2.7	1.5
	3	19	40	2	7	K′	1.9	1.1
	8	18	10	15	18	K′	2.4	2.0

1.2 Data reduction

1.2.1 The NGC6752 observations

Removal of the dark current and bias from each frame is performed automatically by the software which corrects for detector non-linearity. Pixel-to-pixel variations in quantum efficiency were removed from the 1991 data by dividing each frame by an appropriate flat-field frame, consisting of a median filter of an odd number, typically nine, of object and sky frames taken close in time to each object frame.

A more complex data reduction procedure was required for the 1992 data, where flat-fielding was done by subtracting a relevant median sky frame, constructed as above, and then dividing the result by a dome flat. This alternative method of processing was necessary to remove the effects of excess thermal radiation reaching the detector not directly from the primary and secondary mirrors. The source of this excess radiation, and it's path through the telescope optics is not well understood. The reflective baffles around the telescope secondary mirror, which reduce the excess radiation, are no longer used because when they are in place the detector suffers from severe ghosting, with reflected light from bright stars as much as 3° away from the field centre producing significant nebulosity on an image.

Many of the processed frames from 1992 showed a curious odd-even column striping, with quite a complex shape over the array. Though this shape seemed to remain fairly constant, the amplitude of the stripes varied with time in an unpredictable way, and did not correlate with sky background flux. The effect was evident in frames with different exposure times, in exposures taken with the full array and with the smaller 31x31 window, and could also be seen upon subtracting neighbouring dark frames. The western most three or four rows of the array were seen to have anomalously large fluxes when the striping was seen, though were normal when it was not, and the amplitude of the stripes increased with the excess counts in these rows. The effect would also come and go quite unpredictably. Neither we, nor the Anglo-Australian Observatory staff have encountered such behaviour before, nor can find any explanation for it.

The first step in the removal of this effect was to determine if it was an additive or multiplicative factor. This had to be done on the raw frames, to avoid an additive factor becoming multiplicative in the reduction process. The procedure was to subtract two nearby frames containing images of globular cluster stars, and to examine cross sections of rows which passed through stellar images to determine if the amplitude of the stripes varied with the increased flux. This is not an ideal test, because pixel-to-pixel variations in quantum efficiency still remain, but it suggested that the striping was an additive factor.

A procedure was developed to normalise the striping so that it was removed by standard processing. First, two dark frames were subtracted, one from the other, leaving a frame (hereafter 'the mask') containing the striping only. Then, for each frame to be processed (an 'object' frame), all of the frames ('the skies') to be included in the median filtered sky were subtracted from it, one at a time, and the mask scaled and added to the skies, leaving frames with the striping effect normalised to the object frame. These frames were median filtered to produce a median sky frame, and the reduction procedure completed as normal. Fortunately the dome frames did not appear to be affected by the striping. Where the above procedure did not work, or some low level striping remained, Fourier processing was used to remove it. A few frames could not be processed at all, and were discarded. Fourier processing only was used on stripy standard frames, since the striping effect was small, though not negligible, compared to the flux from the standards.

Cosmetic defects such as bad pixels and cosmic ray strikes were removed at this point by interpolation from surrounding pixels; the interpolation routine had to be run twice on each frame to remove the 3x3 group of dead pixels known as the 'beauty spot'.

A constant, determined for each frame from the median value in a 100x100 pixel box centred on the frame, was added to each frame to normalise the sky-only signal to an arbitrarily chosen value, typically 1000 counts. The sky values were not normalised to zero as is usual, because the mosaicing routine fills out the resultant mosaic to a rectangle by adding pixels of zero counts; by normalising to a value well above zero, we were able to have DAOPHOT ignore these extra pixels.

Next, the images of five stars, common to each set of jittered object frames and covering a range of magnitudes, were chosen and the centroids determined, from which the mean offsets between the frames were calculated. Stars which were obviously double or in crowded regions were not used. Mosaics were constructed using the nearest integer offsets to the mean offsets. Column 6 in Table 2 gives the number of frames constituting each mosaic.

Instrumental magnitudes and (x,y) positions were determined for images on the frames by use of the classic (version I) DAOPHOT/ALLSTAR point spread function fitting package of Stetson (1987).

The infrared detections output by DAOPHOT were matched with the optical photometry by iteratively determining a six coefficient transformation between the infrared and optical coordinates. Occasionally a suitable initial estimate of the transformation was available, for example where the observations were made at similar coordinates to previously reduced data, or where the infrared positions could be transformed to the coordinate system of another infrared mosaic and then to the optical coordinate system.

Otherwise, the positions of 20 to 30 images which were easily identifiable on both the infrared mosaics and optical CCD frames were matched by hand to determine the initial transformation, which was then applied to the infrared coordinates. All transformed infrared positions matching an optical detection to better than some maximum separation parameter, which varied but was typically set to two or three times the r.m.s. alignment error at each stage, were found and used to update the transformation. This process was iterated until the r.m.s. separation between the optical and the transformed infrared positions had converged to some stable, low value. In all cases this required only two further iterations after the initial transformation had been found. We have discarded data where the separation between the transformed infrared positions and the optical positions was greater than three times the r.m.s. alignment error determined in the final iteration, and also those where the image was less than eight, or ten in the case of the 1992 data, pixels from the edge of a mosaic. This cutoff, in units of optical pixels, is reported in column 9 of Table 2. The optical plate scales were 0.5 arcseconds pixel^{-1} in field 8 and 0.4 arcseconds pixel^{-1} in the others. Interesting objects which appeared in the infrared images but not the optical images, or vice versa, will be discussed later.

Finally, the instrumental magnitudes were calibrated, and where appropriate the K′ magnitudes were transformed to K as described next.

Figure 1: Residuals with time for the standards of 4/5 May 1991. Coefficients were determined from a linear fit as described in the text.

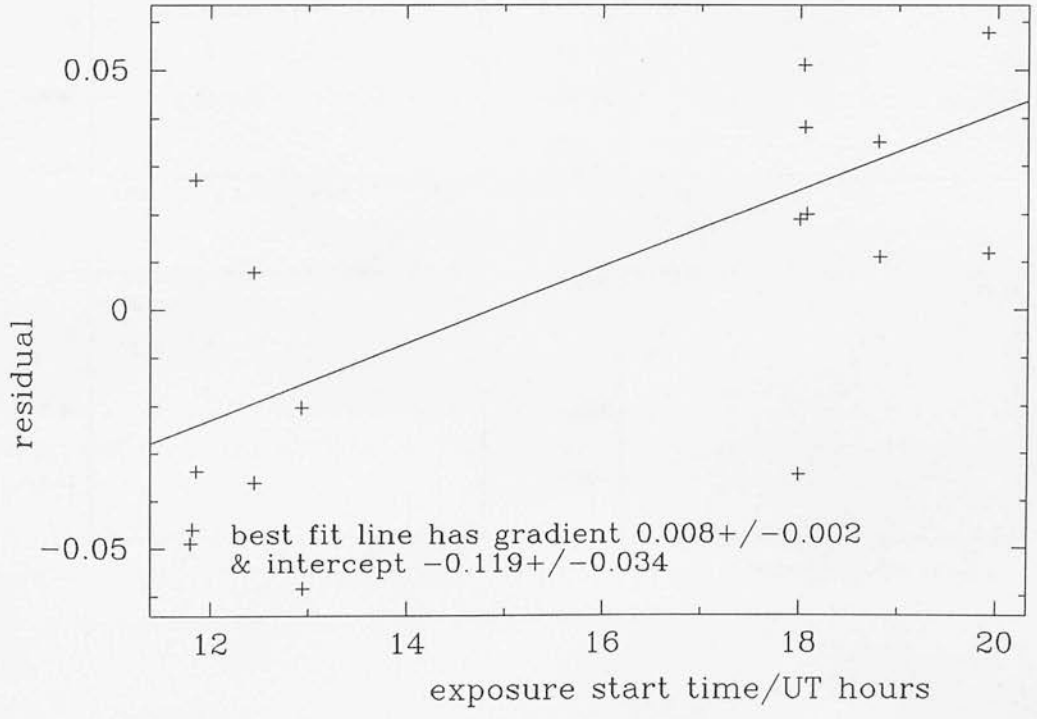

Figure 2: Residuals against airmass and time for the standards of 4/5 May 1991 (a and b), 5/6 May 1991 (c and d), 16/17 April 1992 (e and f) and 17/18 April 1992 (g and h).

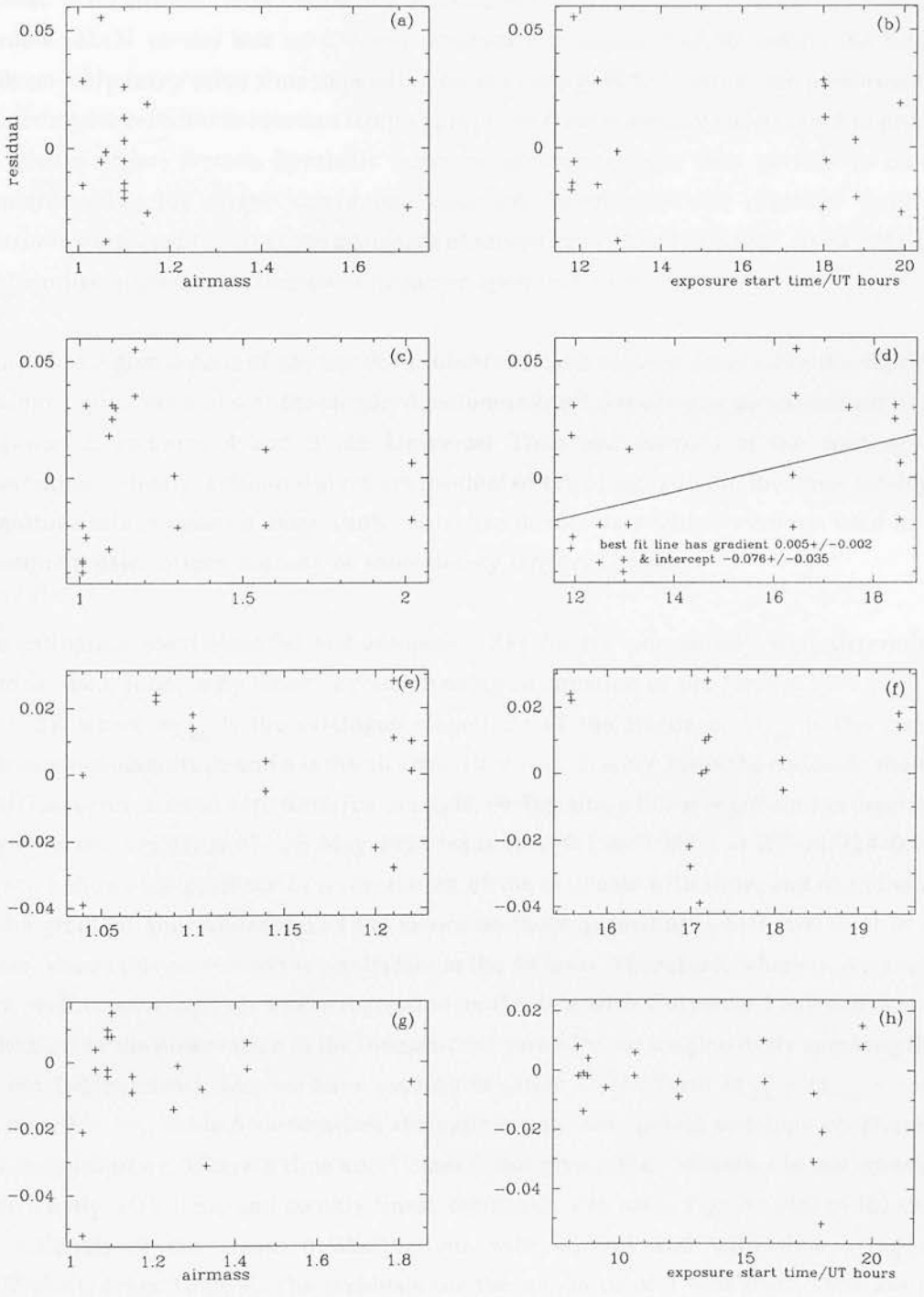

1.2.2 The standard stars

The minimum readout time for the full 128x128 array is 1.4 seconds, which is too long to observe a bright standard without saturating the detector. Therefore, during the 1991 run, bright standards were observed throughout the night with the IRIS25 window, which is a 25x25 pixel subsection at the centre of the array. In 1992, the newly available IRIS31 window (31x31 pixels) was used. These observations consisted of 50 coadds and 0.18 to 0.50s on-chip integration time depending on the seeing. Flat-fielding was performed by extracting the relevant subsection from appropriate frames already constructed to process the cluster object frames. Synthetic aperture photometry was then performed on the standards using the largest convenient aperture. Seven arcsecond diameter synthetic apertures were used for all of the standards observed in 1991 and on 16/17 April 1992. For all the other nights, nine arcsecond diameter apertures were used.

Tables 3 to 7 give details of the standards observed each night as detailed in the captions. Column 1 gives the name of the standard, columns 2 and 3 the instrumental and catalogue magnitudes, columns 4 and 5 the Universal Time and airmass at the start of the observation. Finally, column 6 gives the residual of the observation in the sense catalogue magnitude minus reduced magnitude. Asterisks denote data which were not used in the subsequent calculations because of anomalously large residuals.

The extinction coefficient (ε) and zeropoint (ZP) for the photometry were determined from all the standards by linear regression using an equation of the form $m_{cat} - m_{raw} = -\varepsilon.a + ZP$ where m_{cat} is the catalogue magnitude of the standard, m_{raw} is the raw or instrumental magnitude and a is the airmass. However, in some cases the residuals showed significant correlations with time; for example, performing a linear regression as described above on the standards of 4/5 May 1991 leads to ε=0.136±0.045 and ZP=21.924±0.052. Figure 1 shows the presence of a correlation of the residuals with time, and examination of the gradient and intercept and the errors on these quantities, which are inset in the figure, shows this correlation is significant at the 4σ level. Therefore, where necessary we have performed a multiple linear regression on the data with Universal Time and airmass at the start of the observation as the independent variables (although strictly speaking they are not independent), i.e., we have used an equation of the form $m_{cat} - m_{raw} = -\varepsilon a + b(t/hours) + ZP$. Table 8 summarises the extinctions, zero-points and time coefficients where appropriate. Where a time coefficient is not given, the residuals did not correlate significantly with time, and so only linear regression was used. Figures 2(a) to (h) show the residuals of the standard observations with airmass and with time using the coefficients from Table 8. The residuals for the standards of 19/20 April 1992 are not plotted and are discussed next.

Since the seeing on the night of 19/20 April was so variable, we have been forced to use

Table 3: Data for standard stars from 4/5 May 1991.

Star (HD)	Instrumental Magnitude	Catalogue Magnitude	Universal Time (start)	Airmass	Residual (catalogue - reduced)
122414	-13.487	8.238	11.804	1.10	-0.017
122414	-13.490	8.238	11.815	1.10	-0.014
106807	-13.158	8.65	11.851	1.05	0.056
106807	-13.097	8.65	11.863	1.05	-0.005
116383	-12.012	9.782	12.436	1.01	0.029
116383	-11.968	9.782	12.450	1.01	-0.015
122414	-13.521	8.238	12.929	1.06	-0.001
122414	-13.483	8.238	12.939	1.06	-0.039
122414	-13.417	8.238	17.987	1.72	-0.024
122414	-13.469	8.238	17.998	1.73	0.029
177619	-13.535	8.29	18.042	1.10	0.027
177619	-13.522	8.29	18.054	1.10	0.014
177619	-13.504	8.29	18.065	1.10	-0.004
177619	-13.519	8.29	18.796	1.10	0.004
177619	-13.495	8.29	18.806	1.10	-0.020
177619	-13.535	8.29	19.901	1.15	0.020
177619	-13.489	8.29	19.912	1.15	-0.027
mean					0.001±0.024

only the subset of the standard observations towards the end of the night where the seeing was more stable. There are too few observations in this subset to determine an extinction coefficient, and so we have arbitrarily set $\varepsilon_{K'}$=0.1 magnitudes airmass^{-1} from which we determine ZP=24.140±0.038. This gives a mean residual of 0.000±0.038. Although this is a somewhat arbitrary choice of $\varepsilon_{K'}$, the absolute calibrations of the mosaics have only a very weak dependence on the value of the extinction coefficient because the standards and NGC6752 frames were observed at comparable airmasses. For instance, if we had instead chosen a value of $\varepsilon_{K'}$=0.3 magnitudes airmass^{-1}, the corrections applied to the instrumental magnitudes of the two field 3 and the field 8 mosaics would have been only -0.002, 0.000 and 0.012 magnitudes different respectively.

The NGC6752 and standard observations taken on 17/18 and 19/20 April 1992 used the K′ filter rather than K. This filter has been discussed by Wainscoat & Cowie (1992), and provides a sensitivity some 0.6 magnitudes better than K. The advantage which we gained from this extra sensitivity on the nights with poor seeing is offset somewhat by some serious disadvantages of this filter. Firstly, the short wavelength end of the K′ bandpass

Table 4: Data for standard stars from 5/6 May 1991.

Star (HD)	Instrumental Magnitude	Catalogue Magnitude	Universal Time (start)	Airmass	Residual (catalogue - reduced)
122414	-13.502	8.238	11.919	1.09	-0.030
122414	-13.550	8.238	11.930	1.09	0.018
116383	-11.970	9.782	11.957	1.02	-0.025
116383	-12.026	9.782	11.967	1.02	0.031
116383	-11.960	9.782	12.490	1.01	-0.036
116383	-11.976	9.782	12.500	1.01	-0.020
116383	-11.956	9.782	12.975	1.01	-0.040
116383	-11.961	9.782	12.986	1.01	-0.035
84090	-13.202	8.50	13.077	1.57	-0.020
84090	-13.234	8.50	13.086	1.57	0.012
122414	-13.513	8.238	16.377	1.29	0.001
122414	-13.490	8.238	16.385	1.30	-0.021
177619	-13.507	8.29	16.432	1.17	0.035
177619	-13.527	8.29	16.443	1.17	0.055
177619	-13.508	8.29	17.498	1.11	0.030
177619*	-13.578	8.29	17.509	1.11	0.100
177619	-13.504	8.29	18.427	1.10	0.025
177619	-13.510	8.29	18.436	1.10	0.031
122414	-13.421	8.238	18.526	2.02	-0.018
122414	-13.445	8.238	18.535	2.02	0.006
mean					0.000±0.028

is defined not by the filter, but by atmospheric water vapour absorbtion lines, meaning that the bandpass could be variable if the atmospheric water vapour content varies. Secondly, there are no K′ IRIS standards. We have set the catalogue K′ magnitudes of the standards by assuming the relation determined by Wainscoat & Cowie: (K-K′) = -0.22(H-K).

1.2.3 The absolute calibration of the mosaics

The absolute calibration was transferred to the mosaics by the following procedure.

The point spread functions produced by DAOPHOT during the photometry of the mosaics were used to clean each mosaic of all images but those of a few stars selected to be both

Table 5: Data for standard stars from 16/17 April 1992.

Star (HD)	Instrumental Magnitude	Catalogue magnitude	Universal Time (start)	Airmass	Residual (catalogue - reduced)
122414	-15.781	8.24	15.559	1.08	0.024
122414	-15.779	8.24	15.571	1.08	0.022
122414	-15.740	8.24	16.981	1.20	-0.022
122414	-15.731	8.24	16.996	1.21	-0.028
159402	-15.863	8.15	17.109	1.04	-0.039
159402	-15.902	8.15	17.123	1.04	0.000
177619	-15.721	8.29	17.168	1.22	0.010
177619	-15.713	8.29	17.181	1.22	0.001
177619	-15.743	8.29	17.194	1.21	0.028
177619	-15.726	8.29	17.208	1.21	0.011
177619	-15.764	8.29	18.088	1.14	0.004
177619	-15.756	8.29	18.101	1.14	-0.005
177619*	-15.829	8.29	18.768	1.11	0.041
177619*	-15.815	8.29	18.779	1.11	0.027
159402*	-15.870	8.15	18.829	1.04	-0.080
159402*	-15.789	8.15	18.839	1.04	-0.161
177619	-15.828	8.29	19.468	1.10	0.018
177619	-15.825	8.29	19.481	1.10	0.014
mean					0.003±0.019

as bright and as uncrowded by neighbouring stars as possible. Synthetic aperture photometry, with two sky apertures, was performed on these images using the appropriate sized aperture. This was repeated on frames where images of *all* stars had been removed and the residual flux left behind by the DAOPHOT subtraction thus found. For each star measured the quantity $ZP_{DAO} = r_{ap} - r_{DAO} + ZP_{ap}$ was found and the mean calculated, weighting by the square of (flux/residual flux). ZP is the zero point, r refers to a raw magnitude and subscripts ap and DAO refer to aperture and DAOPHOT values. This scheme gives most weight to the brightest stars and also to those whose images have subtracted well, indicating that the image was well modelled by the point spread function.

The mean airmass for each mosaic and, if appropriate, the mean Universal Time, were used to calculate the final correction to be applied to the DAOPHOT instrumental magnitudes, which are reported in Table 9. Of more importance than the values themselves are the errors, which are the weighted standard deviations of the quantity $ZP_{DAO} = r_{ap} - r_{DAO} + ZP_{ap}$ determined for each star. An idea of the systematic uncertainties inherent in

Table 6: Data for standard stars from 17/18 April 1992.

Star (HD)	Instrumental Magnitude	Catalogue Magnitude	Universal Time (start)	Airmass	Residual (catalogue - reduced)
84090	-15.545	8.51	8.337	1.09	0.009
84090	-15.535	8.51	8.349	1.09	-0.001
GL390	-17.900	6.11	8.547	1.26	0.001
GL390	-17.889	6.11	8.559	1.25	-0.012
84090	-15.538	8.51	8.720	1.06	-0.001
84090	-15.543	8.51	8.742	1.06	0.005
122414	-15.661	8.26	9.400	1.85	0.041
122414	-15.521	8.26	9.412	1.85	-0.099
122414	-15.622	8.26	9.452	1.83	-0.001
122414	-15.697	8.26	10.583	1.43	0.003
122414	-15.704	8.26	10.596	1.43	0.010
122414	-15.735	8.26	12.313	1.15	0.001
122414	-15.730	8.26	12.333	1.15	-0.004
122414	-15.620	8.26	15.666	1.09	0.014
122414	-15.609	8.26	15.743	1.09	0.000
144212	-15.621	8.26	17.659	1.32	-0.004
144212	-15.596	8.26	17.673	1.33	-0.027
159402	-15.778	8.15	17.991	1.03	-0.049
159402	-15.809	8.15	18.006	1.03	-0.019
177619	-15.737	8.30	19.574	1.10	0.014
177619	-15.731	8.30	19.592	1.10	0.007
mean					-0.005±0.027

the photometric calibration can therefore be gained by combining these errors in quadrature with the errors on ZP_{ap} from Tables 3 to 7, though this does not include the error in the correction to zero airmass which may contribute a further 2% or so.

The K′ magnitudes were transformed to K using K = K′ - 0.012(V-K′), a correction determined using the catalogue colours of the standards observed on 17/18 April.

A star-by-star comparison of the field 5 photometry of 4/5 May 1991 and 16/17 April 1992 revealed a discrepancy with the latter photometry being systematically fainter. We have adjusted the zeropoint of the 16/17 April data to bring them into agreement with the 4/5 and 5/6 May data, a change of 0.178 magnitudes. As can be seen from Table 5, during the analysis of the standards of 16/17 April 1992 we discarded the four

Table 7: Data for standard stars from 19/20 April 1992.

Star (HD)	Instrumental Magnitude	Catalogue Magnitude	Universal Time (start)	Airmass	Residual (catalogue - reduced)
122414	-15.687	8.26	16.918	1.22	-0.071
177619	-15.717	8.30	16.999	1.21	-0.002
177619	-15.731	8.30	17.010	1.21	0.012
177619	-15.756	8.30	18.218	1.12	0.028
177619	-15.721	8.30	18.230	1.12	-0.007
177619	-15.781	8.30	19.599	1.10	0.051
177619	-15.751	8.30	19.608	1.10	0.021
159402	-15.843	8.15	19.803	1.12	-0.035
mean					0.000±0.036

Table 8: Summary of the extinction and time coefficients and the zeropoints derived from the standard stars.

Date	Waveband	Extinction coefficient ε	time coefficient b	ZP
4/5 May 1991	K	0.191	0.009	21.846
5/6 May 1991	K	0.100	-	21.879
16/17 April 1992	K	0.288	0.028	23.872
17/18 April 1992	K'	0.205 0.273	-0.010 0.041	24.353 (T<1535h) 23.521 (T>1535h)
19/20 April 1992	K'	assume 0.1	-	24.140

observations of HD177619 and HD159402 with 18.7 < Universal Time/hours < 18.9 because they showed unreasonably large residuals. Since the mean Universal Time of the field 5 mosaic was ~19.1 hours, it is not unreasonable to assume that the patch of non-photometric weather also affected these observations. Further evidence for this can be seen by examining the star-by-star values of ZP_{DAO} calculated during the calibration. After discarding those values where the quantity |(residual flux)/(star flux)| was high, the values of ZP_{DAO} show a standard deviation of ~0.1 magnitudes. For comparison, the standard deviation found in a similar way when calibrating the 5/6 May 1991 field 5 mosaic was only ~0.02 magnitudes, and the value found when calibrating the field 8 mosaic again from 16/17 April was ~0.03 magnitudes. The existence of this zero-point discrepancy is therefore disappointing, but not surprising.

Table 9: Corrections to the mosaic instrumental magnitudes.

Date (UT)	Field	Waveband	Correction to the DAOPHOT instrumental magnitudes
4/5 May 1991	5	K	-3.232±0.016
	8	K	-3.241±0.006
5/6 May 1991	5	K	-3.085±0.016
	8	K	-3.019±0.015
16/17 April 1992	5	K	-1.273±0.058
	8	K	-1.451±0.026
17/18 April 1992	5	K'	-2.027±0.059
19/20 April 1992	3	K'	-1.520±0.046
	3	K'	-1.269±0.027
	8	K'	-1.366±0.020

Finally the photometric results have been combined, weighting approximately in the ratios of the number of frames in each mosaics, although these weights were also adjusted to take account of the scatter in the individual colour-magnitude diagrams. The results are summarised in Table 10. Column 1 gives the Penny & Dickens identification number, to which 3000, 5000, or 8000 has been added to signify the field, and the remaining columns give V, (B-V), (V-K) and σ_K the weighted quadrature combination of the individual DAOPHOT K errors. We include in this table and the following discussion only the data which have measurements from *at least* two separate mosaics. No reddening corrections have been applied to the data presented in Table 10. Henceforth a subscript zero will be used to indicate magnitudes or colours corrected for interstellar extinction and reddening.

Figures 3(a) to (c) show the agreement between the photometry in fields 3, 5 and 8 over the 5 nights. Figure 3(a) shows data for all points matching between the two field 3 mosaics from the night of 19/20 April 1992; the three stars which have optical data are marked with the Penny & Dickens identification numbers. Figures 3(b) and (c) show only data for stars which also have optical counterparts. Inspection of figure 3(b) shows systematic offsets of ~5 to 10% between the 4/5 May 1991 field 5 observations and the others. Since this is only slightly larger than the scatter exhibited by the data points, we have made no attempt to correct for it. The size of the effect will be reduced when the weighted average of the data is taken. Note also that the K magnitudes derived for field 5 stars 8, 9, 11 and 14 from the 17/18 April 1992 mosaic appear to be discrepant, and have

Table 10: NGC6752 photometry.

ID	V	(B-V)	(V-K)	σ_K	ID	V	(B-V)	(V-K)	σ_K
3006	15.63	0.68	1.93	0.01	8061	19.92	0.77	1.90	0.10
3012	16.28	0.65	1.75	0.02	8069	20.03	0.80	2.19	0.07
3017	16.50	0.59	1.59	0.02	8074	20.12	0.86	2.11	0.12
5002	15.82	0.65	1.87	0.01	8077	20.14	0.85	2.26	0.09
5003	16.08	0.72	1.80	0.01	8084	20.26	0.57	1.50	0.26
5004	16.27	0.76	1.74	0.01	8085	20.26	0.87	2.31	0.06
5005	16.65	0.53	1.65	0.01	8086	20.29	0.89	2.22	0.10
5006	16.74	0.53	1.46	0.02	8088	20.36	0.85	2.35	0.08
5008	17.00	0.43	1.41	0.01	8089	20.40	0.92	2.38	0.07
5009	17.02	1.16	3.00	0.01	8095	20.55	0.94	2.38	0.09
5010	17.06	0.65	1.65	0.01	8097	20.60	0.91	2.41	0.08
5011	17.12	0.43	1.41	0.01	8098	20.60	1.01	2.51	0.11
5014	17.27	0.43	1.34	0.03	8104	20.80	0.85	1.99	0.14
5015	17.49	0.43	1.33	0.03	8106	20.83	0.99	2.66	0.09
5016	17.67	0.51	1.55	0.02	8107	20.84	0.99	2.62	0.10
5017	17.74	0.45	1.39	0.02	8113	21.00	1.05	2.69	0.12
5020	17.86	0.44	1.39	0.03	8114	21.03	0.81	2.14	0.18
5021	17.86	0.45	1.23	0.04	8116	21.14	1.11	2.87	0.12
5022	17.95	0.46	1.32	0.03	8120	21.23	1.12	2.72	0.10
5025	18.22	0.49	1.31	0.04	8124	21.24	1.18	3.13	0.13
5026	18.25	0.49	1.43	0.03	8125	21.25	1.28	3.07	0.09
5027	18.30	0.48	1.32	0.05	8128	21.32	1.17	2.71	0.15
5028	18.38	0.51	1.62	0.02	8134	21.42	1.18	3.09	0.16
5031	18.44	0.52	1.34	0.04	8140	21.51	1.45	3.54	0.10
5032	18.50	0.53	1.42	0.05	8145	21.57	1.23	2.93	0.13
5035	18.63	0.50	1.54	0.04	8146	21.58	1.27	2.95	0.12
5036	18.66	0.55	1.62	0.03	8147	21.59	1.24	2.96	0.13
5037	18.66	0.52	1.51	0.06	8151	21.67	1.27	2.73	0.23
5038	18.73	0.54	1.68	0.05	8154	21.70	1.30	3.04	0.17
5040	18.74	0.54	1.49	0.06	8155	21.70	1.17	3.02	0.14
5041	18.77	0.54	1.48	0.04	8157	21.74	1.29	3.08	0.13
5043	18.81	0.52	1.60	0.04	8160	21.78	1.30	3.12	0.15
5044	18.81	0.52	1.44	0.07	8176	21.97	1.33	3.11	0.20
5047	18.89	0.58	1.70	0.06	8180	22.03	1.30	3.13	0.19
5048	18.91	0.56	1.57	0.04	8182	22.04	1.31	2.93	0.22
5049	18.94	0.56	1.56	0.04	8185	22.12	2.26	5.14	0.06
5050	18.99	0.60	1.54	0.06	8188	22.15	2.25	5.05	0.03
5051	19.00	0.62	1.67	0.04	8192	22.21	1.14	4.26	0.09
8002	18.28	0.49	1.37	0.04	8193	22.26	1.47	3.09	0.23
8004	18.35	0.48	1.38	0.04	8194	22.27	1.45	3.32	0.25
8005	18.37	0.51	1.62	0.03	8195	22.29	1.38	3.14	0.29
8008	18.53	2.00	4.62	0.01	8202	22.39	1.56	3.05	0.43
8010	18.56	0.38	1.60	0.03	8203	22.39	1.57	3.45	0.18
8015	18.67	0.52	1.62	0.04	8207	22.40	1.39	3.23	0.25
8016	18.70	0.46	1.61	0.05	8216	22.49	1.49	3.45	0.22
8017	18.70	0.63	1.89	0.03	8226	22.57	1.84	4.28	0.15
8018	18.70	0.54	1.55	0.04	8232	22.58	1.19	4.40	0.08
8020	18.92	0.56	1.65	0.06	8236	22.62	1.44	3.18	0.34
8022	18.93	0.48	1.69	0.06	8237	22.63	1.63	3.80	0.29
8027	19.13	0.80	2.16	0.04	8253	22.77	1.50	3.31	0.31
8028	19.13	0.63	1.65	0.04	8256	22.78	2.05	4.54	0.11
8030	19.13	0.62	1.75	0.05	8260	22.82	1.45	3.68	0.25
8036	19.34	0.69	1.71	0.06	8274	22.98	1.48	3.21	0.45
8037	19.35	0.69	1.98	0.05	8278	23.00	1.61	3.74	0.31
8039	19.42	0.67	2.02	0.06	8279	23.00	2.37	5.60	0.04
8044	19.52	0.66	1.94	0.06	8291	23.07	2.29	5.21	0.06
8045	19.52	0.70	2.06	0.06	8303	23.14	1.48	5.00	0.10
8050	19.64	0.76	2.00	0.05	8331	23.29	1.90	4.03	0.43
8053	19.72	0.80	2.32	0.04	8338	23.32	1.52	3.63	0.40
8055	19.76	0.73	2.05	0.06	8395	23.75	1.84	4.69	0.28
8057	19.83	0.76	2.06	0.09	8401	23.80	0.90	4.17	0.59
8058	19.85	1.28	3.27	0.02					

Figure 3: Agreement between (a) the field 3 and (b) the field 5 photometry.

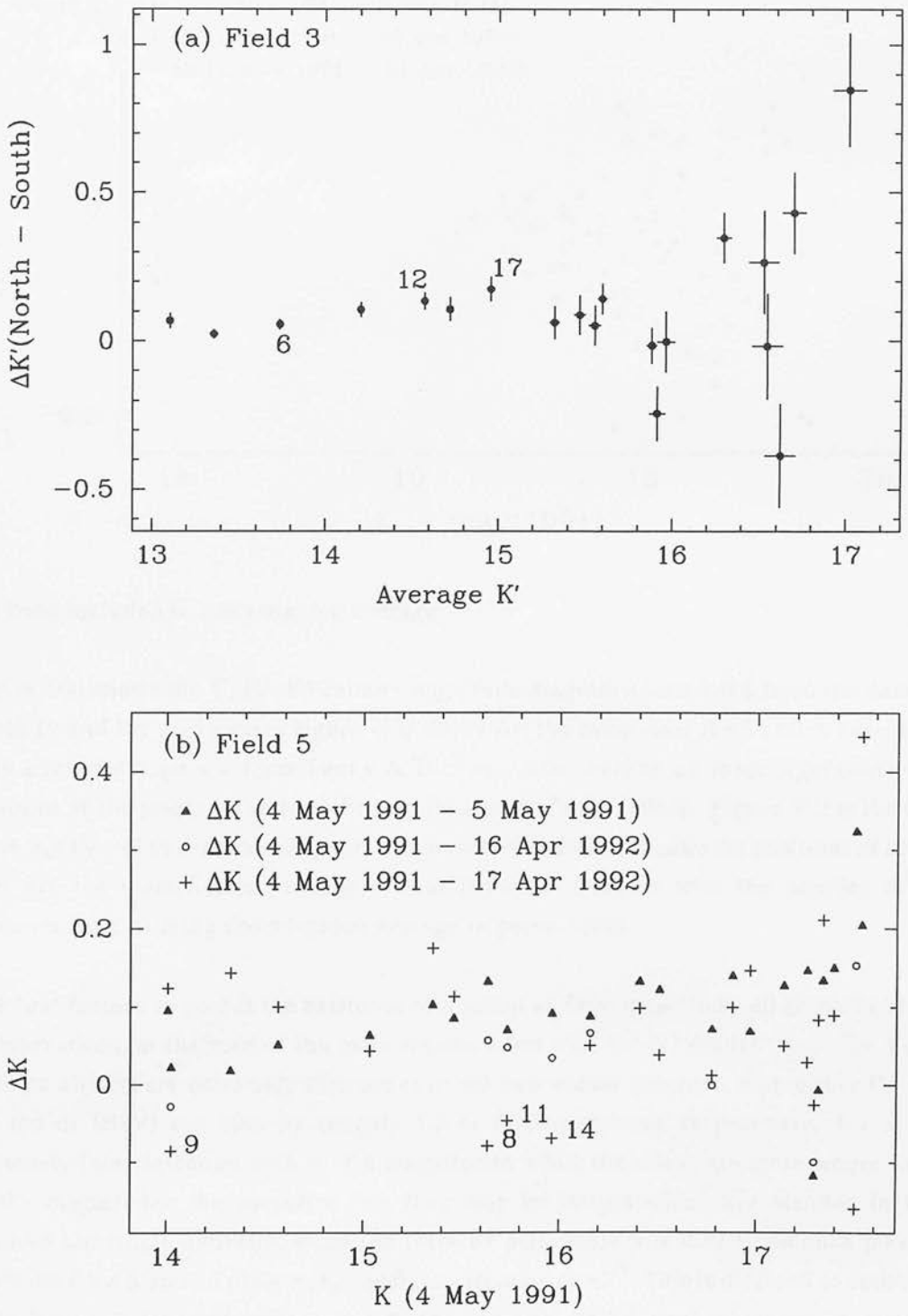

Figure 3(c): Agreement between the field 8 photometry.

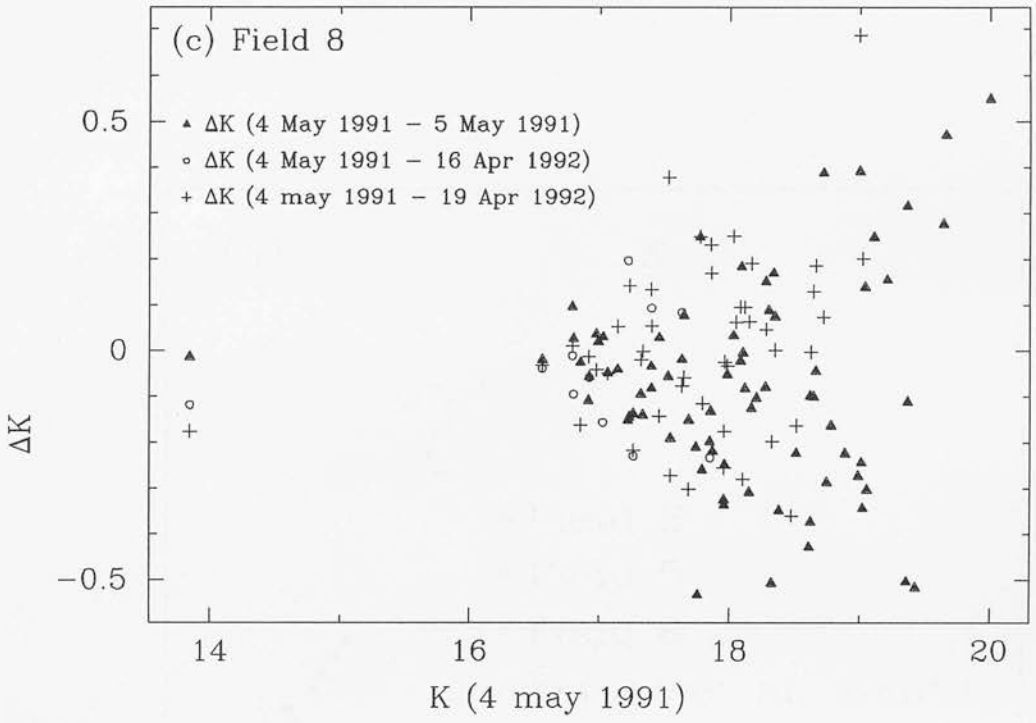

not been included in the weighted average.

Figure 4(a) shows the V, (V-K) colour-magnitude diagram constructed from the data in Table 10 and for comparison figure 4(b) shows for the same stars the V, (B-V) diagram with photometry purely from Penny & Dickens. Also marked on these figures are the positions of the giants taken from Frogel, Persson & Cohen (1983). Figure 4(c) is the (B-V) versus (V-K) two-colour diagram. The numbers indicated beside the positions of some stars are the identification numbers from Penny & Dickens with the number of K measurements forming the weighted average in parentheses.

The first feature to note is the existence of a group of faint detections, all from the field 8 observations, at the base of the main sequence but with (V-K) redder than ~3.6. Four of these objects are extremely discrepant in the two-colour diagram, with either (V-K) too red or (B-V) too blue by roughly 1.5 or 0.75 magnitude respectively. 401 is an extremely faint detection with σ_K~0.6 magnitudes, while the others are more secure with σ_K~0.1 magnitudes. We speculate that they may be images which are blended in the infrared but single optically, since the infrared plate scale was 0.79 arcseconds pixel^{-1} while the field 8 optical plate scale was 0.5 arcseconds pixel^{-1}. This is difficult to confirm since Penny & Dickens remark that "...only enough stars [were] measured in certain magnitude ranges to define the various sequences." We may therefore expect an unknown but significant number of detections to be missing from their tabulation. Star 303 has no

Figure 4(a): The V, (V-K) colour-magnitude diagram for data in Table 8.

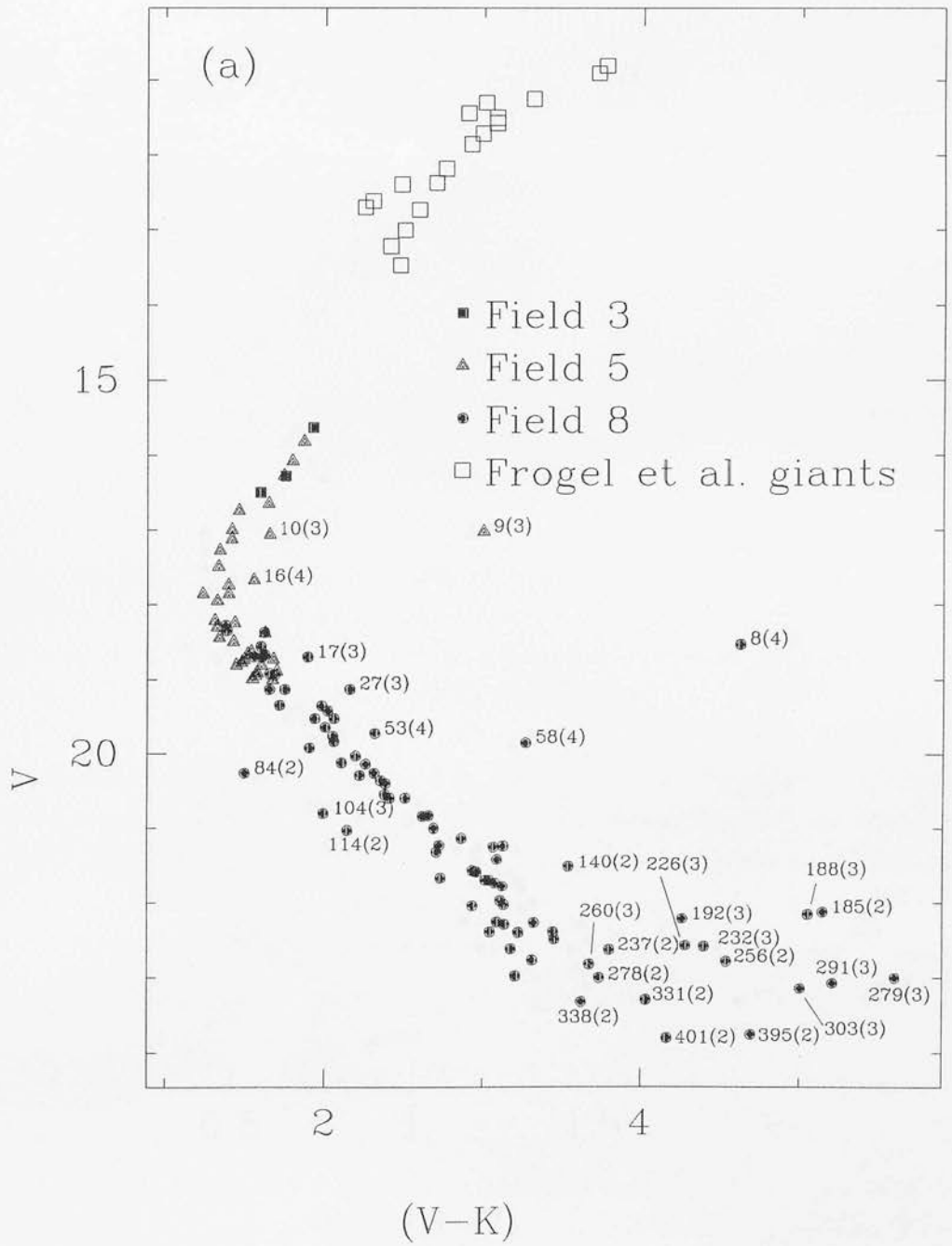

Figure 4(b): The V, (B-V) colour-magnitude diagram for data in Table 8.

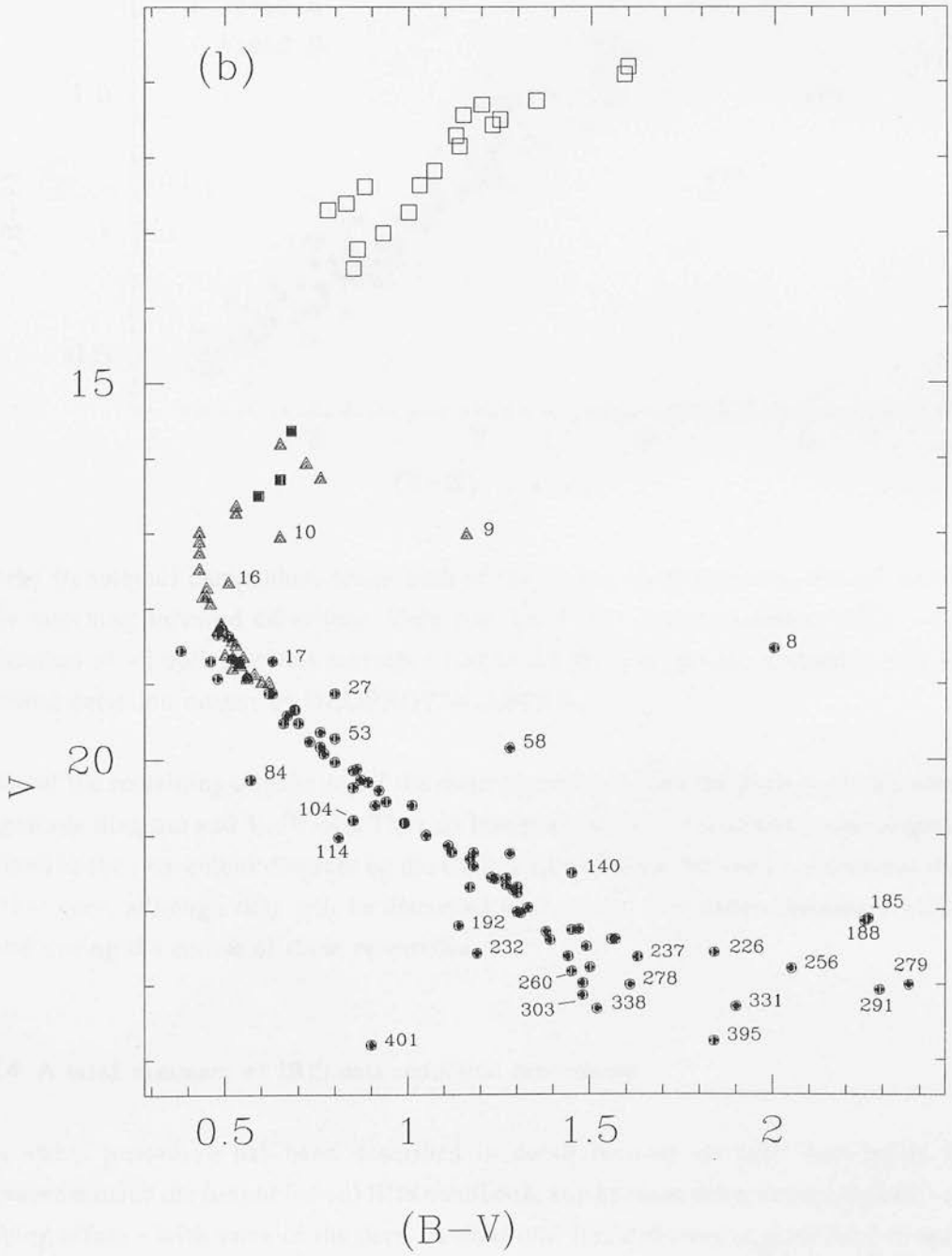

Figure 4(c): The two colour diagram for the stars shown in figures 4(a) and (b).

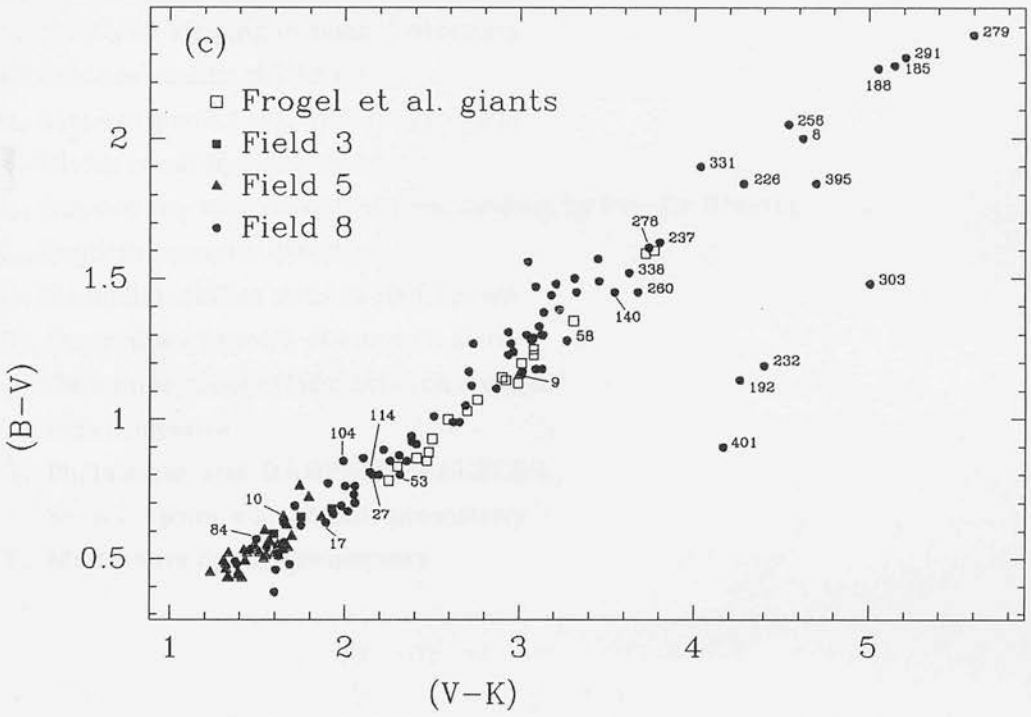

nearby (tabulated) companion, while both of the closest companions to 192 (37 and 86) have matching infrared detections. Only star 232 has a close companion (372), with a separation of ~4 optical pixels corresponding to 2.6 infrared pixels, without a matching infrared detection output by DAOPHOT/ALLSTAR.

Many of the remaining objects lie off the main sequence in both the purely optical colour-magnitude diagram and V, (V-K). They do however continue the almost linear sequence defined in the two-colour diagram by the main-sequence data. We shall not consider them further here, although they will be discussed later, along with other anomalous objects found during the course of these researches.

1.2.4 A brief summary of IRIS data reduction procedures.

The above procedure has been described in detail because no such description has appeared outside the (unpublished) IRIS handbook, and because there were problems - the striping effect - with some of the data. A brief one-line summary is given here to make future reference to the procedure easier to follow.

1... Linearise (the routine also removes dark & bias)
2... Normalise to 1 second on-chip integration time
3... Normalise striping in skies if necessary
4... Produce median sky frames
5... Subtract median sky from object frames
6... Divide result by dome flat
7... Remove any remaining low-level striping by Fourier filtering
8... Deglitch cosmetic defects
9... Normalise median skies to 1000 counts
10... Determine centroids of common stars
11... Determine mean offsets between frames
12... Create mosaics
13... Photometer with DAOPHOT/ALLSTAR
14... Set zero-point via aperture photometry
15... Match with optical photometry

2 47 TUCANA OBSERVATIONS

Infrared photometry of stars in the globular cluster 47 Tuc, with complementary optical photometry from the work of Hesser *et al.* (1987), was obtained at the Anglo-Australian Observatory with IRIS on the nights of 3/4 February 1991, 19/20 and 20/21 September 1991.

2.1 Field 3

The observations of the night of 3/4 February 1991 were made in service mode by D. Allen and colleagues, and comprised part of the IRIS commissioning program. From constraints on the time allowed for the project and estimates of the sensitivity of the array, we selected as the target area the North-East corner of the Hesser *et al.* field F3. The coordinates of the field centre were measured on Schmidt plate J3670, held in the United Kingdom Schmidt Telescope Unit plate library at the Royal Observatory, Edinburgh, and are $00^h21^m57.0^s$ right ascension, -72°16′09″ declination (equinox 1950).

We received a total of 17 K band images taken in a spiral jitter pattern around this field centre with offsets of ±8 arcseconds in each coordinate, and consisting of 30 coadds and 1.55 seconds on-chip integration time. Since this was our first experience with data from IRIS, the data reduction procedure followed that used with IRCAM data where steps 5 and 6 of section 1.2.4 are replaced by the single step of dividing each object frame by the

median sky frame. The reduction procedure was complicated by flexure in the camera optics roughly half-way through the observations, causing a discontinuous change in the array flat-field structure. The flexure appeared to occur suddenly and actually during data-taking; the affected frame could not be flat-fielded, and was discarded.

Four observations of the G5V standard star HD1274 bracketing the field F3 observations were also made using the IRIS25 window and consisting of 20 coadds and 0.25 second exposures; these served to set the photometric zero-point via synthetic aperture photometry with 7 arcsecond diameter apertures. The photometry of these standards is reported in Table 11. Using linear regression we determined the zero-point and extinction coefficient to be ZP=21.58±0.07 magnitudes and ε=0.12±0.04 magnitudes airmass^{-1} respectively. The final column of Table 11 reports the residual in the sense catalogue magnitude minus reduced magnitude. Although four standards is barely sufficient to determine an extinction coefficient, the value of 0.12 magnitudes airmass^{-1} is reasonable for the Siding Springs site.

Of much more concern is the comment made by the Anglo-Australian Observatory staff that weather conditions at the time of the observations were 'not really photometric'. We have performed synthetic aperture photometry of four bright, relatively uncrowded stars on the individual frames comprising the mosaic, again with seven arcsecond diameter apertures, and the instrumental magnitudes are reported in Table 12, as are the magnitudes of the stars measured on the mosaic. Since there is only random scatter apparent in the photometry of Table 12, and given that the standards show only small residuals, we conclude that there is no evidence to suggest any non-photometric behaviour.

From the 601 objects identified and photometered with DAOPHOT and ALLSTAR, ~100 were rejected because their errors were larger than expected for their magnitude. After determining the transformation between the infrared and optical coordinate systems, a remaining 235 objects had an optical counterpart matching to better than three times the r.m.s. alignment error of the coordinate transformation, which was 0.13 optical pixels or ~0.08 arcseconds. Photometry of these 235 objects is reported in Table 13, where the identification numbers are those of Hesser *et al.*

2.2 Field 1

J and K' photometry of stars in the Hesser *et al.* field F1 were obtained with IRIS as the result of a joint proposal to the Australian Time Allocation Committee from our group and K. Mighell & T. Harrison of Mount Stromlo and Siding Springs Observatory. The data were taken on the nights of 19/20 & 20/21 September 1991 by Mighell & Harrison, and subsequently reduced and analysed by us. Both nights were photometric with good seeing,

Table 11: Standard star observations of 3/4 February, 1991.

	Raw magnitude (m_{cat} - m_{raw})	Airmass	Residual
1	21.39	1.59	0.00
2	21.39	1.59	0.00
3	21.36	1.96	0.02
4	21.33	1.96	-0.01

Table 12: Relative photometry of four stars on the 3/4 February 1991 47 Tuc Field F3 frames.

Frame number	Star A	Star B	Star C	Star D
1	-9.31	-9.32	-9.64	-9.48
2	-9.35	-9.35	-9.60	-9.44
3	-9.34	-9.37	-9.62	-9.49
4	-9.31	-9.36	-9.60	-9.45
5	-9.34	-9.33	-9.58	-9.37
6	-9.33	-9.29	-9.58	-9.33
7	-9.23	-9.33	-9.61	-9.46
8	-9.32	-9.36	-9.61	-9.50
9	-9.29	-9.28	-9.59	-9.47
10	-9.33	-9.29	-9.58	-
11	-9.33	-9.36	-9.61	-9.45
12	-9.30	-9.32	-9.59	-9.41
13	-9.33	-9.29	-9.58	-9.39
14	-9.31	-9.29	-9.57	-9.32
15	-9.28	-9.31	-	-9.47
16	-9.35	-9.36	-9.61	-9.44
mosaic	-9.32	-9.32	-9.60	-9.42

Table 13: 47 Tuc field F3 photometry from 3/4 February, 1991.

Star	V	(B-V)	(V-K)	σ_K	Star	V	(B-V)	(V-K)	σ_K
30016	13.826	0.758	2.053	0.041	30361	17.183	0.553	1.433	0.075
30028	14.049	0.689	1.969	0.016	30366	17.190	0.698	1.694	0.063
30033	14.068	0.781	2.105	0.016	30378	17.208	0.403	1.494	0.078
30037	14.083	0.714	2.007	0.044	30396	17.221	0.706	1.796	0.054
30044	14.103	0.779	2.056	0.029	30410	17.232	0.670	1.795	0.031
30050	14.135	0.808	2.056	0.031	30425	17.247	0.616	1.466	0.061
30064	14.521	0.914	2.517	0.029	30430	17.251	0.730	1.647	0.053
30065	14.531	0.925	2.453	0.054	30435	17.254	0.735	1.736	0.039
30068	14.553	0.908	2.548	0.020	30438	17.255	0.693	1.645	0.032
30069	14.563	0.965	2.440	0.037	30439	17.255	0.601	1.617	0.091
30070	14.564	0.933	2.491	0.028	30445	17.260	0.651	1.503	0.039
30097	15.420	0.873	2.289	0.034	30456	17.273	0.655	1.483	0.078
30105	15.557	0.843	2.208	0.021	30460	17.275	0.614	1.656	0.055
30106	15.585	0.841	2.247	0.023	30462	17.277	0.736	1.640	0.078
30112	15.729	0.841	2.199	0.035	30465	17.279	0.629	1.504	0.053
30113	15.732	0.841	2.222	0.022	30471	17.283	0.580	1.346	0.080
30114	15.750	0.979	1.804	0.047	30475	17.285	0.618	1.521	0.055
30115	15.768	0.409	1.211	0.035	30484	17.299	0.503	1.312	0.106
30119	15.830	0.821	2.198	0.034	30493	17.311	0.615	1.546	0.041
30120	15.830	0.854	2.253	0.031	30499	17.314	0.715	1.281	0.092
30125	15.950	0.789	2.086	0.057	30506	17.324	0.678	1.261	0.070
30128	16.003	0.805	2.073	0.018	30514	17.334	0.566	1.329	0.077
30135	16.115	0.835	2.118	0.053	30517	17.338	0.397	1.645	0.055
30142	16.251	0.769	2.078	0.051	30519	17.341	0.570	1.426	0.057
30144	16.267	0.720	1.987	0.036	30520	17.342	0.637	1.621	0.079
30147	16.289	0.420	1.132	0.067	30534	17.356	0.595	1.440	0.047
30170	16.488	0.827	2.085	0.032	30549	17.374	0.590	1.112	0.098
30193	16.618	0.779	2.170	0.025	30559	17.385	0.695	1.556	0.058
30202	16.660	0.771	2.132	0.024	30570	17.402	0.530	1.476	0.074
30208	16.693	0.689	2.156	0.035	30576	17.407	0.575	1.418	0.045
30213	16.735	1.071	2.827	0.049	30587	17.420	0.571	1.386	0.061
30216	16.738	0.769	2.105	0.040	30592	17.426	0.496	1.982	0.069
30248	16.914	0.813	2.147	0.041	30616	17.457	0.537	1.583	0.041
30249	16.914	0.710	1.880	0.048	30629	17.471	0.471	1.507	0.075
30262	16.954	0.673	1.934	0.061	30640	17.482	0.730	1.281	0.080
30270	16.990	0.813	1.945	0.040	30645	17.490	0.506	1.562	0.072
30282	17.010	0.696	2.106	0.043	30661	17.506	0.581	1.228	0.084
30307	17.081	0.581	1.711	0.054	30675	17.527	0.690	1.475	0.075
30316	17.106	0.740	1.901	0.046	30711	17.564	0.645	1.470	0.084
30319	17.110	0.776	1.804	0.084	30724	17.581	0.576	1.449	0.094
30325	17.122	0.800	2.005	0.035	30734	17.588	0.685	1.580	0.075
30327	17.126	0.820	1.768	0.053	30747	17.599	0.509	1.236	0.075
30330	17.128	1.157	1.821	0.072	30751	17.603	0.578	1.536	0.046
30332	17.132	0.748	1.670	0.067	30758	17.615	0.825	1.359	0.075
30335	17.134	0.830	1.788	0.050	30775	17.638	0.551	1.382	0.064
30343	17.148	0.708	1.824	0.062	30780	17.640	0.614	1.290	0.113
30347	17.154	0.565	1.688	0.045	30793	17.653	0.578	1.467	0.094
30348	17.155	0.603	2.101	0.063	30795	17.657	0.609	1.456	0.089
30359	17.180	0.363	1.100	0.096	30803	17.668	0.653	1.321	0.147
30360	17.183	0.658	2.007	0.054	30805	17.672	0.520	1.483	0.080

Table 13 continued

Star	V	(B-V)	(V-K)	σ_K	Star	V	(B-V)	(V-K)	σ_K
30815	17.683	0.541	1.564	0.083	31318	18.101	0.461	1.303	0.143
30816	17.685	0.509	1.588	0.078	31342	18.119	0.584	1.398	0.154
30828	17.696	0.398	1.728	0.087	31343	18.122	0.426	1.345	0.128
30836	17.699	0.623	1.503	0.091	31345	18.125	0.693	1.531	0.162
30837	17.699	0.588	1.594	0.073	31347	18.128	0.736	1.496	0.083
30846	17.708	0.560	1.489	0.089	31349	18.130	0.717	1.217	0.117
30860	17.719	0.487	1.436	0.067	31379	18.149	0.647	1.502	0.086
30862	17.721	0.675	0.605	0.123	31389	18.160	0.517	1.657	0.079
30875	17.737	0.611	1.477	0.055	31395	18.162	0.693	1.734	0.118
30880	17.742	0.688	1.398	0.094	31396	18.163	0.517	1.178	0.195
30885	17.744	0.454	1.318	0.121	31432	18.194	0.491	0.752	0.319
30898	17.755	0.550	1.360	0.087	31446	18.203	0.546	1.445	0.135
30903	17.759	0.507	1.389	0.068	31470	18.224	0.700	1.534	0.197
30917	17.772	0.649	1.431	0.116	31473	18.226	0.268	1.494	0.089
30952	17.808	0.516	1.560	0.057	31481	18.233	0.683	1.231	0.139
30958	17.810	0.436	1.203	0.117	31524	18.264	0.434	1.774	0.057
30960	17.813	0.699	1.234	0.117	31535	18.270	0.187	2.011	0.121
30968	17.819	0.556	1.166	0.116	31546	18.280	0.505	1.587	0.087
30984	17.835	0.611	1.462	0.089	31556	18.291	0.718	1.143	0.221
30988	17.837	0.456	1.609	0.082	31557	18.292	0.548	1.459	0.091
30993	17.840	0.485	1.968	0.059	31568	18.303	0.606	1.365	0.246
31002	17.847	0.630	1.590	0.109	31597	18.334	0.716	1.367	0.145
31014	17.855	0.550	1.325	0.104	31598	18.337	0.820	1.425	0.148
31030	17.866	0.738	1.266	0.091	31622	18.355	0.595	1.654	0.105
31039	17.870	0.527	1.067	0.140	31630	18.361	0.627	1.193	0.218
31047	17.876	0.550	1.582	0.101	31631	18.361	0.574	1.405	0.138
31088	17.912	0.415	1.716	0.141	31634	18.363	0.628	1.410	0.171
31091	17.917	0.646	1.111	0.109	31713	18.434	0.726	1.099	0.235
31110	17.929	0.513	1.522	0.093	31733	18.445	0.623	1.427	0.139
31121	17.941	0.561	1.405	0.069	31736	18.447	0.581	1.095	0.191
31131	17.946	0.516	1.479	0.104	31741	18.451	0.990	1.068	0.174
31141	17.952	0.793	1.499	0.095	31756	18.461	0.765	1.489	0.201
31157	17.969	0.685	1.680	0.131	31763	18.467	0.425	1.818	0.099
31188	17.995	0.527	1.104	0.088	31775	18.477	0.677	1.374	0.152
31190	17.997	0.779	1.698	0.121	31811	18.504	0.739	1.770	0.138
31193	17.998	0.550	1.469	0.108	31824	18.510	0.903	1.660	0.108
31234	18.035	0.506	1.552	0.071	31854	18.538	0.840	1.747	0.088
31245	18.043	0.704	1.880	0.082	31872	18.559	0.710	1.490	0.163
31248	18.044	0.594	1.739	0.091	31878	18.566	0.683	1.659	0.141
31250	18.048	0.606	1.522	0.111	31886	18.573	0.619	2.128	0.133
31254	18.050	0.539	1.369	0.145	31895	18.582	0.577	1.793	0.217
31255	18.050	0.887	1.812	0.085	31900	18.587	0.517	1.231	0.154
31265	18.056	0.603	1.476	0.083	31919	18.597	0.593	1.080	0.162
31275	18.069	0.261	1.726	0.077	31922	18.601	0.743	1.701	0.149
31276	18.070	0.610	1.151	0.180	31927	18.607	0.541	1.650	0.111
31288	18.080	0.649	1.375	0.092	31939	18.614	0.534	1.571	0.126
31296	18.087	1.007	1.422	0.131	31942	18.616	0.814	1.032	0.267
31297	18.087	0.648	0.880	0.148	31947	18.623	0.498	1.599	0.184
31303	18.090	-0.059	1.910	0.064	31956	18.627	0.645	1.689	0.094
31309	18.094	0.657	1.670	0.099	31971	18.639	0.693	1.816	0.167

Table 13 continued

Star	V	(B-V)	(V-K)	σ_K	Star	V	(B-V)	(V-K)	σ_K
31976	18.647	0.367	1.542	0.138	32348	18.968	1.336	1.720	0.203
31981	18.651	0.839	2.050	0.114	32364	18.981	0.164	2.338	0.095
31985	18.656	0.810	1.608	0.176	32369	18.985	0.811	2.035	0.224
32014	18.684	0.401	1.564	0.183	32398	19.014	0.621	1.830	0.186
32032	18.691	0.676	1.338	0.161	32410	19.026	0.980	1.685	0.096
32043	18.704	0.509	1.846	0.213	32411	19.027	0.737	1.918	0.202
32074	18.722	1.019	1.632	0.159	32427	19.042	0.687	2.211	0.145
32100	18.741	0.601	1.306	0.155	32465	19.081	0.530	2.192	0.103
32110	18.750	0.539	1.837	0.137	32468	19.083	0.656	1.822	0.189
32122	18.765	0.808	1.227	0.239	32488	19.106	0.813	1.273	0.371
32127	18.770	0.831	1.716	0.198	32498	19.122	0.571	1.698	0.267
32142	18.781	0.733	1.831	0.182	32562	19.218	0.678	1.562	0.303
32176	18.824	0.605	1.702	0.114	32584	19.239	0.680	2.296	0.164
32178	18.824	0.603	1.498	0.158	32588	19.255	0.711	2.171	0.167
32221	18.860	0.614	1.900	0.123	32641	19.350	0.856	1.497	0.233
32238	18.876	0.469	1.381	0.191	32691	19.426	0.666	2.050	0.162
32287	18.918	0.618	1.858	0.128	32780	19.679	1.296	2.072	0.142
32336	18.956	0.977	2.151	0.142					

except for an interruption by cloud during the first night, causing a loss of ~1.5 hours.

Tables 14 and 15 detail the photometry of the standard stars. These standards were observed with the IRIS31 window, and consisted of 30 coadds and 0.3 seconds on-chip integration time. Standards in Tables 14 and 15 whose names are prefixed by 'L' are red giant stars from the list of Lee (1977). The catalogue magnitudes were taken from the published photometry of Frogel *et al.* (1981) and transformed from the CIT to the AAO photometric system using the transformations of Elias *et al.* (1983) which are reproduced - after slight rearrangement - in equations 1. The zero-points and extinction and time

$$
\begin{aligned}
K_{AAO} &= K_{CIT} + 0.011 \\
H_{AAO} &= \frac{(H-K)_{CIT}}{0.954} + K_{CIT} + 0.015 \\
J_{AAO} &= \frac{(J-K)_{CIT}}{0.897} + K_{CIT} + 0.004
\end{aligned}
\qquad (1)
$$

coefficients determined from the standards are summarised in Table 16, and the residuals against airmass and against time are shown in figure 5. On the two nights, frames comprising four K' and three J jittered mosaics were obtained in overlapping regions of field F1, and can be located by means of the finding charts provided in Appendix A of this thesis. Details of these observations are given in Table 17, which lists for each mosaic

Table 14: Standard star observations of 19/20 September 1991.

Star (HD)	Instrumental Magnitude	Catalogue magnitude	Universal Time (start)	Airmass	Residual (catalogue - reduced)
		The K' Standards			
1274	-13.380	8.39	9.312	1.83	-0.002
1274	-13.378	8.39	9.324	1.82	-0.005
218814	-12.541	9.25	9.492	1.47	-0.012
218814	-12.540	9.25	9.500	1.47	-0.013
DM-597287	-13.249	8.57	9.593	1.15	-0.004
DM-597287	-13.248	8.57	9.605	1.15	-0.005
194107	-13.470	8.38	9.810	1.05	0.017
1274*	-13.175	8.39	9.883	1.66	-0.225
1274	-13.389	8.39	9.905	1.66	-0.012
1274	-13.439	8.39	11.126	1.42	0.012
1274	-13.448	8.39	11.138	1.41	0.019
1274	-13.444	8.39	11.736	1.33	0.005
1274	-13.438	8.39	11.750	1.33	-0.001
1274	-13.453	8.39	12.359	1.27	0.006
1274	-13.443	8.39	12.370	1.27	-0.005
1274	-13.450	8.39	12.895	1.23	-0.004
1274	-13.437	8.39	12.908	1.23	-0.017
1274	-13.441	8.39	13.481	1.21	-0.019
1274*	-13.417	8.39	13.491	1.20	-0.043
1274	-13.459	8.39	13.956	1.19	-0.005
1274	-13.459	8.39	13.968	1.19	-0.005
20223*	-13.134	8.68	15.021	1.16	-
20223*	-11.102	8.68	15.038	1.16	-
18847	-13.130	8.68	16.514	1.03	-0.003
18847	-13.119	8.68	16.531	1.03	-0.014
18847	-13.127	8.68	16.540	1.03	-0.005
1274	-13.415	8.39	16.673	1.28	-0.003
1274	-13.414	8.39	16.682	1.28	-0.004
L3501	-13.195	8.62	16.787	1.40	0.012
L3501	-13.188	8.62	16.797	1.41	0.005
1274	-13.421	8.39	17.408	1.36	0.002
1274	-13.409	8.39	17.418	1.36	-0.010
1274	-13.416	8.39	17.949	1.44	-0.004
1274	-13.402	8.39	17.958	1.44	-0.018
L3501	-13.191	8.62	18.503	1.60	0.005
L3501	-13.181	8.62	18.519	1.60	-0.005
L4503	-12.338	9.47	18.677	1.62	0.003
L4503	-12.352	9.47	18.689	1.62	0.017
L1510	-13.010	8.80	18.730	1.63	0.009
L1510	-13.001	8.80	18.741	1.63	0.000
L2426	-13.283	8.54	18.843	1.65	0.017
L2426	-13.273	8.54	18.854	1.65	0.007
1274	-13.399	8.39	18.879	1.62	-0.019
1274	-13.388	8.39	18.892	1.62	-0.030
7644	-12.571	9.22	19.022	1.38	-0.019

Table 14 continued

Star (HD)	Instrumental Magnitude	Catalogue Magnitude	Universal Time (start)	Airmass	Residual (catalogue - reduced)
7644	-12.565	9.22	19.030	1.38	-0.025
15911	-12.331	9.48	19.064	1.19	-0.009
15911	-12.339	9.48	19.074	1.19	-0.002
20223	-13.163	8.68	19.171	1.10	0.023
20223	-13.147	8.68	19.180	1.10	0.008
29250	-12.463	9.37	19.205	1.01	0.010
29250	-12.475	9.37	19.214	1.01	0.022
		The J Standards			
1274	-12.742	8.80	9.357	1.81	-0.009
1274	-12.731	8.80	9.367	1.81	-0.020
218814*	-12.182	9.35	9.430	1.49	-0.068
218814*	-12.174	9.35	9.449	1.48	-0.078
DM-597287	-12.743	8.89	9.658	1.15	-0.019
DM-597287	-12.748	8.89	9.670	1.15	-0.014
194107	-12.883	8.79	9.751	1.05	0.006
1274	-12.784	8.80	9.941	1.65	0.008
1274	-12.769	8.80	9.949	1.65	-0.007
1274	-12.843	8.80	11.155	1.41	0.030
1274	-12.836	8.80	11.176	1.41	0.024
1274	-12.829	8.80	11.710	1.34	0.006
1274	-12.831	8.80	11.724	1.34	0.008
1274	-12.845	8.80	12.336	1.27	0.011
1274	-12.842	8.80	12.350	1.27	0.008
1274	-12.838	8.80	12.920	1.23	-0.002
1274	-12.823	8.80	12.929	1.23	-0.017
1274	-12.832	8.80	13.459	1.21	-0.011
1274	-12.829	8.80	13.470	1.21	-0.014
1274	-12.852	8.80	13.979	1.19	0.006
1274	-12.837	8.80	13.991	1.19	-0.009
20223*	-11.512	8.83	15.056	1.16	-
20223*	-11.940	8.83	15.086	1.15	-
18847	-12.568	9.01	16.551	1.03	0.001
18847	-12.527	9.01	16.560	1.03	-0.040
1274	-12.777	8.80	16.693	1.28	0.012
1274	-12.777	8.80	16.703	1.28	0.011
L3501	-11.959	9.59	16.747	1.40	-0.012
L3501	-11.970	9.59	16.756	1.40	-0.001
1274	-12.785	8.80	17.446	1.36	0.012
1274	-12.788	8.80	17.455	1.37	0.015
1274	-12.784	8.80	17.899	1.43	0.008
1274	-12.785	8.80	17.907	1.43	0.009
1274	-12.765	8.80	17.919	1.43	-0.011
L3501	-11.993	9.59	18.546	1.60	0.005
L3501	-11.987	9.59	18.554	1.60	-0.002
L4503	-11.290	10.27	18.633	1.61	-0.017

Table 14 continued

Star (HD)	Instrumental Magnitude	Catalogue Magnitude	Universal Time (start)	Airmass	Residual (catalogue - reduced)
L4503	-11.295	10.27	18.645	1.61	-0.013
L1510	-11.841	9.75	18.769	1.64	0.008
L1510	-11.850	9.75	18.777	1.64	0.017
L2426	-12.071	9.52	18.806	1.64	0.012
L2426	-12.047	9.52	18.815	1.65	-0.012
1274	-12.765	8.80	18.919	1.63	-0.016
7644	-12.067	9.50	18.974	1.37	-0.029
7644	-12.068	9.50	18.989	1.37	-0.028
15911	-12.107	9.47	19.101	1.20	-0.030
15911	-12.125	9.47	19.111	1.20	-0.012
20223	-12.802	8.83	19.134	1.09	0.019
20223	-12.809	8.83	19.143	1.09	0.025
29250	-12.158	9.47	19.240	1.01	0.009
29250	-12.161	9.47	19.249	1.01	0.011

Table 15: Standard star observations of 20/21 September 1991.

Star (HD)	Instrumental Magnitude	Catalogue Magnitude	Universal Time (start)	Airmass	Residual (catalogue - reduced)
		The K' Standards			
193727	-13.082	8.81	8.831	1.13	0.004
193727	-13.054	8.81	8.846	1.13	-0.025
194107	-13.500	8.38	8.974	1.09	-0.009
194107	-13.474	8.38	8.981	1.09	-0.035
1274	-13.407	8.39	9.086	1.88	-0.033
1274	-13.409	8.39	9.102	1.87	-0.031
1274	-13.438	8.39	9.879	1.65	-0.015
1274	-13.424	8.39	9.889	1.65	-0.029
1274	-13.458	8.39	10.517	1.51	-0.002
1274	-13.446	8.39	10.525	1.51	-0.015
L3501	-13.259	8.62	11.175	1.51	0.034
L3501	-13.245	8.62	11.184	1.50	0.020
1274	-13.482	8.39	11.707	1.33	0.015
1274	-13.474	8.39	11.718	1.33	0.007
L3501	-13.239	8.62	11.828	1.44	0.013
L3501	-13.234	8.62	11.836	1.44	0.008
1274	-13.478	8.39	12.497	1.26	0.011
1274	-13.475	8.39	12.506	1.26	0.008
L3501	-13.240	8.62	12.574	1.38	0.014
L3501	-13.230	8.62	12.583	1.38	0.005
L4503	-12.397	9.47	12.686	1.37	0.022
L4503	-12.419	9.47	12.694	1.37	0.044
L1510	-13.052	8.80	12.751	1.38	0.013
L1510	-13.071	8.80	12.759	1.37	0.031
L2426	-13.342	8.54	12.859	1.37	0.037
15911	-12.332	9.48	12.933	1.42	-0.024
15911	-12.329	9.48	12.942	1.42	-0.027
202964	-13.545	8.29	13.130	1.08	-0.027
202964	-13.552	8.29	13.139	1.08	-0.020
1274	-13.462	8.39	14.244	1.19	0.002
1274	-13.460	8.39	14.254	1.19	0.000
L3501	-13.249	8.62	14.417	1.32	0.032
L3501	-13.247	8.62	14.425	1.32	0.030
1274	-13.472	8.39	14.963	1.19	0.017
1274	-13.431	8.39	14.972	1.19	-0.024
1274	-13.463	8.39	15.512	1.21	0.013
1274	-13.454	8.39	15.521	1.21	0.004
1274	-13.426	8.39	16.119	1.24	-0.017
1274	-13.423	8.39	16.127	1.24	-0.020
1274	-13.403	8.39	17.269	1.35	-0.022
1274	-13.403	8.39	17.278	1.35	-0.022
1274	-13.394	8.39	18.338	1.52	-0.010
1274	-13.395	8.39	18.348	1.52	-0.009
L4503	-12.311	9.47	18.879	1.66	0.005
L4503	-12.305	9.47	18.902	1.67	0.000

Table 15 continued

Star (HD)	Instrumental Magnitude	Catalogue Magnitude	Universal Time (start)	Airmass	Residual (catalogue - reduced)
L3501	-13.135	8.62	19.026	1.69	-0.019
L3501	-13.138	8.62	19.034	1.70	-0.014
L2426	-13.251	8.54	19.052	1.70	0.019
L2426	-13.238	8.54	19.060	1.70	0.006
L4503	-12.294	9.47	19.176	1.72	-0.006
L4503	-12.298	9.47	19.192	1.72	-0.001
15911	-12.315	9.48	19.224	1.22	-0.013
15911	-12.301	9.48	19.233	1.22	-0.027
1274*	-13.043	8.39	19.454	1.79	-0.331
1274*	-13.248	8.39	19.463	1.80	-0.125
		The J Standards			
193727	-12.716	8.99	8.884	1.12	-0.043
193727	-12.732	8.99	8.895	1.12	-0.027
194107	-12.918	8.79	8.926	1.09	-0.046
194107	-12.925	8.79	8.936	1.09	-0.040
1274	-12.806	8.80	9.130	1.87	0.000
1274	-12.792	8.80	9.138	1.86	-0.016
1274	-12.818	8.80	9.924	1.64	-0.019
1274	-12.823	8.80	9.932	1.63	-0.016
1274	-12.852	8.80	10.436	1.52	0.000
1274	-12.860	8.80	10.444	1.52	0.009
L3501	-12.080	9.59	11.138	1.51	0.026
L3501	-12.096	9.59	11.147	1.51	0.042
1274	-12.905	8.80	11.748	1.33	0.038
1274	-12.932	8.80	11.757	1.32	0.062
L3501	-12.090	9.59	11.868	1.43	0.031
L3501	-12.057	9.59	11.876	1.43	-0.001
1274	-12.887	8.80	12.460	1.26	0.017
1274	-12.885	8.80	12.472	1.26	0.015
L3501	-12.063	9.59	12.609	1.38	0.006
L3501	-12.040	9.59	12.618	1.38	-0.017
L4503	-11.346	10.27	12.652	1.37	-0.031
L4503	-11.351	10.27	12.661	1.37	-0.025
L1510	-11.963	9.75	12.789	1.37	0.064
L1510	-11.939	9.75	12.799	1.37	0.040
L2426	-12.139	9.52	12.826	1.37	0.014
15911	-12.097	9.47	12.997	1.40	-0.068
15911	-12.111	9.47	13.016	1.40	-0.054
202964	-13.030	8.65	13.092	1.07	-0.016
202964	-13.059	8.65	13.102	1.07	0.014
1274	-12.886	8.80	14.297	1.19	0.030
1274	-12.866	8.80	14.320	1.19	0.012
L3501	-12.046	9.59	14.382	1.32	0.005
L3501	-12.068	9.59	14.391	1.32	0.027
1274	-12.857	8.80	14.931	1.19	0.011

Table 15 continued

Star (HD)	Instrumental Magnitude	Catalogue Magnitude	Universal Time (start)	Airmass	Residual (catalogue - reduced)
1274	-12.885	8.80	14.940	1.19	0.040
1274	-12.854	8.80	15.479	1.21	0.020
1274	-12.855	8.80	15.488	1.21	0.022
1274	-12.792	8.80	16.152	1.24	-0.026
1274	-12.798	8.80	16.161	1.25	-0.018
1274	-12.769	8.80	17.303	1.35	-0.012
1274	-12.770	8.80	17.312	1.36	-0.008
1274*	-12.009	8.80	18.320	1.51	-0.727
1274	-12.757	8.80	18.329	1.52	0.023
L4503	-11.238	10.27	18.928	1.67	0.011
L4503	-11.206	10.27	18.936	1.67	-0.020
L3501	-11.913	9.59	18.985	1.69	0.009
L3501	-11.899	9.59	19.003	1.69	-0.004
L2426	-12.005	9.52	19.086	1.70	0.036
L2426	-12.009	9.52	19.094	1.71	0.042
L4503	-11.175	10.27	19.145	1.71	-0.041
L4503	-11.242	10.27	19.153	1.71	0.027
15911	-12.072	9.47	19.257	1.22	-0.033
15911	-12.069	9.47	19.264	1.22	-0.036
1274	-12.618	8.80	19.486	1.80	-0.046
1274	-12.612	8.80	19.494	1.81	-0.050

Table 16: Summary of the extinction and time coefficients and the zero-points derived from the standard stars.

Time range	Filter	Extinction coefficient ε	time coefficient b	Zero-point
		19/20 September 1991		
UT<1400h	J	0.153	-	21.828
	K'	0.083	0.0061	21.863
UT>1630h	J	0.055	0.0155	21.377
	K'	0.035	0.0056	21.755
		20/21 September 1991		
	J	0.186	-0.0150	22.091
	K'	0.084	-0.0071	22.047

Figure 5: Residuals against airmass and Universal Time for the nights of 19/20 & 20/21 September 1991. Respectively 19/20 September K' (a and b) & J (c and d), and 20/21 September K' (e and f) & J (g and h).

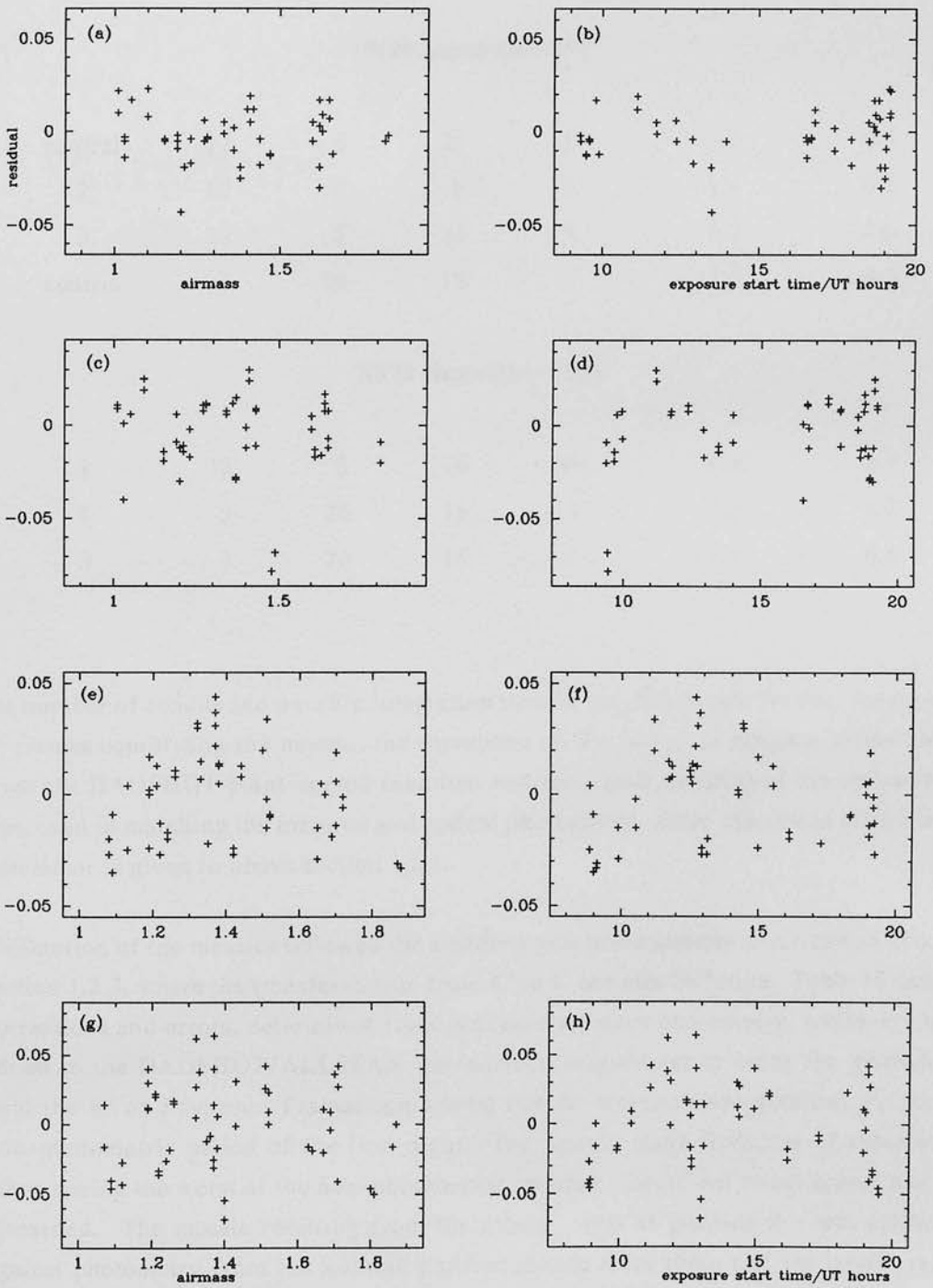

Table 17: Details of the September 1991 47 Tuc observations. The optical pixel scale used by Hesser *et al.* is ~0.58 arcseconds pixel^{-1}.

Position	N_{coadds}	t_{int}/s	N_{final}	Filter	Seeing (FWHM/ arcseconds)	cutoff/ optical pixels
			19/20 September 1991			
central	12	5	23	K'	1.0	0.5
2	12	5	8	K'	1.1	0.6
3	12	5	16	K'	1.2	0.6
central	3	20	16	J	1.1	0.5
			20/21 September 1991			
1	12	5	16	K'	0.9	0.7
1	3	20	16	J	1.0	0.7
3	3	20	16	J	0.9	0.6

the number of coadds and on-chip integration time of the component frames, the number of frames comprising the mosaic, the waveband of the filter, an estimate of the seeing from the DAOPHOT point-spread function, and the cutoff, in units of the optical pixel size, used in matching the infrared and optical photometry. More discussion of this latter parameter is given in above section 1.2.1.

Calibration of the mosaics followed the standard procedure already described in detail in section 1.2.3, where the transformation from K' to K can also be found. Table 18 lists the corrections and errors, determined from synthetic aperture photometry, which are to be added to the DAOPHOT/ALLSTAR instrumental magnitudes to bring the photometry onto the K' or J system. Frames comprising two K' mosaics were obtained during the non-photometric period of the first night. The mosaic made from one of these sets - taken during the worst of the non-photometric weather - could not be calibrated and was discarded. The mosaic resulting from the others - that at position 2 - was calibrated against photometry from the 'central' position mosaic since these had the largest region of overlap.

Figure 6 shows the agreement between the photometry in the overlapping regions.

Figure 6: The agreement between (a) the K', and (b) the J photometry in the overlapping portions of 47 Tuc field 1 central position and positions 1 & 3.

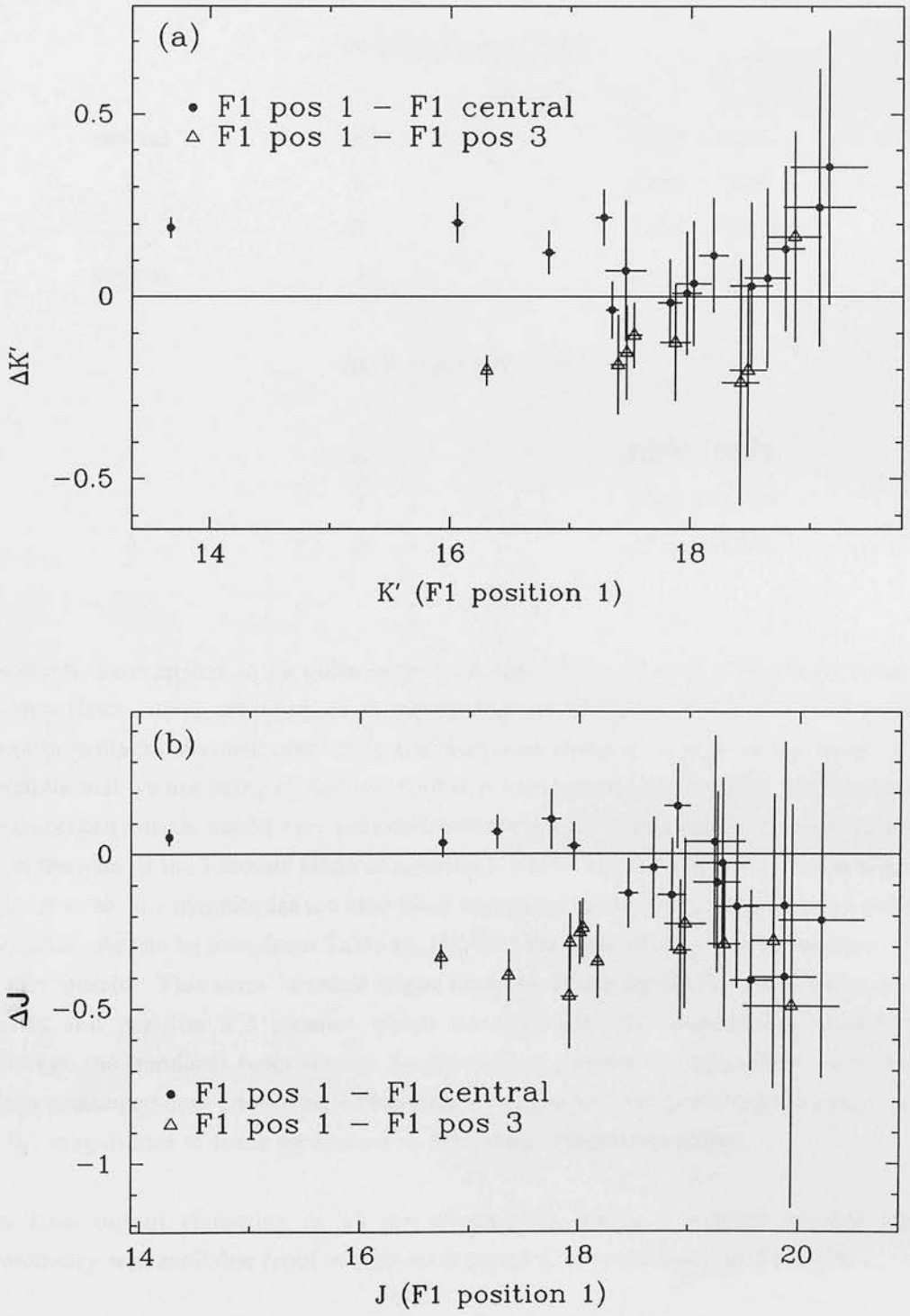

Table 18: Corrections to be added to the DAOPHOT instrumental magnitudes to produce AAO K' or J magnitudes.

Field	Filter	Correction to the DAOPHOT instrumental magnitudes
	19/20 September 1991	
central	K'	-3.228 ± 0.032
2	K'	-2.868 ± 0.008
3	K'	-3.280 ± 0.010
central	J	-3.414 ± 0.055
	20/21 September 1991	
1	K'	-2.974 ± 0.013
1	J	-3.505 ± 0.109
3	J	-3.532 ± 0.006

Although there appear to be quite large systematic offsets in the photometry from the various fields, none are seen when examining the V, (V-K') and V, (V-J) colour-magnitude diagrams constructed from the individual mosaics, except for J position 1. We conclude that we are being misled by small number statistics in figure 6. Unfortunately, the discarded mosaic would have provided more overlap if it had been possible to calibrate it. In the case of the J mosaic taken at position 1, the V, (V-J) colour-magnitude diagram appears to be ~0.1 magnitudes too blue when compared to the central position and position 3 mosaics. As can be seen from Table 18, this is at the limit of the error on the zero-point of this mosaic. This error is much larger than the errors set on the zero-points of the central and position 3 J mosaics which are 0.06 and 0.01 magnitudes respectively. Although the standards from around the time of the position 1 mosaic show no evidence of any prolonged non-photometric behaviour, we have arbitrarily shifted the J zero-point by 0.1 magnitudes to force agreement in the colour-magnitude planes.

The final output consisting of all the photometry, taking a straight average where photometry was available from two or more mosaics, is reproduced in Table 19.

Table 19: The field F1 photometry.

Number	Optical ID	B	V	J	K'	σ_J	$\sigma_{K'}$
1	10049	18.983	18.409	17.566	-	0.055	-
2	-	-	-	17.903	-	0.070	-
3	10124	20.654	19.859	18.475	-	0.128	-
4	-	-	-	18.583	-	0.130	-
5	10156	21.345	20.428	18.644	-	0.099	-
6	-	-	-	18.784	-	0.098	-
7	-	-	-	18.943	-	0.157	-
8	10303	23.110	21.820	18.960	-	0.250	-
9	10233	22.382	21.252	19.009	-	0.150	-
10	-	-	-	19.048	-	0.135	-
11	10220	22.229	21.149	19.048	-	0.122	-
12	10221	22.249	21.157	19.055	-	0.166	-
13	-	-	-	19.271	-	0.219	-
14	-	-	-	19.311	-	0.169	-
15	10294	23.063	21.768	19.342	-	0.146	-
16	10261	22.430	21.507	19.419	-	0.218	-
17	10329	23.283	21.981	19.431	-	0.181	-
18	-	-	-	19.438	-	0.406	-
19	10252	22.648	21.422	19.441	-	0.168	-
20	-	-	-	19.499	-	0.203	-
21	-	-	-	19.551	-	0.197	-
22	-	-	-	19.570	-	0.309	-
23	-	-	-	19.581	-	0.239	-
24	10421	23.886	22.397	19.606	-	0.195	-
25	-	-	-	19.677	-	0.285	-
26	10326	23.333	21.968	19.684	-	0.209	-
27	10497	23.903	22.650	19.685	-	0.231	-
28	10340	23.345	22.063	19.703	-	0.179	-
29	-	-	-	19.722	-	0.326	-
30	10229	21.429	21.197	19.736	-	0.174	-
31	10575	24.444	22.896	19.739	-	0.187	-
32	-	-	-	19.796	-	0.307	-
33	10492	23.844	22.638	19.802	-	0.246	-
34	10207	21.771	21.070	19.822	-	0.147	-
35	-	-	-	19.827	-	0.307	-
36	-	-	-	19.846	-	0.364	-
37	10358	23.514	22.157	19.863	-	0.449	-
38	10210	21.843	21.099	19.881	-	0.240	-
39	10364	23.453	22.184	19.881	-	0.416	-
40	10641	24.550	23.072	19.884	-	0.220	-
41	-	-	-	19.889	-	0.263	-
42	10536	24.210	22.796	19.895	-	0.354	-
43	-	-	-	19.957	-	0.283	-
44	-	-	-	19.962	-	0.238	-
45	10475	23.758	22.607	19.977	-	0.389	-
46	-	-	-	19.986	-	0.377	-
47	10647	24.561	23.096	20.000	-	0.318	-
48	10562	24.253	22.865	20.008	-	0.332	-
49	10481	24.212	22.618	20.023	-	0.270	-
50	-	-	-	20.046	-	0.297	-

Table 19 continued

Number	Optical ID	B	V	J	K'	σ_J	$\sigma_{K'}$
51	-	-	-	20.058	-	0.495	-
52	10489	23.966	22.635	20.058	-	0.299	-
53	10527	24.254	22.769	20.062	-	0.432	-
54	-	-	-	20.063	-	0.302	-
55	10694	24.711	23.213	20.071	-	0.336	-
56	-	-	-	20.074	-	0.583	-
57	10610	24.474	22.988	20.111	-	0.427	-
58	-	-	-	20.114	-	0.352	-
59	-	-	-	20.115	-	0.257	-
60	10758	25.004	23.401	20.118	-	0.312	-
61	-	-	-	20.120	-	0.377	-
62	10455	23.999	22.549	20.136	-	0.292	-
63	10292	22.615	21.739	20.144	-	0.414	-
64	10816	25.491	23.555	20.151	-	0.272	-
65	-	-	-	20.159	-	0.338	-
66	10603	24.595	22.972	20.163	-	0.261	-
67	-	-	-	20.173	-	0.266	-
68	10711	24.650	23.259	20.192	-	0.309	-
69	-	-	-	20.204	-	0.337	-
70	10609	24.580	22.987	20.204	-	0.454	-
71	10275	22.244	21.612	20.217	-	0.302	-
72	10231	21.677	21.210	20.219	-	0.415	-
73	-	-	-	20.229	-	0.297	-
74	10322	22.528	21.944	20.232	-	0.325	-
75	10507	24.425	22.678	20.232	-	0.327	-
76	-	-	-	20.235	-	0.435	-
77	10561	24.290	22.857	20.256	-	0.315	-
78	-	-	-	20.276	-	0.466	-
79	-	-	-	20.282	-	0.498	-
80	-	-	-	20.283	-	0.485	-
81	10256	22.120	21.447	20.288	-	0.476	-
82	-	-	-	20.302	-	0.385	-
83	-	-	-	20.307	-	0.379	-
84	-	-	-	20.310	-	0.478	-
85	-	-	-	20.343	-	0.701	-
86	10780	24.764	23.470	20.363	-	0.255	-
87	-	-	-	20.365	-	0.333	-
88	-	-	-	20.370	-	0.338	-
89	-	-	-	20.376	-	0.420	-
90	10267	22.413	21.536	20.386	-	0.467	-
91	10263	21.990	21.515	20.396	-	0.399	-
92	-	-	-	20.397	-	0.319	-
93	-	-	-	20.403	-	0.370	-
94	10726	24.954	23.305	20.424	-	0.489	-
95	-	-	-	20.439	-	0.340	-
96	-	-	-	20.448	-	0.329	-
97	10618	23.868	23.009	20.460	-	0.450	-
98	10807	25.013	23.528	20.482	-	0.408	-
99	-	-	-	20.497	-	0.828	-
100	-	-	-	20.513	-	0.590	-

Table 19 continued

Number	Optical ID	B	V	J	K'	σ_J	$\sigma_{K'}$
101	10829	24.780	23.595	20.519	-	0.519	-
102	11132	25.750	24.504	20.540	-	0.412	-
103	-	-	-	20.544	-	0.619	-
104	10276	22.261	21.613	20.557	-	0.450	-
105	-	-	-	20.558	-	0.460	-
106	10362	22.496	22.181	20.558	-	0.476	-
107	-	-	-	20.562	-	0.527	-
108	-	-	-	20.584	-	0.492	-
109	-	-	-	20.613	-	0.453	-
110	-	-	-	20.627	-	0.562	-
111	-	-	-	20.643	-	0.626	-
112	-	-	-	20.662	-	0.429	-
113	-	-	-	20.711	-	0.578	-
114	-	-	-	20.715	-	0.555	-
115	-	-	-	20.737	-	0.785	-
116	-	-	-	20.741	-	0.602	-
117	-	-	-	20.747	-	0.705	-
118	10837	24.977	23.618	20.748	-	0.710	-
119	-	-	-	20.750	-	0.635	-
120	-	-	-	20.751	-	0.502	-
121	11073	24.996	24.291	20.764	-	0.602	-
122	-	-	-	20.766	-	0.775	-
123	-	-	-	20.775	-	0.584	-
124	-	-	-	20.777	-	0.914	-
125	-	-	-	20.786	-	0.623	-
126	-	-	-	20.788	-	0.722	-
127	-	-	-	20.789	-	0.519	-
128	-	-	-	20.803	-	0.607	-
129	-	-	-	20.808	-	0.454	-
130	-	-	-	20.838	-	0.468	-
131	-	-	-	20.839	-	0.799	-
132	-	-	-	20.841	-	0.690	-
133	-	-	-	20.846	-	0.562	-
134	-	-	-	20.856	-	0.612	-
135	-	-	-	20.867	-	0.930	-
136	10442	22.799	22.481	20.871	-	0.500	-
137	-	-	-	20.880	-	1.239	-
138	-	-	-	20.899	-	0.746	-
139	10776	24.980	23.458	20.929	-	0.608	-
140	-	-	-	20.960	-	0.931	-
141	-	-	-	20.962	-	0.831	-
142	-	-	-	20.967	-	0.679	-
143	-	-	-	20.967	-	0.925	-
144	-	-	-	20.975	-	0.779	-
145	-	-	-	20.995	-	0.808	-
146	-	-	-	21.061	-	1.051	-
147	-	-	-	21.080	-	0.882	-
148	-	-	-	21.117	-	0.849	-
149	-	-	-	21.142	-	0.967	-
150	-	-	-	21.146	-	1.142	-

Table 19 continued

Number	Optical ID	B	V	J	K'	σ_J	$\sigma_{K'}$
151	–	–	–	21.148	–	0.840	–
152	–	–	–	21.182	–	1.131	–
153	–	–	–	21.210	–	1.097	–
154	–	–	–	21.231	–	0.884	–
155	–	–	–	21.241	–	1.359	–
156	–	–	–	21.312	–	0.903	–
157	–	–	–	21.322	–	1.733	–
158	–	–	–	21.328	–	1.107	–
159	–	–	–	21.329	–	0.928	–
160	–	–	–	21.369	–	1.315	–
161	–	–	–	21.376	–	0.880	–
162	–	–	–	21.409	–	1.647	–
163	–	–	–	21.422	–	1.032	–
164	–	–	–	21.442	–	1.434	–
165	–	–	–	21.472	–	1.389	–
166	–	–	–	21.476	–	1.346	–
167	–	–	–	21.512	–	1.160	–
168	–	–	–	21.524	–	1.159	–
169	–	–	–	21.563	–	1.109	–
170	–	–	–	21.624	–	1.653	–
171	–	–	–	21.677	–	1.206	–
172	–	–	–	21.853	–	1.540	–
173	–	–	–	22.080	–	2.418	–
174	10001	14.868	14.137	12.910	12.373	0.043	0.029
175	10003	15.936	15.052	13.498	12.796	0.006	0.003
176	10004	16.442	15.651	14.289	13.550	0.014	0.010
177	10005	18.538	17.146	14.839	13.805	0.013	0.013
178	–	–	–	–	14.082	–	0.087
179	10012	18.438	17.264	15.303	14.443	0.014	0.006
180	10006	17.814	17.169	–	15.466	–	0.016
181	10017	18.262	17.481	16.101	15.514	0.013	0.015
182	10009	17.813	17.191	16.124	15.544	0.015	0.019
183	–	–	–	–	15.564	–	0.046
184	10008	17.779	17.186	16.184	15.652	0.020	0.015
185	10013	17.879	17.322	16.352	15.788	0.014	0.018
186	10051	19.418	18.424	16.785	15.925	0.023	0.021
187	10015	17.958	17.404	16.480	15.978	0.021	0.018
188	10079	20.297	19.209	16.960	15.981	0.045	0.022
189	10069	19.874	18.821	16.856	16.020	0.022	0.018
190	10020	18.095	17.560	16.617	16.055	0.020	0.019
191	10019	18.085	17.541	16.630	16.166	0.034	0.023
192	10024	18.301	17.764	16.842	16.304	0.026	0.017
193	10159	21.982	20.465	17.176	16.311	0.025	0.027
194	10021	18.221	17.678	16.996	16.358	0.031	0.030
195	10023	18.282	17.743	16.959	16.409	0.020	0.021
196	10032	18.484	17.931	16.975	16.435	0.021	0.027
197	10028	18.431	17.878	16.943	16.464	0.027	0.024
198	10029	18.447	17.888	16.939	16.481	0.019	0.027
199	10030	18.465	17.902	17.046	16.503	0.047	0.039
200	10033	18.419	17.933	17.042	16.527	0.034	0.026

Table 19 continued

Number	Optical ID	B	V	J	K'	σ_J	$\sigma_{K'}$
201	10061	19.509	18.699	17.204	16.558	0.017	0.035
202	-	-	-	18.405	16.628	0.142	0.075
203	10041	18.799	18.225	17.227	16.699	0.027	0.027
204	10037	18.677	18.137	17.267	16.722	0.028	0.022
205	10121	21.028	19.826	17.579	16.727	0.047	0.043
206	10042	18.859	18.270	17.277	16.790	0.030	0.025
207	10057	19.157	18.561	17.709	16.834	0.037	0.086
208	10045	18.970	18.377	17.377	16.841	0.026	0.034
209	10054	19.072	18.470	17.606	16.879	0.042	0.039
210	10071	19.795	18.967	17.531	16.908	0.032	0.037
211	10058	19.210	18.596	17.557	16.925	0.045	0.032
212	-	-	-	17.736	16.934	0.102	0.068
213	10135	21.332	20.102	17.795	16.952	0.045	0.036
214	10053	19.018	18.438	17.417	16.961	0.025	0.037
215	10271	22.727	21.583	18.494	16.978	0.083	0.043
216	10056	19.077	18.483	17.460	16.980	0.027	0.031
217	10066	19.451	18.792	17.631	17.023	0.027	0.042
218	10065	19.406	18.778	17.657	17.103	0.039	0.055
219	10055	19.065	18.471	17.794	17.122	0.074	0.071
220	10513	24.583	22.699	18.865	17.153	0.096	0.040
221	10067	19.448	18.796	17.741	17.160	0.048	0.030
222	10062	19.331	18.703	17.641	17.162	0.031	0.044
223	-	-	-	18.197	17.211	0.085	0.078
224	10286	23.233	21.710	18.003	17.217	0.039	0.040
225	10260	22.909	21.505	18.151	17.272	0.063	0.045
226	10060	19.204	18.618	17.666	17.291	0.045	0.036
227	10697	25.355	23.225	19.146	17.337	0.166	0.098
228	10105	20.303	19.529	18.104	17.355	0.082	0.084
229	10086	20.114	19.373	17.951	17.356	0.036	0.045
230	10075	19.784	19.094	17.990	17.368	0.040	0.034
231	10074	19.738	19.044	17.929	17.372	0.066	0.073
232	-	-	-	19.262	17.388	0.173	0.052
233	10081	19.979	19.291	18.257	17.424	0.101	0.096
234	10100	20.256	19.491	18.175	17.450	0.080	0.077
235	-	-	-	-	17.460	-	0.133
236	10089	20.103	19.404	18.074	17.467	0.041	0.079
237	10093	20.178	19.436	18.140	17.472	0.084	0.047
238	10087	20.113	19.378	18.188	17.491	0.051	0.068
239	10088	20.119	19.396	18.159	17.495	0.046	0.048
240	10084	20.053	19.355	18.041	17.524	0.052	0.055
241	10107	20.317	19.534	18.170	17.545	0.044	0.056
242	10284	23.208	21.700	18.970	17.545	0.122	0.062
243	10085	20.073	19.363	18.114	17.548	0.046	0.064
244	10103	20.271	19.515	18.242	17.559	0.073	0.062
245	10108	20.320	19.570	18.267	17.566	0.063	0.074
246	10106	20.283	19.532	18.163	17.572	0.045	0.056
247	10082	20.058	19.323	18.074	17.575	0.039	0.082
248	10091	20.189	19.422	18.206	17.586	0.048	0.045
249	10109	20.330	19.573	18.277	17.598	0.057	0.085
250	-	-	-	19.506	17.598	0.177	0.069

Table 19 continued

Number	Optical ID	B	V	J	K'	σ_J	$\sigma_{K'}$
251	10115	20.458	19.673	18.308	17.599	0.059	0.046
252	10097	20.131	19.461	-	17.602	-	0.091
253	10113	20.417	19.648	18.397	17.635	0.059	0.080
254	10094	20.182	19.442	-	17.677	-	0.102
255	10112	20.446	19.644	18.282	17.677	0.050	0.061
256	10116	20.451	19.673	18.310	17.701	0.052	0.059
257	10139	21.016	20.143	18.564	17.796	0.056	0.047
258	-	-	-	19.819	17.831	0.350	0.071
259	10257	22.429	21.471	19.084	17.832	0.173	0.091
260	10133	20.911	20.060	18.568	17.836	0.070	0.066
261	10142	21.058	20.175	18.553	17.838	0.105	0.097
262	10167	21.538	20.557	18.686	17.839	0.095	0.067
263	10157	21.423	20.432	18.505	17.859	0.076	0.089
264	10154	21.319	20.392	18.761	17.863	0.095	0.090
265	10114	20.386	19.650	18.530	17.870	0.085	0.092
266	10148	21.234	20.316	18.685	17.880	0.079	0.073
267	10176	21.680	20.669	18.913	17.881	0.121	0.077
268	10155	21.328	20.414	18.758	17.897	0.095	0.094
269	10141	21.014	20.151	18.600	17.916	0.090	0.070
270	10145	21.085	20.197	18.517	17.917	0.061	0.074
271	10125	20.690	19.871	18.587	17.920	0.109	0.100
272	10181	21.703	20.732	18.961	17.922	0.091	0.069
273	10127	20.706	19.893	18.478	17.923	0.068	0.098
274	10138	21.031	20.137	18.445	17.934	0.059	0.077
275	10169	21.045	20.598	19.130	17.938	0.138	0.079
276	-	-	-	-	17.956	-	0.122
277	10122	20.641	19.831	18.487	17.971	0.062	0.082
278	10136	20.976	20.116	18.628	17.974	0.084	0.086
279	-	-	-	18.840	17.977	0.100	0.085
280	10153	21.311	20.389	18.725	17.990	0.097	0.100
281	10198	22.102	20.992	19.003	18.003	0.110	0.067
282	10150	21.308	20.367	18.751	18.008	0.082	0.085
283	10149	21.263	20.330	18.631	18.009	0.063	0.078
284	10208	22.097	21.085	-	18.023	-	0.166
285	10178	21.652	20.678	18.741	18.040	0.113	0.102
286	10144	20.996	20.186	18.738	18.055	0.100	0.075
287	10132	20.869	20.031	18.866	18.055	0.069	0.061
288	10162	21.453	20.501	18.726	18.062	0.088	0.109
289	-	-	-	-	18.071	-	0.158
290	10219	22.201	21.147	18.863	18.117	0.120	0.116
291	-	-	-	19.153	18.128	0.135	0.103
292	10170	21.586	20.604	18.924	18.133	0.126	0.064
293	-	-	-	-	18.135	-	0.127
294	10175	21.637	20.666	18.871	18.144	0.090	0.083
295	10171	21.598	20.621	18.773	18.155	0.085	0.114
296	10251	22.528	21.410	19.169	18.155	0.113	0.076
297	10212	22.212	21.104	19.038	18.186	0.113	0.077
298	10255	22.525	21.429	19.041	18.190	0.116	0.119
299	10220	22.229	21.149	-	18.201	-	0.095
300	10303	23.110	21.820	-	18.241	-	0.250

Table 19 continued

Number	Optical ID	B	V	J	K'	σ_J	$\sigma_{K'}$
301	10184	21.791	20.768	18.867	18.244	0.146	0.135
302	10193	21.926	20.888	19.009	18.256	0.141	0.112
303	10239	22.454	21.295	19.263	18.269	0.191	0.096
304	10249	22.502	21.369	19.403	18.277	0.238	0.128
305	-	-	-	-	18.279	-	0.219
306	10200	22.062	21.008	18.999	18.280	0.197	0.137
307	10242	22.518	21.322	19.545	18.293	0.186	0.158
308	10278	22.879	21.649	19.518	18.313	0.134	0.103
309	10177	21.645	20.673	18.965	18.332	0.087	0.117
310	10110	20.135	19.634	18.914	18.344	0.103	0.102
311	10187	21.789	20.809	18.932	18.344	0.105	0.085
312	10607	24.669	22.979	19.264	18.346	0.140	0.128
313	-	-	-	-	18.353	-	0.274
314	10227	22.282	21.192	19.173	18.358	0.114	0.128
315	10409	23.698	22.355	19.759	18.361	0.431	0.279
316	10209	22.201	21.098	19.015	18.362	0.097	0.116
317	10214	22.199	21.114	19.109	18.362	0.105	0.122
318	10225	22.291	21.185	19.412	18.364	0.204	0.146
319	-	-	-	-	18.368	-	0.104
320	10270	22.769	21.580	19.435	18.406	0.220	0.126
321	10264	22.690	21.517	19.227	18.418	0.208	0.099
322	10258	22.660	21.479	19.353	18.482	0.147	0.096
323	10375	23.640	22.220	19.656	18.507	0.222	0.151
324	10304	23.106	21.823	19.548	18.512	0.162	0.114
325	10253	22.589	21.426	19.340	18.523	0.220	0.192
326	10152	21.132	20.381	19.129	18.536	0.114	0.169
327	10311	23.141	21.871	19.571	18.556	0.186	0.210
328	10168	21.314	20.581	19.315	18.558	0.177	0.140
329	10261	22.430	21.507	-	18.580	-	0.119
330	-	-	-	-	18.583	-	0.152
331	-	-	-	-	18.587	-	0.185
332	10294	23.063	21.768	-	18.642	-	0.168
333	-	-	-	19.370	18.677	0.138	0.102
334	-	-	-	-	18.690	-	0.191
335	-	-	-	-	18.691	-	0.200
336	10344	23.355	22.071	19.720	18.699	0.263	0.169
337	-	-	-	-	18.710	-	0.245
338	10317	23.420	21.920	19.572	18.710	0.133	0.201
339	10300	23.039	21.811	19.788	18.714	0.287	0.123
340	10240	22.461	21.295	19.524	18.715	0.172	0.160
341	10359	23.436	22.163	19.682	18.719	0.206	0.136
342	-	-	-	-	18.723	-	0.113
343	10439	23.841	22.471	19.461	18.749	0.183	0.139
344	10279	22.874	21.665	19.313	18.760	0.240	0.189
345	10350	23.551	22.117	19.593	18.762	0.318	0.179
346	10312	23.269	21.878	-	18.767	-	0.363
347	-	-	-	-	18.776	-	0.269
348	-	-	-	-	18.785	-	0.144
349	-	-	-	-	18.790	-	0.218
350	10348	23.414	22.115	-	18.795	-	0.219

Table 19 continued

Number	Optical ID	B	V	J	K'	σ_J	$\sigma_{K'}$
351	-	-	-	-	18.805	-	0.216
352	-	-	-	-	18.807	-	0.149
353	-	-	-	-	18.818	-	0.236
354	10495	24.231	22.647	20.180	18.818	0.310	0.191
355	10387	23.625	22.281	20.050	18.823	0.253	0.171
356	10364	23.453	22.184	-	18.828	-	0.301
357	10164	21.289	20.530	19.179	18.840	0.153	0.158
358	10532	23.927	22.773	19.656	18.841	0.183	0.160
359	-	-	-	-	18.856	-	0.224
360	-	-	-	-	18.857	-	0.213
361	10443	23.771	22.486	19.775	18.882	0.180	0.152
362	10335	23.352	22.039	19.523	18.890	0.170	0.196
363	-	-	-	-	18.892	-	0.277
364	10197	21.710	20.990	19.805	18.896	0.241	0.191
365	-	-	-	-	18.913	-	0.130
366	-	-	-	-	18.915	-	0.174
367	-	-	-	20.120	18.916	0.216	0.153
368	10417	23.752	22.375	20.003	18.922	0.266	0.149
369	-	-	-	19.678	18.949	0.224	0.247
370	10341	22.442	22.068	-	18.950	-	0.177
371	10636	24.620	23.052	-	18.954	-	0.179
372	10396	23.561	22.311	19.599	18.955	0.214	0.179
373	10739	24.720	23.355	-	18.959	-	0.207
374	10505	23.990	22.672	19.871	18.967	0.227	0.267
375	10399	23.779	22.333	19.757	18.975	0.188	0.275
376	10412	23.752	22.366	19.618	18.987	0.186	0.183
377	10654	23.848	23.113	20.282	18.992	0.324	0.241
378	10507	24.425	22.678	-	18.993	-	0.295
379	10739	24.720	23.355	20.171	18.999	0.433	0.291
380	-	-	-	-	19.010	-	0.427
381	10589	24.228	22.936	-	19.012	-	0.306
382	-	-	-	-	19.023	-	0.357
383	-	-	-	-	19.032	-	0.267
384	10452	23.881	22.524	19.877	19.042	0.274	0.225
385	-	-	-	-	19.068	-	0.269
386	10488	23.999	22.634	-	19.078	-	0.320
387	-	-	-	-	19.083	-	0.278
388	-	-	-	-	19.085	-	0.289
389	10608	24.318	22.987	20.097	19.097	0.356	0.219
390	10814	24.768	23.554	20.268	19.101	0.548	0.330
391	10520	24.181	22.745	19.806	19.106	0.267	0.172
392	-	-	-	-	19.109	-	0.421
393	10459	23.955	22.555	19.848	19.110	0.180	0.182
394	10561	24.290	22.857	-	19.111	-	0.216
395	-	-	-	-	19.115	-	0.320
396	-	-	-	-	19.122	-	0.482
397	10935	24.373	23.885	-	19.174	-	0.333
398	10605	24.410	22.974	20.007	19.175	0.305	0.336
399	-	-	-	-	19.183	-	0.282
400	-	-	-	-	19.185	-	0.445

Table 19 continued

Number	Optical ID	B	V	J	K'	σ_J	$\sigma_{K'}$
401	-	-	-	-	19.187	-	0.541
402	-	-	-	-	19.224	-	0.380
403	10371	23.670	22.210	19.804	19.231	0.248	0.258
404	-	-	-	-	19.248	-	0.382
405	-	-	-	20.225	19.272	0.407	0.270
406	-	-	-	-	19.296	-	0.275
407	10627	24.456	23.028	-	19.331	-	0.410
408	-	-	-	-	19.337	-	0.277
409	-	-	-	-	19.345	-	0.395
410	-	-	-	-	19.356	-	0.289
411	-	-	-	-	19.362	-	0.492
412	-	-	-	-	19.377	-	0.413
413	-	-	-	-	19.377	-	0.284
414	-	-	-	20.517	19.400	0.474	0.380
415	-	-	-	-	19.412	-	0.294
416	-	-	-	-	19.414	-	0.439
417	-	-	-	-	19.443	-	0.314
418	-	-	-	-	19.456	-	0.326
419	-	-	-	-	19.486	-	0.612
420	-	-	-	-	19.488	-	0.451
421	-	-	-	-	19.494	-	0.373
422	-	-	-	-	19.509	-	0.573
423	-	-	-	-	19.520	-	0.424
424	-	-	-	-	19.540	-	0.450
425	-	-	-	-	19.617	-	0.319
426	-	-	-	-	19.693	-	0.599
427	-	-	-	-	19.720	-	0.443
428	-	-	-	-	19.737	-	0.392
429	-	-	-	-	19.744	-	0.570
430	-	-	-	-	19.744	-	0.432
431	-	-	-	-	19.814	-	0.667
432	-	-	-	-	19.891	-	0.532
433	-	-	-	-	19.952	-	0.883
434	-	-	-	-	20.022	-	0.941
435	-	-	-	-	20.035	-	0.761
436	-	-	-	-	20.076	-	1.234
437	-	-	-	-	20.098	-	0.843
438	-	-	-	-	20.118	-	1.163
439	-	-	-	-	20.161	-	0.878
440	-	-	-	-	20.208	-	1.101
441	-	-	-	-	20.252	-	0.986
442	-	-	-	-	20.272	-	0.983
443	-	-	-	-	20.303	-	1.154
444	-	-	-	-	20.395	-	1.328
445	-	-	-	-	20.400	-	1.033
446	-	-	-	-	20.415	-	1.150
447	-	-	-	-	20.577	-	1.636
448	-	-	-	-	20.580	-	1.035
449	-	-	-	-	20.716	-	1.459
450	-	-	-	-	20.726	-	1.516

Table 19 continued

Number	Optical ID	B	V	J	K'	σ_J	$\sigma_{K'}$
451	-	-	-	-	20.795	-	1.843
452	-	-	-	-	20.861	-	2.624
453	-	-	-	-	20.958	-	1.592

Table 20: Standard star observations from 10/11 June 1990.

Star	Instrumental Magnitude	Zero-point	Airmass	Corrected Zero-point	Residual (catalogue - reduced)
HD105601	-13.477	20.162	1.06	20.226	-0.011
HD105601	-13.473	20.158	1.06	20.222	-0.015
HD105601	-13.493	20.178	1.06	20.242	0.005
HD105601	-13.474	20.159	1.06	20.223	-0.014
HD105601	-13.495	20.180	1.06	20.244	0.007
HD106965	-12.855	20.170	1.06	20.234	-0.003
HD106965	-12.839	20.154	1.06	20.218	-0.019
HD136754	-13.025	20.160	1.01	20.221	-0.016
HD136754	-13.021	20.156	1.00	20.216	-0.021
M13_A4	-6.345	20.190	1.06	20.254	0.017
M13_A4	-6.293	20.138	1.06	20.202	-0.035
HD161903	-13.181	20.201	1.29	20.278	0.041
HD161903	-13.172	20.192	1.30	20.270	0.033
M15_X10	-6.882	20.192	1.02	20.253	0.016
GL811.1	-13.234	20.164	1.25	20.239	0.002
GL811.1	-13.220	20.150	1.25	20.225	-0.012
HD201941	-13.565	20.185	1.10	20.251	0.014
HD201941	-13.558	20.178	1.10	20.244	0.007

Table 21: Standard star observations from 16/17 June 1990.

Star	Instrumental Magnitude	Zero-point	Airmass	Corrected Zero-point	Residual (catalogue - reduced)
HD106965	-12.942	20.257	1.05	20.320	0.040
HD106965	-12.907	20.222	1.05	20.285	0.005
HD136754	-13.099	20.234	1.36	20.316	0.036
HD136754	-13.066	20.201	1.36	20.283	0.003
HD136754	-13.066	20.195	1.17	20.265	-0.015
HD136754	-13.056	20.191	1.17	20.261	-0.019
HD201941	-13.592	20.212	1.26	20.288	0.008
HD201941	-13.564	20.184	1.26	20.260	-0.020
GL811.1	-13.262	20.192	1.34	20.272	-0.008
GL811.1	-13.241	20.171	1.34	20.251	-0.029
GL811.1	-13.245	20.175	1.26	20.251	-0.029
GL811.1	-13.222	20.152	1.26	20.228	-0.052
HD201941	-13.603	20.223	1.11	20.290	0.010
HD201941	-13.568	20.188	1.11	20.255	-0.025
M13_A14	-7.100	20.250	1.33	20.330	0.050
M13_A14	-7.057	20.207	1.33	20.287	0.007
M13_A4	-6.391	20.236	1.05	20.299	0.019
M13_A4	-6.376	20.221	1.05	20.284	0.004
M15_P11	-7.186	20.181	1.03	20.243	-0.037

3 M13 OBSERVATIONS

Observations of stars in M13 were carried out under photometric conditions on the nights of 10/11 and 16/17 June 1990 with the common-user InSb array camera IRCAM [see McLean, 1987, 1989 and McLean *et al.*, 1989], operating in 0.62 arcsecond pixel^{-1} plate scale and mounted at the F35 focal station of the United Kingdom Infrared Telescope.

3.1 Standard Stars

The results of synthetic aperture photometry of the standard star observations, including standards from the (unpublished) UKIRT faint standards list, with eight arcsecond

diameter apertures, are summarised in Tables 20 and 21. The techniques used to process IRCAM standard star observations have been discussed extensively elsewhere (e.g., Dixon, 1992), and are not reproduced here. Since there was insufficient airmass coverage among the standards to determine the extinction coefficient, a typical K band extinction for Mauna Kea of 0.06 magnitudes airmass^{-1} has been assumed. The standard stars were observed at similar airmasses to the M13 observations, so the relative airmass corrections are, in any case, small. Zero-points of 20.237±0.019 and 20.280±0.022 were determined for the nights of 10/11 and 16/17 June respectively.

3.2 Deep M13 observations

We selected for deep study an area at the North-East corner of the Richer & Fahlman (1986) optical CCD study of this cluster, the field centre being located approximately at coordinates (250,360) on figure 1 of that paper. On the two nights we obtained respectively 14 and 27 frames, each consisting of 6 coadds and 45 seconds on-chip integration time, of the field centre and in a spiral jitter pattern around it with offsets of typically ±5 arcseconds in each coordinate.

Two mosaics were constructed employing fractional pixel offsets, one consisting of all 14 frames from the first night and the other of 24 frames from the second night, and photometered using DAOPHOT/ALLSTAR.

The instrumental magnitudes were transformed to the UKIRT photometric system via synthetic aperture photometry on each mosaic after subtraction of all but a few selected bright stars. The results are summarised in Table 22. We also attempted to set the photometric zero-point by applying to the faint photometric standards the same point-spread function that produced the instrumental magnitudes of the M13 stars. There was some mismatch between the point-spread function of the M13 mosaic stars and that of the standards, which are some two magnitudes brighter. This effect manifested itself by leaving residuals after the standards had been subtracted by DAOPHOT/ALLSTAR; the residuals were estimated using synthetic apertures, and the zero-points determined were corrected by this amount. These results are summarised in Table 23. When calculating the final correction to be made to the instrumental magnitudes, the results from fitting the point-spread function to the faint standards were given quarter weight.

Because of the relatively small number of stars involved, matching of our photometry with that of Richer & Fahlman was done by eye and ruler; only stars which appeared on both of our mosaics and in the optical tabulation were considered further. Figure 7 shows, for the stars meeting this criterion, a plot of the difference in K magnitude determined independently from the two nights' photometry against the mean of these values. It is

Table 22: Photometric calibration of the mosaics.

Star	aperture magnitude	DAOPHOT magnitude	Correction to instrumental magnitude
		10/11 Jun 1990	
28	15.53	20.47	-4.94
21	17.39	22.32	-4.93
8	17.61	22.60	-4.99
		16/17 Jun 1990	
28	15.66	20.45	-4.79
16	16.96	21.64	-4.68
21	17.51	22.35	-4.84

Table 23: Photometric calibration of the mosaics from fitting the point-spread functions to the faint standards.

Star	Catalogue magnitude	DAOPHOT magnitude	Residual correction	Corrected DAOPHOT magnitude	Correction to instrumental magnitude
		10/11 Jun 1990			
M13_A4	13.845	18.609	0.25	18.80	-4.96
M13_A4	13.845	18.635	0.21	18.79	-4.95
M15_X10	13.31	18.052	0.11	18.10	-4.79
		16/17 Jun 1990			
M13_A14	13.15	18.130	-0.06	17.99	-4.84
M13_A14	13.15	18.032	0.08	18.03	-4.88
M13_A4	13.845	18.791	0.02	18.75	-4.90
M13_A4	13.845	18.602	0.22	18.76	-4.91

Table 24: M13 photometry.

Star	B	σ_B	V	σ_V	K	σ_K
16	18.633	0.007	18.193	0.007	16.87	0.01
20	18.835	0.007	18.412	0.007	17.14	0.01
21	19.295	0.013	18.855	0.007	17.55	0.02
17	19.359	0.013	18.941	0.007	17.67	0.02
14	20.057	0.017	19.586	0.013	18.21	0.03
24	20.501	0.017	19.954	0.013	18.29	0.06
33	20.402	0.017	19.898	0.013	18.30	0.09
11	20.385	0.017	19.865	0.013	18.39	0.05
19	20.673	0.017	20.096	0.017	18.51	0.06
22	21.162	0.018	20.519	0.017	18.80	0.08
103	21.736	0.018	21.148	0.018	19.05	0.11
26	22.055	0.062	21.988	0.018	19.08	0.14
18	21.580	0.018	20.836	0.017	19.14	0.07
109	22.798	0.062	21.774	0.018	19.19	0.19
23	22.491	0.062	21.602	0.018	19.29	0.13
30	23.311	0.103	22.235	0.062	19.31	0.22
111	22.793	0.062	22.129	0.062	19.48	0.24
201	22.618	0.062	21.718	0.018	19.48	0.10
110	22.759	0.062	21.685	0.018	19.49	0.25
104	23.155	0.103	22.244	0.062	19.53	0.21
106	23.483	0.103	22.327	0.062	19.83	0.13

Figure 7: Differences between the photometry of the nights of 10/11 and 16/17 June 1990.

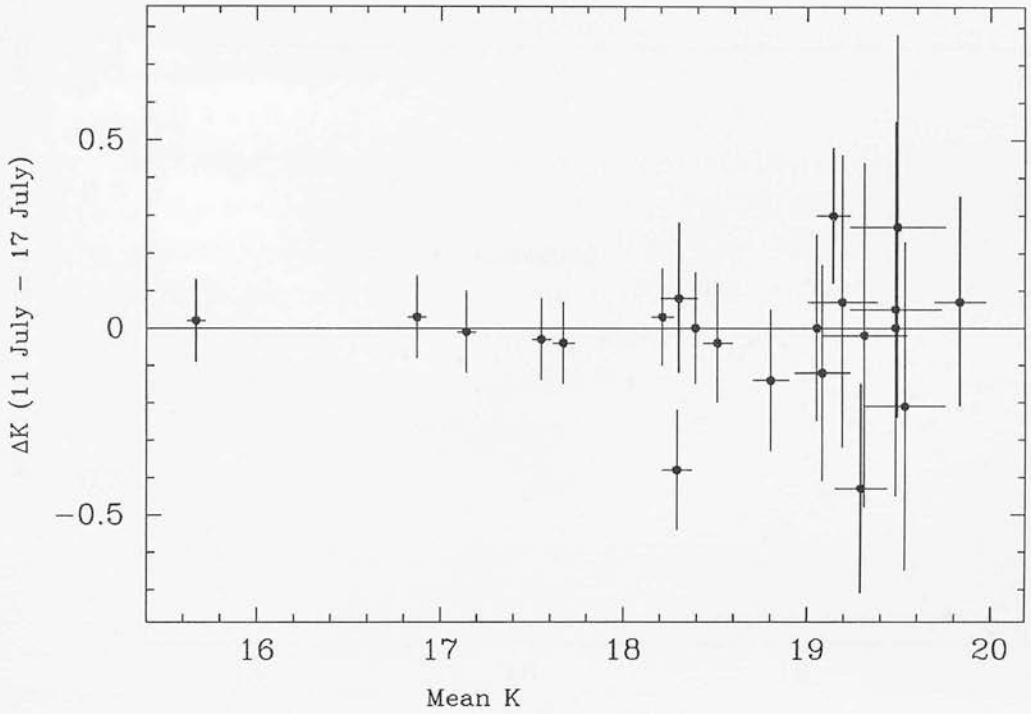

obvious from inspection of this figure that the agreement between the two nights' photometry is satisfactory and that any systematic errors present in the K photometry amount to less than ~0.05 magnitudes. The adopted K value for each star was calculated by taking the mean of the two independently derived values corrected to zero airmass. These K magnitudes, together with the Richer & Fahlman B and V values are presented in Table 24. No correction for foreground extinction has been included in these values.

4 M30 OBSERVATIONS

K(2.2μm) band observations of stars in the globular cluster M30 were made with IRCAM on the same nights, and with the same configuration, as the M13 observations described in the previous section. To be certain of including stars from the horizontal branch to below the main-sequence turn-off, we selected for study a strip one IRCAM frame wide and running North-South in the area with optical photometry by Richer, Fahlman & VandenBerg (1988). On the nights of 10/11 and 16/17 June 1990 we obtained respectively 5 and 33 frames consisting of 6 coadds and 45 seconds on-chip integration time; the latter representing 3 separate passes of the same area, each 11 frames long. Each frame was offset by ~16 arcsecond of declination from the preceding frame; since the Richer *et al.* CCD frames were not oriented exactly North-South, each successive frame was offset by ~4 arcseconds to the West.

Figure 8: The agreement between the M30 K photometry from 10/11 and 16/17 June 1990.

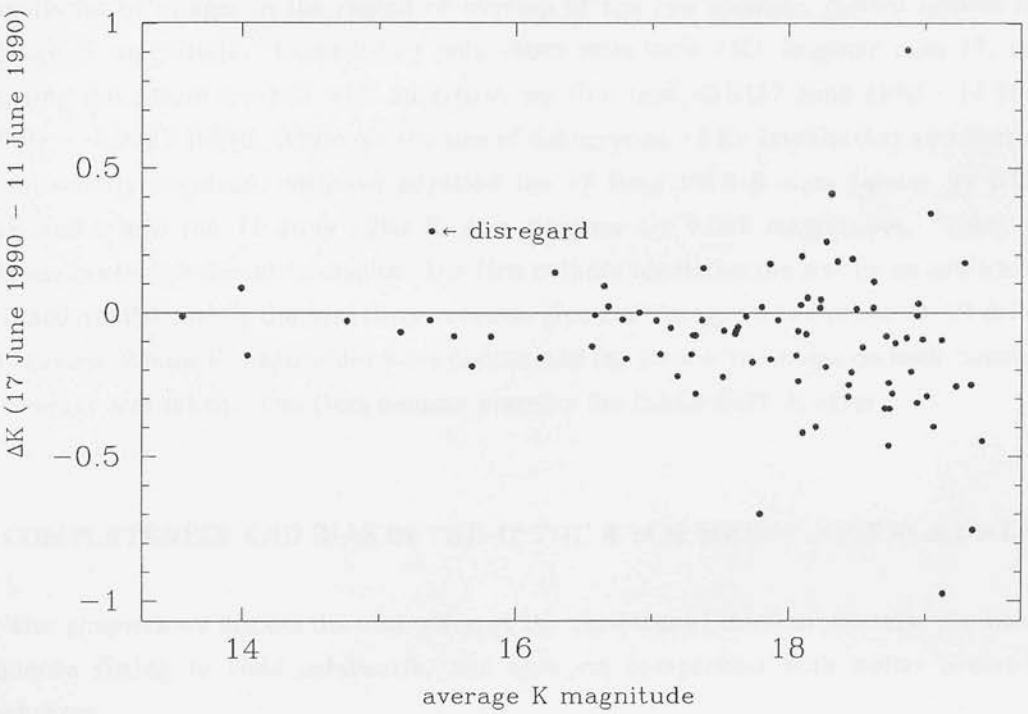

Table 25: Corrections to the M30 instrumental magnitudes.

Date	Correction to the DAOPHOT instrumental magnitudes
10/11 June 1990	-4.871 ± 0.056
16/17 June 1990	-4.652 ± 0.017

4.1 The Standard Stars

The standard star observations were discussed in section 3.1.

4.2 Data Reduction

Two mosaics were constructed, photometered with DAOPHOT/ALLSTAR and calibrated, using procedures described in previous sections. Table 25 presents the corrections,

determined by aperture photometry, which bring the DAOPHOT instrumental magnitudes of the mosaics onto the UKIRT K system. Figure 8 shows the difference between the K magnitudes of images in the region of overlap of the two mosaics, plotted against the average K magnitude. Considering only those stars with <K> brighter than 17, and omitting the datum marked with an arrow, we find that $<\Delta K(17 \text{ June } 1990 - 11 \text{ June } 1990)> = -0.041 \pm 0.090$. Although the size of the error on $<\Delta K>$ implies that a correction is not strictly required, we have adjusted the 17 June 1990 K data fainter by 0.021 magnitudes and the 11 June 1990 K data brighter by 0.020 magnitudes. Table 26 summarises the photometric results. The first column identifies the star by an arbitrarily assigned number, while the next three columns give the V magnitude and the (B-V) & (V-K) colours. Where K magnitudes were determined for stars with images on both mosaics, an average was taken. The final column presents the DAOPHOT K error.

5 COMPLETENESS AND BIAS IN THE 47 TUC & M30 MAIN-SEQUENCE DATA

In later chapters we discuss the derivation of the distances of the four clusters, via main-sequence fitting to field subdwarfs, and ages via comparison with stellar evolution isochrones.

As a prelude, we discuss the results of experiments to determine and quantify the completeness of the main-sequence data, the size of any bias in the magnitudes, and the reliability of the errors, determined by DAOPHOT/ALLSTAR. We used representative mosaics on which the stellar images are crowded [M30 - 16/17 June 1990] and relatively uncrowded [47 Tuc - 19/20 September 1991 K'].

The experiments were performed using ADDSTAR, the facility within DAOPHOT which allows the addition of artificial stars of known magnitudes to an image using the point-spread function constructed when the image was photometered. The new image can then be reduced again, the fraction of artificial stars recovered can be found, and a comparison of their magnitudes and errors made with the input parameters.

In order for the conclusions to be valid also for the data on the original frames, it is necessary not to significantly increase the level of crowding by adding too many artificial stars. Stetson (1987) recommends that the number of artificial stars added should be ~10% of the number of real images.

Table 26: M30 photometry.

Star	V	(B-V)	(V-K)	σ_K	Star	V	(B-V)	(V-K)	σ_K
1	14.832	0.680	2.385	0.018	65	18.712	0.396	1.185	0.049
2	15.056	0.504	1.416	0.025	68	18.759	0.414	1.080	0.095
3	15.269	0.187	0.597	0.009	71	18.795	0.406	1.174	0.101
4	15.393	0.069	0.322	0.011	72	18.800	0.431	1.427	0.077
5	15.475	0.044	0.319	0.013	73	18.818	0.405	1.505	0.103
6	15.640	0.706	2.080	0.004	74	18.822	0.379	1.031	0.110
7	15.701	0.684	2.137	0.012	75	18.842	0.448	1.590	0.115
8	15.729	-0.012	0.181	0.010	76	18.843	0.411	1.208	0.111
9	15.889	-0.056	0.069	0.016	77	18.850	0.385	1.195	0.119
11	16.045	-0.076	-0.140	0.030	78	18.851	0.430	1.372	0.108
12	16.086	0.659	2.048	0.020	79	18.855	0.410	1.238	0.082
13	16.130	0.672	2.139	0.027	80	18.859	0.423	1.324	0.092
14	16.181	0.677	2.030	0.024	81	18.862	0.436	1.062	0.119
15	16.580	0.655	1.958	0.025	82	18.866	0.425	1.319	0.079
16	16.767	0.616	2.004	0.009	84	18.871	0.397	1.242	0.073
17	16.941	0.653	1.909	0.042	86	18.887	0.391	0.786	0.091
19	17.293	0.631	1.921	0.017	87	18.895	0.414	1.173	0.104
20	17.506	0.608	1.826	0.025	88	18.896	0.437	1.282	0.126
21	17.808	0.649	1.901	0.051	90	18.906	0.421	1.298	0.052
22	17.829	0.564	1.762	0.034	92	18.930	0.496	1.195	0.102
23	17.956	0.529	1.603	0.062	95	18.988	0.390	1.651	0.102
24	17.965	0.521	1.678	0.047	98	19.052	0.390	1.548	0.127
27	18.082	0.465	1.499	0.031	99	19.068	0.430	1.550	0.059
28	18.084	0.496	1.432	0.037	100	19.072	0.479	1.089	0.167
29	18.102	0.462	1.522	0.054	101	19.073	0.457	1.137	0.110
30	18.121	0.478	1.441	0.061	103	19.089	0.410	1.397	0.115
32	18.146	0.473	1.497	0.047	104	19.094	0.412	1.230	0.070
33	18.171	0.403	1.610	0.035	105	19.104	0.329	1.416	0.067
36	18.215	0.435	1.403	0.034	107	19.114	0.414	1.193	0.092
37	18.242	0.431	1.420	0.054	108	19.127	0.407	1.312	0.209
39	18.272	0.398	1.280	0.109	109	19.130	0.416	1.327	0.110
43	18.364	0.397	1.456	0.032	110	19.142	0.381	1.406	0.156
44	18.373	0.453	1.588	0.044	111	19.187	0.346	1.319	0.115
45	18.383	0.407	1.352	0.082	112	19.192	0.410	1.940	0.115
46	18.408	0.424	1.376	0.046	115	19.220	0.387	1.106	0.156
47	18.421	0.373	1.359	0.046	116	19.230	0.453	1.588	0.185
48	18.426	0.409	1.240	0.062	117	19.232	0.400	0.963	0.126
50	18.427	0.416	1.308	0.063	118	19.237	0.436	0.764	0.217
52	18.473	0.399	1.295	0.085	120	19.240	0.418	1.317	0.101
53	18.479	0.396	1.103	0.052	121	19.261	0.439	1.267	0.121
54	18.494	0.399	1.278	0.102	122	19.298	0.437	1.482	0.124
56	18.519	0.379	1.381	0.050	125	19.319	0.379	1.353	0.203
57	18.522	0.431	1.469	0.044	126	19.322	1.406	3.958	0.020
58	18.576	0.368	1.256	0.051	128	19.335	0.399	1.364	0.144
59	18.586	0.384	1.395	0.141	130	19.344	0.473	1.206	0.144
60	18.598	0.473	1.295	0.144	133	19.380	0.407	1.312	0.119
61	18.678	0.367	1.378	0.056	134	19.384	0.412	1.486	0.173
62	18.696	0.414	1.378	0.051	135	19.389	0.469	1.109	0.220
63	18.698	0.394	1.408	0.058	136	19.396	0.448	1.517	0.190
64	18.708	0.419	1.342	0.050	137	19.402	0.410	1.292	0.152

Table 26 continued

Star	V	(B-V)	(V-K)	σ_K	Star	V	(B-V)	(V-K)	σ_K
138	19.411	0.435	1.320	0.168	216	19.997	0.497	1.358	0.329
139	19.415	0.452	1.586	0.202	217	20.000	0.527	1.987	0.144
140	19.421	0.464	1.434	0.127	218	20.010	0.530	1.953	0.302
142	19.426	0.430	1.590	0.198	219	20.013	0.471	1.578	0.290
143	19.429	0.429	1.227	0.170	220	20.021	0.444	2.011	0.156
145	19.445	0.472	1.604	0.133	221	20.022	0.462	1.761	0.249
147	19.475	0.604	1.313	0.155	222	20.029	0.656	1.313	0.225
148	19.484	0.380	0.637	0.466	225	20.057	0.486	1.699	0.123
149	19.508	0.434	1.213	0.146	226	20.060	0.515	1.565	0.122
151	19.521	0.444	1.446	0.158	227	20.063	0.455	1.848	0.253
153	19.531	0.359	1.434	0.086	228	20.066	0.515	1.420	0.236
156	19.558	0.424	1.421	0.114	229	20.072	0.593	1.439	0.222
157	19.560	0.434	1.308	0.251	230	20.073	0.442	1.520	0.258
158	19.560	0.446	1.506	0.094	232	20.089	0.422	1.410	0.217
159	19.561	0.444	1.534	0.122	233	20.097	0.407	1.517	0.379
161	19.595	0.491	1.399	0.137	234	20.102	0.484	1.944	0.157
162	19.596	0.477	1.697	0.155	235	20.116	0.502	1.275	0.305
163	19.606	0.487	1.143	0.155	236	20.119	0.586	1.636	0.167
165	19.645	0.466	1.412	0.129	238	20.132	0.595	1.034	0.342
166	19.668	0.437	0.955	0.164	240	20.139	0.543	2.263	0.168
167	19.675	0.539	1.445	0.097	242	20.150	0.555	1.212	0.234
168	19.689	0.453	1.089	0.273	243	20.152	0.512	2.085	0.182
169	19.692	0.371	1.430	0.137	244	20.177	0.539	2.052	0.297
171	19.698	0.487	1.453	0.170	247	20.195	0.540	1.654	0.166
172	19.699	0.503	1.423	0.130	248	20.197	0.487	1.364	0.390
173	19.703	0.503	1.245	0.102	249	20.198	0.566	1.789	0.162
174	19.706	0.412	1.507	0.166	250	20.203	0.565	2.019	0.190
175	19.712	0.409	1.645	0.158	251	20.204	0.494	1.831	0.152
179	19.739	0.472	1.467	0.179	252	20.212	0.505	1.502	0.225
180	19.743	1.549	4.359	0.035	254	20.230	0.543	1.244	0.288
181	19.757	0.447	2.444	0.103	255	20.231	0.554	1.678	0.292
182	19.770	0.466	1.682	0.160	260	20.245	0.504	0.537	0.881
183	19.780	0.449	1.404	0.149	263	20.251	0.530	1.379	0.380
185	19.819	0.477	1.592	0.165	264	20.253	0.502	1.391	0.236
187	19.823	0.466	1.088	0.153	265	20.262	0.552	1.916	0.141
190	19.844	0.503	1.472	0.179	266	20.264	0.539	1.765	0.199
193	19.852	0.561	1.637	0.266	268	20.271	0.547	1.714	0.329
196	19.867	0.496	1.938	0.216	269	20.273	0.536	1.344	0.233
197	19.870	0.474	1.435	0.120	271	20.291	0.570	1.670	0.226
198	19.883	0.477	1.180	0.153	272	20.302	0.518	1.418	0.321
199	19.889	0.552	1.762	0.096	273	20.307	0.567	1.603	0.202
202	19.908	0.459	1.500	0.295	274	20.321	0.509	2.063	0.261
203	19.920	0.537	1.464	0.242	276	20.324	0.505	1.545	0.178
206	19.940	0.492	1.534	0.207	280	20.381	0.442	1.674	0.285
207	19.940	0.481	1.626	0.117	281	20.383	0.539	1.325	0.275
208	19.951	0.382	1.249	0.263	282	20.389	0.536	1.292	0.316
210	19.964	0.514	1.526	0.150	283	20.398	0.640	1.697	0.268
211	19.964	0.494	1.810	0.121	284	20.400	0.521	1.347	0.359
212	19.967	0.468	1.519	0.186	285	20.405	0.580	1.110	0.473
213	19.985	0.468	1.774	0.165	286	20.408	0.789	2.065	0.161

Table 26 continued

Star	V	(B-V)	(V-K)	σ_K	Star	V	(B-V)	(V-K)	σ_K
289	20.421	0.560	1.907	0.173	366	20.751	0.802	2.233	0.159
290	20.423	0.655	1.381	0.356	367	20.762	0.659	1.348	0.475
291	20.432	0.524	0.907	0.619	368	20.763	0.852	2.538	0.174
292	20.432	0.131	2.054	0.271	371	20.778	0.545	1.848	0.306
294	20.441	0.503	1.819	0.162	376	20.796	0.611	1.750	0.280
295	20.442	0.664	2.026	0.192	377	20.820	0.693	2.605	0.253
297	20.446	0.658	1.451	0.427	378	20.822	0.466	2.194	0.374
298	20.463	0.749	1.650	0.323	379	20.823	0.348	3.360	0.119
299	20.469	0.489	1.951	0.159	381	20.827	0.600	1.811	0.255
300	20.471	0.575	1.554	0.440	382	20.831	0.731	1.608	0.251
302	20.481	0.679	1.471	0.269	385	20.847	0.708	2.259	0.266
303	20.492	0.634	1.781	0.384	386	20.849	0.672	1.650	0.327
304	20.503	0.511	1.556	0.223	389	20.859	0.688	1.790	0.565
305	20.517	0.606	1.672	0.353	391	20.865	0.635	1.527	0.382
306	20.528	0.509	1.258	0.495	392	20.867	0.581	2.367	0.235
307	20.530	0.492	1.898	0.228	393	20.869	0.490	1.896	0.516
309	20.536	0.562	1.811	0.238	401	20.897	0.529	2.087	0.302
310	20.540	0.810	2.499	0.130	403	20.923	0.672	1.805	0.405
311	20.541	0.505	1.725	0.249	405	20.925	0.853	2.167	0.201
312	20.544	0.479	0.965	0.571	408	20.952	0.628	1.804	0.310
313	20.549	0.577	1.268	0.399	409	20.959	0.752	1.773	0.304
318	20.567	0.555	1.784	0.308	411	20.960	0.525	2.488	0.221
319	20.568	0.722	1.838	0.162	413	20.971	0.878	2.353	0.126
322	20.571	0.578	2.105	0.127	415	20.981	0.568	1.769	0.516
323	20.578	0.523	1.600	0.299	420	21.015	0.966	2.277	0.229
324	20.578	0.571	1.905	0.257	421	21.017	0.653	2.553	0.287
325	20.582	0.721	1.643	0.283	423	21.030	0.494	2.134	0.365
328	20.595	0.555	1.765	0.420	425	21.045	0.721	2.049	0.501
329	20.610	0.676	1.909	0.268	426	21.047	0.473	2.151	0.292
332	20.620	0.651	1.852	0.389	430	21.061	0.465	3.185	0.168
334	20.632	0.604	2.260	0.222	431	21.063	1.122	4.402	0.045
336	20.636	0.584	1.508	0.265	434	21.081	0.785	2.127	0.301
338	20.644	0.631	1.357	0.400	435	21.083	0.666	1.715	0.462
339	20.646	0.595	1.385	0.570	437	21.096	0.702	2.105	0.232
340	20.656	0.583	1.590	0.472	440	21.102	0.410	1.756	0.330
341	20.657	0.589	1.529	0.349	441	21.103	0.804	2.342	0.294
343	20.662	1.094	1.893	0.232	442	21.103	0.701	1.867	0.322
344	20.665	0.600	1.611	0.334	444	21.116	0.920	2.302	0.312
345	20.665	0.628	1.870	0.249	446	21.141	0.766	2.162	0.211
346	20.666	0.591	2.441	0.174	450	21.156	0.677	1.929	0.503
349	20.677	0.655	1.599	0.484	451	21.158	0.884	1.949	0.431
351	20.688	0.593	1.957	0.157	454	21.166	0.679	2.397	0.388
352	20.688	0.827	1.746	0.337	455	21.168	0.643	2.182	0.397
356	20.702	0.566	2.092	0.188	456	21.173	0.674	2.178	0.247
357	20.709	0.592	2.149	0.244	458	21.194	0.622	2.539	0.240
358	20.722	0.617	1.459	0.784	459	21.195	0.723	2.731	0.316
359	20.724	0.537	1.437	0.413	464	21.221	1.022	3.303	0.179
361	20.731	0.661	1.783	0.320	469	21.246	0.676	1.873	0.425
364	20.738	0.575	1.701	0.247	470	21.252	0.720	3.090	0.155
365	20.748	0.571	2.738	0.156	477	21.275	0.537	1.937	0.397

Table 26 continued

Star	V	(B-V)	(V-K)	σ_K	Star	V	(B-V)	(V-K)	σ_K
481	21.311	0.407	2.965	0.141	559	21.628	0.914	2.205	0.724
484	21.320	0.736	2.201	0.233	562	21.645	0.469	2.419	0.376
485	21.327	0.765	2.397	0.519	565	21.659	0.406	2.683	0.437
487	21.333	1.267	3.096	0.126	571	21.717	0.979	2.565	0.346
489	21.337	0.628	2.004	0.338	576	21.746	0.667	3.253	0.236
490	21.340	0.753	2.203	0.359	584	21.791	0.316	3.531	0.145
494	21.351	0.429	2.454	0.231	585	21.794	0.201	3.965	0.202
496	21.369	0.734	1.735	0.858	593	21.831	0.297	2.951	0.287
500	21.375	0.953	2.273	0.404	595	21.833	0.747	2.071	0.780
503	21.384	0.695	2.884	0.235	601	21.860	0.670	2.119	0.640
510	21.409	0.666	2.132	0.584	605	21.898	0.729	2.934	0.522
512	21.411	0.666	3.300	0.152	610	21.956	0.969	2.533	0.649
515	21.426	0.561	2.716	0.225	612	21.958	0.628	3.254	0.202
519	21.451	0.701	2.125	0.387	617	21.992	1.234	3.158	0.365
521	21.456	0.819	2.617	0.267	619	21.998	0.914	2.604	0.631
523	21.465	0.841	2.461	0.457	624	22.055	0.150	3.427	0.374
533	21.504	0.758	1.765	0.975	649	22.231	0.780	3.276	0.441
538	21.525	0.748	2.388	0.359	661	22.291	1.028	2.869	0.560
547	21.560	0.876	2.174	0.702	665	22.320	0.901	3.309	0.272
550	21.576	0.668	2.682	0.188	677	22.415	0.860	3.024	0.344
551	21.580	0.785	2.734	0.360	681	22.439	0.904	3.600	0.371
558	21.618	0.867	3.578	0.214	688	22.487	1.018	2.893	0.632

5.1 M30 artificial star experiments

For this experiment we used the mosaic constructed from data taken on 16/17 June 1990, which covered the greatest area observed in M30. Figure 9 shows the K, (B-V) diagram determined from photometry solely from this image matched with the Richer *et al.* (1988) optical data.

During data reduction DAOPHOT identified and photometered a total of 430 objects on this frame, although some were later rejected because their errors were too large for their magnitudes. We were therefore constrained to adding ~50 artificial stars to the frame. Unfortunately, the experiments were complicated somewhat by the unusual shape of the mosaic, which had been padded out by pixels of zero counts to make a rectangular array, and because ADDSTAR ignored both the upper and lower limits on valid data set within DAOPHOT. ADDSTAR would thus add stars into the padding, which had roughly the same area as the valid data. We therefore added twice the number of desired stars at random positions on the rectangular array, and deleted by hand those that fell within the padding.

Two frames, with respectively 42 and 57 artificial stars with random positions and random

Figure 9: The K, (B-V) colour-magnitude diagram of M30, with data from the 16/17 June 1990 mosaic only.

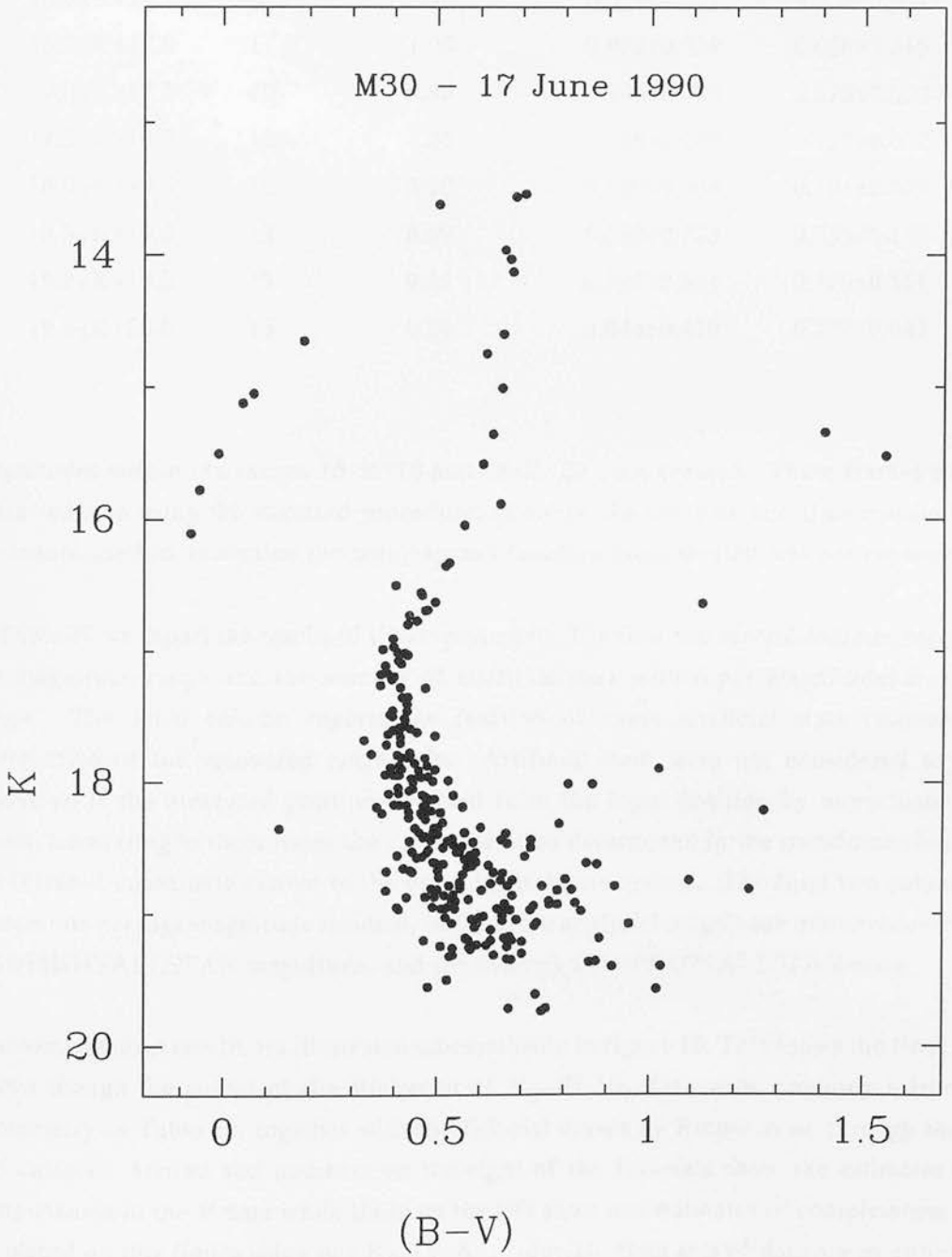

Table 27: Results of the M30 artificial star experiments. Quoted errors are standard deviations of the mean.

Magnitude range	N_{added}	Completeness factor	$\langle \Delta K$(artificial - recovered)$\rangle$	$\langle \sigma_K \rangle$
$16.0 \leq K < 16.5$	9	1.00	0.019±0.021	0.038±0.021
$16.5 \leq K < 17.0$	11	1.00	0.072±0.239	0.060±0.015
$17.0 \leq K < 17.5$	10	0.80	0.190±0.285	0.075±0.024
$17.5 \leq K < 18.0$	12	1.00	0.088±0.248	0.127±0.037
$18.0 \leq K < 18.5$	10	0.80	0.169±0.404	0.191±0.078
$18.5 \leq K < 19.0$	13	0.69	0.589±0.723	0.250±0.157
$19.0 \leq K < 19.5$	19	0.42	0.724±0.631	0.275±0.161
$19.5 \leq K < 20.0$	15	0.20	0.844±0.410	0.277±0.063

magnitudes within the ranges $16 < K < 18$ and $18 < K < 20$ were created. These frames were again reduced using the standard procedure, although the complex and time consuming procedure used to determine the point-spread function from scratch was not repeated.

In Table 27 we report the results of this experiment. The first and second columns reports the magnitude range and the number of artificial stars with input magnitudes in this range. The third column reports the fraction of these artificial stars recovered, irrespective of the recovered magnitude. Artificial stars were not considered to be recovered if the measured position deviated from the input position by more than 1.5 pixels, amounting to three times the r.m.s. deviation determined in the transformation of the infrared coordinate system to the optical coordinate system. The final two columns present the average magnitude residual, in the sense artificial magnitude minus recovered DAOPHOT/ALLSTAR magnitude, and the average DAOPHOT/ALLSTAR error.

The completeness results are illustrated schematically in figure 10. This shows the fiducial drawn though the subset of the Richer *et al.* V_0, $(B-V)_0$ data with matching infrared photometry in Table 26, together with the fiducial drawn by Richer *et al.* through their full dataset. Arrows and numbers on the right of the fiducials show the estimates of completeness in the V data while those on the left show our estimates of completeness in K, placed on this figure using our K_0, $(V-K)_0$ fiducial. Both sets of data are essentially complete down to ~0.5 magnitudes below the main-sequence turn-off; the dip in completeness to 0.8 in the interval $17.0 \leq K < 17.5$ is possibly due to small-number statistics.

Note also by comparing the final two columns of Table 27, that, apart again from the

Figure 10: The completeness of the M30 data. Figures to the right indicate completeness in the optical data while those to the left indicate completeness in the infrared data.

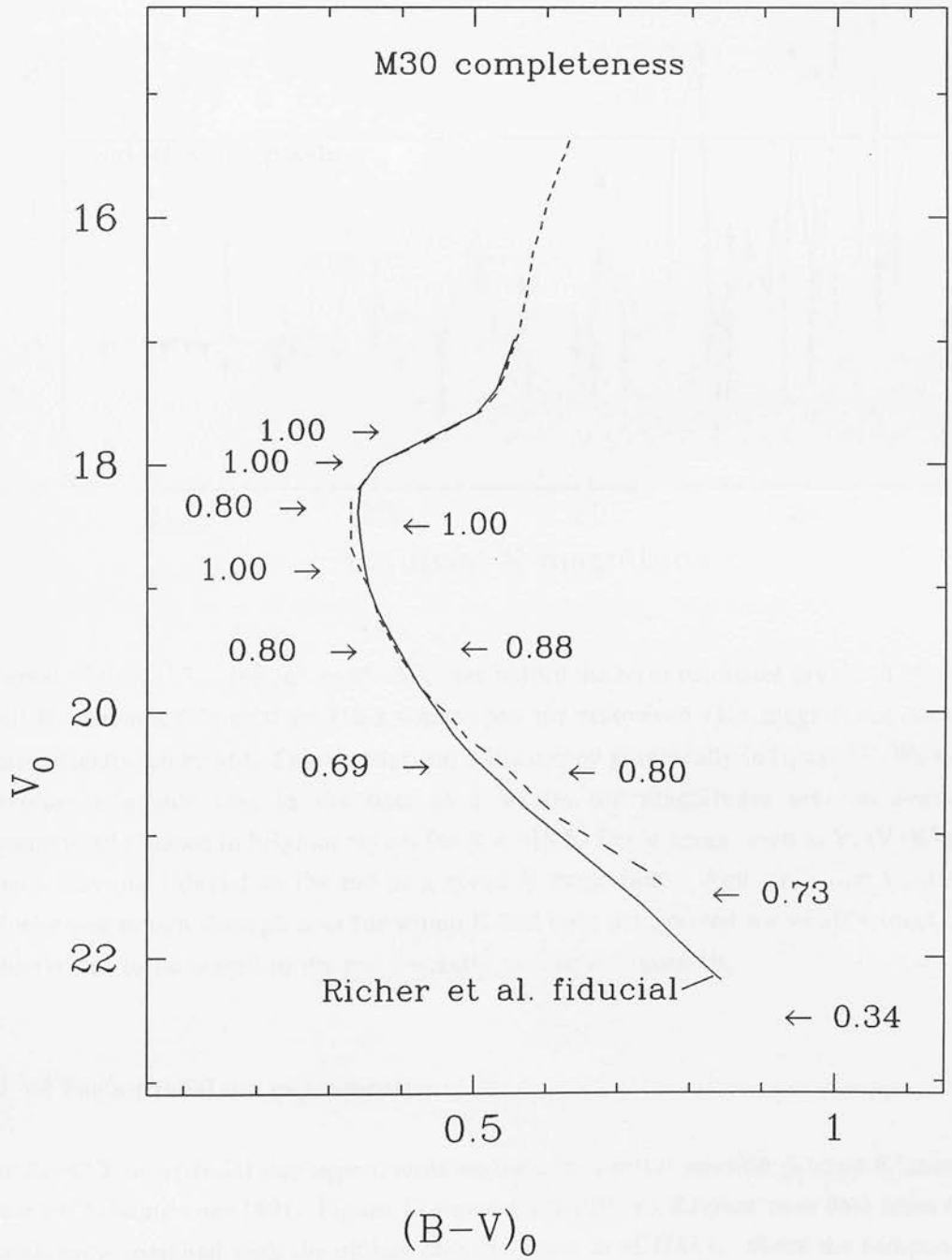

Figure 11: Results of the M30 artificial star experiments. Note that artificial stars recovered with discrepant magnitudes also have discrepant positions and thus may have been mismatched due to crowding.

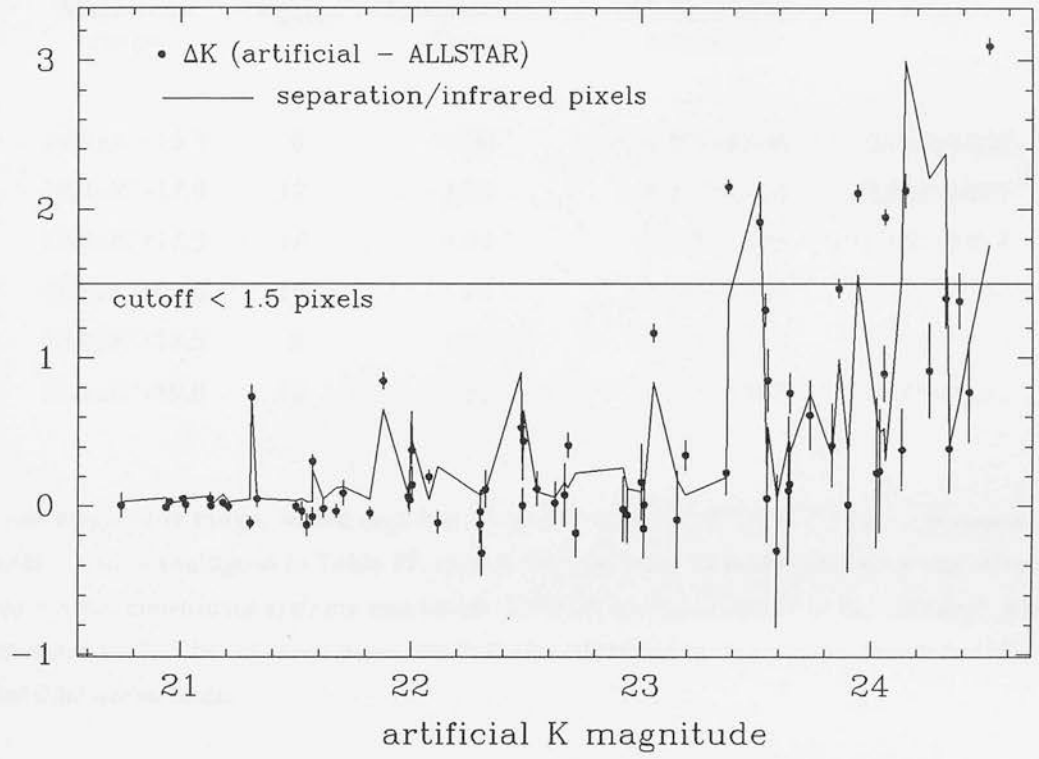

interval $17.0 \leq K < 17.5$, the values of $\langle \Delta K \rangle$ are within the error estimates provided by $\langle \sigma_K \rangle$ until K becomes fainter than ~18.5 whereupon the recovered $\langle K \rangle$ magnitudes become systematically too bright. This comparison is illustrated graphically in figure 11. We must therefore conclude that in the data as a whole, the magnitudes are, on average, systematically biased to brighter values for $K > \sim 18.5$. In a diagram such as V, (V-K) this would bias the fiducial to the red at a given V magnitude. And since our V, (B-V) fiducial was drawn through data for which K had been determined we would expect that fiducial also to be biased to the red - exactly as seen in figure 10.

5.2 47 Tuc artificial star experiments

For the 47 Tuc artificial star experiments we used the central position jittered K' mosaic from 19/20 September 1991. Figure 12 shows the K, (B-V) diagram with data from this mosaic only, matched with the optical data of Hesser *et al.* (1987). Since the component frames were observed in the more conventional spiral jitter pattern, we did not encounter the same problems with ADDSTAR which complicated the M30 experiments.

Three new frames were created from this mosaic, each of which had 20 artificial stars in

Table 28: Results of the 47 Tuc artificial star experiments. Quoted errors are standard deviations of the mean.

Magnitude range	N_{added}	Completeness factor	$<\Delta K'$(artificial - recovered)	$<\sigma_{K'}>$
$16.0 \leq K' < 16.5$	8	1.00	-0.003±0.036	0.023±0.002
$16.5 \leq K' < 17.0$	12	1.00	0.027±0.060	0.033±0.005
$17.0 \leq K' < 17.5$	10	1.00	0.038±0.095	0.061±0.014
$17.5 \leq K' < 18.0$	10	1.00	0.007±0.069	0.072±0.012
$18.0 \leq K' < 18.5$	8	1.00	0.078±0.212	0.112±0.030
$18.5 \leq K' < 19.0$	12	0.67	0.314±0.752	0.150±0.054

a one magnitude range, which together cover the range $16 < K' < 19$. Table 28 presents the results, and is analogous to Table 27, except that the transformation between the infrared and optical coordinate systems was better defined, so that a cutoff of 0.4 infrared pixels has been used. The infrared pixel size is 0.79 arcseconds in this case, whereas for M30 it was 0.62 arcseconds.

The completeness factors are again shown illustratively, along side the V_0, $(B-V)_0$ fiducials, in figure 13. It is obvious that the data are essentially complete along the entire length of the main sequence. Indeed the completeness fraction of 0.67 in the faintest bin may be an underestimate, since two of the unrecovered artificial stars were lost in the noise of a badly fitted bright star near the edge of the mosaic.

Also note that the average residual $<\Delta K'>$ is within the limit set by $<\sigma_{K'}>$ down the entire length of the main sequence except for the faintest bin, as is shown graphically in figure 14. This indicates that the colour of the main sequence is not biased as was the M30 main sequence, and this can be further seen in the excellent agreement between our V_0, $(B-V)_0$ fiducial and that of Hesser *et al.*

Figure 12: The K', (B-V) colour-magnitude diagram of 47 Tuc, with data only from the 19/20 September 1991 field 1 central position mosaic.

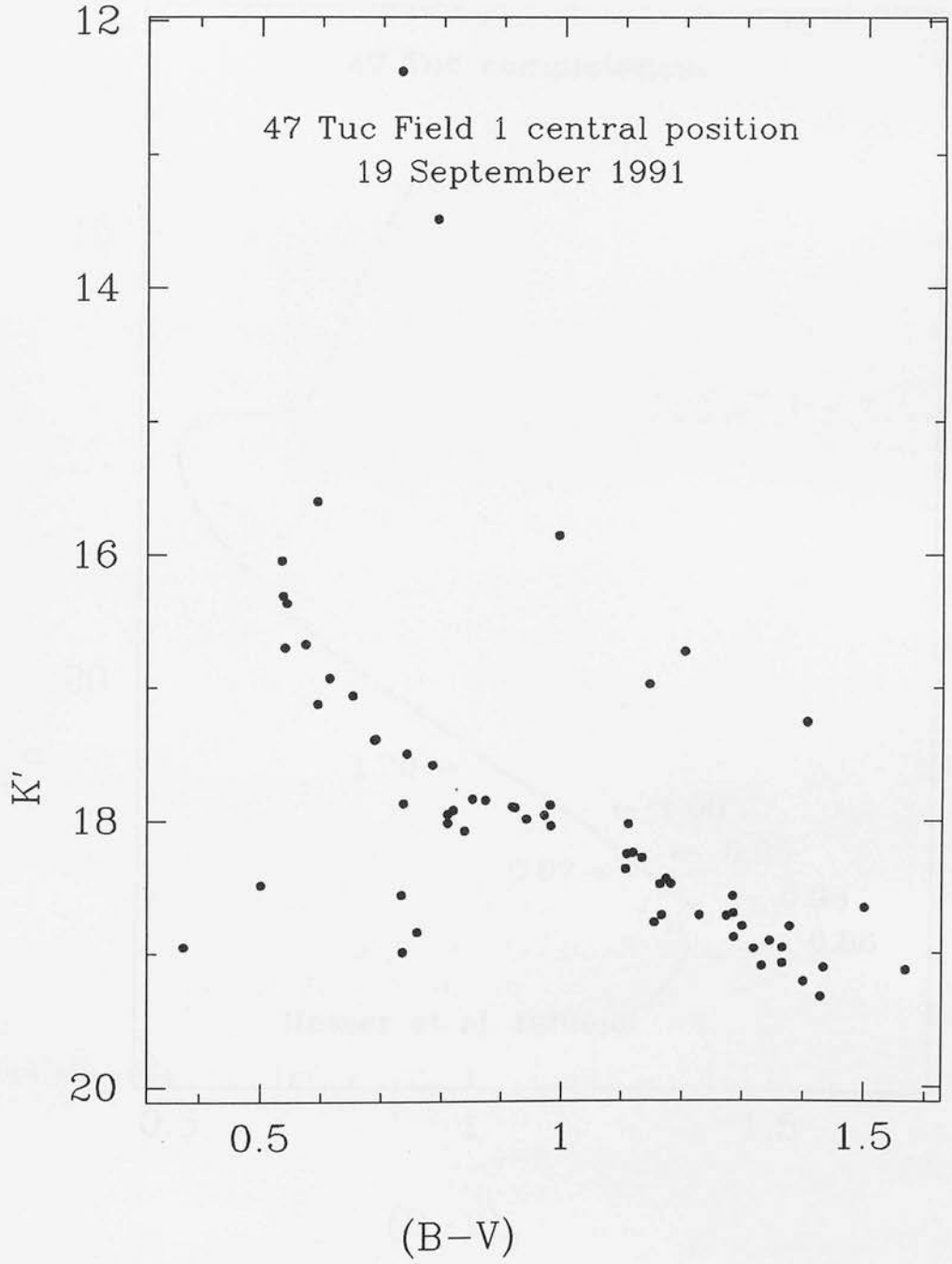

Figure 13: The completeness of the 47 Tuc data. Figures to the right indicate completeness in the optical data while those to the left indicate completeness in the infrared data.

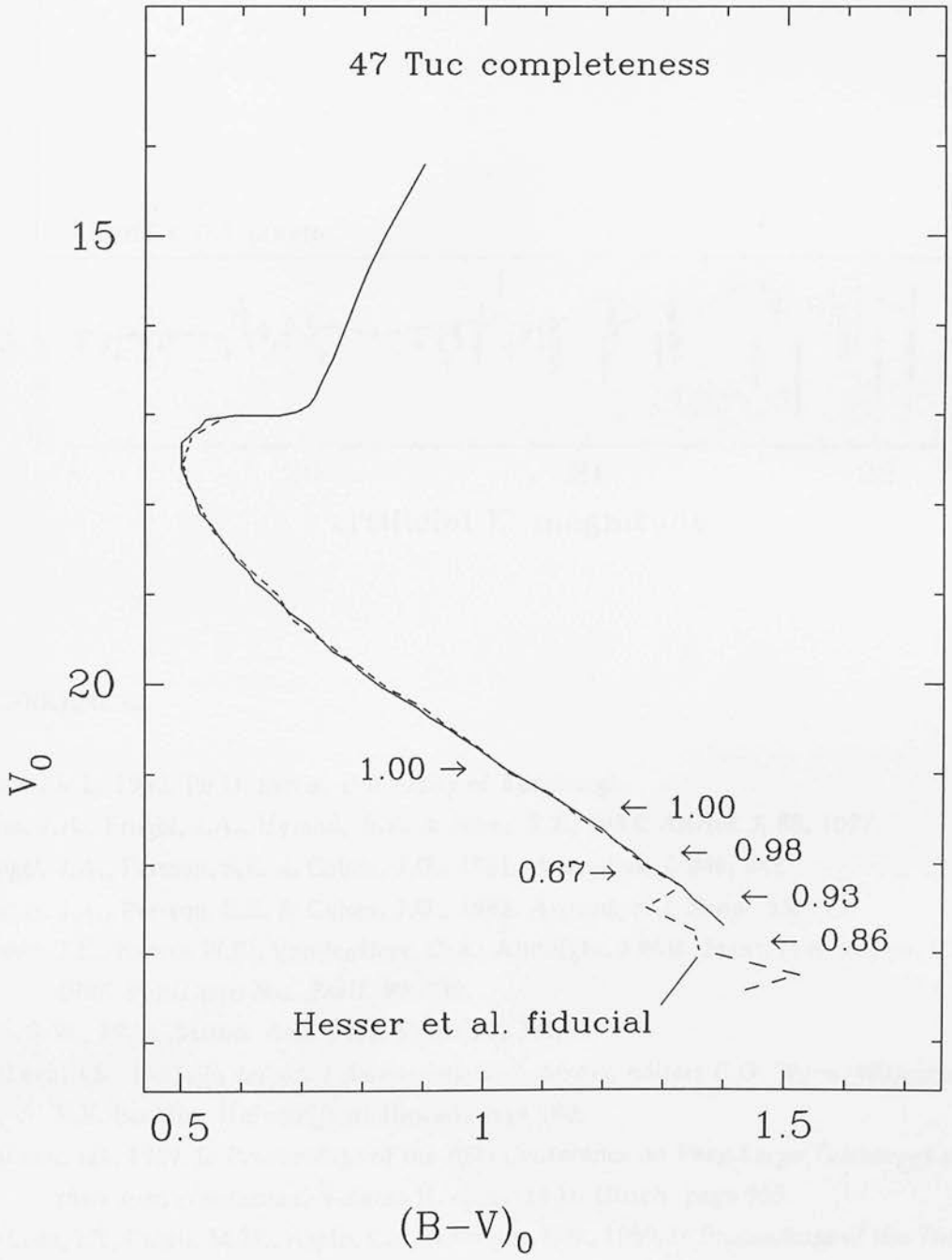

Figure 14: Results of the 47 Tuc artificial star experiments.

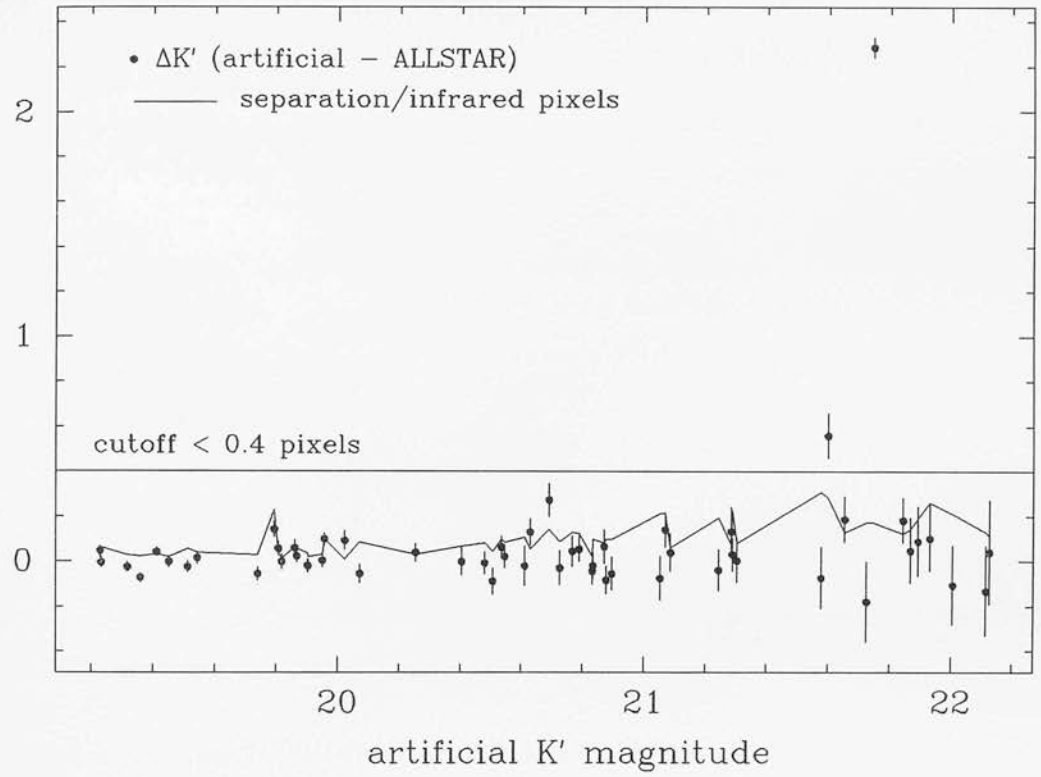

REFERENCES

Dixon, R.I., 1992. Ph.D. thesis, University of Edinburgh.

Elias, J.H., Frogel, J.A., Hyland, A.R. & Jones, T.J., 1983. *Astron. J.* **88,** 1027.

Frogel, J.A., Persson, S.E. & Cohen, J.G., 1981. *Astrophys. J.* **246,** 842.

Frogel, J.A., Persson, S.E. & Cohen, J.G., 1983. *Astrophys. J. Suppl.* **53,** 713.

Hesser, J.E., Harris, W.E., VandenBerg, D.A., Allwright, J.W.B., Shott, P. & Stetson, P.B., 1987. *Publs astr. Soc. Pacif.* **99,** 739.

Lee, S-W., 1977. *Astron. Astrophys. Suppl.* **27,** 381.

McLean, I.S., 1987. In *Infrared Astronomy with Arrays,* editors C.G. Wynn-Williams & E.E. Becklin, University of Hawaii, page 180.

McLean, I.S., 1989. In Proceedings of the *ESO Conference on Very Large Telescopes and their Instrumentation,* Volume II, editor M.H. Ulrich, page 955.

McLean, I.S., Casali, M.M., Aspin, C.A. & Wright, G.S., 1989. In Proceedings of the *Third NASA Ames Infrared Detectors Workshop,* editor C. McCreight, page 183.

Penny, A.J. & Dickens, R.J., 1986. *Mon. Not. Roy. astr. Soc.* **220,** 845.

Richer, H.B. & Fahlman, G.G., 1986. *Astrophys. J.* **304,** 273.

Richer, H.B., Fahlman, G.G. & VandenBerg, D.A., 1988. *Astrophys. J.* **329,** 187.

Stetson, P.B., 1987. *Publs astr. Soc. Pacif.* **99,** 191.
Wainscoat, R.J. & Cowie, L.L., 1992. preprint.

Chapter 2

Globular Cluster Distances and Ages

" The stars can be near or distant, according as we need them. Do you suppose our mathematicians are unequal to that? Have you forgotten doublethink? "
- George Orwell, 1984.

ABSTRACT

This chapter is concerned with the derivation of the distances and ages of the globular clusters M13, M30, NGC6752 and 47 Tuc, using colour-magnitude data incorporating the infrared photometry presented in Chapter 1.

In section 1 we discuss the Bergbusch & VandenBerg V, (B-V) and V, (V-K) isochrones, which are the most up-to-date self-consistent set of models available, paying particular attention to the methods used by the authors to convert the theoretical luminosities and temperatures to the V, (B-V) [VandenBerg (1992) and Bergbusch & VandenBerg (1992)] and to the V, (V-K) [Bell (1992)] observational planes.

In section 2 we summarise the available values of foreground reddening and chemical composition for each cluster from the recent literature, and give some discussion of the methods used in their determinations. The value of foreground reddening for M30 is found to be controversial, with values ranging from E[B-V]=0.01 to 0.07. We adopt the higher value of E[B-V]=0.07 and further justify this later in the chapter.

The chemical composition of 47 Tuc stars is also found to be controversial. As Pilachowski, Sneden & Wallerstein (1983) point out, abundance measurements of 47 Tuc stars tend to give [Fe/H]~-0.65 where light-element abundances are measured or [Fe/H]~-1 where iron-peak elements are measure. They also note that while [Fe/H]~-0.8 is a good compromise, the concept of an average abundance should be avoided. Given this apparent decoupling of the elemental abundances, we discuss whether isochrones with scaled-solar abundances can be used to derive meaningful results for 47 Tuc. We argue that when the enhancement of α-process elements is taken into account, using the scaling scheme of Straniero, Chieffi & Salaris (1991) - which was criticised as being too simplistic by

VandenBerg (1992) - isochrones more metal rich than the 'compromise' abundance of [Fe/H]=-0.78 should be used.

Section 3 is concerned with the derivation of cluster distances by main-sequence fitting to subdwarfs. We discuss the pros and cons of determining distances using this method; chief amongst the cons is the application of the controversial Lutz-Kelker corrections to the subdwarf magnitudes. The basic parameters of a sample of 5 field subdwarfs with <[Fe/H]>=-1.4 are presented, as are corrections to the subdwarf absolute magnitudes at fixed colour, determined differentially between the Bergbusch & VandenBerg isochrones, to enable distances to be determined to the more metal rich or poor clusters.

We also present results of simulations involving fitting the isochrones to the subdwarfs, to illustrate the sensitivity of the subdwarf-determined distances to various sources of error. We find that the distances determined by main-sequence fitting in the V, (V-K), the K, (V-K) and the K, (B-V) planes are less sensitive to some systematic shifts than are the distances determined from V, (B-V). We find that these mixed optical-infrared planes also give distances which are less sensitive to small photometric errors than those from V, (B-V) until the K photometric error exceeds 2 to 3 times the equivalent V photometric error. The distances from K, (B-V) are the least sensitive to small photometric errors, although critical discussion is given, warning that the results of this simulation at least should be approached with caution.

Distances determined in K, (B-V) are also the least sensitive to incorrectly adopted values of R, the ratio of total-to-selective extinction, although the distances from all the planes are found to be equally sensitive to small errors (±0.03 magnitudes) in the adopted cluster foreground reddening.

When considering the sensitivity of the derived distances to errors in the adopted cluster chemical abundance of ±0.4 dex about [Fe/H]~-1.4, all planes are found to fare equally, underestimating the distance by ~0.21 magnitudes at the metal-rich end of the range and overestimating the distance by ~0.15 magnitudes at the metal-poor end.

Finally, distances to each cluster are derived, and are summarised in Table 16.

Section 4 is concerned with estimating cluster ages using the distance and reddening independent (V-K) and (B-V) colour differences between the cluster turn-offs and the subgiant branches. We calibrate these parameters, to derive absolute ages, using the isochrones. VandenBerg, Bolte & Stetson (1991) have warned that such ages are untrustworthy because the subgiant branch colour are just too sensitive to present uncertainties in convective theory and colour-temperature equations. Despite this, such ages are independent of any global correction to the isochrone colours, such as that

suggested by Bell (1992) for the V, (V-K) isochrones, and so these ages could offer important constraints when compared to ages derived directly from the isochrones and cluster colour-magnitude data.

In section 5 we use the observed colours of the subgiant branches to determine if the adopted reddenings are internally consistent among our four clusters. Variations in age and abundance are removed using the isochrones. Most weight is given to the (B-V) comparisons, since the discussion of section 4 renders us suspicious of the (V-K) colours. We find marginal evidence that the reddening adopted for M30 is 0.01 to 0.02 magnitudes too high, although the evidence is too marginal to allow a definitive statement about this. There is good agreement between the derived and adopted relative reddenings of 47 Tuc and NGC6752 or M13, all of which have less controversial reddenings that M30.

Absolute ages are determined in section 6 by comparing the isochrones directly to the cluster colour-magnitude diagrams. The V, (B-V) isochrones agree well with the entire observed colour-magnitude diagram of each of the four clusters, while only in the case of 47 Tuc is there satisfactory agreement between the colour-magnitude diagram and the V, (V-K) isochrones. The observed and theoretical V, (V-K) giant branches of both M13 and NGC6752 disagree, suggesting that the 0.12 magnitude correction to the isochrone (V-K) colours is not appropriate at low metallicity and low gravity. We are unfortunately unable to ascertain if this discrepancy persists at extremely low abundances, there being no infrared photometry of M30 giants.

Finally, in section 7, we compare the ages derived from the two methods, and assign best overall ages to the clusters, as summarised in Table 25. Since the available evidence suggests that it is only at the abundance of 47 Tuc where the global 0.12 magnitude correction to the V, (V-K) isochrone colours, suggested by Bell (1992), is appropriate, we adopt for the other three clusters the mean of the ages determined from Δ(B-V) and directly from the V, (B-V) isochrones. We must await the 'new' isochrones presented in Chapter 4 before our K data can be used to the fullest in deriving ages for these clusters.

For 47 Tuc, we find good agreement between the ages derived from the V, (V-K) and V, (B-V) isochrones. We also find good agreement between the ages derived from Δ(V-K) and Δ(B-V). However, the ages derived from these two methods are discrepant unless a metallicity intermediate between [Fe/H]=-0.65 and [Fe/H]=-0.78 is assumed, as was suggested when the reddenings of the clusters were intercompared.

1 BERGBUSCH & VANDENBERG MODEL ISOCHRONES

Bergbusch & VandenBerg (1992) have recently made available to the community their latest theoretical stellar evolution models and isochrones [see also VandenBerg 1992]. These have been calculated at ten metallicities in the range $-2.26 \leq [Fe/H] \leq -0.47$, and with oxygen enhancements whose functionality with [Fe/H] is reproduced in equations 1. The other metals are assumed to have scaled-solar values. The values of [Fe/H] at which the

$$\begin{aligned} [O/Fe] &= -0.5[Fe/H] && [Fe/H] \geq -1 \\ [O/Fe] &= -0.2[Fe/H] + 0.3 && [Fe/H] < -1 \end{aligned} \qquad (1)$$

models were calculated are reproduced in Table 1, together with the values of [O/Fe], the helium mass fraction Y and the metal mass fractions including and excluding the oxygen enhancement, respectively Z and Z_0.

In calculating these models, the surface boundary conditions were set by interpolation in a grid of model atmosphere results, rather than the more widely adopted, but unphysical procedure of integrating the equations of stellar structure in conjunction with an assumed temperature versus optical depth relation. The zero-point of the temperature scale was then set by selecting α, the ratio of mixing length to pressure scale height, to normalise to the observed parameters of the metal-poor field dwarf Groombridge 1830 (HD103095). The values of α used in the $[Fe/H] > -1.3$ models were arbitrarily changed to force agreement of the models with the slopes of the Frogel, Persson & Cohen (1981) globular cluster fiducial giant-branches.

1.1 Bolometric corrections and (B-V) colour transformations

In this section we briefly summarise the discussion given by VandenBerg (1992) regarding the transformation of the theoretical model luminosities and temperatures to V magnitudes and (B-V) colours. It is not, however, intended to replace the superior discussion given by VandenBerg himself.

The feature which makes the Bergbusch & VandenBerg calculations the best set of self-consistent models to date is their use of the same model atmosphere results which provided the surface boundary conditions to also provide the colour to effective temperature transformations and bolometric corrections. These model results are based on the MARCS results published by Bell & Gustaffson (1978) and VandenBerg & Bell (1985) and also the Kurucz (1979) ATLAS6 results. The ranges of temperature, gravity and abundance where these results are used are as follow:

Table 1: The abundance parameters at which Bergbusch & VandenBerg tabulate their stellar evolution models.

[Fe/H]	[O/Fe]	Y	Z	Z_0
-2.26	0.75	0.2350	0.000323	0.00010
-2.03	0.70	0.2350	0.000497	0.00017
-1.78	0.66	0.2351	0.000816	0.00030
-1.66	0.63	0.2352	0.001030	0.00040
-1.48	0.60	0.2354	0.001460	0.00060
-1.26	0.55	0.2358	0.002227	0.00100
-1.03	0.50	0.2368	0.003470	0.00170
-0.78	0.39	0.2391	0.005100	0.00300
-0.65	0.30	0.2413	0.006012	0.00400
-0.47	0.23	0.2454	0.008000	0.00600

Bell & Gustaffson (1978)

$$-2 \leq [A/H] \leq 0 \quad 4000 \leq T_e/K \leq 6000 \quad 0.75 \leq \log_{10}(g/cm\ s^{-2}) \leq 3.00$$

VandenBerg & Bell (1985)

$$4500 \leq T_e/K \leq 7000 \quad 3.00 < \log_{10}(g/cm\ s^{-2}) \leq 4.50$$

Kurucz (1979)

$$T_e > 7000K \quad 2.00 < \log_{10}(g/cm\ s^{-2}) \leq 4.50$$

As has been pointed out on many occasions, there are systematic differences between the colours and bolometric corrections of these three studies, and the regions of overlap are sufficiently small to render impossible a comprehensive correction of one grid to another. See, for example, the discussion in Dixon (1992). However, VandenBerg has made the following adjustments to the above results.

For the grid of bolometric corrections, he first makes small adjustments to each of the above such that $BC_\odot = -0.12$. The Kurucz results are then normalised to the VandenBerg & Bell results to extend the latter to $T_e > 7000K$. For giants with $T_e < 4000K$, the bolometric corrections were determined from an M-giant (V-K) versus T_e relation and a K

bolometric magnitude versus (V-K) relation. The higher gravity values are by linear interpolation between these and bolometric corrections determined for dwarf stars with $\log_{10}(g/cm\ s^{-2})=5$.

For the transformation to (B-V), the VandenBerg & Bell model colours were shifted to the red by ~0.03 magnitudes to normalise to the Bell & Gustaffson colours. Additional redward shifts were also applied to the synthetic colours of the very cool high-gravity models. Detailed information on the sizes of these shifts can be obtained from figures 9 and 10 of VandenBerg (1992).

1.2 The transformation to V, (V-K) by Bell (1992)

In his paper discussing the derivation of the V, (V-K) and K, (V-K) isochrones from the Bergbusch & VandenBerg results, Bell (1992) finds a discrepancy of ~0.12 magnitudes between the predicted temperature versus (V-K) relation and the observed relation defined by the works of Glass and of Saxner & Hammerbäck. He attributes this to a discrepancy in the K magnitudes predicted by the MARCS model atmospheres (Bell, 1991, private communication), and notes that no simple linear transformation exists to allow the theoretical (V-K) colours to be normalised to the observations. However he also finds that applying a global blueward correction of 0.12 magnitudes to the isochrone (V-K) colours produces good agreement of the theoretical giant branch with photometry of 47 Tuc giants and with our preliminary, unpublished subgiant and main-sequence turn-off photometry of that cluster for a reasonable age, distance and composition.

To prevent the following discussion from degenerating into a mere examination of parameter space, we shall also apply this global correction to all the isochrone K magnitudes unless explicitly stated otherwise. It should be borne in mind that future work may show this global correction to be incorrect.

2 BASIC CLUSTER PARAMETERS

In order to derive absolute distances and ages of globular clusters, we must have *a priori* knowledge both of the abundance of chemical elements in the globular cluster stars, and of the foreground reddening to the clusters. In this section, we present tables summarising some determinations of these parameters for M30, M13, NGC6752 and 47 Tuc from the recent literature. We also follow each table with some discussion, since the information in them cannot be taken at face value, and without reference to the discussion given by the original authors.

Not all of the determinations tabulated below are independent, but may rely on data from other studies mentioned in the tables. In the case of the abundance determinations, for example, different studies of the same cluster may adopt slightly different values of foreground reddening or ratio of total-to-selective extinction. The abundances are usually given relative to the solar values, and undoubtedly some of the differences between independent studies are due to differences in the adopted solar chemical-abundance parameters; few authors bother to mention the adopted solar values. Also, the quoted abundances are not all on the same scale. Where an author has collected data for many clusters, and subjected them to homogeneous analysis, the resulting abundances are on a given scale, defined by the *relative* cluster abundances. The zero-points and gradients of different scales may disagree, however. If these abundances are then used to calibrate other abundance indicators, for example DDO photometric colours, these will also produce abundances on the calibrating scale. Two of the prevalent abundance scales are those defined by the works of Zinn, and Cohen and their co-workers. Specific references and discussion of the differences between these scales follows below.

In adopting abundances for our clusters, we have taken weighted averages, and we use the dispersion between the separate determinations as a measure of the real uncertainty in setting the absolute abundance.

2.1 The metallicity of NGC6752

Table 2 summarises recent abundance determinations for NGC6752.

Bell, Hesser & Cannon (1984) determine [Fe/H] by using three photometric indices from Cannon (1974). Of these three indices, two rely on knowing accurately the colour and magnitude of the intersection of the horizontal and red giant branches. $(B-V)_{0,g}$ is the dereddened colour of the giant branch at the level of the horizontal branch, while S is the gradient of a line joining the intersection of these two branches to a point on the giant branch 2.5 V magnitudes brighter. In a cluster with a poorly populated horizontal branch, these parameters are not well defined. The third determination involves ΔV, the V magnitude difference between the horizontal branch and the giant branch measured at $(B-V)_0=1.4$, and is also difficult to define for a cluster without a fully populated horizontal branch.

Carney (1979a) determines the value of [Fe/H]=-1.5 from $\delta(U-B)_{0.6} = 0.22\pm0.03$. Using this value and the calibration of $\delta(U-B)_{0.6}$ with [Fe/H] from Carney (1979b), viz

$$[Fe/H]=0.11-2.90\delta_{0.6}-18.68\delta_{0.6}^2 \qquad (2)$$

Table 2: NGC6752 metallicity determinations.

[Fe/H]	Source	Method
-1.79	Mallia (1977)	medium dispersion spectra of 7 stars
-1.5	Carney (1979a)	$\delta(U-B)_{0.6}$
-1.55	Zinn (1980)	integrated light (Q39)
-1.4	Norris *et al.* (1981)	DDO photometry of 16 giants
-1.39	Frogel, Cohen & Persson (1983)	$(J-K)_0$(GB) and $(V-K)_0$(GB)
-1.32	Pilachowski *et al.* (1983)	0.3Å echelle spectra of 3 giants
-1.1	Bell, Hesser & Cannon (1984)	$(B-V)_{0,g}$
-1.0	*ibid*	ΔV
-1.3	*ibid*	S
-1.5	*ibid*	3 to 4Å spectra of 26 stars
-1.55	Zinn & West (1984)	<Q39> from three methods
-1.64	Webbink (1985)	$(B-V)_{0,g}$
-1.61	Gratton *et al.* (1986)	high dispersion spectra
-1.62	Straniero & Chieffi (1991)	V, (B-V) isochrone fitting

gives [Fe/H]=-1.43. An error of ±0.02 in $\delta_{0.6}$ corresponds to an error in [Fe/H] of ±0.3 dex. See Sandage & Fouts (1987) and references therein for other calibrations of $\delta_{0.6}$ with [Fe/H].

Norris *et al.* (1981) use intermediate band DDO photometry of six 'apparently anomalous' asymptotic giant branch stars and of ten giants taken from the study by Bessel & Norris together with a calibration by Osborn (1971) to derive [Fe/H]=-1.4, which they adopt. They also note that a newer calibration of the DDO parameters with metallicity, based on revised abundances for M3, M13, M15 and M92 by Cohen, leads to [Fe/H]=-1.6.

Bell *et al.* (1984) have obtained spectra of 26 stars ranging from the red giant tip to the main-sequence turn-off with resolutions of ~4Å. Assuming a true distance modulus of 13.5 magnitudes and E[B-V]=0.05, they deduce an overall metal abundance of [Fe/H]≈-1.5 by comparison of various observed and synthetic M_v vs spectral index diagrams. Zero-point shifts have been applied to some of the observed spectral indices to facilitate the best fit with the synthetic values. The existence of such shifts is thought to be plausible because the spectra were obtained with a narrow slit, and the absolute fluxes are affected

by refraction losses. The sense of the zero-point shift is to reduce the derived abundance.

We have adopted [Fe/H]=-1.5±0.3 for NGC6752.

2.2 The reddening of NGC6752

The reddening to NGC6752 is low, as can be seen from Table 3.

Carney (1979a) adopts E[B-V]=0.04, by combining determinations from several methods, including comparison of the (U-B), (B-V) two-colour diagrams of NGC6752 and M13, combining data for the seven hottest horizontal branch stars with mean luminosity class III colours, and by using DDO photometry of population I giants with corrections for the metal difference between the giants and NGC6752.

Zinn (1980) uses (g-r) and literature (B-V) values to estimate the reddenings to his program clusters. The relation between the reddening-free parameters and intrinsic colours is defined using literature reddening estimates for 45 clusters with reddenings determined to accuracies of better than ±0.05 magnitudes. For NGC6752 he derives E[B-V] = 0.00±0.03. However, NGC6752 was one of the clusters used in the calibration, with an input value of E[B-V]=0.04±0.02.

It is also possible to estimate the reddening to NGC6752 using the neutral hydrogen column densities of Burstein & Heiles (1978). It is not possible to use the full method of Burstein & Heiles because there are no galaxy counts available for the direction of NGC6752, but it is possible to estimate E[B-V] by assuming a constant gas-to-dust ratio. Equation 7 from that paper gives the relation between the HI column density N_H and E[B-V], viz:

$$E[B-V] = -(0.055\pm0.006) + (0.443\pm0.018)\times10^{-3}\left(\frac{N_H}{2.23\times10^{18} cm^{-2}}\right) \qquad (3)$$

Taking $N_H/2.23\times10^{18}$ cm^{-2} = 226 from Table 1 of the Burstein & Heiles paper leads to E[B-V]=0.05±0.01. Note, however, that NGC6752 was again one of the clusters used to calibrate the above equation, with an input parameter of E[B-V]=0.04.

We have adopted E[B-V]=0.04±0.01. E[V-K] and A_K have been determined from formulae taken from Rieke & Lebofsky (1985): E[V-K] = (2.744±0.024)E[B-V] and $A_K = 0.112A_V$. We have used Turner's (1976) value of R = 3.08±0.03 for the ratio of total-to-selective extinction.

Table 3: Optical reddening estimates for NGC6752.

E[B-V]	Source	Method
0.05±0.01	Cannon & Stobie (1973)	Seven hottest blue horizontal-branch stars
0.05±0.01	Burstein & Heiles (1978)	HI column density assuming constant gas-to-dust ratio
0.04±0.01	Carney (1979a)	Various - see below
0.00±0.03	Zinn (1980)	(g-r) and (B-V)

2.3 The metallicity of M13

Abundance determinations of M13 are presented in Table 4.

The determination by Butler may be less than trustworthy since it depends on measurements from only three variables which are known to be peculiar (Richer & Fahlman 1986 and references therein); Butler himself notes that the horizontal branch of M13 would be anomalously blue for his derived metallicity. The Zinn scale probably systematically underestimates by a small amount the metallicity of clusters with blue horizontal branches such as those of M13 and NGC6752, which have Lee (1991) horizontal branch indices of C=0.97 and 1.00 respectively. The definition of C is reproduced in equation 4, where B, V and R are the numbers of blue, variable and red horizontal-branch stars respectively. An equation quantifying this underestimation was given by Frogel, Cohen & Persson (1983) and is reproduced in equation 5.

We adopt [Fe/H]=-1.4±0.3.

$$C = \frac{B-R}{B+V+R} \tag{4}$$

$$[Fe/H] = 0.95[Fe/H]_{Zinn} - 0.07 \tag{5}$$

2.4 The reddening of M13

Literature foreground reddenings of M13 are presented in Table 5. Following Richer & Fahlman (1986), who take the mean value from the studies of Sandage (1970), McClure & Racine (1969) and Crawford & Barnes (1969), we adopt E[B-V]=0.02±0.01

Table 4: M13 metallicity determinations.

[Fe/H]	Source	Method
-1.69±0.3	Osborn (1973)	DDO photometry of 6 red giants
-1.03±0.2	Butler (1975)	ΔS measurements of variables V5, V8 & V9
-1.4±0.3	Bell & Dickens (1980)	FeI equivalent widths
-1.42±0.1	Pilachowski, Wallerstein & Leep (1980)	High resolution spectroscopy
-1.73±0.1	Zinn (1980)	Photometry of integrated cluster light
-1.47±0.15	Frogel, Cohen & Persson (1983)	$(V-K)_0$(GB) & $(J-K)_0$(GB)
-1.4 (+0.4,-0.8)	Richer & Fahlman (1986)	$\delta_{0.6}$
-1.54±0.15	Lehnert, Bell & Cohen (1991)	High-dispersion spectra of 10 red giants

Table 5: Optical reddening estimates for M13.

E[B-V]	Source	Method
0.00	Sandage (1964)	(1) two-colour diagram of ~40 field stars, and (2) comparing colours of blue horizontal branch stars with field A stars
0.016±0.016	Crawford & Barnes (1969)	Photometry of A & F stars giving E[b-y] = 0.011 ± 0.011
0.03±(>)0.02	Sandage (1969)	two-colour diagram of horizontal-branch stars
0.00±0.02	McClure & Racine (1969)	Broad-band photometry of late-type giants
0.03±0.02	Sandage (1970)	adopted

2.5 The metallicity of M30

Abundance determinations of M30 are presented in Table 6.

In his study of M30, Bolte (1987) used the Zinn & West (1984) calibration of ΔV with [Fe/H], together with his value of ΔV=3, to derive [Fe/H]=-1.86. Recall that ΔV is the

Table 6: M30 metallicity determinations.

[Fe/H]	Source	Method
-2.26 ± 0.07	Zinn (1980)	Q39
-1.84 ± 0.08	Bica & Pastoriza (1983)	DDO $C(42 - 45)_0$
-2.32 ± 0.12	Pilachowski (1984)	Q39 with a correction for horizontal branch type
-2.15 ± 0.15	Zinn & West (1984)	<Q39>
-2.19	Webbink (1985)	$(B-V)_{0,g}$
-1.86	Bolte (1987)	ΔV
-1.77	*ibid*	Floating best fit of VandenBerg & Bell isochrones

V magnitude difference between the horizontal branch and the giant branch at $(B-V)_0$=1.4. The giant branch brighter than V~14.5 is not well populated in Bolte's colour-magnitude diagram, making ΔV difficult to define. Indeed the giant branch to the red of (B-V)~1.1 is defined by only one point at (B-V)~1.4. Also, ΔV is reddening dependent. Bolte adopts E[B-V]=0.02, but as we shall see later in section 5, this value is probably too low. Since ΔV increases with E[B-V], a value higher than 3 would lead to a lower value of [Fe/H]. We also note, as did Bolte, that Zinn & West only define the relation between ΔV and [Fe/H] for $\Delta V \leq 2.9$ since sensitivity to metallicity is lost for higher values. This again makes [Fe/H]=-1.86 an upper limit.

Comparing his V, (B-V) colour-magnitude data with the VandenBerg & Bell isochrones and allowing heavy metal abundance, distance modulus and reddening to 'float' as free parameters, Bolte determined a best fit also with a high value of [Fe/H] and with a much higher value of E[B-V] than he originally adopted {[Fe/H]=-1.77, E[B-V]=0.05, $(m-M)_V$=14.65 and age~16.5 Gyr}.

We adopt [Fe/H]=-2.25±0.30

2.6 The reddening of M30

The foreground reddening to M30 is somewhat controversial. Over the past three decades determinations have ranged from E[B-V]=0.01 to 0.07. In Table 7 we list published estimates of the foreground optical reddening to M30. We adopt the value of E[B-

Table 7: Optical reddening estimates for M30.

E[B-V]	Source	Method
0.06 ± 0.02	Dickens (1972)	Photographic photometry of 6 field stars compared with Johnson (1964) (U-B) vs (B-V) relation for luminosity class V stars
0.03 ± 0.03	Burstein & Heiles (1978)	HI column density & galaxy counts
0.04 ± 0.01	*ibid*	Assuming constant gas-to-dust ratio
0.01 ± 0.03	Zinn (1980)	(g-r) and (B-V)
0.01 ± 0.02	Bica & Pastoriza (1983)	Average of values from BV & DDO photometry (E[B-V] = -0.01) and the Zinn (1980) value
0.068 ± 0.035	Richer, Fahlman & VandenBerg (1988)	Comparison in (U-B) vs (B-V) of horizontal branch stars with Johnson (1966) population I fiducial
0.05	Piotto et al. (1990)	16 Gyr isochrone with Z=0.000497, Y=0.24 & [O/Fe]=0.7

V]=0.07±0.04 determined by Richer *et al.* (1988), and further justification for this choice is given later in this chapter. Indeed, an important result of section 5 is the confirmation of this higher value of the M30 reddening relative to the less controversial reddenings of 47 Tuc and NGC6752 via a comparison of the near-vertical subgiant branches of these clusters in the V, V-K and V, B-V colour-magnitude diagrams.

2.7 The metallicity of 47 Tuc

The heavy-element abundance of the globular cluster 47 Tuc is also controversial. As pointed out by Pilachowski, Sneden & Wallerstein (1983), abundance determinations tend to cluster around [m/H]~-0.65 where light-metal abundances have been measured, or around [m/H]~-1 for measurements of iron-peak element abundances. They also note that, while [Fe/H]~-0.8 seems to be a good compromise, the concept of an 'average' metallicity should be avoided.

In Table 8 we summarise determinations of the abundance of metals in 47 Tuc stars from the recent literature, using the usual convention where [X/Y] is the logarithmic abundance ratio by number of elements X and Y relative to the sun. The original notation is from

Table 8: 47 Tuc metallicity determinations.

Abundance	Source	Method
[Fe/H]=-0.87	Lee (1977)	UV excess relative to the Hyades
[Fe/H]=-0.66±0.14	Bica & Pastoriza (1983)	DDO $C(42 - 45)_0$
[Fe/H]=-0.59±0.25	Frogel *et al.* (1983)	$(J-K)_0$(GB) & $(V-K)_0$(GB)
[Fe/H]=-1.09±0.20 [O/Fe]=+0.15±0.30 $[m_\alpha/Fe]$=+0.5	Pilachowski, Sneden & Wallerstein (1983)	0.3Å resolution spectra of two giants
<[Fe/H]>=-0.71±0.08	Zinn & West (1984)	<Q39>, DDO photometry, ΔV and other indicators
[Fe/H]=-0.75	Webbink (1985)	$(B-V)_{0,g}$
[FeI/H]=-0.82±0.03 [MgI/FeI]=+0.14±0.19 [SiI/FeI]=+0.35±0.04 [CaI/FeI]=-0.03±0.05 [TiI/FeI]=+0.24±0.07	Gratton, Quarta & Ortolani (1986)	High-dispersion spectroscopy
[Fe/H]=-0.81±0.02 (m.e.) [O/Fe]=+0.33 $[m_\alpha/Fe]$=+0.22±0.03 (m.e.)	Brown & Wallerstein (1992)	High-resolution CCD spectra of four giants

Helfer, Wallerstein & Greenstein (1959). Then, for example, $[m_\alpha/Fe]$ parameterises the enhancement, over iron, of the α-process elements oxygen, neon, magnesium, silicon, sulphur, titanium and so on.

If the abundances of individual metals in the stars of 47 Tuc are 'decoupled', that is, are not scaled-solar, then they cannot be characterised by only the one or two parameters,

such as [Fe/H] and [O/Fe], which fully characterise the abundances of all the metals in the scaled-solar composition stellar evolution calculations.

Stellar evolution models have yet to be calculated for an arbitrary mixture of metallicities, since, as VandenBerg (1992) points out, neither the opacities or model atmosphere calculations exist which would permit this. This immediately begs the following two questions. Can the existing scaled-solar metallicity isochrones be compared with the colour-magnitude observations of 47 Tuc to derive meaningful astrophysical parameters for the cluster, and if so, which metallicity isochrones should be used?

Specifically, consider the α-element enhancement in 47 Tuc. Although the scatter in the determinations of different studies is unfortunately large, it seems likely that in 47 Tuc the α-process elements are enhanced with respect to iron, and that the enhancement is probably in the range $\sim 0.2 < [m_\alpha/Fe] < \sim 0.5$. If the enhancement follows those seen, particularly for oxygen, in metal-poor field dwarf stars, then perhaps $[m_\alpha/Fe] > \sim 0.3$. Unfortunately the functionality of field-star oxygen enhancement with metallicity is also controversial - see the discussion in Section 2 of VandenBerg (1992) and papers by Bessel, Sutherland & Ruan (1991) and by Spite & Spite (1991).

$$\log_{10}(Z) = [Fe/H] + \log_{10}\left(0.6369 \times 10^{[m_\alpha/Fe]} + 0.3631\right) - 1.658 \qquad (6)$$

Straniero, Chieffi & Salaris (1991) have recently proposed a formula, reproduced in equation 6, which allows scaled-solar models to be corrected for an α-enhancement, given by $[m_\alpha/Fe]$, simply by rescaling to a new value of heavy-metal mass fraction Z. If we substitute $[Fe/H] \sim -1$ and $[m_\alpha/Fe] \sim 0.4$ into equation 6 we determine $Z \sim 4.3 \times 10^{-3}$. From Table 1 of VandenBerg (1992) we find that the isochrone with [Fe/H]=-0.65 and [O/Fe]=0.30 has a value of heavy metal mass fraction, *excluding* the oxygen enhancement, of $Z_0 = 4 \times 10^{-3}$.

The quality of the determinations of the α-enhancement of 47 Tuc stars precludes a more precise determination. However even from this handwaving argument, it would seem that we should compare our 47 Tuc colour-magnitude data to (scaled-solar abundance) isochrones which are more metal rich than the 'compromise' metallicity of $[Fe/H] \sim -0.8$.

This scheme for rescaling the isochrone metallicity to take into account an enhancement of the α-process elements, derived by Straniero *et al.* and reproduced in equation 6, was criticised by VandenBerg (1992) for being too simplistic. The enhancement of the α elements, with the exception of oxygen, will effect the stellar evolution calculations through their contribution to the opacity, and the relation implicitly assumes that the opacity at all values of temperature, pressure and density scales only with the number of

α nuclei. This assumption may be questionable, especially for lower abundances where free-free transitions of electrons from hydrogen and helium are the dominant source of interior opacity.

The stellar evolution calculations for low-metallicity stars should therefore be largely independent of the abundance of the α-process elements, excluding oxygen, upon which they sensitively depend through nucleosynthesis via the carbon-nitrogen-oxygen chain. For this reason, we should probably not apply the same rescaling to the low-metallicity scaled-solar isochrones before comparing them to our colour-magnitude data for M30 [and M13 & NGC6752].

2.8 The reddening of 47 Tuc

Values of the foreground reddening to 47 Tuc from the literature cover a range of ~0.07 magnitudes in E[B-V], giving the appearance that the true value of E[B-V] is as poorly defined as that of M30. However, most values tend to cluster around E[B-V]=0.04±0.01 (see Table 9) which we adopt, as did Hesser *et al.* (1987). We note that Bica & Pastoriza (1983) actually calculated E[B-V]=0.14, and their adopted value, quoted in Table 9, is the average of this value and other literature values from Zinn (1980).

3 CLUSTER DISTANCES FROM SUBDWARFS

3.1 Pros and cons of subdwarf derived distances

The idea behind deriving globular cluster distances from subdwarfs is simple enough. A fiducial main sequence is defined in a colour-absolute-magnitude plane by the positions of population II field subdwarf stars of accurately known parallax and similar abundance to the cluster in question. The observed cluster main sequence is then corrected for foreground reddening and the vertical magnitude shift necessary to overlay the apparent magnitude of the cluster main sequence onto the absolute magnitude of the fiducial sequence is the distance modulus.

Such a purely observational method produces distances which are independent of any assumptions about, for example, the brightness of the horizontal branch, and it's variation with abundance, or the brightness of the brightest cluster giants. Both of these latter have been used to derive cluster distances, and both are controversial.

The subdwarf method has several problems associated with it, however. First, it is observationally intensive, as it requires the cluster main sequence to be accurately defined

Table 9: Optical reddening estimates for 47 Tuc.

E[B-V]	Source	Method
0.03±0.02	Crawford & Snowden (1975)	uvbyβ photometry of 26 foreground A & F stars
0.03	Hesser & Philip (1976)	uvbyβ photometry of 10 early type stars
0.04±0.01	Lee (1977)	(U-B) vs (B-V) diagram of field stars
0.05±0.01	Burstein & Heiles (1978)	HI column density, assuming constant gas-to-dust ratio
0.08±0.04	Bica & Pastoriza (1983)	BV & DDO photometry

to a depth of at least 3 V magnitudes below the main-sequence turn-off. This causes problems when working in the infrared, due to the current small size of infrared detectors, forcing observers to compromise between achieving great depth on a few stars and covering a large enough area to populate well the main sequence. The main-sequence fitting method is also not viable for extragalactic clusters where photometry of individual stars, whether below the turn-off or not, is not possible.

Second, the number of field subdwarfs with accurately known parallax and of the correct composition for comparison with any significantly metal-poor population is pitifully small, and the number with infrared photometry smaller still [see, for example, Laird, Carney & Latham (1988)].

Third, there are the Lutz-Kelker corrections to consider; despite three decades of study, the existence and size of these corrections is still controversial. At their most basic (Lutz & Kelker 1973) these correct a Malmquist bias caused by observational errors on the parallax. Consider observing a parallax-limited, equivalent to a volume-limited, sample of stars in some solid angle forming a cone of space about a line of sight. A given parallax $\pi \pm \sigma_\pi$ defines some distance $d \pm \sigma_d$ along the line of sight. However, the *volume* in the cone between d and $d+\sigma_d$ is greater than that between $d-\sigma_d$ and d. For, say, a constant space density of stars, more stars will be scattered into the cone, by observational errors, from the larger volume outside than will be scattered out from the smaller volume inside. Thus the sample of stars at a given parallax π, not just at the limiting parallax, will be biased towards fainter magnitudes. The Lutz-Kelker corrections give the amount by which the parallax-determined absolute magnitude of a star must be made brighter to correct for this bias. The corrections increase with σ_π/π, meaning that those stars which are furthest away and/or have the largest errors on their parallax determinations have the largest Lutz-

Kelker corrections. Later studies of the Lutz-Kelker effect incorporate dynamical and space density models in their derivations [see, for example, Smith 1987a and 1987b; see also Koen 1992 for estimates of the confidence intervals on the corrections].

3.2 Basic subdwarf data

The metallicities, absolute visual magnitudes and (V-K) colours for five subdwarfs of known parallax and of similar metal content to M13 and NGC6752 have been taken from Table II of Laird, Carney & Latham (1988) and are reproduced here in Table 10, as are the trigonometric parallaxes (π) and errors (σ_π) from Sandage (1983). The final column gives ΔM, the amount that must be added to the absolute magnitudes to correct for the full Lutz-Kelker effect, which was determined by linear interpolation in Table I of Lutz & Kelker (1973) using the values of σ_π/π from column six of our Table 10. There are in fact seven stars ostensibly suitable for comparison with M13 and NGC6752 in the Laird *et al.* Table II. However we have disregarded two of these, both on the basis of poor fits to model isochrones. After correcting for differences in metallicity between the subdwarfs, Laird *et al.* themselves disregarded HD194598 as having a greater deviation from the isochrones (both with and without oxygen enhancement) than was allowed by the errors. Similarly we disregarded HD64090, which Straniero & Chieffi (1991) note fits their models poorly compared to the other subdwarfs.

We note that the Laird *et al.* absolute visual magnitude of HD201891 is some 0.3 magnitudes fainter than the value used by Straniero & Chieffi. However, with the brighter value, this star lies above the Straniero & Chieffi isochrone and fits only at the limit of the error bars (their figure 3), whereas using the fainter value of M_V=5.43 lowers this star almost exactly onto the isochrone. Indeed, using the Laird *et al.* M_V values for the other subdwarfs also tends to reduce the residuals from the isochrone, although it does not improve the position of the discrepant HD64090 enough to warrant inclusion. The colour differences between the two studies are negligible.

Table II of Laird *et al.* lists parameters of only three stars with [Fe/H]<-1.5, and since HD140283 is now known to be a subgiant, this leaves only BD+66°268, at [Fe/H]=-2.06, with similar metallicity to M30. Similarly, there are only two stars with compositions similar to 47 Tuc at [Fe/H]=-0.65 and none for the more metal poor 'compromise' abundance of [Fe/H]~-0.8.

Although several studies in the past have determined cluster distances based on main sequence fits to only one subdwarf, usually Groombridge 1830 (HD103095), we have adopted the more widely used procedure of correcting the observed parameters of the larger sample of [Fe/H]~-1.4 subdwarfs for the difference between their abundance and

Table 10: Basic data for the five intermediate metallicity subdwarfs.

Star	[Fe/H]	M_V	(B-V)	(V-K)	$(\pi\pm\sigma_\pi)$/mas	ΔM
HD25329	-1.33	7.17	0.865	2.275	53±4	-0.06
HD103095	-1.36	6.76	0.750	2.015	116±5	-0.02
HD134439	-1.46	6.98	0.760	2.040	37±4	-0.13
HD134440	-1.46	7.36	0.850	2.280	37±4	-0.13
HD201891	-1.42	5.43	0.510	1.420	41±6	-0.26

that of M30 or 47 Tuc. We have also included in the sample of subdwarfs information for BD+66°268 [M_V=6.72±0.24, (B-V)=0.650, (V-K)=1.835, π=(23.0±2.7) milli-arcseconds & ΔM=-0.16]. Our *modus oparandi* for this correction is that adopted by Laird, Carney & Latham, who change the absolute magnitudes of the subdwarfs at fixed colour, by an amount determined differentially between isochrones of the relevant abundances. Other authors have opted to apply corrections to the subdwarf colours keeping the absolute magnitudes fixed. Neither of these methods mimic a physical change, in the sense that if one could somehow add extra metals to a star, both temperature (colour) and luminosity would change. However, provided the isochrones reproduce the shape of the real main sequence, both of these methods are analogous. We have adopted the Laird, Carney & Latham method to keep fixed the subdwarf colours, which have smaller errors than the absolute magnitudes, and also so that, when correcting to more metal rich abundances, the reddest subdwarfs should not become even redder and be matched to fainter main-sequence stars where the observational errors are larger. This latter is a very slight effect in the case of our data, however, since the 47 Tuc main sequence is very well defined.

The corrections to M_V and M_K in each colour magnitude plane were estimated using the 16 Gyr Bergbusch & VandenBerg isochrones in the same plane differentially between [Fe/H]=-1.48 [-2.03 for BD+66°268] for the original sample of subdwarfs and [Fe/H]=-2.26 for M30, or [Fe/H]=-0.65 and -0.78 for 47 Tuc. The values of ΔV and ΔK to be added to the absolute magnitudes in planes with (V-K) and (B-V) as the colour, are shown in Table 11.

Two comments must be made regarding the contents of Table 11. First, note that the correction to be applied to the absolute V magnitude of BD+66°268 in V, (V-K), to change the abundance from [Fe/H]=-2.03 to -2.26 was calculated to be -0.04 magnitudes. This is in the wrong sense; a more metal deficient subdwarf should be fainter than a metal-rich subdwarf. The V, (V-K) [Fe/H]=-2.03 isochrone main sequences cross over those of the [Fe/H]=-2.26 such that to the red of the crossover point the [Fe/H]=-2.03 isochrone is

Table 11: Corrections to be added to the subdwarf absolute magnitudes to convert to the indicated abundances.

Star	[Fe/H]=-2.26	[Fe/H]=-0.65		[Fe/H]=-0.78	
	ΔV	ΔV	ΔK	ΔV	ΔK
	Corrections to V, (V-K) and K, (V-K)				
HD25329	0.10	-0.36	-0.37	-0.31	-0.31
HD103095	0.08	-0.35	-0.35	-0.28	-0.29
HD134439	0.08	-0.35	-0.35	-0.29	-0.29
HD134440	0.10	-0.36	-0.36	-0.32	-0.31
HD201891	0.17	-0.48	-0.48	-0.37	-0.37
BD+66°268	-0.04	-0.47	-0.46	-0.40	-0.39
	Corrections to V, (B-V) and K, (B-V)				
HD25329	0.27	-0.45	-0.40	-0.36	-0.33
HD103095	0.24	-0.48	-0.41	-0.39	-0.33
HD134439	0.24	-0.47	-0.41	-0.38	-0.33
HD134440	0.26	-0.45	-0.39	-0.37	-0.32
HD201891	0.40	-	-	-	-
BD+66°268	0.06	-0.74	-0.61	-0.62	-0.51

fainter - in the case of the 16 Gyr isochrone this crossover occurs at (V-K)~1.73 and M_V~6.15. This crossover is not seen in the V, (B-V) isochrones; it could indicate incorrect metallicity dependencies either of Bell's bolometric corrections, or of his suggested colour shift, or both. Second, the colour of HD201891 is to the blue of the turn-off of the 16 Gyr [Fe/H]=-0.65 isochrone, although not of the [Fe/H]=-0.78 isochrone. It can, however, be corrected to both of these abundances in V, (V-K) or K, (V-K). We have not included it in the sample of subdwarfs in V, (B-V) or K, (B-V) at either [Fe/H]=-0.65 or -0.78, but it is included in V, (V-K) and K, (V-K). Looking ahead to the distance determinations of 47 Tuc from these subdwarfs, we shall see that the r.m.s. fitting errors to the fiducials are similar, indicating that both samples match the shape of the respective fiducials equally well.

3.3 Sensitivity of the subdwarf fits to various sources of error

In sections 3.4 to 3.6 below we use the subdwarf information of the previous section to derive distances to the four clusters by main-sequence fitting. First, though, we present the results of simulations, involving subdwarf fits (without Lutz-Kelker corrections) to the isochrones, in an attempt to determine which, if any, of the colour-magnitude planes that we have at our disposal will produce distances which are least sensitive to the likely sources of error.

Such determinations have already been presented by Buckley & Longmore (1992), although in the absence of the Bergbusch & VandenBerg optical isochrones we used the Straniero & Chieffi V, (B-V) models, and matched these with the Bergbusch & VandenBerg V, (V-K) isochrones from Bell (1992) to form K, (B-V). As we pointed out at the time, these two sets of models use different input physics; we now present a re-analysis, using only the Bergbusch & VandenBerg isochrones. Our *a priori* expectations, however, are that the conclusions reached by Buckley & Longmore will not be substantially changed; as VandenBerg (1992) points out, the Straniero & Chieffi isochrones have similar upper main sequences in V, (B-V) to those Bergbusch & VandenBerg, even though the M_{bol} versus $\log_{10}(T_e/K)$ loci differ.

3.3.1 Sensitivity to systematic shifts

An important result of these simulations is the reduced sensitivity to systematic errors of the distances determined from the V, (V-K), K, (V-K) and K, (B-V) planes compared to those determined from V, (B-V).

For this simulation we used the 16 Gyr [Fe/H]=-1.48, [O/Fe]=0.60 isochrones. The systematic shifts were simulated by arranging 5% shifts in B and V and 5, 10 and 15% shifts in K, such that the colour of the isochrone was made redder by 10% in (B-V) and by 10, 15 and 20% in (V-K). These criteria also determine in which direction the magnitude of the isochrone should shift for V, (B-V), V, (V-K) and K, (V-K) but not K, (B-V) for which we shift K to both fainter and brighter magnitudes. The results are summarised in Table 12 where Δ is the shifted minus the unshifted distance modulus. Since $\Delta_{V,\ (V-K)}$, $\Delta_{K,\ (V-K)}$ and $\Delta_{K,\ (B-V)}$ are all less than $\Delta_{V,\ (B-V)}$, this indicates that the distances derived from subdwarf fitting in the V, (V-K), the K, (V-K) and the K, (B-V) planes are all affected less by the systematic shifts described above than those determined in V, (B-V). This is not a full simulation involving every possible combination of systematic shift in each colour; indeed, it is possible to arrange some shifts where the distances determined from the optical-infrared planes fare worse than those determined from V, (B-V). It does, however, indicate that distances derived from subdwarf fitting

Table 12: The sensitivity of the distance moduli to systematic shifts in the isochrones. The K, (V-K) results are identical to those for V, (V-K).

$\frac{\delta_K}{magnitudes}$	$\frac{\Delta_{V,(V-K)}}{\Delta_{V,(B-V)}}$	$\frac{\Delta_{K,(B-V)}}{\Delta_{V,(B-V)}}$
0.05	0.30	0.52, 0.32
0.10	0.54	0.62, 0.22
0.15	0.80	0.72, 0.12

in optical-infrared colour-magnitude planes are less sensitive to *some* systematic effects than are distances derived from V, (B-V).

3.3.2 Sensitivity to small photometric errors

If it is assumed that the dominant source of noise in an observation is the 'shot' noise of photons from the source if the source is brighter than the sky background, or of photons from the sky if it is not, then given a magnitude m_1 and error $\sigma(m_1)$ at that magnitude, it is possible to calculate the error $\sigma(m_2)$ at another magnitude m_2 via equation 7 if both m_1 and m_2 are fainter than the sky background, or equation 8 if both are brighter than the sky background. It is trivial to combine the two above equations if m_1 and m_2 are on opposite sides of the sky background. Note that the former equation applies exclusively to our M13 observations since the K band sky is very bright, typically ~13.5 magnitudes per square arcsecond above Mauna Kea.

Equations 7 and 8 have been used to add a realistic run of photometric errors to the isochrone mentioned in section 3.3.1, and the scheme used for this is briefly outlined now. Realistic values of the B and V errors at the M13 main-sequence turn-off were determined to be $\sigma_{V,MSTO}$=0.005 and $\sigma_{B,MSTO}$=0.004 magnitudes. Together with the isochrone turn-off magnitudes of V_{MSTO}=4.24 and B_{MSTO}=4.62 and the sky magnitudes per square arcsecond corrected for distance modulus (V_{sky}=7.09 and B_{sky}=7.59) these define the run of photometric errors in B and V. A value of $\sigma_{K,MSTO}$ was chosen to be some multiple of $\sigma_{V,MSTO}$ and coupled with K_{MSTO}=3.07 to define the run of K photometric errors. At each point on the isochrone, say V, V-K, an error box was defined to be $V\pm\sigma_V$, $(V-K)\pm\sqrt{(\sigma_V^2+\sigma_K^2)}$. Two new isochrones were defined which passed through the upper

$$\sigma(m_2) = \sigma(m_1)10^{0.4(m_2-m_1)} \qquad (7)$$

$$\sigma(m_2) = \sigma(m_1)10^{0.2(m_2-m_1)} \quad (8)$$

and lower corners of the error box, as shown schematically in figure 1. The true, 'upper' and 'lower' isochrones were fitted to the subdwarfs, without Lutz-Kelker corrections, and the differences in 'distance moduli' found. The above steps were repeated in all the colour-magnitude planes for several values of $\sigma_{K,MSTO}$. Figures 2(a) and (b) present the difference in 'distance moduli' from the mixed optical-infrared isochrones compared to that from the purely optical isochrone, in the sense distance from true isochrone minus distance from (a) the 'upper' isochrone and (b) the 'lower' isochrone, against the ratio $\sigma_{K,MSTO}/\sigma_{V,MSTO}$. Points falling below one on the ordinate indicate where the mixed optical-infrared isochrones give distances from subdwarf fitting which are less sensitive to small photometric errors than the purely optically derived distances.

We find that the distances determined from the subdwarfs in V, (V-K) and K, (V-K) are less sensitive to small photometric errors than those determined in V, (B-V) until σ_K is greater than 2 to 3 times σ_V. The tracks which show the K, (B-V) results are somewhat different than those which appeared in Buckley & Longmore (1992), which unfortunately contained an error; the value of B_{MSTO} was accidentally set ~0.8 magnitudes too bright, leading to an overestimate of the errors at fainter magnitudes.

Of course, a fiducial derived from data containing random photometric errors will not pass through the upper or lower corners of the 1σ error boxes - a systematic depth-dependent error would be needed for this to happen. However, the 'upper' and 'lower' isochrones set limits between which a fiducial should lie. Thus the absolute effects of the simulated photometric errors on the derived distances will be grossly exaggerated, but comparing one plane with another - as in figures 2(a) and (b) - should indicate the *relative* effects of the photometric errors. We realise, though, that the results presented in figures 2(a) and (b) are only strictly valid if some depth-dependent systematic error causes a derived fiducial to lie completely to one side or the other of the true location. Such systematic effects could be caused by crowding and incompleteness - as seen in our M30 main-sequence data, or by problems with photometric colour equations - where the depth dependence may be in reality a colour dependence. See for example the discussion in section 6.2 regarding the differences found between the NGC6752 lower main-sequence fiducials of Penny & Dickens and other authors. More reasons why the results of this simulation should not be taken at face value are mentioned at the end of section 3.3.4 below.

Clearly, further simulations, possibly along the lines of a Monte-Carlo simulation, are required.

Figure 1: Schematic showing how the 'upper' and 'lower' isochrones were defined.

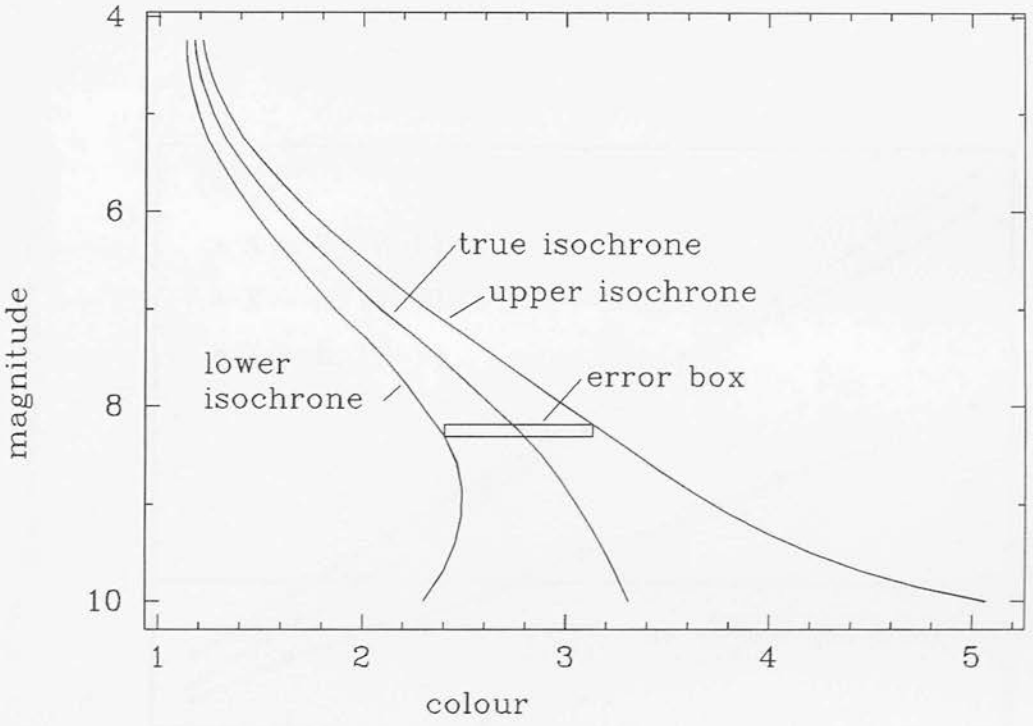

3.3.3 Sensitivity to errors in adopted cluster reddening

To illustrate the sensitivity of the distance determination to errors in the ratio of total-to-selective extinction, we give here a specific example where R - R_{true} = -1 and the assumed original reddening to the 'cluster' is E[B-V]=0.4. Although we used a metallicity appropriate to M13, this example is perhaps more appropriate to M4 where R may be as high as 4 (Liu & Janes, 1990, Dixon & Longmore, 1993). In this case we determined $\Delta_{K,\ (B-V)}$=-0.04±0.13 while $\Delta_{V,\ (V-K)}$=0.29±0.16 and $\Delta_{V,\ (B-V)}$=-0.40±0.16 where Δ is distance modulus(R_{true}) - distance modulus(R). Figure 3 presents results again for R-R_{true}=-1 and for reddenings in steps of 0.05 magnitudes between E[B-V]=0.05 and 0.40.

For the more conventional value of R=3.08 the distances derived from each plane are, within the errors, affected equally by small errors (±0.03 magnitudes) in the value of E[B-V], as shown in figure 4. The distances from V, (V-K) are *slightly* more sensitive and at the extreme ends of the range of E[B-V] considered here, give distances large or smaller by 0.01 to 0.02 magnitudes than those from V, (B-V). The r.m.s. fitting errors in V, (V-K), however, are less than those in the other planes, indicating that the subdwarfs give a tighter fit to the isochrones in this plane.

Figure 2: The sensitivity of distances derived from subdwarf fitting to small photometric errors.

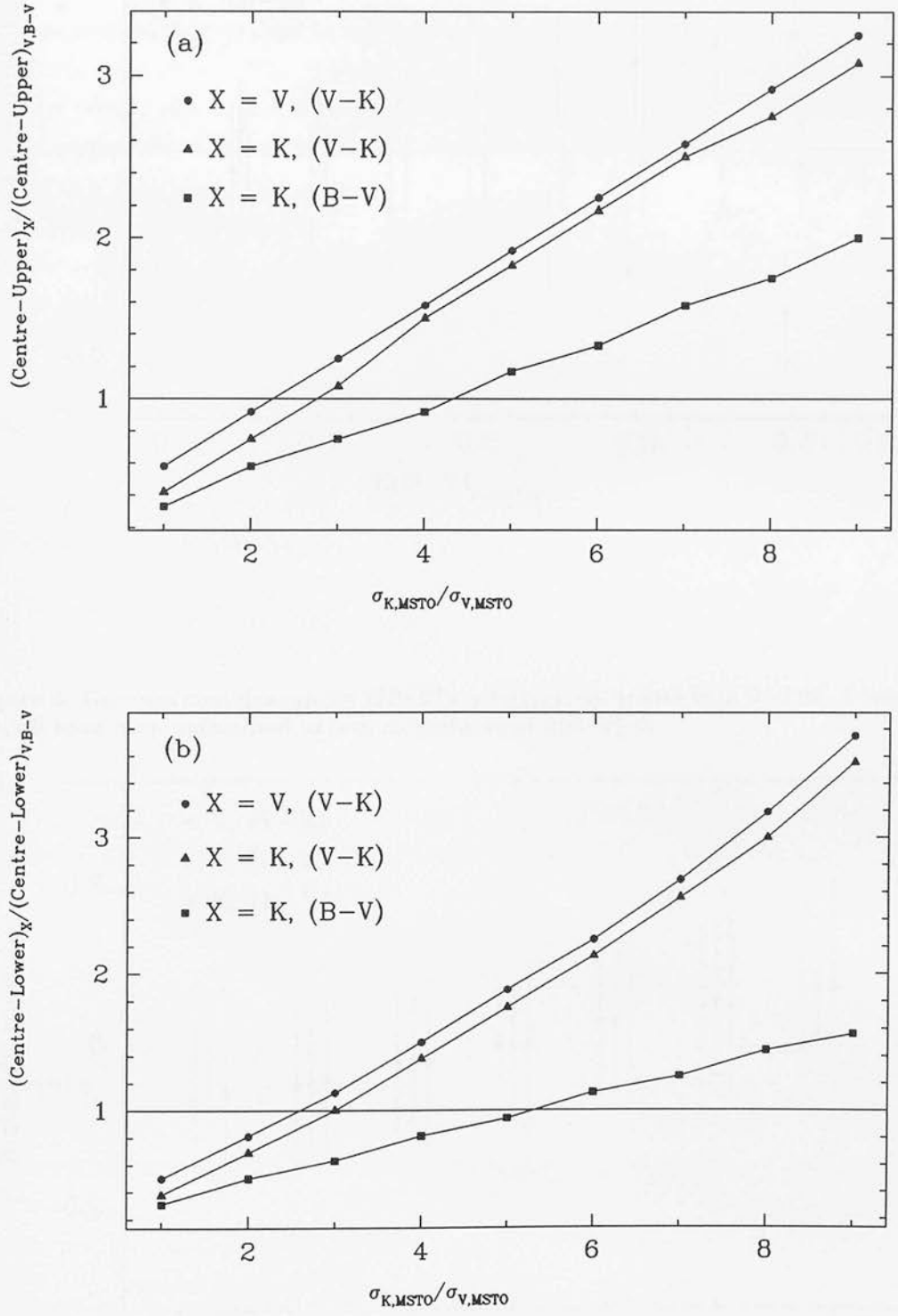

Figure 3: Δ distance modulus plotted against 'cluster' reddening for $R-R_{true}=-1$.

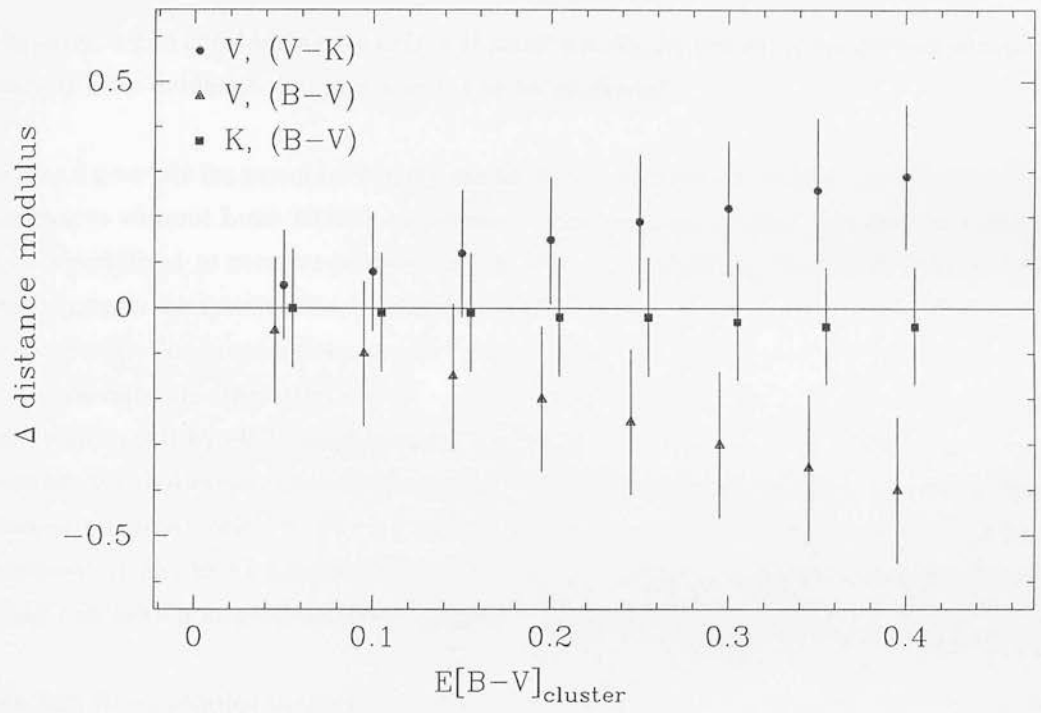

Figure 4: Distance modulus against E[B-V] for 16 Gyr isochrones with R=3.08. Distance moduli have been normalised to zero magnitudes at E[B-V]=0.

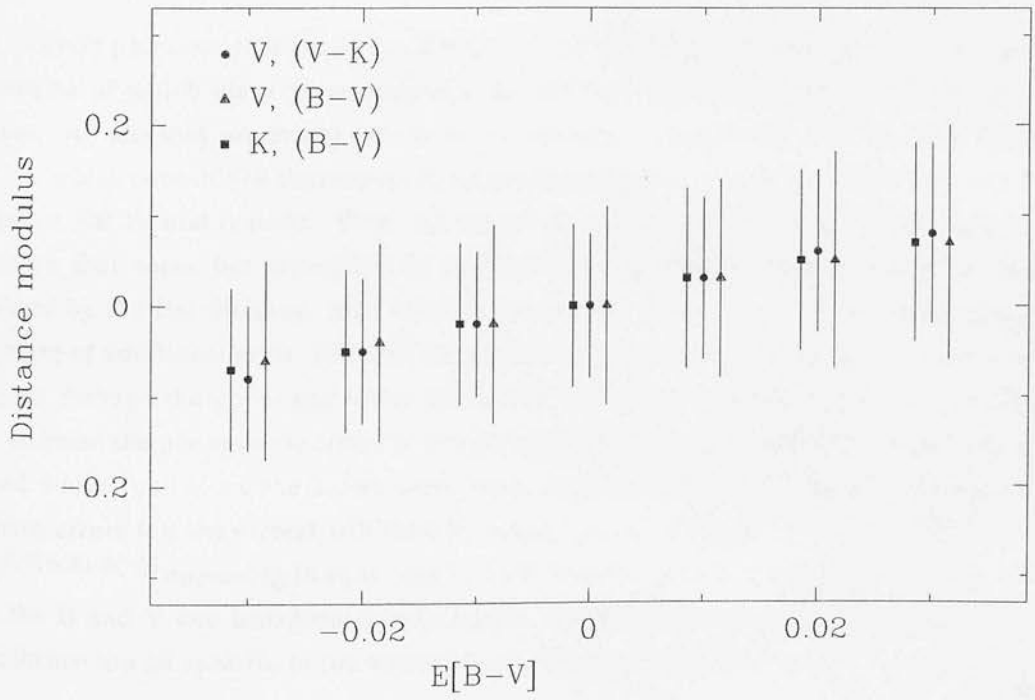

3.3.4 Sensitivity to metallicity errors

Similarly, when considering the effect of small metallicity errors on the derived distances, there is little evidence that any plane is to be preferred.

Figure 5 presents the results of fitting the 16 Gyr isochrones of various metallicities to the subdwarfs without Lutz-Kelker corrections. The 'distance moduli' thus determined have been normalised to zero magnitudes at [Fe/H]=-1.4, which required 0.00, 0.04 and 0.02 magnitudes to be systematically added to the V, (V-K), V, (B-V) and K, (B-V) distances respectively. Considering the metallicity range [Fe/H]=-1.4±0.4 we find that all the planes will overestimate the distance by ~0.15 magnitudes at the metal-poor end and underestimate it by ~0.21 magnitudes at the metal-rich end. It is only at the very extreme ends of this ±0.4 range, and outside it, where differences in the sensitivities of the planes become apparent, with V, (V-K) showing the least sensitivity and V, (B-V) the most. However, if one had a colour-magnitude diagram complete with giant branch, say, it is likely that such a large abundance mismatch would be very obvious.

The best fit quadratics through the data points are given by equations 9, where those for the individual planes are given prior to normalisation to zero at [Fe/H]=-1.4.

$$\begin{aligned} d &= -0.172[Fe/H]^2 - 0.830[Fe/H] - 0.821 && V,(V-K) \\ d &= -0.200[Fe/H]^2 - 1.105[Fe/H] - 1.195 && V,(B-V) \\ d &= -0.200[Fe/H]^2 - 1.026[Fe/H] - 1.065 && K,(B-V) \\ \Delta d &= -0.191[Fe/H]^2 - 0.987[Fe/H] - 1.007 && \textit{combined} \end{aligned} \qquad (9)$$

We should point out that the above simulations do not present a definitive answer to the question of which plane gives distances that are less sensitive to the various sources of error. At best they are meant only to be illustrative. In particular, the results of section 3.3.2, which determined the sensitivity to small photometric errors, should be treated with caution for several reasons. First, the actual photometric errors will not be due just to photon shot noise, but depending on the instrument used may contain additional errors caused by the flat-fielding, read noise or bias subtraction to name a few array-specific sources of additional error. Second, the errors will *not* produce a fiducial sequence which passes through the upper and lower corners of the 1σ error boxes. Third, it is difficult to estimate the photometric errors at any given point, such as the main-sequence turn-off used above, and since the errors were small, significant changes could be introduced. These errors (on the errors) will then be magnified by the factors of $10^{0.4[m(2)-m(1)]}$ or $10^{0.2[m(2)-m(1)]}$ appearing in equations 7 and 8. Fourth, most of the parameters used, such as the B and V sky background magnitudes, the distance modulus and the age of the isochrone are all specific to the observing site or the cluster in question.

Figure 5: The sensitivity of distances derived from subdwarf fitting to errors in the adopted metallicity of the cluster. Distance moduli have been normalised to zero magnitudes at [Fe/H]=-1.4.

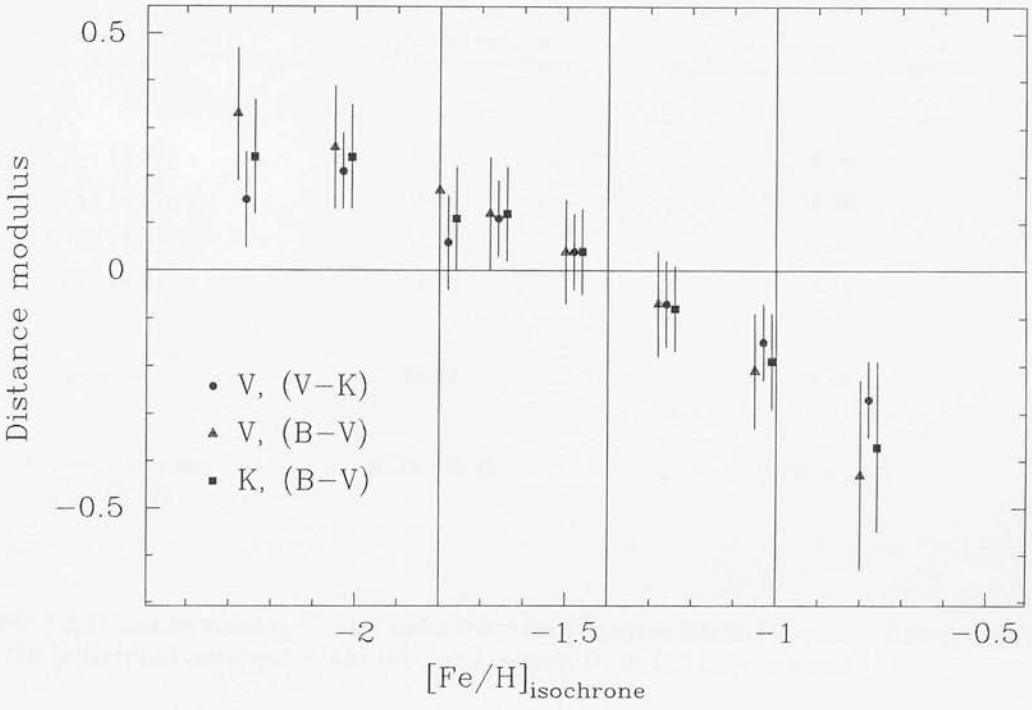

The method of determining distances from subdwarf fitting, then, will depend on many factors, including the sizes of the estimated internal and systematic errors in the photometry, the size of the cluster reddening, and whether there is evidence for an anomalous value of the ratio of total-to-selective extinction R. At the least, a comparison of distances determined separately in each plane may highlight for example, a potentially discrepant value of R.

3.4 The distance to M13

Although our K photometric data for M13 define the main-sequence turn-off region accurately, the main sequence at the colours of the subdwarfs shows considerable scatter, as can be seen from V, (V-K), K, (V-K) and K, (B-V) colour-magnitude diagrams in figure 2 of Buckley & Longmore (1992). This makes it difficult to objectively determine a distance to M13 in these planes. We have, however, determined distances in these three planes since the K data offer a photometrically independent contribution. We have also determined a distance in the V, (B-V) plane *containing only those stars with matching K data*, for comparison with the distance determined from the full optical dataset, in order to glean an idea of any systematic errors introduced by the limited dataset.

Table 13: Distance moduli for M13 from the subdwarf fits. In view of the scatter in the data, and the errors involved in fitting the subdwarfs by eye, the error on these figures is probably ±0.15 magnitudes.

Colour-magnitude plane	True distance modulus (no Lutz-Kelker corrections)	True distance modulus (full Lutz-Kelker corrections)
V_0, $(V-K)_0$	14.27	14.44
K_0, $(V-K)_0$	14.25	14.36
V_0, $(B-V)_0$	14.26	14.45
K_0, $(B-V)_0$	14.30	14.52
mean	**14.27**	**14.44**
Richer & Fahlman V_0, $(B-V)_0$	14.25 ± 0.13	14.37 ± 0.15

Table 14: Distance moduli of NGC6752 from least squares fits to fiducials. Errors quoted on the individual determinations are r.m.s. errors from the least squares fit.

Colour-magnitude plane	True distance modulus (no Lutz-Kelker corrections)	True distance modulus (full Lutz-Kelker corrections)
V_0, $(V-K)_0$	13.01 ± 0.11	13.13 ± 0.14
K_0, $(V-K)_0$	13.03 ± 0.11	13.15 ± 0.16
V_0, $(B-V)_0$	13.01 ± 0.13	13.13 ± 0.17
K_0, $(B-V)_0$	13.02 ± 0.13	13.14 ± 0.18
mean	**13.02 ± 0.12**	**13.14 ± 0.16**
Penny & Dickens (1986) V_0, $(B-V)_0$	12.99 ± 0.13	13.11 ± 0.17

A best fit by eye of the subdwarfs directly to the M13 main sequence has been performed in each plane and the results summarised in Table 13, together with the means in each case. In order to perform the fit by eye without being influenced by previously determined results, a colleague was asked to apply an offset to the magnitudes in each plane, leaving the colours unchanged, and the fit was performed without knowledge of these shifts. The distances determined, both with and without Lutz-Kelker corrections, are in good agreement with those determined from our subdwarfs and the V, (B-V) fiducial of Richer & Fahlman (1986). The dwarfs have been marked on figures 2(a) to (c)

of Buckley & Longmore corrected to the mean distance modulus without the Lutz-Kelker corrections.

We thus determine a distance modulus for M13 of 14.27 magnitudes without Lutz-Kelker corrections or 14.44 magnitudes with full Lutz-Kelker corrections. We estimate the errors to be ±0.15 magnitudes. These correspond to distances of 7.1 and 7.7 kpc.

3.5 The distance to NGC6752

Our NGC6752 main sequence is much better defined than that of M13, but still consists of too few stars to define the fiducial objectively. A smooth sequence was drawn by hand through the data on each colour-magnitude plane, digitised and transferred to the computer where distance moduli were found by least squares fitting to the subdwarf data. The least squares fits were performed such that the squared magnitude difference of the subdwarfs about the fiducial was minimised. This formulation was used because the subdwarf colours have small errors compared to the uncertainties in their absolute magnitudes, which are dominated by errors in the parallax. The results are presented in Table 14, as is the fit of the subdwarfs to the fiducial of Penny & Dickens (1986). The mean distance determined from the four optical-infrared colour-magnitude planes is in very good agreement with that determined from the fiducial drawn through the full optical dataset by Penny & Dickens, indicating that negligible bias has been introduced by our used of the smaller datasets.

As an aside, it is worth mentioning that we also determined the distances using the by-eye method employed for the M13 data, and also by fitting isochrone main sequences to the colour-magnitude data, the latter then being corrected onto the subdwarf absolute magnitude scale by fitting the isochrones to the subdwarfs. From these two methods we determined distances without Lutz-Kelker corrections of 13.05±0.18 and 13.03±0.24 magnitudes respectively, which are in excellent agreement with those determined from the fiducials.

We adopt a distance modulus for NGC6752 of 13.03±0.18 magnitudes determined without Lutz-Kelker corrections, or 13.15±0.20 magnitudes including full Lutz-Kelker corrections. These correspond to distances of 4.0 or 4.3 kpc respectively.

3.6 The distances to 47 Tuc and M30

Fiducials were drawn, again by hand, through the 47 Tuc colour-magnitude diagrams, and transferred to the computer. The results of the subdwarf fits, using the subdwarfs

Table 15: Distance moduli of 47 Tuc and M30 from least squares fits of subdwarfs to fiducials. Quoted errors are r.m.s. errors from the least squares fits. Numbers in parentheses indicate the number of subdwarfs used in the fits.

Plane	True distance modulus from fiducials	
	No Lutz-Kelker corrections	Full Lutz-Kelker corrections
47 Tuc [Fe/H]=-0.78 [O/Fe]=0.39		
V_0, $(V-K)_0$	13.17±0.10 (6)	13.29±0.09 (6)
K_0, $(V-K)_0$	13.17±0.11 (6)	13.30±0.11 (6)
V_0, $(B-V)_0$	13.15±0.15 (5)	13.25±0.11 (5)
K_0, $(B-V)_0$	13.11±0.14 (5)	13.21±0.10 (5)
mean	13.15±0.13	13.26±0.10
Hesser *et al.* V_0, $(B-V)_0$	13.11±0.16 (5)	13.21±0.12 (5)
47 Tuc [Fe/H]=-0.65 [O/Fe]=0.30		
V_0, $(V-K)_0$	13.23±0.10 (6)	13.36±0.11 (6)
K_0, $(V-K)_0$	13.24±0.11 (6)	13.36±0.12 (6)
V_0, $(B-V)_0$	13.24±0.14 (5)	13.34±0.10 (5)
K_0, $(B-V)_0$	13.19±0.13 (5)	13.29±0.09 (5)
mean	13.23±0.12	13.34±0.11
Hesser *et al.* V_0, $(B-V)_0$	13.20±0.15 (5)	13.30±0.11 (5)
M30 [Fe/H]=-2.26 [O/Fe]=0.75		
Richer *et al.* V_0, $(B-V)_0$	14.54±0.11 (4)	14.68±0.12 (4)

corrected to [Fe/H]=-0.65 and the 'compromise' abundance of [Fe/H]=-0.78, are shown in Table 15.

Remembering the results of the artificial star experiments on the M30 mosaics, discussed in Chapter 1, which indicated that the main sequences in our colour-magnitude diagrams are biased to the red by incompleteness and crowding errors, we have determined the distance to M30 by fitting our subdwarfs corrected to [Fe/H]=-2.26, to the V, (B-V)

fiducial of Richer et al. (1988) only. The fact that we have not used the V, (V-K) subdwarfs, means that the distance estimate is unaffected by the problem of the abundance correction for BD+66°268 discussed in section 3.2 above. The distance to M30 is also reported in Table 15.

For 47 Tuc we determine distances of 4.4 and 4.7 kpc respectively without and with full Lutz-Kelker corrections if, as we argued in section 2.7, the abundance is [Fe/H]=-0.65, while we determine distances of 4.3 and 4.5 kpc if the abundance is [Fe/H]=-0.78.

The adopted distance moduli from each cluster determined from the subdwarfs both with and without Lutz-Kelker corrections are summarised in Table 16. We must wait until section 6, where we use these distances to compare the colour-magnitude diagrams to the isochrones, before making any further comment about which abundance to select for 47 Tuc.

Before we use these distances to derive ages from isochrones, in the next section we discuss the derivation of distance and reddening independent ages.

4 DISTANCE AND REDDENING INDEPENDENT AGE ESTIMATES

VandenBerg, Bolte & Stetson (1990) were the first to use the (B-V) colour difference between the main-sequence turn-off and the subgiant branch as a diagnostic of the age of globular clusters [see also Sarajedini & Demarque (1990) who made a similar proposal independently]. They used this diagnostic, which is independent of cluster distance and reddening and also photometric zero-point errors, to search for age differences among clusters of similar abundances. They further remark that, although it is possible to calibrate the Δ(B-V) versus age relation with theoretical isochrones, the ages thus determined could not be relied upon because the colour of the subgiant branch predicted from theoretical models is too sensitive to uncertainties in convection theory and colour transformations, amongst other things.

However, the (V-K) colour difference between the turn-off and subgiant branch, when calibrated from the isochrones is independent not only of reddening and so forth, *but also of any systematic shifts in the isochrone colours*, such as the 0.12 magnitude correction suggested by Bell (1992). While we wholeheartedly agree with the warning given by VandenBerg, Bolte & Stetson, we believe that absolute ages derived from both Δ(V-K) and Δ(B-V) calibrated by the isochrones, could offer an important constraint on cluster ages *when compared to absolute ages derived from the isochrones matched to the cluster colour-magnitude diagrams.* In this case, we expect that any problems in the subgiant-branch colours will show up as mismatches between the colour-magnitude diagrams and

Table 16: Summary of the distances determined for each cluster from main-sequence fitting to subdwarfs. Distances with and without full Lutz-Kelker corrections are given.

Cluster	True distance moduli		
	No Lutz-Kelker corrections	Full Lutz-Kelker corrections	
M30	14.54±0.11	14.68±0.12	
M13	14.27±0.15	14.44±0.15	
NGC6752	13.02±0.12	13.14±0.16	
	13.23±0.12	13.34±0.11	[Fe/H]=-0.65
47 Tuc	13.15±0.13	13.26±0.10	[Fe/H]=-0.78

the isochrones.

Following VandenBerg, Bolte & Stetson, the (V-K) and (B-V) colours of the subgiant branch are determined at a level which is 2.5 V magnitudes brighter than a point 0.05 magnitudes to the red of the turn-off in (V-K) or (B-V). They chose this point on the main sequence as a reference point because the main sequence is flat enough there to match two colour-magnitude diagrams. Provided it is done consistently, however, the exact level at which the subgiant branch colour is determined is unimportant.

Figures 6, 7 and 8 show both Δ(V-K) and Δ(B-V) as functions of age, calculated from the Bergbusch & VandenBerg isochrones with the abundances of M30, M13 & NGC6752 and 47 Tuc respectively. Note the greater (V-K) colour differences between the isochrone turn-offs and the subgiant branches compared to the (B-V) colour differences. This indicates that for comparable photometric accuracy, ages derived from Δ(V-K) should be more accurate by a factor of ~2 than those derived from Δ(B-V), whether absolute or relative.

In Table 17 we present the observed main-sequence turn-off and subgiant branch colours determined from the same fiducials used to derive distances in the previous section. We also tabulate these quantities determined from the fiducials drawn through the full optical datasets by the authors noted in the table. In each case there is excellent agreement between the values of Δ(B-V) determined from our fiducials and from those determined from fiducials drawn through the full optical datasets. The errors on the colours were estimated by eye based on the scatter of the data around the fiducials. Since the subgiant branch is almost vertical in both V, (V-K) and V, (B-V) the scatter about the fiducial is the dominant source of error on the colour of the subgiant branch, rather than any error

Figure 6: The (V-K) and (B-V) colour differences between the main-sequence turn-off and the subgiant branch versus age from the Bergbusch & VandenBerg isochrones of suitable abundance for comparison with M30 data.

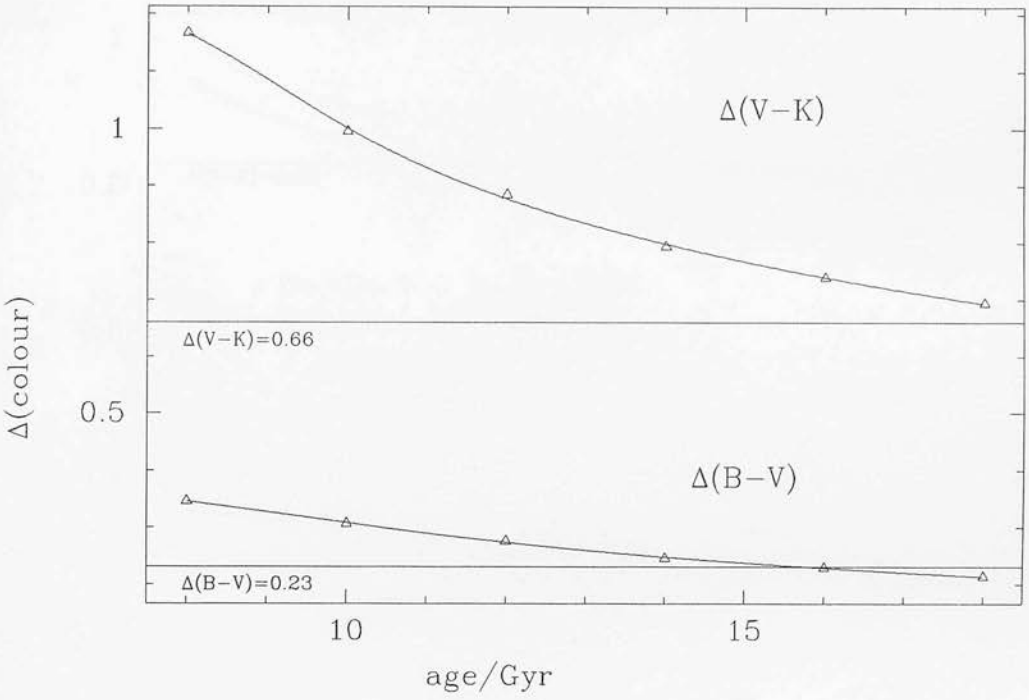

Figure 7: The (V-K) and (B-V) colour differences between the main-sequence turn-off and the subgiant branch versus age from the Bergbusch & VandenBerg isochrones of suitable abundance for comparison with M13 and NGC6752 data.

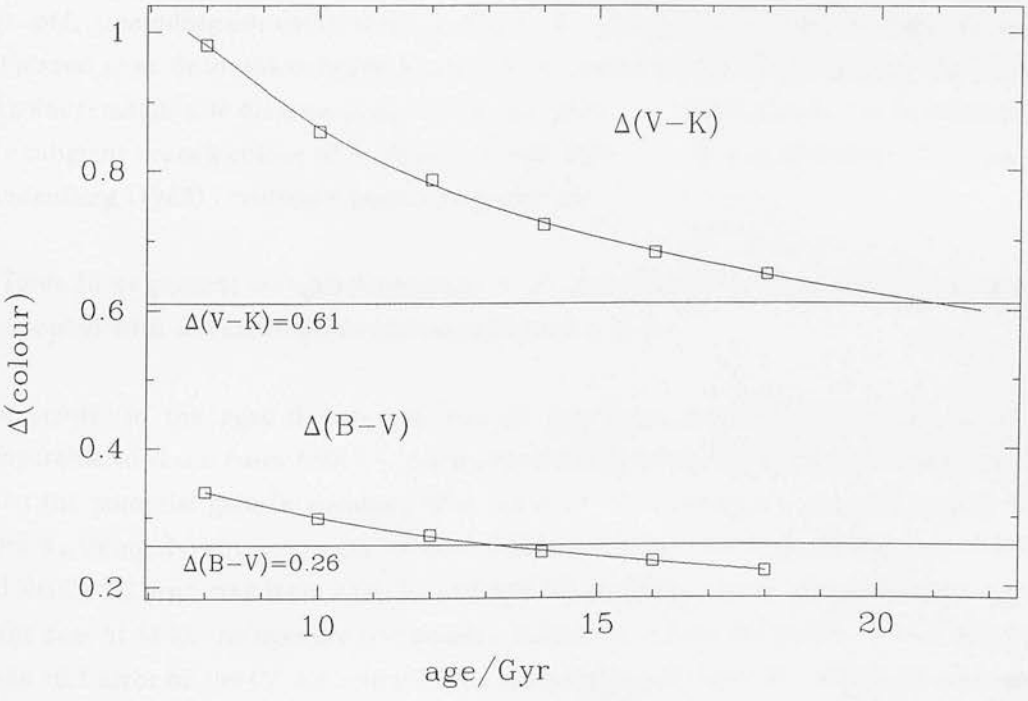

Figure 8: The (V-K) and (B-V) colour differences between the main-sequence turn-off and the subgiant branch versus age from the Bergbusch & VandenBerg isochrones of suitable abundance for comparison with 47 Tuc data.

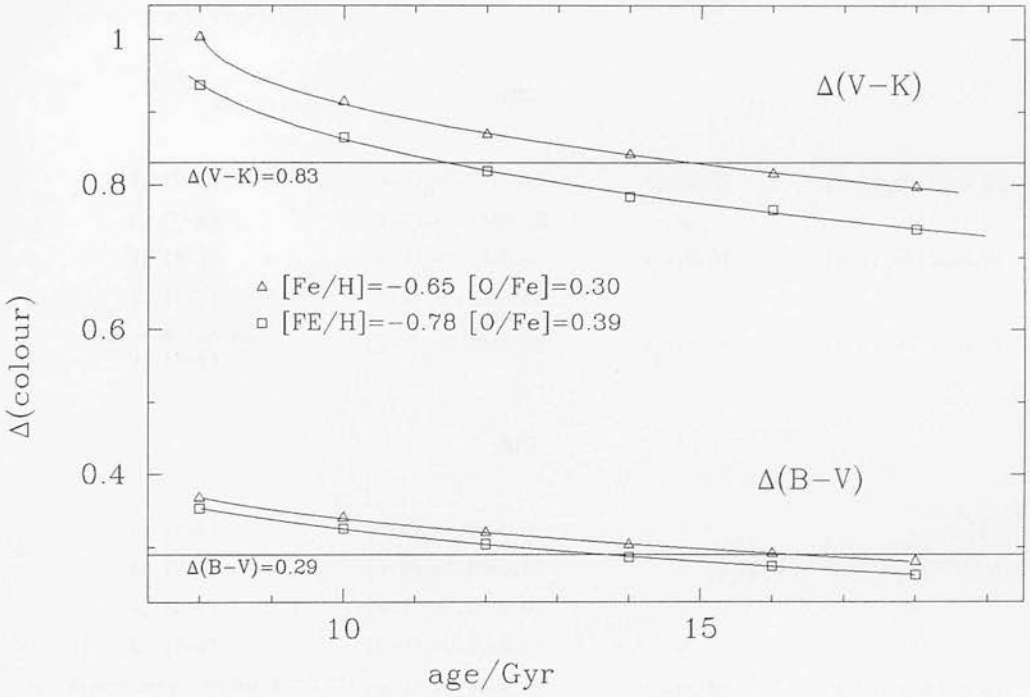

which has propagated from the error in fixing the fiducial point 0.05 magnitudes to the red of the turn-off.

Unfortunately the V, (V-K) colour-magnitude diagram of M13 does not extend above the turn-off, precluding our determination of Δ(V-K) in that cluster. Note also that we have not placed an error on the subgiant branch (V-K) colour of NGC6752 because the V, (V-K) colour-magnitude diagram contains too few points to enable an error to be estimated. The subgiant branch colour of M30 determined from the fiducial of Richer, Fahlman & VandenBerg (1988) involved a small extrapolation.

In Table 18 we present the ages determined from the observed values of Δ(V-K) and Δ(B-V) coupled with the calibrations shown in figures 6 to 8.

The errors on the ages determined for 47 Tuc from Δ(V-K), which are roughly comparable to those from Δ(B-V), are disappointing, given the comments made earlier about the potential gain in accuracy of a factor of ~2 in the ages compared to Δ(B-V). More worrying, however, are the ~4 and ~8 Gyr discrepancies between the ages of M30 and NGC6752 predicted from Δ(V-K) and Δ(B-V), with the former giving the older ages. In the case of M30, the ages are comparable *within the errors*, the bulk of which are due to the ±0.1 error on the (V-K) colour of the main-sequence turn-off. Although we could

Table 17: Main-sequence turn-off and subgiant branch parameters.

Plane	Turn-off colour	subgiant branch parameters	
		magnitude[a]	colour
	M30		
V, (V-K)	$(V-K)_0=1.07\pm0.10$	$V_0=16.67$	$(V-K)_0=1.75\pm0.03$
K, (V-K)	$(V-K)_0=1.11\pm0.10$	-	-
V, (B-V)	$(B-V)_0=0.33\pm0.02$	$V_0=16.87$	$(B-V)_0=0.56\pm0.01$
K, (B-V)	$(B-V)_0=0.33\pm0.02$	-	-
Richer & Fahlman V, (B-V)	$(B-V)_0=0.34\pm0.02$	$V_0=16.94$	$(B-V)_0=0.56\pm0.01$
	M13		
V, (V-K)	$(V-K)_0=1.20\pm0.01$	-	-
K, (V-K)	$(V-K)_0=1.20\pm0.01$	-	-
V, (B-V)	$(B-V)_0=0.39\pm0.01$	-	-
K, (B-V)	$(B-V)_0=0.39\pm0.01$	-	-
VandenBerg, Bolte & Stetson V, (B-V)	$(B-V)_0=0.39\pm0.01$	$V_0=16.89$	$(B-V)_0=0.65\pm0.01$
	NGC6752		
V, (V-K)	$(V-K)_0=1.21\pm0.03$	$V_0=15.54$	$(V-K)_0=1.82$
K, (V-K)	$(V-K)_0=1.21\pm0.05$	-	-
V, (B-V)	$(B-V)_0=0.39\pm0.01$	-	-
K, (B-V)	$(B-V)_0=0.39\pm0.01$	-	-
Penny & Dickens V, (B-V)	$(B-V)_0=0.39\pm0.01$	$V_0=15.58$	$(B-V)_0=0.65\pm0.01$
	47 Tuc		
V, (V-K)	$(V-K)_0=1.29\pm0.04$	$V_0=15.48$	$(V-K)_0=2.12\pm0.04$
K, (V-K)	$(V-K)_0=1.28\pm0.04$	-	-
V, (B-V)	$(B-V)_0=0.50\pm0.02$	$V_0=15.73$	$(B-V)_0=0.79\pm0.02$
K, (B-V)	$(B-V)_0=0.50\pm0.02$	-	-
Hesser *et al.* V, (B-V)	$(B-V)_0=0.50\pm0.00$	$V_0=15.78$	$(B-V)_0=0.80\pm0.02$

[a]The subgiant-branch magnitudes determined from V, (V-K) should not be compared with those determined from V, (B-V). The fiducial point on the main-sequence was taken to be 0.05 magnitudes to the red of the turn-off in both colours, which is further down the main sequence in V, (B-V) than in V, (V-K).

Table 18: Reddening and distance independent ages from Δ(V-K) and Δ(B-V).

Isochrone	Cluster age/Gyr
M30 age from Δ(V-K)=0.66±0.10	
[Fe/H]=-2.26 [O/Fe]=0.75	19.7 (-4.4,+6.5)
M30 age from Δ(B-V)=0.23±0.02	
[Fe/H]=-2.26 [O/Fe]=0.75	15.8 (-2.0,+2.6)
M13 age from Δ(B-V)=0.26±0.01	
[Fe/H]=-1.48 [O/Fe]=0.60	13.1 (-0.9,+1.1)
NGC6752 age from Δ(V-K)=0.61	
[Fe/H]=-1.48 [O/Fe]=0.60	21.0
NGC6752 age from Δ(B-V)=0.26±0.01	
[Fe/H]=-1.48 [O/Fe]=0.60	13.1 (-0.9,+1.1)
47 Tuc age from Δ(V-K)=0.83±0.06	
[Fe/H]=-0.78 [O/Fe]=0.39	11.5 (-2.4,+3.9)
[Fe/H]=-0.65 [O/Fe]=0.30	14.9 (-4.0,+5.9)
47 Tuc age from Δ(B-V)=0.29±0.03	
[Fe/H]=-0.78 [O/Fe]=0.39	13.6 (-3.2,+4.8)
[Fe/H]=-0.65 [O/Fe]=0.30	16.2 (-4.3,+5.6)

Table 19: Adopted ages for each cluster determined from Δ(V-K) and Δ(B-V).

Cluster	age/Gyr	
M30	17.1±2.0	
M13	13.1 (-0.9,+1.1)	
NGC6752	13.1 (-0.9.+1.1)	
47 Tuc	15.6±3.5	[Fe/H]=-0.65
	12.4±3.0	[Fe/H]=-0.78

not place an error on the colour of the NGC6752 subgiant branch, the error on the colour of the turn-off leads to lower limits on the errors in the age from Δ(V-K) of (-2.3,+2.6) Gyr. The errors on the ages from Δ(V-K) and Δ(B-V) are thus not large enough to explain the discrepancy.

We consider that the age determined for NGC6752 from Δ(V-K) is likely to be less reliable than that from Δ(B-V). Inspection of figure 4(a) from Chapter 1 shows that the subgiant branch colour is determined at a level which lies between the brightest two points with K observations by us; the brightest of these is from field 3 while the other is from the field 5 observations. Therefore any small systematic errors in the relative zero-points of the photometry of these fields would lead to an error in the age. We must remember this discrepancy, though, when we make comparisons between the colour-magnitude diagrams and the isochrones; it is possible that the discrepancy is caused by the effects which VandenBerg, Bolte and Stetson have warned against. Another, related, explanation could be that the correction to the isochrone (V-K) colours determined by Bell to be a constant 0.12 magnitudes is, in reality, not a constant but a function of gravity and abundance.

Our adopted ages from this method for each cluster, taking a weighted average where appropriate, are summarised in Table 19.

5 DO THE ADOPTED REDDENINGS FORM A CONSISTENT PICTURE?

The adopted reddening for at least one of our clusters - M30 - is controversial, and so it would be advantageous to have some means of intercomparing the reddenings of all our clusters, to check for internal consistency. To do this we require to match the colours of some suitable near-vertical feature of the cluster colour-magnitude diagrams. Once variations between cluster ages and abundances have been taken into account, any

remaining colour difference should be due only to differences between foreground reddening. Since we will need to explicitly remove age and abundance variations, a desirable property of our 'near-vertical feature' would be that it's colour is relatively insensitive to these.

We use the colour of the subgiant branch near the base - in fact, defined at the same level used to calculate Δ(V-K) and Δ(B-V) - to intercompare our relative cluster reddenings. However, we shall actually adopt a slightly different approach than the one described above. Since we already have dereddened fiducials, it is easier to compare the difference in colour between the cluster subgiant branches *with the reddening removed* to the difference expected from just the abundance and age differences. The two methods are equivalent since any mismatches found in the second method are due to errors in our adopted reddenings.

The observed colours of the cluster subgiant branches are available in Table 17, but are also reproduced in Table 20 for convenience. Figure 9 shows the variation of the subgiant branch colours, found from the Bergbusch & VandenBerg isochrones. Note that the (V-K) colours in this figure do *not* include the 0.12 magnitude correction recommended by Bell (1992); we use the information in these figures differentially, but care must be exercised if using the absolute values.

Table 21 compares the expected colour difference between the cluster subgiant branches, using the adopted ages from Table 19, with those observed. Fortunately the subgiant branch colours are not sensitive functions of age; in the case of NGC6752 we have adopted the age determined from Δ(B-V), but using an age ~8 Gyr older would lead to a downward revision of the (V-K) colour of the subgiant branch by only ~0.01 magnitudes and no change to the (B-V) colour.

Consider first the (B-V) comparisons, which have smaller errors than the (V-K) comparisons - due to the limited (V-K) data; in principle (V-K) is the better colour with which to work. There is extremely good agreement in the predicted and observed subgiant branch colour differences between NGC6752 and M13. The value of δ(B-V)=0.09±0.01 between the observed (B-V) colours of the NGC6752 and M30 subgiant branches is marginally outside the allowed errors when compared to the expected value of δ(B-V)=0.074±0.002, suggesting that either the reddening adopted for M30 is too high by 0.01 to 0.02 magnitudes, or that the adopted reddening for NGC6752 is too low by the same amount, or a combination of both. The observed colour differences in the comparisons involving 47 Tuc and either NGC6752 or M13 lie midway between the values expected from the [Fe/H]=-0.65 and [Fe/H]=-0.78 models, although within the errors the observed value is consistent with either. The observed colour difference between 47 Tuc and M30 favours the higher abundance, although within the errors it too is consistent with the

Table 20: The subgiant branch colours of M13, M30, 47 Tuc & NGC6752, reproduced from Table 17.

Cluster	Subgiant branch colours	
	$(V-K)_0$	$(B-V)_0$
M13	-	0.65±0.01
M30	1.75±0.03	0.56±0.01
47 Tuc	2.12±0.04	0.79±0.02
NGC6752	1.82	0.65±0.01

Table 21: Comparison of the observed colour differences between dereddened cluster subgiant branches and those calculated from the models, using adopted metallicities and ages.

Clusters	δ(V-K) models	δ(V-K) observed	δ(B-V) models	δ(B-V) observed
47 Tuc - NGC6752				
[Fe/H]=-0.65	0.29±0.03	0.30±0.04	0.161±0.004	0.14±0.02
[Fe/H]=-0.78	0.20±0.01		0.122±0.003	
47 Tuc - M13				
[Fe/H]=-0.65	-	-	0.161±0.004	0.14±0.02
[Fe/H]=-0.78	-		0.122±0.003	
47 Tuc - M30				
[Fe/H]=-0.65	0.36±0.03	0.37±0.05	0.235±0.004	0.23±0.02
[Fe/H]=-0.78	0.27±0.01		0.196±0.004	
NGC6752 - M30	0.07±0.01	0.07±0.03	0.074±0.002	0.09±0.01
NGC6752 - M13	-	-	0.000±0.001	0.00±0.01

Figure 9: (a) the (V-K), and (b) the (B-V) colours of the subgiant branch, determined from the Bergbusch & VandenBerg isochrones, as a function of age and abundance.

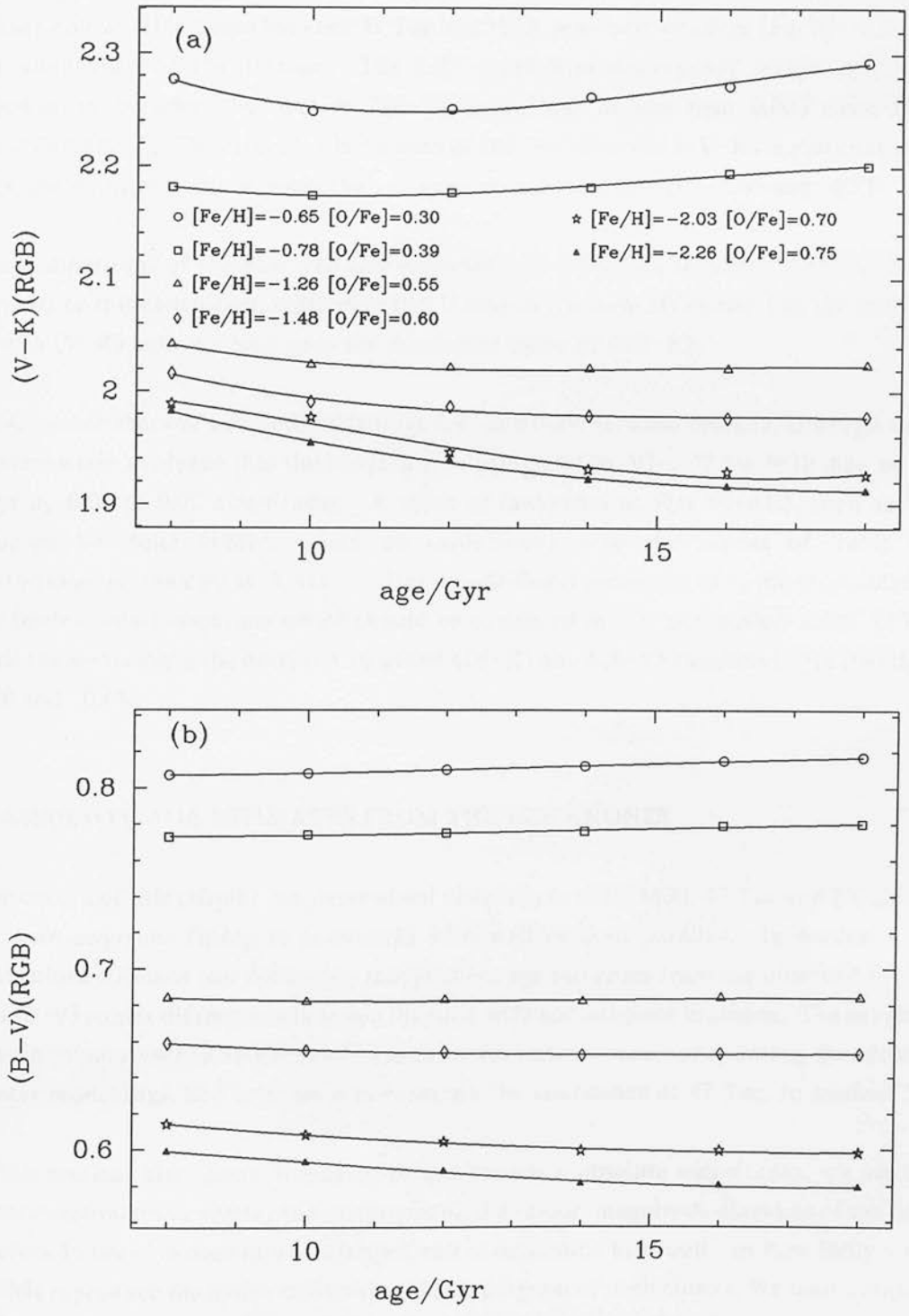

midway point.

Now consider the comparisons in (V-K). Setting aside for the moment those comparisons involving NGC6752, which we found to have an anomalous value of Δ(V-K) compared to Δ(B-V), we see that there is excellent agreement in the observed and predicted subgiant branch colour differences between 47 Tuc and M30, provided we adopt [Fe/H]=-0.65 for the abundance of the former. The 0.01 magnitude discrepancy would lead to a discrepancy between the relative E[B-V] reddenings of less than 0.005 since E[V-K]=2.744E[B-V]. The errors are large enough that the observed δ(V-K) is also consistent with the point midway between the values expected from [Fe/H]=-0.65 and -0.78.

The comparisons of the observed and expected δ(V-K) values involving NGC6752 also re-enforce this conclusion, suggesting that it may be the turn-off rather than the subgiant branch (V-K) colour which gave the discrepant value of Δ(V-K).

We conclude that our adopted reddenings are consistent between clusters, although there is some slight evidence that the adopted reddening of E[B-V]=0.07 for M30 may be too high by 0.01 to 0.02 magnitudes. A value as low value as E[B-V]=0.02, such as was adopted by Bolte (1987), would be inconsistent with the results of Table 21. Unfortunately, the data in this table offer no additional constraint as to the abundance of the (scaled-solar) isochrone which should be compared to the (non-scaled-solar) 47 Tuc data; the errors make the observed values of δ(V-K) and δ(B-V) consistent with [Fe/H]=-0.78 and -0.65.

6 ABSOLUTE AGE ESTIMATES FROM THE ISOCHRONES

In section 3 of this chapter, we determined distances to M13, M30, 47 Tuc and NGC6752 by main-sequence fitting to subdwarfs with well defined parallax. In section 4 we determined distance and reddening independent age estimates from the observed (V-K) and (B-V) colour differences between the turn-offs and subgiant branches. The subgiant branch colours were further employed to check for internal consistency among the adopted cluster reddenings, and to attempt to constrain the abundance of 47 Tuc, in sections 5.

In this section, after some discussion of the isochrone absolute magnitudes, we use the distance estimates to overlay the isochrones on the colour-magnitude diagrams of the four clusters, in order to determine their ages, and to determine how well - or how badly - the models reproduce the entire colour-magnitude diagram of each cluster. We then compare these ages with the distance and reddening independent ages. Finally we summarise our best estimate of the age of each cluster.

6.1 Are the isochrone absolute magnitudes correct?

The isochrone absolute magnitudes are calculated from the theoretical luminosities of the stellar evolution models, using a bolometric correction determined from model atmospheres for a given temperature, gravity and chemical composition. The absolute magnitudes will thus depend on which model atmosphere or atmospheres are used - and if more than one is used, on how their results are combined - and also on how the results were normalised originally. Some authors normalise their grids of bolometric corrections so that the smallest correction is zero, while others normalise to an observed bolometric correction, such as that of the Sun.

The isochrone absolute magnitudes should thus be treated with some caution; in particular there is no *a priori* reason to expect any two sets of isochrones, of different abundance, not to have some zero-point shift, which may be a function of temperature, gravity or abundance, and there is no way of knowing, without further information, which of the absolute magnitude systems is the correct one, if either.

In order to take this into account we have fixed the absolute magnitude systems of the two sets of Bergbusch & VandenBerg isochrones - the V, (B-V) isochrones from Bergbusch & VandenBerg (1992) and the V, (V-K) isochrones from Bell (1992) - by main-sequence fitting to the field subdwarfs used to determine cluster distances. The results of this fitting give information not only on the offset between the isochrone absolute magnitude system and the true system defined by the subdwarfs, at least at high gravity, but also offer corrections which can be applied before the isochrones are compared to globular cluster colour-magnitude data. Note also that provided any offset is not a function of abundance, the method of correcting the subdwarfs to different abundances by correcting their absolute magnitudes at constant colour, as outlined in section 3.2, is independent of the offset. The method of correcting colour at constant absolute magnitude is not independent.

The results of fitting the 16 Gyr isochrones to the subdwarfs are presented in Table 22. The 16 Gyr isochrone was chosen because that was the age of the isochrones used differentially to correct the subdwarfs to different abundances. All but HD201891 have colours which place them on the sections of the isochrone main-sequences which are coincident at all ages, so the choice of isochrone age is immaterial for these. However, HD201891 does lie at a colour where the isochrones follow slightly different loci for different ages, and so some slight variation of isochrone 'distance modulus' with age can be expected. For comparison, the results in Table 23 are of the fit of the 8 Gyr isochrones to the subdwarfs. The differences between the results of the 8 and 16 Gyr fits are small compared to the r.m.s. fitting errors.

Table 22: True 'distance moduli' of the 16 Gyr V, (V-K) and V, (B-V) isochrones from main-sequence fits to subdwarfs. The numbers in parentheses indicate the number of subdwarfs used in the fits.

Plane	True 'distance modulus' of isochrone	
	No Lutz-Kelker corrections	Full Lutz-Kelker corrections
	[Fe/H]=-0.65 [O/Fe]=0.30	
V, (V-K)	0.02±0.09 (6)	0.15±0.10 (6)
V, (B-V)	-0.05±0.12 (5)	0.05±0.08 (5)
	[FE/H]=-0.78 [O/Fe]=0.39	
V, (V-K)	0.03±0.09 (6)	0.15±0.10 (6)
V, (B-V)	-0.04±0.12 (5)	0.06±0.08 (5)
	[Fe/H]=-1.48 [O/Fe]=0.60	
V, (V-K)	0.04±0.08 (5)	0.16±0.11 (5)
V, (B-V)	0.00±0.11 (5)	0.12±0.12 (5)
	[Fe/H]=-2.26 [O/Fe]=0.75	
V, (V-K)	0.03±0.09 (6)	0.15±0.10 (6)
V, (B-V)	-0.03±0.11 (6)	0.10±0.12 (6)

When comparing the isochrones to cluster colour-magnitude data, we use the corrections from Table 22, that is from the 16 Gyr isochrones, to correct the isochrone absolute magnitudes; for any constant cluster distance modulus, applying a separate correction for each age would lead to the isochrone lower main-sequences not being coincident at all ages, which is unphysical.

Table 23: True 'distance moduli' of the 8 Gyr V, (V-K) and V, (B-V) isochrones from main-sequence fits to subdwarfs. The numbers in parentheses indicate the number of subdwarfs used in the fits.

Plane	True 'distance modulus' of isochrone	
	No Lutz-Kelker corrections	Full Lutz-Kelker corrections
	[Fe/H]=-0.65 [O/Fe]=0.30	
V, (V-K)	0.07±0.13 (6)	0.19±0.17 (6)
V, (B-V)	-0.03±0.11 (5)	0.07±0.07 (5)
	[FE/H]=-0.78 [O/Fe]=0.39	
V, (V-K)	0.06±0.12 (6)	0.19±0.15 (6)
V, (B-V)	-0.03±0.11 (5)	0.07±0.07 (5)
	[Fe/H]=-1.48 [O/Fe]=0.60	
V, (V-K)	0.06±0.09 (5)	0.18±0.13 (5)
V, (B-V)	0.01±0.12 (5)	0.13±0.14 (5)
	[Fe/H]=-2.26 [O/Fe]=0.75	
V, (V-K)	0.03±0.10 (6)	0.16±0.11 (6)
V, (B-V)	-0.03±0.11 (6)	0.10±0.12 (6)

6.2 Comparison of isochrones and NGC6752 & M13 colour-magnitude data

Figures 10 to 13 show the V_0, $(V-K)_0$ and V_0, $(B-V)_0$ colour-magnitude diagrams of NGC6752 and M13, the two clusters with similar abundances ([Fe/H]~-1.5). The V_0, $(B-V)_0$ diagrams show the full optical datasets from Penny & Dickens (1986) and from Richer & Fahlman (1986). Also marked on these diagrams is the photometry of red giant branch stars from Frogel, Persson & Cohen (1983) and Cohen, Frogel & Persson (1978), the subdwarfs and the fiducials from which the distances were determined. We have overlaid on these figures the Bergbusch & VandenBerg isochrones corrected to true distance

Figure 10: The V_0, $(V-K)_0$ colour-magnitude diagram of NGC6752, with the Bergbusch & VandenBerg isochrones overlaid.

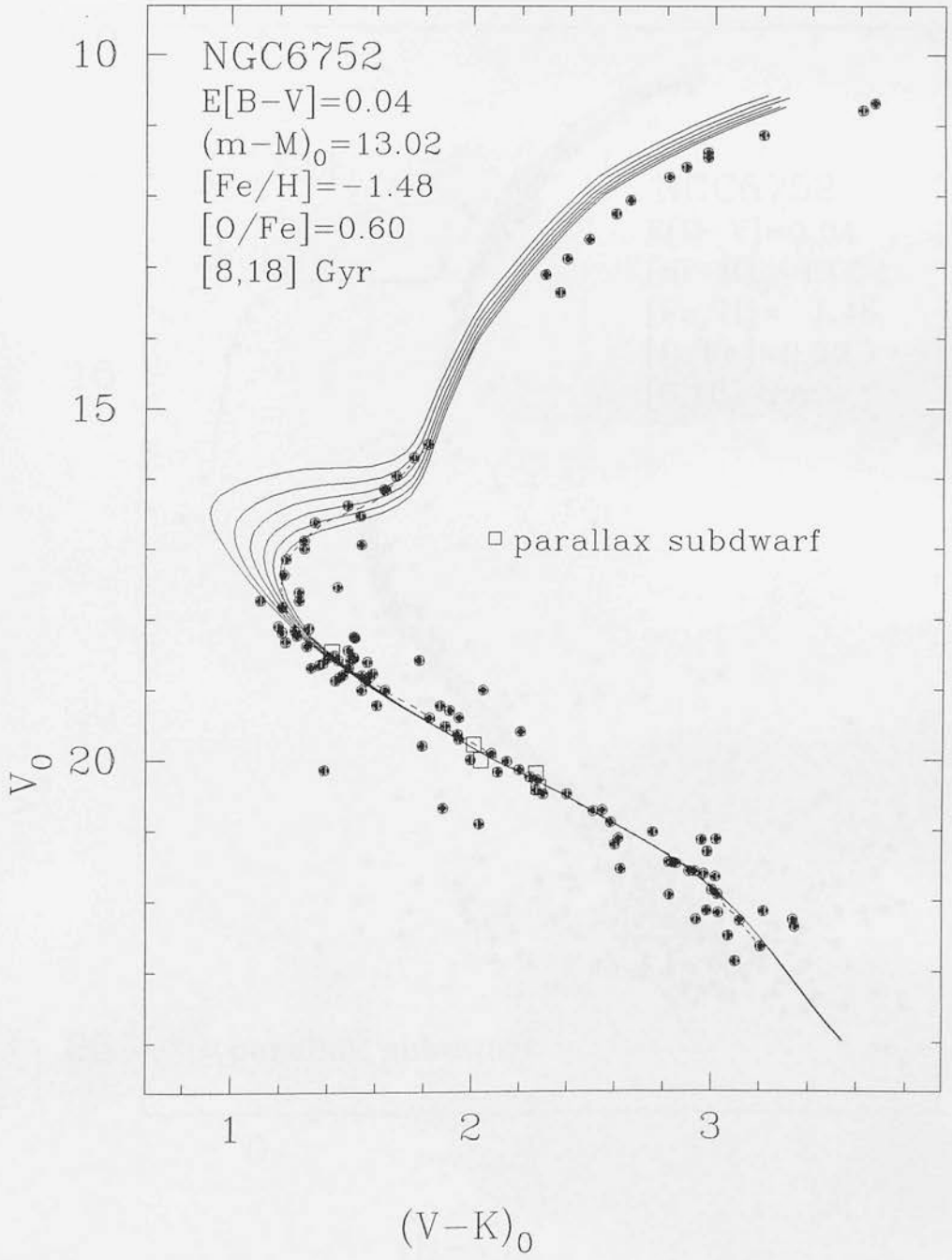

Figure 11: The V_0, $(B-V)_0$ colour-magnitude diagram of NGC6752, with the Bergbusch & VandenBerg isochrones overlaid. Also shown is the zero-age horizontal-branch locus of Dorman (1992).

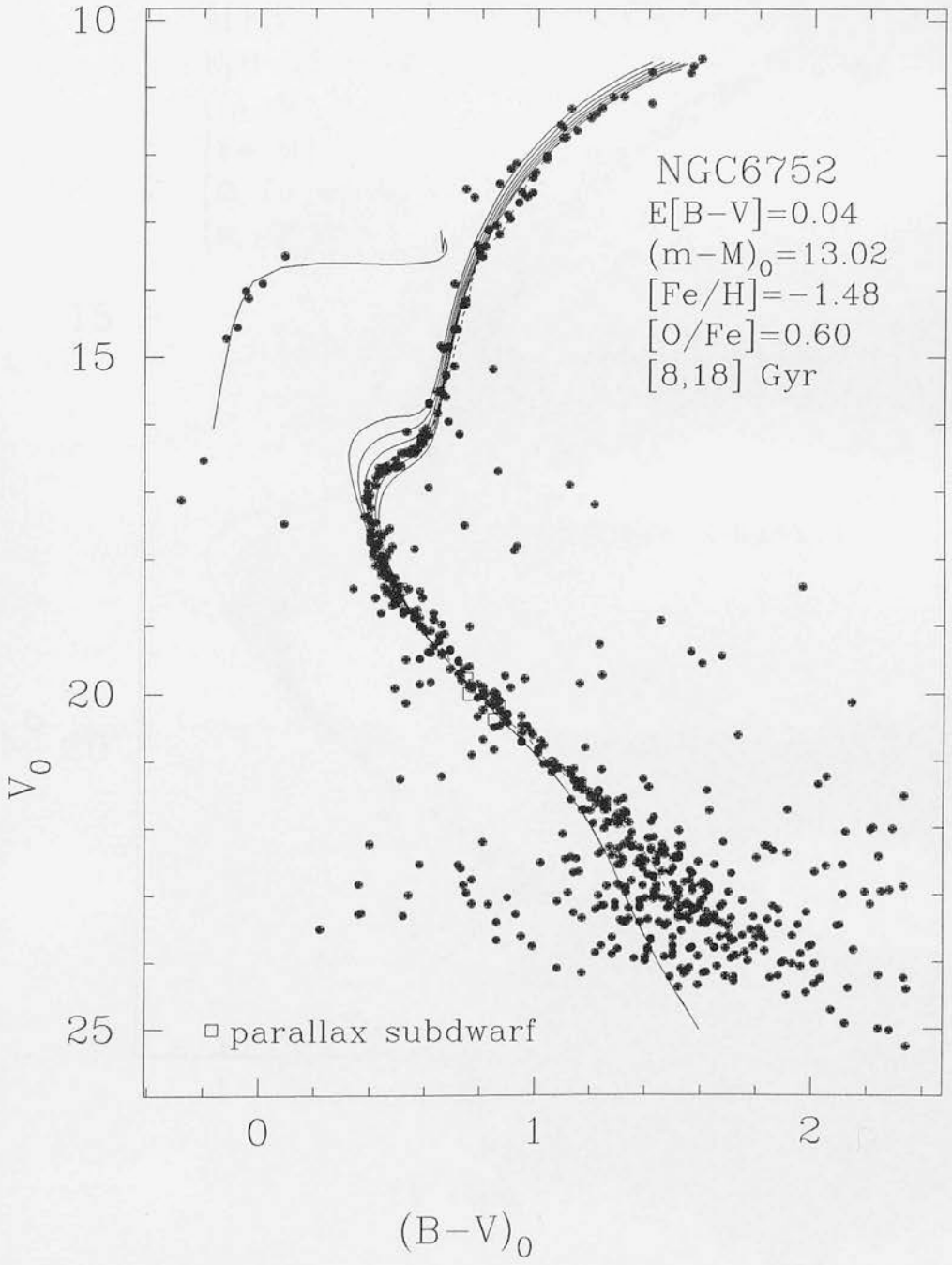

Figure 12: The V_0, $(V-K)_0$ colour-magnitude diagram of M13.

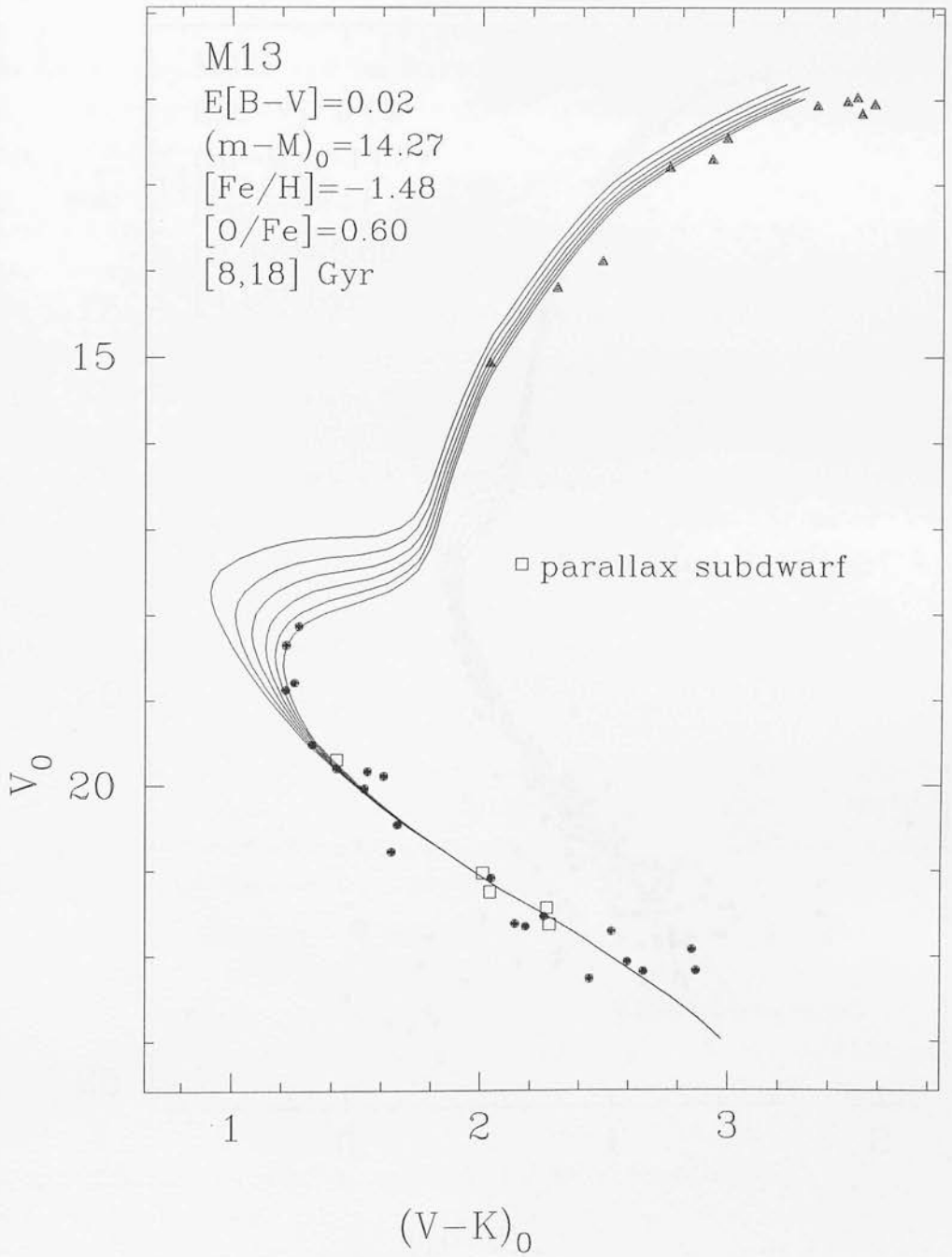

Figure 13: The V_0, $(B-V)_0$ colour-magnitude diagram of M13 with the full optical dataset of Richer & Fahlman (1986).

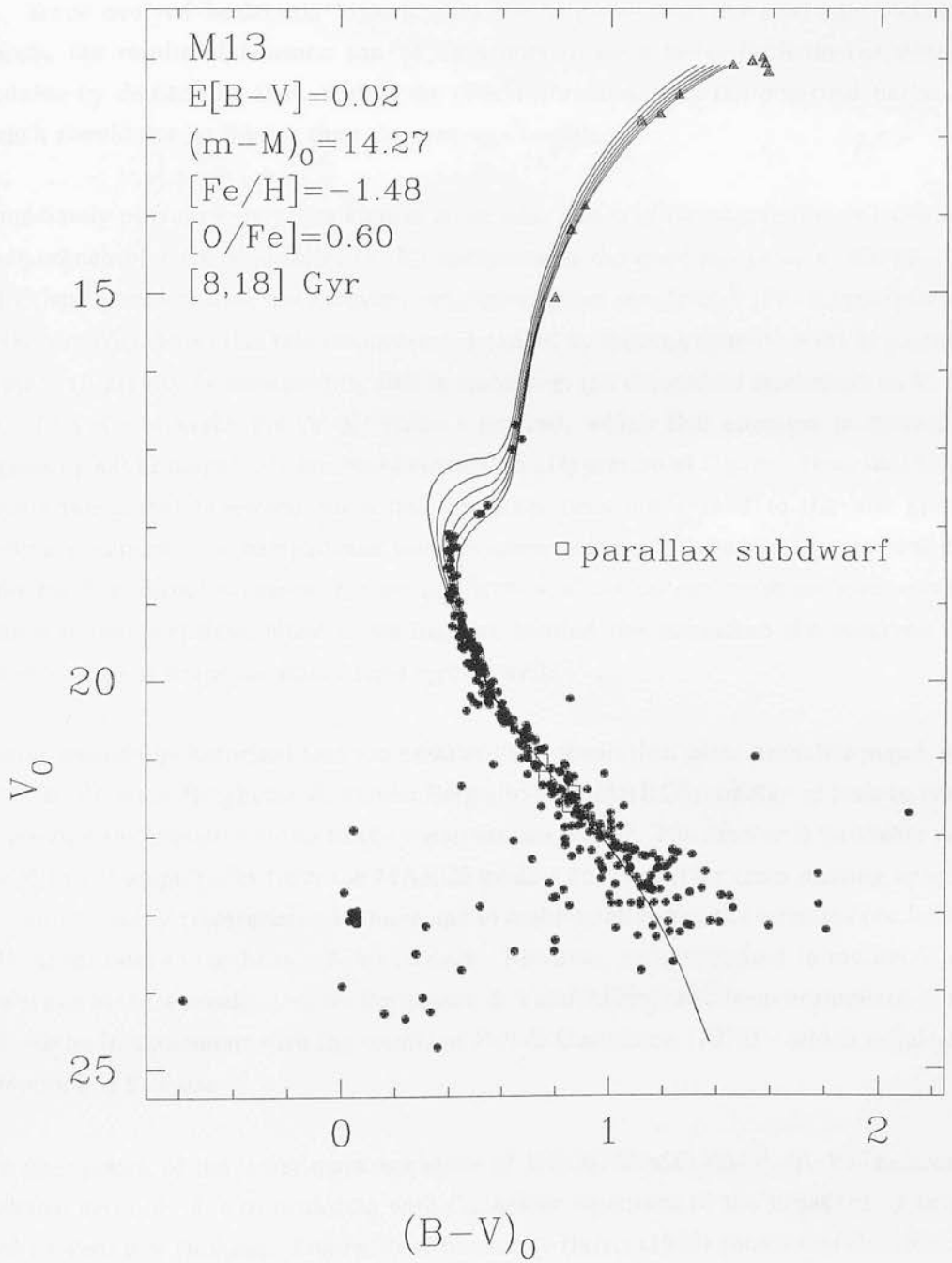

moduli, without Lutz-Kelker corrections, of 13.02 and 14.27 magnitudes respectively, and correcting onto the subdwarf absolute magnitude scale via the corrections presented in Table 22.

The purely optical colour-magnitude diagram of NGC6752 also has the zero-age horizontal-branch locus of Dorman (1992) marked, again with the correction from Table 22. Since evolved horizontal-branch stars are brighter than the zero-age horizontal branch, the results of Dorman can be used only to set a lower limit on the distance modulus by demanding that, within the observational scatter, the observed horizontal branch should not be fainter than the zero-age models.

Immediately obvious from these figures is the poor match of the theoretical and observed giant branch of NGC6752 in V, (V-K) compared to the good match in V, (B-V). The M13 giant branch shows more scatter, but also matches poorly in V, (V-K) compared to V, (B-V). We suspect that this conundrum is caused by missing opacity in the K passband of the high gravity models used by Bell to transform the theoretical isochrones to V, (V-K). This would make the (V-K) colours too red, which Bell attempts to correct by suggesting a 0.12 magnitude blueward correction. Inspection of figure 1 from Bell (1992) reveals the global blueward correction probably does not extend to the low gravity isochrone colours. The comparisons between observation and theory in figures 10 and 12 offer the first direct evidence that the application of the correction to the giant-branch models is inappropriate, since if we had not applied the correction the observed and theoretical giant branches would have agreed well.

Should we then be surprised that the observed and theoretical giant branches match well in V, (B-V), since Bergbusch & VandenBerg also used MARCS models - at least in part - to provide the transformation to the observational plane? The answer is 'probably not'. The B and V magnitudes from the MARCS models do also suffer from missing opacity, as found by many researchers who have had to make small redward corrections of 0.03 or 0.04 magnitudes to isochrone (B-V) colours. However, as summarised in section 1, the model atmosphere results used by Bergbusch & VandenBerg have been normalised to the red - to be in agreement with the results of Bell & Gustafsson (1978) - which required a correction of this size.

The poor match of the lower main-sequence of NGC6752 with the V, (B-V) isochrones is almost certainly due to problems with the colour equations of the broad-band filters used by Penny & Dickens. Figure 36 of Stetson & Harris (1988) shows that the fiducial of NGC6752 tabulated by Penny & Dickens crosses over to the red of the 47 Tuc fiducial for $(B-V)_0 > 1.2$. The fiducial from figure 8 of VandenBerg, Bolte & Stetson shows the discrepancy is present for $(B-V)_0 > \sim 0.5$. The good agreement of the Penny & Dickens fiducial, marked on figure 10, with the isochrone main-sequences for $(B-V) < \sim 0.9$ suggest

that it is not until redder colours that the discrepancy is significant. Interestingly, the observed and theoretical main-sequences in the V, (V-K) colour-magnitude diagram of figure 11 agree well along the entire length, suggesting that the discrepancy in V, (B-V) is solely due to problems with the B photometry. The good agreement of the distances derived from subdwarfs in V, (V-K) and V, (B-V) indicates that the bias in the V, (B-V) main sequence has not affected the distance determination.

For NGC6752 we determine an age of (18±3) Gyr from the V, (V-K) colour-magnitude diagram. In V, (B-V) the points at the turn-off and below give an age of (12±2) Gyr while the points between the turn-off and the base of the subgiant branch suggest (15±1) Gyr leading to a weighted mean of (14±1) Gyr.

For M13 we determine and age of (18±2) Gyr from V, (V-K). From the points at the turn-off and below in V, (B-V) we determine an age of (14±2) Gyr while the three points on the redward sweep between the turn-off and the subgiant branch follow the 16 Gyr isochrone. We thus assign an age to M13 from the V, (B-V) isochrones of (15.0±1.4) Gyr. These errors are lower limits determined from the internal scatter in the photometry only, and do not take into account the errors which would be introduced by systematic uncertainties in the reddening or photometric zero-points.

6.3 Comparison of isochrones and 47 Tuc colour-magnitude data

Figures 14 and 15 show respectively the V_0, $(V-K)_0$ and the V_0, $(B-V)_0$ colour-magnitude diagrams of 47 Tuc on which the relevant Bergbusch & VandenBerg isochrones have been overlaid. The purely optical data shown consist of all of the photometry from fields F1 and F3 of Hesser *et al.* (1987), the latter limited to V<17.2. Photometry of giant-branch stars from Frogel, Persson & Cohen (1981) is also shown. The fiducial, however, is that drawn by Hesser *et al.* through their full composite diagram.

Each figure consists of part (a), with isochrones of abundance [Fe/H]=-0.65, which we have argued should reproduce the 47 Tuc colour-magnitude diagram well when α-element enhancement is taken into account, and part (b) with isochrones of the more metal-poor 'compromise' abundance of [Fe/H]=-0.78. As usual, the isochrone absolute magnitude scale has been corrected to that of the subdwarfs without Lutz-Kelker corrections.

There is obviously a colour mismatch of ~0.02 to 0.04 magnitudes in (B-V) between the photometry of the giants from Frogel, Persson & Cohen (1981) and the field F3 giants. The fiducial drawn by Hesser *et al.* through their composite colour-magnitude diagram agrees with the latter, although they did not use the photometry of their inner fields to define the giant branch, choosing instead to use photographic photometry from Lee (1977)

Figure 14(a): The V_0, $(V-K)_0$ colour-magnitude diagram of 47 Tuc, showing the Bergbusch & VandenBerg isochrones from Bell (1992) with [Fe/H]=-0.65 [O/Fe]=0.30. The giant branch photometry is from Frogel, Cohen & Persson (1981).

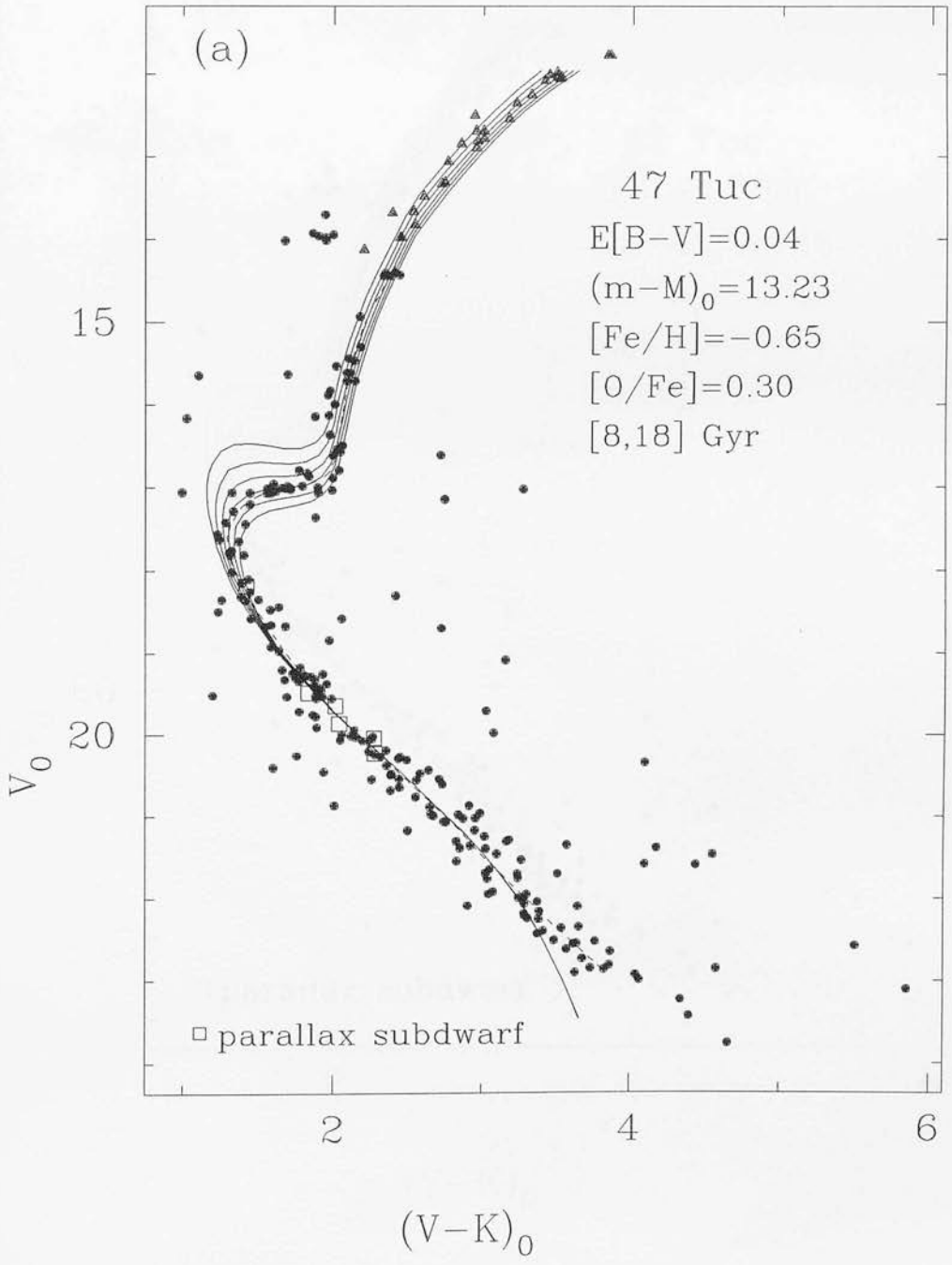

Figure 14(b): As (a) but showing the isochrones with [Fe/H]=-0.78 [O/Fe]=0.39.

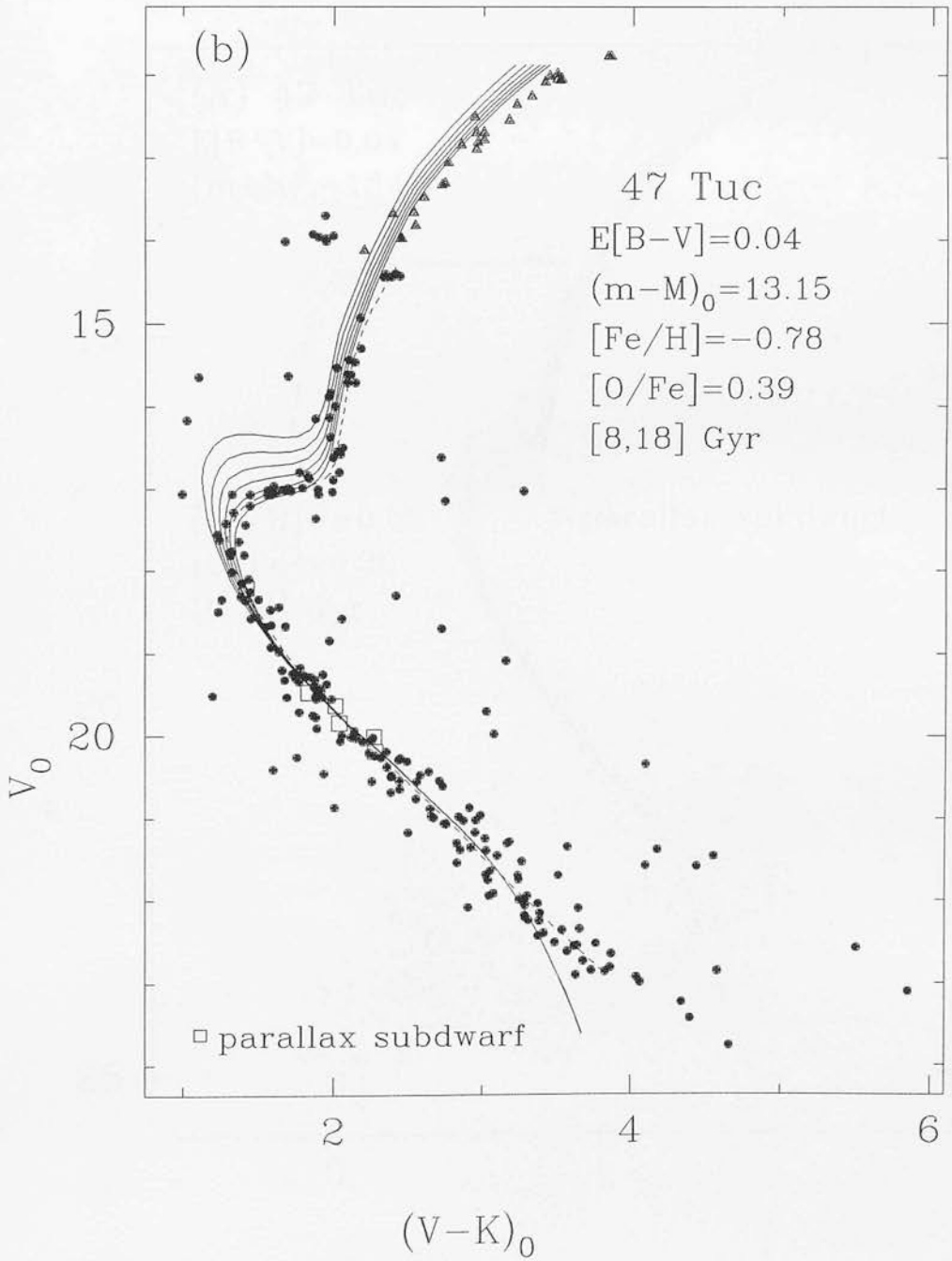

Figure 15(a): The V_0, $(B-V)_0$ colour-magnitude diagram of 47 Tuc. Also shown are the Bergbusch & VandenBerg (1992) isochrones and Dorman (1992) zero-age horizontal-branch with [Fe/H]=-0.65 [O/Fe]=0.39.

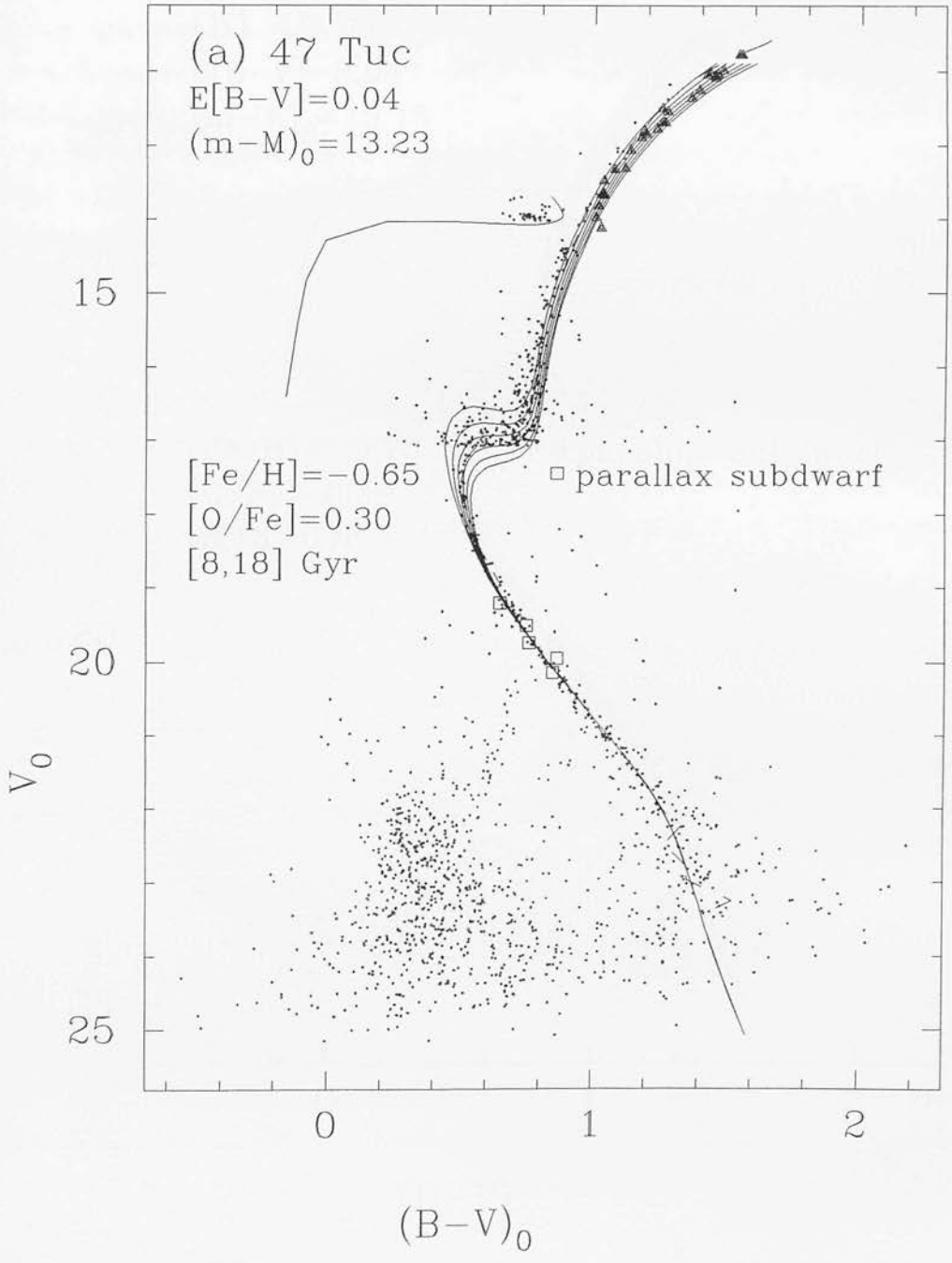

Figure 15(b): As (a) but showing the isochrones and zero-age horizontal branch with [Fe/H]=-0.78 [O/Fe]=0.39.

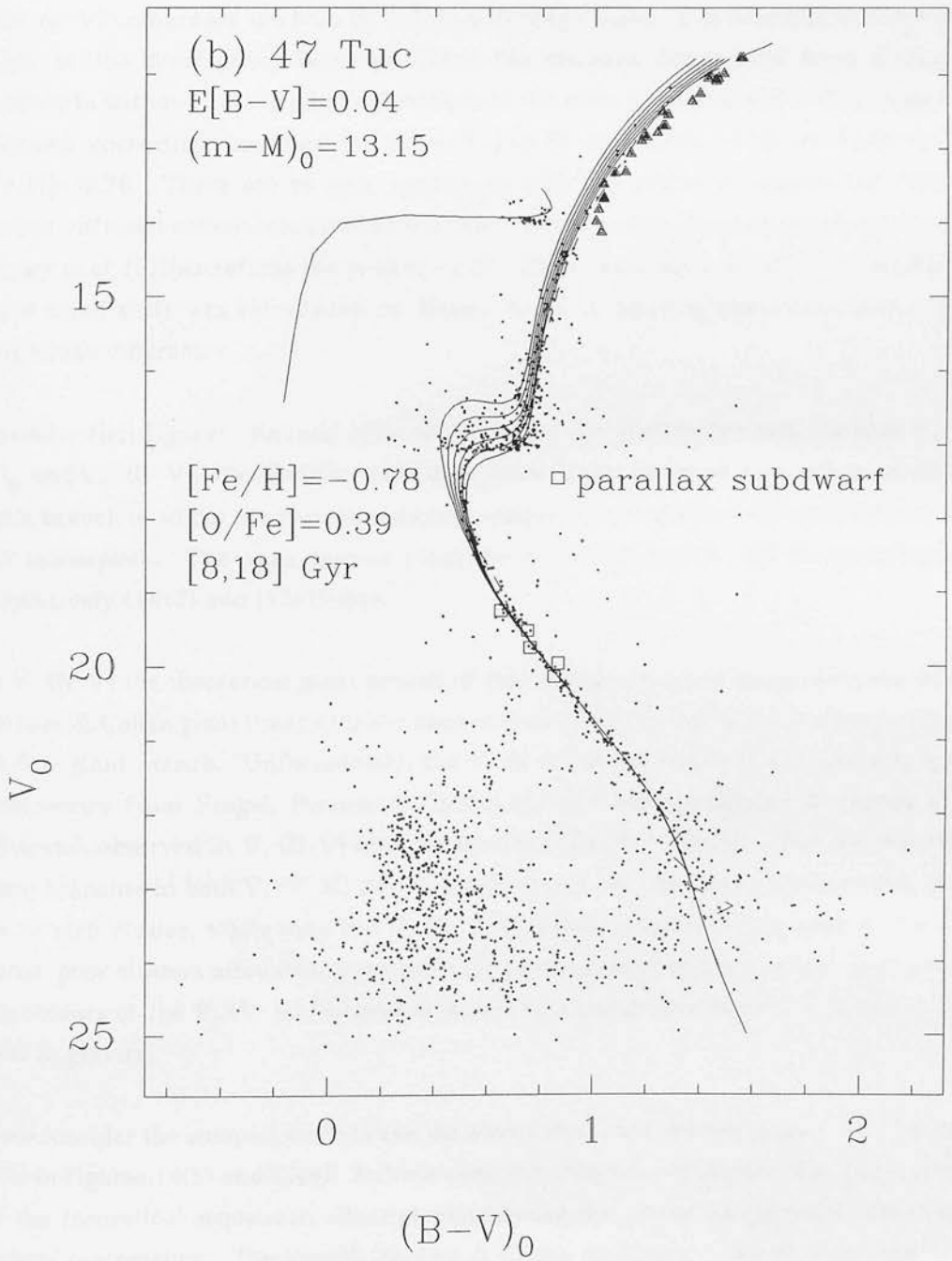

and Hesser & Hartwick (1977). This mismatch is surprising, since the optical photometry tabulated by Frogel, Persson & Cohen is part of the photoelectric photometry used by Lee (1977) to calibrate the photographic photometry. A comparison of the Lee ring 7 photographic photometry and the photoelectric photometry reveals no systematic mismatch, and yet the fiducial tabulated by Hesser *et al.* is ~0.02 to 0.04 magnitudes to the blue of both. Hesser *et al.* note in appendix E that there is a reasonable possibility that their (B-V) colours are too blue by 0.01 to 0.02 magnitudes. It is doubtful that this is the cause of the discrepancy however, since the distance determined from fitting the subdwarfs without Lutz-Kelker corrections to the main sequence with a 0.02 magnitude redward correction becomes $(m-M)_0$=13.11±0.17 at [Fe/H]=-0.65 or 13.01±0.17 at [Fe/H]=-0.78. These are in poor agreement with the distances determined from the optical-infrared colour-magnitude diagrams. Also the note added in proof at the end of Hesser *et al.* further refutes the possibility of a (B-V) zero-point error. It is possible that some small shift was introduced by Hesser *et al.* in creating their composite colour-magnitude diagram.

Consider first figures 14(a) and 15(a) with the [Fe/H]=-0.65 isochrones. In both V_0, $(V-K)_0$ *and* V_0, $(B-V)_0$ the [Fe/H]=-0.65 isochrones fit the observed data well from the red giant branch to all but the very faintest main-sequence stars, where the observational data are incomplete. The ages derived from the V, (V-K) and V, (B-V) isochrones are respectively (14±2) and (13±1) Gyr.

In V, (B-V) the theoretical giant branch of this age agrees much better with the Frogel, Persson & Cohen giant branch than it does with the fiducial which is matched by the 8 or 10 Gyr giant branch. Unfortunately, the V, (V-K) giant branch is defined only by the photometry from Frogel, Persson & Cohen, so it is not possible to determine if the mismatch observed in V, (B-V) also persists in V, (V-K). The fact that the theoretical giant branches in both V, (V-K) *and* V, (B-V) match the observed giant branches of this metal-rich cluster, while only the V, (B-V) branches matched in the case of the more metal-poor clusters discussed in the previous section, suggests that the true correction to the colours of the V, (V-K) isochrones should be a function of chemical composition as well as gravity.

Now consider the comparison between the observations and the isochrones with [Fe/H]=-0.78 in figures 14(b) and 15(b). In both cases the subgiant branch fiducial lies to the red of the theoretical sequences, although considering the scatter in the data, this is not a serious discrepancy. The Frogel, Persson & Cohen giants are likewise to the red of the theoretical giant-branches, although the agreement between the models and the fiducial, drawn by Hesser *et al.* through their composite diagram, is much better. The match of the observed horizontal branch with the theoretical [Fe/H]=-0.78 zero-age horizontal branch is also poor compared to the match with the [Fe/H]=-0.65 models.

From the [Fe/H]=-0.78 V, (V-K) and V, (B-V) models we determine ages of (17±2) and (16±1) Gyr respectively.

6.4 Comparison of isochrones and M30 colour-magnitude data

Figures 16 and 17 show the V_0, $(V-K)_0$ and V_0, $(B-V)_0$ colour-magnitude diagrams of M30, with the [Fe/H]=-2.26 [O/Fe]=0.75 Bergbusch & vandenBerg isochrones overlaid and corrected to a true distance modulus of 14.54 magnitudes. The V_0, $(B-V)_0$ diagram also sports the Dorman (1992) zero-age horizontal-branch of the same abundance.

Immediately obvious is the extent of the redward bias in the V_0, $(V-K)_0$ main-sequence data caused by incompleteness and crowding. Note also the good agreement between the observed and theoretical horizontal branches, which lends further weight to our choice of distance modulus and our adopted reddening of E[B-V]=0.07.

To the best of our knowledge no published infrared photometry of M30 giants exists; we are therefore unable to say if the theoretical V, (V-K) giant branch of this abundance agrees with the observed giant branch, as in V, (B-V), and thus reproduces the behaviour at high abundance found in comparisons with 47 Tuc data, or does not agree, continuing the trend found at the intermediate abundances of M13 and NGC6752.

From the V, (V-K) and V, (B-V) isochrones we determine ages for M30 of (16±3) and (14±2) Gyr respectively.

7 COMPARISON OF DISTANCE AND REDDENING INDEPENDENT AGE ESTIMATES WITH THOSE FROM THE ISOCHRONES

Table 24 summarises the ages determined for each cluster from the comparisons of the isochrones and colour-magnitude diagrams, and compares these with the ages determined from the (V-K) and (B-V) colour differences between the turn-off and subgiant branch.

Note first that the ages derived for M13 and NGC6752 from the V, (V-K) isochrones are in poor agreement with the ages derived from the V, (B-V) isochrones. The ages derived for M30 from the isochrones agree within the internal errors but are still 2 Gyr different. However, the ages determined for 47 Tuc are in good agreement. It is also in 47 Tuc that the theoretical and observed giant branches match in both V, (V-K) and V, (B-V). Thus it is quite probable that the correction of 0.12 magnitudes which Bell suggested should be applied to the isochrone (V-K) colours, and which we have already seen is probably not appropriate for the low-gravity low-abundance colours, is also a function of abundance

Figure 16: The V_0, $(V-K)_0$ colour-magnitude diagram of M30 with the [Fe/H]=-2.26 [O/Fe]=0.75 Bergbusch & VandenBerg isochrones overlaid.

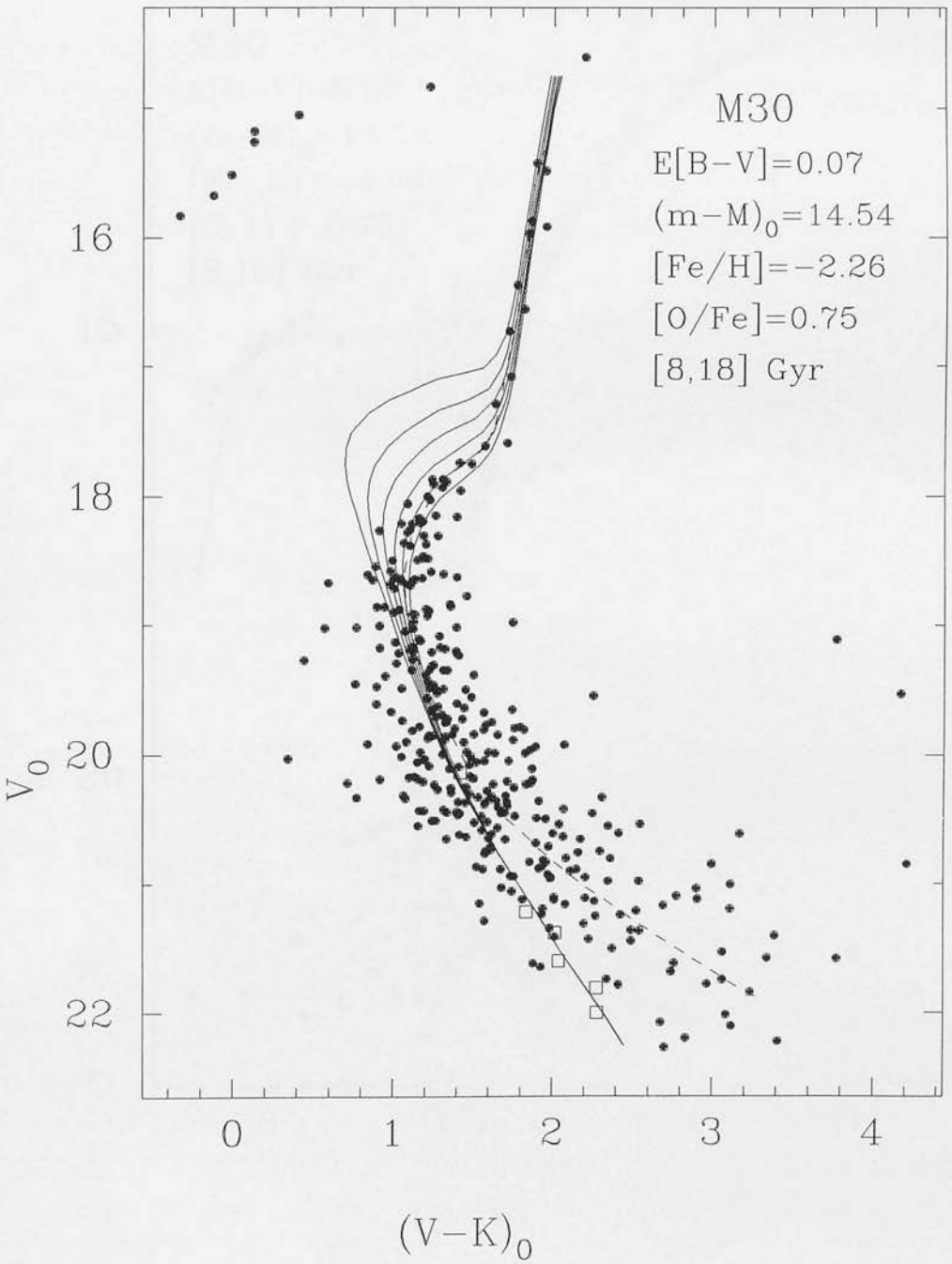

Figure 17: As 16, but showing the full optical data of Richer, Fahlman & VandenBerg (1988) and the Dorman (1992) zero-age horizontal-branch.

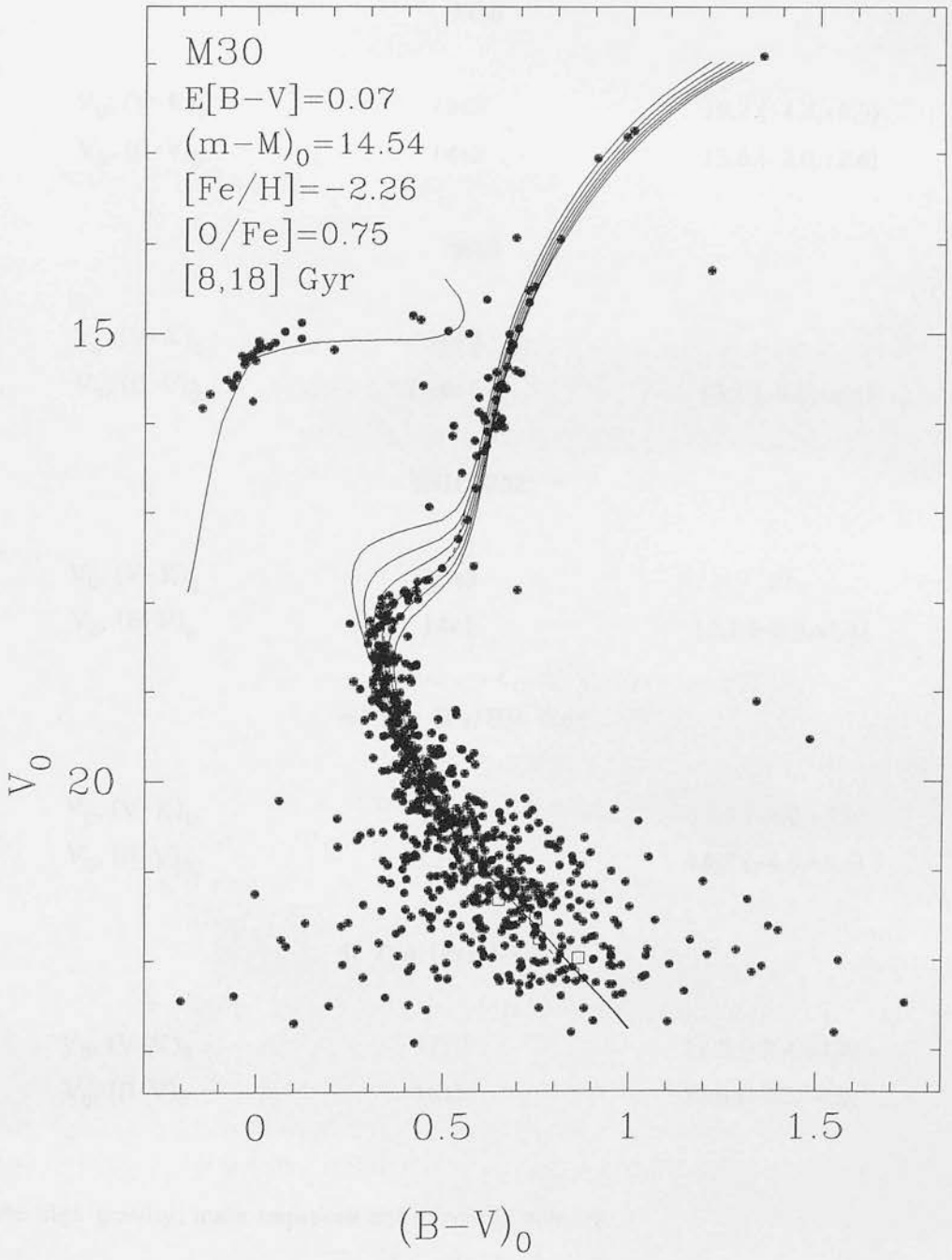

Table 24: A comparison of globular cluster ages derived from Bergbusch & VandenBerg isochrones with ages derived from $\Delta(V-K)$ and $\Delta(B-V)$.

Plane	age/Gyr from colour-magnitude diagram	age/Gyr from Δ
	M30	
V_0, $(V-K)_0$	16±3	19.7 (-4.4,+6.5)
V_0, $(B-V)_0$	14±2	15.8 (-2.0,+2.6)
	M13	
V_0, $(V-K)_0$	18±2	-
V_0, $(B-V)_0$	15.0±1.4	13.1 (-0.9,+1.1)
	NGC6752	
V_0, $(V-K)_0$	18±3	21
V_0, $(B-V)_0$	14±1	13.1 (-0.9,+1.1)
	47 Tuc [Fe/H]=-0.65	
V_0, $(V-K)_0$	14±2	14.9 (-4.0,+5.9)
V_0, $(B-V)_0$	13±1	16.2 (-4.3,+5.6)
	47 Tuc [Fe/H]=-0.78	
V_0, $(V-K)_0$	17±2	11.5 (-2.4,+3.9)
V_0, $(B-V)_0$	16±1	13.6 (-3.2,+4.8)

for the high gravity, main sequence and turn-off colours.

Now consider the ages which result from $\Delta(B-V)$ and $\Delta(V-K)$. The ages from $\Delta(V-K)$ must be treated with caution in the cases of M13 and NGC6752, and probably M30, since any difference between the size of the correction to the model colours at low gravity (giant branch) and high gravity (main-sequence and turn-off) will affect this parameter. The

differences in ages derived from $\Delta(V-K)$ and $\Delta(B-V)$ for NGC6752, and also M30 although the errors are larger in that case, is probably due to this. The ages derived for 47 Tuc from $\Delta(V-K)$ and $\Delta(B-V)$ are in as good agreement with each other as were the ages derived directly from the V, (V-K) and V, (B-V) isochrones. However, they give older ages than direct application of the isochrones at [Fe/H]=-0.65 and younger ages at [Fe/H]=-0.78.

7.1 The best overall ages for each cluster

What ages should we adopt for each cluster, given the discussion in the previous section? In the case of M13, NGC6752 and M30, which are the intermediate and metal-poor clusters in our sample, it is quite clear that the ages derived from the V, (V-K) isochrones, whether by direct comparison to the colour-magnitude diagrams or by their calibration of $\Delta(V-K)$, should be avoided. The colour correction suggested by Bell obviously does not apply to the intermediate metallicity giant branches, whereas is does to those of higher metallicity. We must therefore also be suspicious of applying a correction to the main-sequence and turn-off regions which does not vary with metallicity. Economy of hypothesis would suggest that this is the cause of the discrepancy between the ages derived from the V, (V-K) and V, (B-V) isochrones.

For the intermediate and metal-poor clusters we thus adopt the mean of the ages derived from $\Delta(B-V)$ and by direct comparison of the V, (B-V) isochrones.

Now consider the 47 Tuc ages. The good agreement between both the V, (V-K) and V, (B-V) isochrones over the whole colour-magnitude diagram suggests that the global 0.12 magnitude correction to the (V-K) colours *is* appropriate at this metallicity. We should thus be able to trust the ages derived both directly from the isochrones and from $\Delta(V-K)$ and $\Delta(B-V)$. Yet the two methods give discrepant ages both with [Fe/H]=-0.65 and with [Fe/H]=-0.78. This can be resolved if the isochrones which best reproduce the 47 Tuc colour-magnitude diagram have a chemical abundance intermediate between these two values. Recalling the discussion of the chemical abundance of 47 Tuc stars in section 2.7, we argued that *if* one could rescale the scaled-solar models to take an enhancement of α-process elements into account, and *if* for 47 Tuc stars $[m_\alpha/Fe]\sim0.4$ then we should use isochrones with [Fe/H]~-0.65. In order for in intermediate value of [Fe/H] to be appropriate, a value of $[m_\alpha/Fe]\sim0.3$ would be needed, which is certainly within the range $0.2\leq[m_\alpha/Fe]\leq0.5$ allowed by the observations, and is consistent with the oxygen enhancements [O/Fe]=0.3 to 0.4 at these abundances. Remember also that the most consistent picture among the cluster reddenings - at least when intercomparing the (B-V) colours of the subgiant branches - emerged if the abundance for 47 Tuc was taken to be intermediate between [Fe/H]=-0.65 and [Fe/H]=-0.78.

Table 25: The adopted ages for the four clusters.

Cluster	age/Gyr
M30	14.9±2.6
M13	14.1±1.4
NGC6752	13.6±1.1
47 Tuc	14.6±1.5

Table 25 lists our derived ages for each cluster, and a short explanation of how these ages were derived is given here. As we stated earlier, the ages of the intermediate and metal poor clusters are the averages of the ages determined by direct application of the V, (B-V) isochrones and from Δ(B-V). Since the errors from the two methods are comparable, the largest error was assigned to the average in each case. For 47 Tuc, average error bars were first assigned to all the ages from Δ(V-K) and Δ(B-V). Straight averages of the ages at [Fe/H]=-0.65 and -0.78 were taken for each method, leading to four ages, one from the V, (V-K) isochrones, one from the V, (B-V) isochrones and one each from Δ(V-K) and Δ(B-V). The errors on these four average ages were assigned by taking the average error, rounded to the nearest integer Gyr. The four ages were then combined, weighting by the inverse square of the errors, and an error was assigned also by taking the weighted average of the errors.

In the case of the intermediate and metal poor clusters, the errors on the ages from the isochrones and from Δ(V-K) or Δ(B-V) are not independent, since they derive ultimately from the same data, so it is not correct to combine them in quadrature. This is also the case for 47 Tuc, but there the errors determined from the isochrones and from Δ(V-K) or Δ(B-V) are not comparable, so some weighted combination of the ages and the dependent errors was desirable.

8 CONCLUSIONS

This chapter was concerned with the derivation of the distances and ages of the globular clusters M13, M30, NGC6752 and 47 Tuc, using colour-magnitude data incorporating the infrared photometry from Chapter 1.

In section 1 we discussed the Bergbusch & VandenBerg V, (B-V) and V, (V-K) isochrones, which are the most up-to-date self-consistent set of models available, paying particular attention to the methods used to convert the theoretical luminosities and

temperatures to the V, (B-V) [VandenBerg (1992) and Bergbusch & VandenBerg (1992)] and to the V, (V-K) [Bell (1992)] observational planes.

In section 2 we presented the available values of foreground reddening and chemical composition for each cluster from the recent literature, and gave some discussion of the methods used in their determinations. The value of foreground reddening for M30 was found to be controversial, with values ranging from E[B-V]=0.01 to 0.07. We adopted the higher value of E[B-V]=0.07; further justification for this value was given later in the chapter. The chemical composition of 47 Tuc stars was also found to clearly exhibit non-solar ratios. As Pilachowski, Sneden & Wallerstein (1983) have pointed out, abundance measurements of 47 Tuc stars tend to give [Fe/H]~-0.65 where light-element abundances are measured or [Fe/H]~-1 where iron-peak elements are measure. They also note that while [Fe/H]~-0.8 is a good compromise, the concept of an average abundance should be avoided. Given this apparent decoupling of the elemental abundances, we discussed whether isochrones with scaled-solar abundances could be used to derive meaningful results for 47 Tuc. We argued that when the enhancement of α-process elements is taken into account, using the scaling scheme of Straniero, Chieffi & Salaris (1991) - which was criticised as being too simplistic by VandenBerg (1992) - isochrones more metal rich than the 'compromise' abundance of [Fe/H]=-0.78 should be used. Our adopted abundances and reddenings for each cluster are as follows.

Cluster	Adopted metallicity	Adopted foreground reddening E[B-V]
M30	-2.25±0.30	0.07±0.04
M13	-1.4±0.3	0.02±0.01
NGC6752	-1.5±0.3	0.04±0.01
47 Tuc	-0.65 or -0.78	0.04±0.01

Section 3 was concerned with the derivation of cluster distances by main-sequence fitting to subdwarfs. We discussed the pros and cons of determining distances using this method; chief amongst the cons was the application of the controversial Lutz-Kelker corrections to the subdwarf magnitudes. The basic parameters of a sample of 5 field subdwarfs with $\langle$[Fe/H]$\rangle$=-1.4 were presented, as were corrections to the subdwarf absolute magnitudes at fixed colour, determined differentially between the Bergbusch & VandenBerg isochrones, to enable distances to the more metal rich or poor clusters to be determined.

We also presented results of simulations involving fitting the isochrones to the subdwarfs, to illustrate the sensitivity of the subdwarf-determined distances to various sources of error. We found that the distances determined by main-sequence fitting in the V, (V-K), the K, (V-K) and the K, (B-V) planes were less sensitive to some systematic shifts than were the distances determined from V, (B-V). We found that these mixed optical-infrared planes also gave distances which were less sensitive to small photometric errors than those from V, (B-V) until the K photometric error exceeds 2 to 3 times the equivalent V photometric error. The distances from K, (B-V) were the least sensitive to small photometric errors, although critical discussion was given, warning that the results of this simulation at least should be approached with caution.

Distances determined in K, (B-V) were also the least sensitive to incorrectly adopted values of R, the ratio of total-to-selective extinction, although the distances from all the planes were found to be equally sensitive to small errors (±0.03 magnitudes) in the adopted cluster foreground reddening.

When considering the sensitivity of the derived distances to errors in the adopted cluster chemical abundance of ±0.4 dex about [Fe/H]~-1.4, all planes fared equally, underestimating the distance by ~0.21 magnitudes at the metal-rich end of the range and overestimating the distance by ~0.15 magnitudes at the metal-poor end.

Finally, distances to each cluster were derived, and are summarised in Table 16.

Section 4 was concerned with estimating cluster ages using the distance and reddening independent (V-K) and (B-V) colour differences between the cluster turn-offs and the subgiant branches. These were calibrated to derive absolute ages using the isochrones. VandenBerg, Bolte & Stetson (1991) have warned that such ages are untrustworthy because the subgiant branch colours are just too sensitive to present uncertainties in convective theory and colour-temperature equations. Despite this, such ages are insensitive to any global correction to the isochrone colours, such as that suggested by Bell (1992) for the V, (V-K) isochrones, and we felt that these ages could offer important constraints when compared to ages derived directly from the isochrones and cluster colour-magnitude data.

The ages derived for each cluster from Δ(V-K) and Δ(B-V) are summarised in Table 19. The ages determined from Δ(V-K) for all the clusters bar 47 Tuc disagree with those determined from Δ(B-V).

In section 5 we used the observed colours of the subgiant branches to determine if the adopted reddenings were internally consistent among our four clusters. Variations in age and abundance were removed using the isochrones. Most weight was given to the (B-V) comparisons, since following the discussion in the previous section we were suspicious of

comparisons involving (V-K) - and especially those also involving NGC6752. We found marginal evidence that the reddening adopted for M30 is 0.01 to 0.02 magnitudes too high, although the evidence is too marginal to make a definitive statement about this. A value of E[B-V]=0.02 for M30, as is adopted in some studies, was found to be too low. There is good agreement between the derived and adopted relative reddenings of 47 Tuc and NGC6752 or M13, all of which have less controversial reddenings that M30, whichever abundance is selected for 47 Tuc, although most consistency is found if the abundance of 47 Tuc is midway between [Fe/H]=-0.78 and -0.65.

Absolute ages were determined in section 6 by comparing the isochrones directly to the cluster colour-magnitude diagrams, and are summarised in Table 24. We found that the V, (B-V) isochrones agree well over the entire colour-magnitude diagram of each of the four clusters, while only in the case of 47 Tuc was satisfactory agreement found between the colour-magnitude diagram and the V, (V-K) isochrones. The observed and theoretical V, (V-K) giant branches of both M13 and NGC6752 disagreed, suggesting that the 0.12 magnitude correction to the isochrone (V-K) colours is not appropriate at low metallicity and low gravity. We were unable to ascertain if this discrepancy persisted at the abundance of M30, because there in no infrared photometry of M30 giants.

Finally, in section 7, comparison was made between the ages derived from the two methods, and the best overall ages were adopted and are summarised in Table 25. Since the available evidence suggests that it is only at the abundance of 47 Tuc where the global 0.12 magnitude correction to the V, (V-K) isochrone colours is appropriate, we adopted for the other three clusters the mean of the ages determined from Δ(B-V) and directly from the V, (B-V) isochrones. We must await the 'new' isochrones presented in Chapter 4 before our K data can be used to the fullest in deriving ages for these clusters.

For 47 Tuc, we found good agreement between the ages derived from the V, (V-K) and V, (B-V) isochrones. We also found good agreement between the ages derived from Δ(V-K) and Δ(B-V). However, the ages derived from these two methods are discrepant unless a metallicity intermediate between [Fe/H]=-0.65 and [Fe/H]=-0.78 is assumed, as was suggested when the reddenings of the clusters were intercompared.

REFERENCES

Bell, R.A., 1992. *Mon. Not. Roy. astr. Soc.* **257**, 423.
Bell, R.A. & Dickens, R.J., 1980. *Astrophys. J.* **242**, 657.
Bell, R.A. & Gustaffson, 1978. *Astron. Astrophys. Suppl.* **34**, 229.
Bell, R.A., Hesser, J.E. & Cannon, R.D., 1984. *Astrophys. J.* **283**, 615.
Bergbusch, P.A. & VandenBerg, D.A., 1992. *Astrophys. J. Suppl.* **81**, 163.

Bessel, M.S., Sutherland, R.S. & Ruan, K., 1991. *Astrophys. J. Lett.* **383,** L71.

Bica, E.L.D. & Pastoriza, M.G., 1983. *Astrophys. Space. Sci.* **91,** 99.

Bolte, M.J., 1987. *Astrophys. J.* **319,** 760.

Brown, J.A. & Wallerstein, G., 1992. *Astron. J.* **104,** 1818.

Buckley, D.R.V. & Longmore, A.J., 1992. *Mon. Not. Roy. astr. Soc.* **257,** 731.

Burstein, D. & Heiles, C., 1978. *Astrophys. J.* **225,** 40.

Butler, D., 1975. *Astrophys. J.* **200,** 68.

Cannon, R.D., 1974. *Mon. Not. Roy. astr. Soc.* **167,** 551.

Cannon, R.D. & Stobie, R.S., 1973. *Mon. Not. Roy. astr. Soc.* **162,** 227.

Carney, B.W., 1979a. *Astron. J.* **84,** 515.

Carney, B.W., 1979b. *Astrophys. J.* **233,** 211.

Cohen, J.G., Frogel, J.A. & Persson, S.E., 1978. *Astrophys. J.* **222,** 165.

Crawford, D.L. & Barnes, J.V., 1969. *Astron. J.* **74,** 1008.

Crawford, D.L. & Snowden, M.S., 1975. *Publs astr. Soc. Pacif.* **87,** 561.

Dickens, R.J., 1972. *Mon. Not. Roy. astr. Soc.* **157,** 299.

Dixon, R.I., 1992. Ph.D. thesis, University of Edinburgh.

Dixon, R.I. & Longmore, A.J., 1993. *Mon. Not. Roy. astr. Soc.* accepted.

Dorman, B., 1992. *Astrophys. J. Suppl.* **81,** 221.

Frogel, J.A., Persson, S.E. & Cohen, J.G., 1981. *Astrophys. J.* **246,** 842.

Frogel, J.A., Cohen, J.G. & Persson, S.E., 1983. *Astrophys. J.* **275,** 773.

Frogel, J.A., Persson, S.E. & Cohen, J.G., 1983. *Astrophys. J. Suppl.* **53,** 713.

Gratton, R.G., Quarta, M.L. & Ortolani, S., 1986. *Astron. Astrophys.* **169,** 208.

Helfer, H.L., Wallerstein, G. & Greenstein, J.L., 1959. *Astrophys. J.* **129,** 700.

Hesser, J.E. & Hartwick, F.D.A., 1977. *Astrophys. J. Suppl.* **33,** 361.

Hesser, J.E., Harris, W.E., VandenBerg, D.A., Allwright, J.W.B., Shott, P. & Stetson, P.B., 1987. *Publs astr. Soc. Pacif.* **99,** 739.

Hesser, J.E. & Philip, A.G.D., 1976. *Publs astr. Soc. Pacif.* **88,** 522.

Koen, C., 1992. *Mon. Not. Roy. astr. Soc.* **256,** 65.

Kurucz, R.L., 1979. *Astrophys. J. Suppl.* **40,** 1.

Laird, J.B., Carney, B.W. & Latham, D.W., 1988. *Astron. J.* **95,** 1843.

Lee, S-W., 1977. *Astron. Astrophys. Suppl.* **27,** 381.

Lee, Y-W., 1991. *Astrophys. J. Lett.* **373,** L43.

Lehnert, M.D., Bell, R.A. & Cohen, J.G., 1991. *Astrophys. J.* **367,** 514.

Liu, T. & Janes, K.A., 1990. *Astrophys. J.* **360,** 561.

Lutz, T.E. & Kelker, D.H., 1973. *Publs astr. Soc. Pacif.* **85,** 573.

Mallia, E.D., 1977. *Astron. Astrophys.* **60,** 195.

McClure, R.D. & Racine, R., 1969. *Astron. J.* **74,** 1000.

Norris, J., Cottrell, P.L., Freeman, K.C. & Da Costa, G.S., 1981. *Astrophys. J.* **244,** 205.

Osborn, W., 1971. Ph.D. thesis, Yale University.

Osborn, W., 1973. *Astrophys. J.* **186,** 725.

Penny, A.J. & Dickens, R.J., 1986. *Mon. Not. Roy. astr. Soc.* **220,** 845.

Pilachowski, C.A., 1984. *Astrophys. J.* **281,** 614.

Pilachowski, C.A., Sneden, C. & Wallerstein, G., 1983. *Astrophys. J. Suppl.* **52,** 241.

Pilachowski, C.A., Sneden, C. & Wallerstein, G., 1983. *Astrophys. J. Suppl.* **52,** 241.

Pilachowski, C.A., Wallerstein, G. & Leep, E.M., 1980. *Astrophys. J.* **236,** 508.

Piotto, G., King, I.R., Capaccioli, M., Ortolani, S. & Djorgovski, S., 1990. *Astrophys. J.* **350,** 662.

Richer, H.B. & Fahlman, G.G., 1986. *Astrophys. J.* **304,** 273.

Richer, H.B., Fahlman, G.G. & VandenBerg, D.A., 1988. *Astrophys. J.* **329,** 187.

Rieke, G.H. & Lebofsky, M.J., 1985. *Astrophys. J.* **288,** 618.

Sandage, A.R., 1964. *Observatory* **84,** 245.

Sandage, A.R., 1969. *Astrophys. J.* **157,** 515.

Sandage, A.R., 1970. *Astrophys. J.* **162,** 841.

Sandage, A.R., 1983. *Astron. J.* **88,** 1159.

Sandage, A.R. & Fouts, G., 1987. *Astron. J.* **93,** 74.

Sarajedini, A. & Demarque, P., 1990. *Astrophys. J.* **365,** 219.

Smith, H. Jr., 1987a. *Astron. Astrophys.* **171,** 336.

Smith, H. Jr., 1987b. *Astron. Astrophys.* **171,** 342.

Spite, M. & Spite, F., 1991. *Astron. Astrophys.* **252,** 689.

Stetson, P.B. & Harris, W.E., 1988. *Astron. J.* **96,** 909.

Straniero, O. & Chieffi, A., 1991. *Astrophys. J. Suppl.* **76,** 525.

Straniero, O., Chieffi, A. & Salaris, M., 1991. *Mem. Soc. Astron. Ital.* **63,** 315.

Turner, D.G., 1976. *Astron. J.* **81,** 1125.

VandenBerg, D.A., 1992. *Astrophys. J.* **391,** 685.

VandenBerg, D.A. & Bell, R.A., 1985. *Astrophys. J. Suppl.* **58,** 561.

VandenBerg, D.A., Bolte, M. & Stetson, P.B., 1990. *Astron. J.* **100,** 445.

Webbink, R.F., 1985. International Astronomical Union Symposium **113** 541.

Zinn, R., 1980. *Astrophys. J. Suppl.* **42,** 19.

Zinn, R. & West, M.J., 1984. *Astrophys. J. Suppl.* **55,** 45.

Chapter 3

New Colours from ATLAS9 Model Atmospheres

"Essentia non sunt multiplicanda praeter necessitatem (entities are not to be multiplied except of necessity)" - William of Ockham.

ABSTRACT

We have calculated a new grid of (B-V) and (V-K) colours, and bolometric corrections from ATLAS9 spectral energy distributions with 2 km s^{-1} microturbulent velocity and covering $0 \leq \log_{10}(g/cm\ s^{-2}) \leq 5$, $-5 \leq [Fe/H] \leq +1$, $3500 \leq T_e/K \leq 50000$. The model colours were normalised by assuming that a Vega model has (B-V)=(V-K)=0.

We have attempted to use empirical temperatures of field stars, which were determined, almost independently of model atmospheres, from interferometric angular diameters and observed flux distributions, to check the temperature normalisation of the models. Although the temperatures determined from both (B-V) and (V-K) colours reproduce the empirical temperatures within the errors, the sample is too small and the errors too large to draw any firm conclusions about this.

We make comparisons of the (V-K) vs effective temperature relation derived from the new ATLAS9 models with existing relations derived by Peterson & Carney (1979) and by Fernley (1989) from the ATLAS6 models, until recently the most prevalent of the Kurucz models.

1 INTRODUCTION

Model stellar atmosphere calculations are a vital weapon in the armoury of those studying the galactic globular cluster system, as they provide the link between the luminosity vs effective temperature plane of the theoretical stellar evolution calculations and the colour-magnitude plane of the observations. Also, in some cases, the stellar evolution models themselves depend on model atmosphere results for their surface boundary conditions. This was the case for the Bergbusch & VandenBerg (1992) models discussed in the

previous chapter. VandenBerg (1992) remarks that this *should* lead to more realistic results than the more widely adopted procedure which involves assuming a scaled temperature versus optical depth relation. As we pointed out in the last chapter, the fact that the conversion to observational parameters employs the *same* model atmospheres, makes the Bergbusch & VandenBerg results the best self-consistent set of models presently available.

Recently, Kurucz has made available to the community his ATLAS9 model atmosphere code and results (Kurucz, 1991); these represent the latest iteration of models which have been under continuous development for the last three decades.

Previously, the most widely used of the Kurucz models were those produced by ATLAS6 (Kurucz, 1979), which modelled not only continuous opacity but also included data for ~10^6 atomic lines via the statistical 'opacity distribution function' treatment of line opacity (Strom & Kurucz, 1966). Even with such a large line list, the models still had problems with 'missing' opacity, particularly in the ultraviolet, which, because the models were iterated to flux constancy, meant that the predicted colours were too blue. For F and G stars this discrepancy amounted to ~0.05 magnitudes. The lack of molecular opacity data also meant that the models were not reliable for temperatures less than ~6000K.

The developing maturity of the subject is reflected by the specifications of the new ATLAS9 models. The opacity distribution functions are calculated for a line list which now contains 58×10^6 atomic *and* molecular lines - CH, NH, OH, MgH, SiH, CN, C_2 TiO, H_2, CO and SiO data have been included, along with 42×10^6 lines from the first nine ions of Ca through to Ni. The inclusion of the new data seems to have solved the missing opacity problem (Kurucz, 1992), and makes the models reliable for temperatures greater than ~4000K. Below this, opacity due to triatomic molecules, in particular H_2O, becomes important. Hopefully the near future will see the inclusion of H_2O opacity in the models, although this requires a mammoth computational effort - out of a possible ~10^9 transitions, parameters for 20×10^6 have been calculated (Jørgensen, Jensen & Sørensen, 1993) although this will probably need to double before a realistic treatment of this opacity source can be included in model atmospheres (Jones, 1993, private communication).

The new models also reflect the increased computing power available now, leading to improvement of the numerical accuracy when high or rapidly varying opacity is modelled, and allows more and shallower optical depth layers and more wavelength points to be calculated. Specifically, the new model flux distributions have 1221 wavelength points between 9 and 160000nm, with typically 1, 2 and 10nm spacings in the ultraviolet, visible and infrared. This latter is a welcome improvement when deriving infrared magnitudes

from these flux distributions; now there are 40 flux points within the K band where before there were only points at 1.8 and 2.7μm.

In this Chapter we discuss the derivation of (B-V) and (V-K) colours, and bolometric correction from the 25 January 1993 release of the ATLAS9 spectral energy distributions, including a detailed discussion of the treatment of the terrestrial atmospheric transmission. We attempt to check the temperature normalisation of the models by comparison with the empirically derived temperatures of a sample of metal-rich field stars. Finally, comparison is made of temperatures derived from the new models with the temperature scales of other studies.

2 FILTER PROFILES AND THE TERRESTRIAL ATMOSPHERIC TRANSMISSION

The B and V filter profiles were taken from Buser & Kurucz (1978) and are the same as those given by Ažusienis & Straižys (1969) but without the 'red leak' on the B filter. The effect of this red leak is extremely small, since it has a peak transmission of only 0.00014. The K filter profile is that of the Optical Coating Laboratory, inc. K filter used in the common-user array camera IRCAM, at the operating temperature of 77K (Aspin, 1992, private communication). This profile, with the transmission normalised to unity at the maximum, is reproduced in Table 1.

The optical terrestrial atmospheric extinction has been calculated for Cerro Tololo following the method of Hayes & Latham (1975), which assumes that the extinction is a combination of Rayleigh and aerosol scattering and absorption by Ozone. The optical extinction above Cerro Tololo has been taken as representative of the extinction above a good mountain site. The method is reiterated here and the formulae giving the extinction due to each component of the model are reproduced.

Atmospheric Rayleigh scattering is well understood theoretically, and $A_{Ray}(\lambda,h)$, the extinction in magnitudes per airmass at wavelength λ over an observatory of height h, is given by equations 1, the lower of which is the index-of-refraction term.

$$A_{Ray}(\lambda,h) = 9.4977\times10^{-3}\left(\frac{\lambda}{\mu m}\right)^{-4}\left[\frac{(n-1)_\lambda}{(n-1)_{\lambda=1}}\right]^2 \exp\left(\frac{-h}{7.996km}\right)$$

$$\frac{(n-1)_\lambda}{(n-1)_{\lambda=1}} = 0.23465 + \frac{1.076\times10^2}{146-\left(\frac{\lambda}{\mu m}\right)^2} + \frac{0.93161}{41-\left(\frac{\lambda}{\mu m}\right)^2} \qquad (1)$$

Extinction due to Ozone is given by equation 2, again in terms of the extinction in

Table 1: The IRCAM K filter profile at 77K.

λ/μm	Transmission	λ/μm	Transmission	λ/μm	Transmission
1.94	0.000	2.16	0.923	2.38	0.949
1.96	0.013	2.18	0.923	2.40	0.821
1.98	0.026	2.20	0.897	2.42	0.577
2.00	0.103	2.22	0.872	2.44	0.308
2.02	0.256	2.24	0.872	2.46	0.128
2.04	0.449	2.26	0.923	2.48	0.051
2.06	0.667	2.28	0.974	2.50	0.026
2.08	0.782	2.30	1.000	2.52	0.013
2.10	0.821	2.32	0.974	2.54	0.000
2.12	0.833	2.34	0.949		
2.14	0.885	2.36	0.949		

Table 2: Ozone absorption coefficients.

λ/μm	k_{oz}/cm^{-1} (Table 7-1)	$k_{oz}(18°C)/cm^{-1}$ (Table 7-3)	$k_{oz}(-44°C)/cm^{-1}$ (Table 7-3)
0.30	10.1	9.65	8.88
0.32	0.898	0.898	0.781
0.34	0.064	0.064	0.055
0.36	0.0018	0.0018	-
0.38	0	-	-

$$A_{oz}(\lambda) = 1.11 T_{oz} k_{oz}(\lambda) \qquad (2)$$

magnitudes per airmass at wavelength λ. In this case the extinction does not depend on the observatory height because most atmospheric ozone is located between 10 and 35 km above sea level. T_{oz} is the total amount of ozone above the observatory in atm-cm. Bi-monthly or year-average values of T_{oz} are given as a function latitude by Allen (1963). Rather than assume any specific observation time, we have interpolated within the year-

average values to determine T_{oz}=0.24 atm-cm at the Cerro Tololo latitude of -30.165 degrees. The ozone absorption coefficients (in cm^{-1}) have been taken from Tables 7-1 and 7-3 of Valley (1966). Table 7-3 contains coefficients on a finer wavelength mesh, but over a smaller wavelength range, than the values in Table 7-1, and for temperatures of 18, -44 and -59°C. From examination of these tables we conclude that the coefficients in Table 7-1, which Elterman uses to calculate his atmospheric model, are for Ozone at 18°C. This is rather hot given the altitude at which most atmospheric Ozone is concentrated. However, rather than attempt any potentially unphysical correction of the Table 7-1 values we have adopted the absorption coefficients at 18°C for our model, although this will lead to an overestimate of the extinction due to Ozone. Table 2 reproduces the coefficients where Tables 7-1 and 7-3 overlap, and shows that, except at the shortest wavelengths, the change in absorption coefficient from 18 to -44°C is small. Our choice will be further justified later in this section.

$$A_{aer}(\lambda,h) = A_0\left(\frac{\lambda}{\mu m}\right)^{-\alpha}\exp\left(\frac{-h}{H}\right) \qquad (3)$$

Extinction from scattering due to particulate material in the atmosphere - aerosol scattering - is given by equation 3. We adopt the Hayes & Latham values of H=1.5km and α=0.8. They note that the former value can be in error by as much as a factor of ~2 on any given night. The value adopted for the latter is representative of several sites, and is close to the Cerro Tololo value of 0.81. Hayes & Latham fix the value of A_0 so that at 0.5μm the extinction due to aerosol scattering makes up the difference between the observed extinction and the extinction due to Rayleigh scattering. They chose to do this at 0.5μm to avoid calculating the extinction due to Ozone which is zero at that wavelength. We have calculated values of A_0 at each of the five wavelengths for which an observed extinction for Cerro Tololo is reported in their Table 4, such that aerosol scattering makes up the difference between the observed extinction and the sum of the Rayleigh *and* Ozone extinctions. These values of A_0 are given in Table 3. We adopted the mean of these five values and used equations 1 to 3 to predict the total extinction at each wavelength, and the residuals from the observed extinctions are also reported in Table 3, in the sense observed minus calculated. For comparison, the residuals in parentheses are those calculated by Hayes & Latham by fixing A_0 at 0.5μm, where the residual is zero by definition.

The observed extinction is reproduced very well, certainly to well within the limits to which the extinction by Rayleigh scattering alone can be modelled or the observed extinctions measured, and this further justifies our use of the Ozone absorption coefficients at 18°C.

In figure 1(a) we show the atmospheric transmission - which is trivially determined from the extinctions - against wavelength from each component of the model, together with the

Table 3: Optical extinction parameters for Cerro Tololo.

λ/μm	Observed extinction (magnitudes airmass^{-1})	A_0	Residual extinction (observed - calculated)
0.34	0.680	0.138	0.000 (0.006)
0.36	0.541	0.147	0.005 (0.008)
0.42	0.308	0.138	0.000 (0.003)
0.47	0.215	0.136	0.000 (0.004)
0.50	0.179	0.127	-0.004 (0.000)
mean		0.137	0.000 (0.004)

B and V filter profiles.

The terrestrial atmospheric transmission in the K band has been calculated for Mauna Kea, assuming a precipitable water vapour content of 1.2mm, from IRTRANS transmission spectra (Traub & Stier, 1976) using (unpublished) software from the CGS4 database at the Royal Observatory, Edinburgh. This transmission spectrum, together with the K filter profile of Table 1, is shown in figure 1(b).

3 CALIBRATION OF THE MODEL COLOURS

Linear interpolation was used to place the filters, the atmospheric transmissions at one airmass and the model spectral energy distributions on the same wavelength scale with spacings of 1nm, before multiplying them and integrating numerically. B, V and K magnitudes were defined as in equation 4, where F_λ is the model flux, S_λ is the filter

$$S = -2.5\log_{10}\left(\frac{\int_\lambda F_\lambda S_\lambda A_\lambda d\lambda}{\int_\lambda S_\lambda A_\lambda d\lambda}\right) \qquad (4)$$

profile and A_λ is the terrestrial atmospheric transmission. We calibrated the (B-V) and (V-K) *colours* by adding a constant to each B, V and K, determined by forcing a Vega model to have zero magnitude in each passband. This model, which was supplied to us by Kurucz, had T_e=9400K, $\log_{10}$(g/cm s^{-2})=3.90, [A/H]=-0.5 and microturbulent velocity 0 km s^{-1}.

Figure 1(a): The B and V filter profiles together with the terrestrial atmospheric transmission curves for the three components of the model.

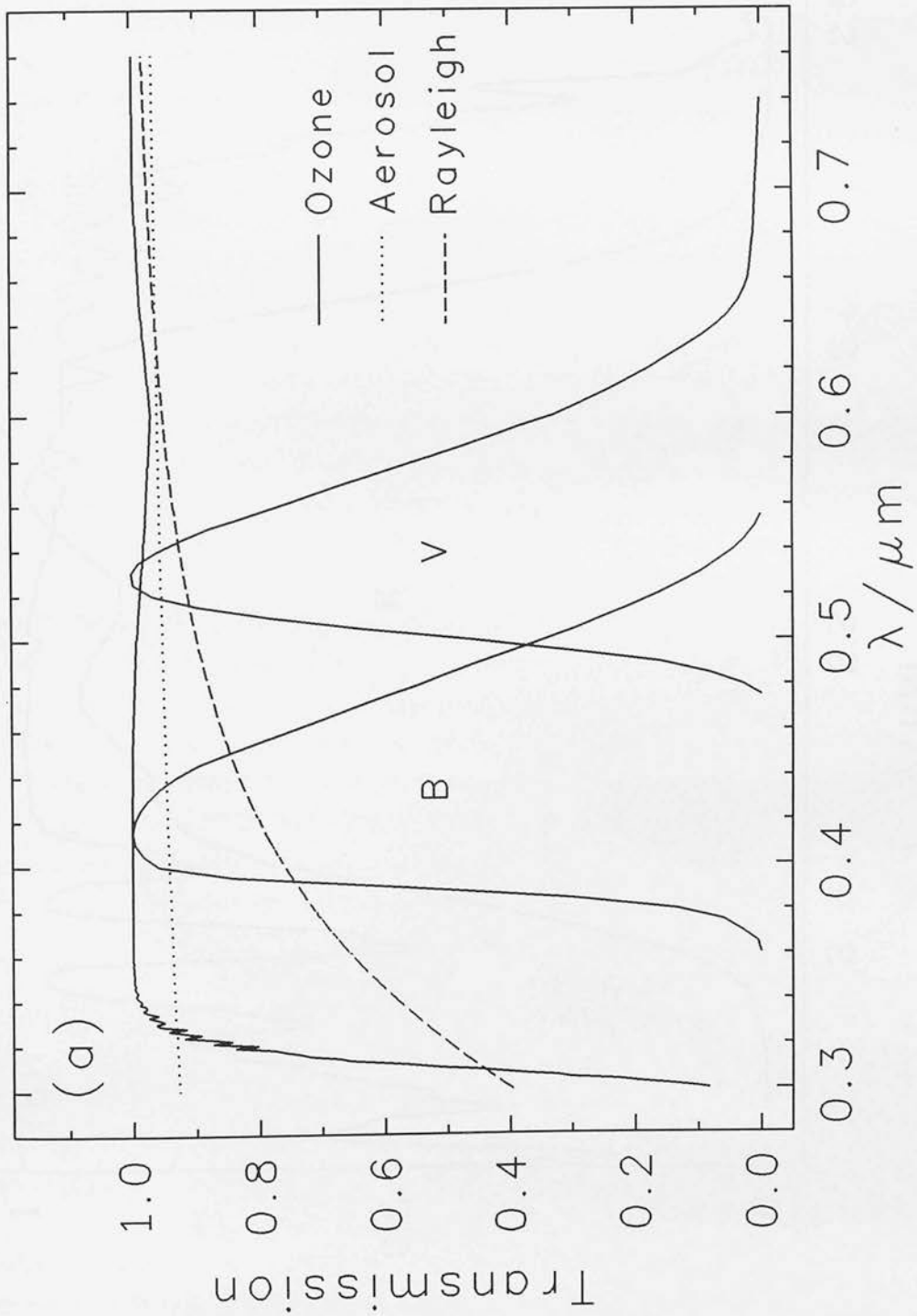

Figure 1(b): The K band filter profile and atmospheric transmission of one airmass with 1.2mm precipitable water vapour content.

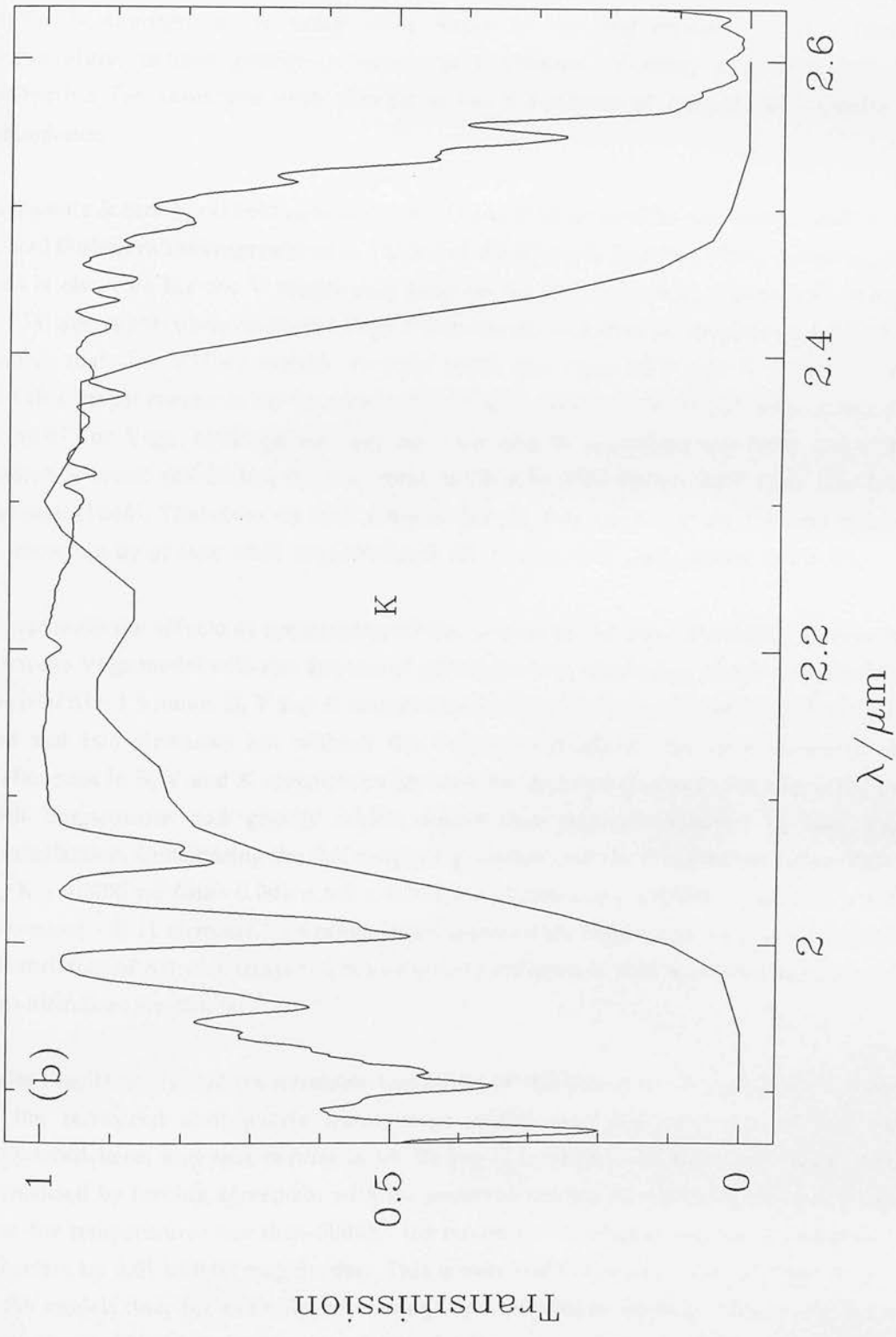

This calibration contains several implicit assumptions which should be examined critically. First it assumes that Vega does indeed have (B-V)=0 on the winter 1951 Johnson system which the B and V filters are designed to reproduce and (V-K)=0 on the mixed Johnson-UKIRT system. Second, it assumes that the normalisation determined from the Vega model is appropriate for every other model in the grid irrespective of effective temperature, surface gravity or heavy metal content. Finally, it assumes that the correction for extinction with airmass is not a function of temperature, gravity or abundance.

Ažusienis & Straižys (1969) note that their U and B filter profiles correspond well to the U and B observations reproduced in Table 2 of Ažusienis & Straižys (1966). Assuming that this is also true for the V magnitudes then for Vega (B-V)=-0.01. Johnson & Morgan (1953) also report observations of Vega which are ostensibly on the original winter system and in that case V=0.03 and (B-V)=0.00. From this value of V and K=0.00 from the UKIRT bright standards list we obtain (V-K)=0.03. However, Fernley (1989) quotes (V-K)=0.01 for Vega, although we have not been able to reproduce this from any of his quoted sources; the closest we can come is (V-K)=-0.03 for an A0V class star from Johnson (1966). Therefore we must assume that the zero-point for the Johnson 'system' is uncertain by *at least* ±0.01 magnitudes in (B-V) and ±0.03 magnitudes in (V-K).

To estimate the effects of normalising all the colours by the same constants, determined from the Vega model with one airmass of atmospheric transmission, we have recalculated the [Fe/H]=-1.5 model B, V and K magnitudes with atmospheric transmissions from zero, one and two airmasses but without the Vega normalisation. We have examined the differences in B, V and K magnitudes between one and two airmasses for any variations with temperature and gravity which would thus not be removed by the Vega normalisation. Considering the full range of gravities, and the temperature range $3500 \leq T_e/K \leq 10000$ we find $-0.001 \leq \Delta K \leq 0.000$ and $-0.006 \leq \Delta V \leq 0.004$, where ΔK = K (2 airmasses) - K (1 airmass). The range in ΔB is somewhat larger, and we present a plot of the variation of ΔB with temperature and gravity in figure 2. The results between one and zero airmasses are similar.

These results imply that the normalisation of the (V-K) colour is not a sensitive function of the terrestrial atmospheric transmission model over the range of temperatures considered here, and that neither is (B-V) for $T_e > \sim 6000K$. If the model colours are normalised by forcing agreement with the observed colours of a hot star, as in this case, then for temperatures less than 6000K, the model (B-V) colours may be systematically uncertain by 0.01 to 0.05 magnitudes. This is over and above any uncertainties inherent in the models due, for example, to missing input physics or opacity. Therefore, if the normalisation is via the observed colours of a hot star, we must exercise caution when comparing observed and model (B-V) colours when $T_e < \sim 6000K$, and vice-versa. It is

Figure 2: The difference in model B magnitudes between two and one airmasses against effective temperature for various gravities.

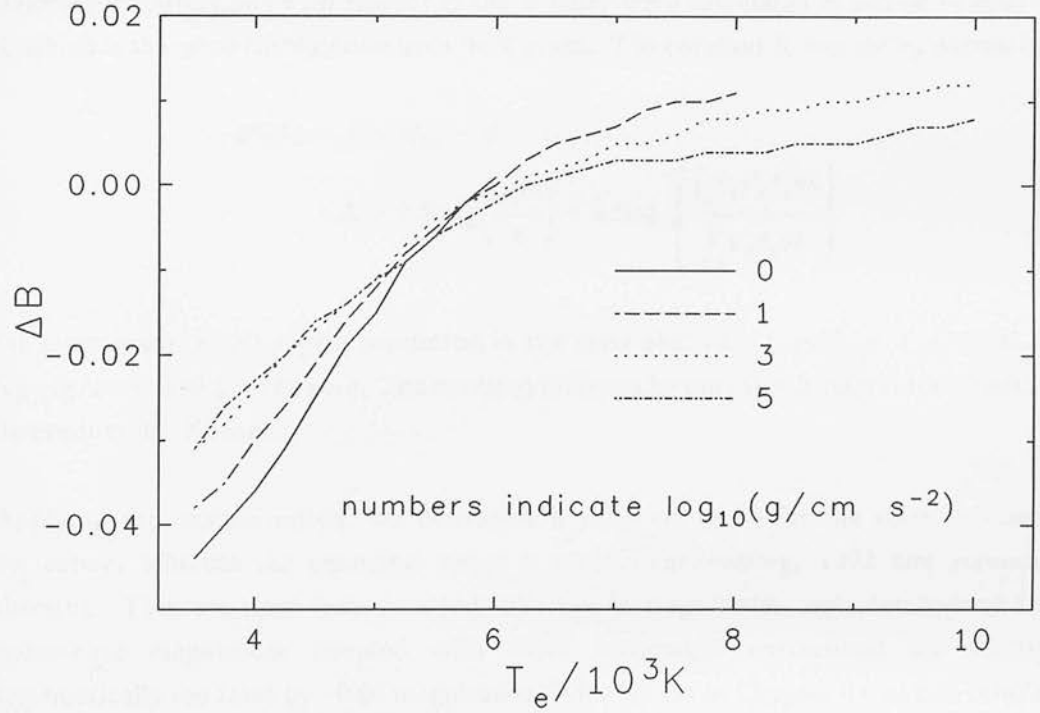

worth remembering that these models do not include opacity due to H_2O, and are unreliable for $T_e < \sim 4000K$.

Older models have had well known normalisation problems, such that if the colours were normalised by forcing agreement with the observed colours of a hot star, the predicted colours of cool stars would be systematically out by a few per-cent, and vice-versa. It is therefore instructive to check our Vega normalised colours for the Sun against observations. Using the spectral energy distribution of a solar model, supplied by Kurucz, with T_e=5777K, $\log_{10}$(g/cm s^{-2})=4.4377, [A/H]=0.0, microturbulent velocity 1.5 km s^{-1} and ratio of mixing length to pressure scale height l/H=1.25, the model solar colours are (B-V)=0.652 and (V-K)=1.502. This value of (B-V) is certainly consistent with the range of $0.63 \leq (B-V) \leq 0.67$ usually adopted for the Sun (see, for example, VandenBerg & Poll (1989), Hayes (1985), Clements & Neff (1979) and references therein). Campins, Rieke & Lebofsky (1985) have determined the solar (V-K) colour to be 1.486±0.025 by taking the mean observed colours of six Hardorp class 1 solar analogue stars, and our predicted value is in excellent agreement with this.

4 BOLOMETRIC CORRECTIONS

Bolometric corrections with respect to the V filter were calculated as shown in equation 5, which is the same formulation used by Kurucz. The constant K was set by normalising

$$\begin{aligned} BC(V) &= K + M_{bol} - V \\ &= K - 2.5\log_{10}\left(\frac{\sigma T^4}{\pi}\right) + 2.5\log_{10}\left(\frac{\int_\lambda F_\lambda V_\lambda A_\lambda d\lambda}{\int_\lambda V_\lambda A_\lambda d\lambda}\right) \end{aligned} \quad (5)$$

the most positive bolometric correction in the solar abundances grid, at T_e=7250K and $\log_{10}(g/cm\ s^{-2})$=0.5, to be zero. The constant differed by only 0.002 magnitudes from that determined by Kurucz.

Applying this normalisation, we determine a value of -0.20 for the solar bolometric correction, whereas the canonical value is -0.12 [VandenBerg, 1992 and references therein]. Thus we must bear in mind that any V magnitudes, say, determined from bolometric magnitudes coupled with these bolometric corrections are probably systematically too faint by ~0.08 magnitudes. We shall see in Chapter 4 that this is indeed the case, and that this zero-point error is constant, at least for high gravities, within the abundance range $-2.26 \leq [Fe/H] \leq -0.65$.

At first sight, it may seem odd that in equation 5 we have set the bolometric magnitude using the equation for the total flux from a black body. It is patently obvious that the spectral energy distribution from a star is *not* that of a black body - hence the need for detailed stellar atmosphere models in the first place. Remember, however, that these stellar models are driven to flux constancy, and so have the same total flux as a black body with effective temperature equal to that of the model.

5 TEMPERATURE NORMALISATION

In this section we discuss the temperature normalisation of the models. We wish to know if, given colour, surface gravity and composition, the new models will reproduce the true effective temperature of a star and which, if either, of the (B-V) or (V-K) colour defined temperatures most closely matches the true stellar temperature.

To answer these questions we need a sample of stars which have accurately known temperatures, gravities, compositions and B, V and K photometry for comparison with the models. Furthermore this information *must* have been derived as independently as possible of other model atmosphere results in order to avoid circularity of argument. We may relax

the condition that gravity be accurately known if the stars under consideration have ~4000<T_e/K<~5800, since, as illustrated in figure 3(a), the (V-K) to effective temperature relation is insensitive to gravity within that range of temperature. For comparison, figure 3(b) shows the (B-V) to effective temperature relation, which is a much more sensitive function of gravity. As a further test of the models, it would also be advantageous to have several large samples of stars meeting the above criteria at several discreet and accurately known compositions.

The sample of stars studied by Code (1975) and Code *et al.* (1976) goes some way towards meeting the criteria outlined above, although to the best of our knowledge, there is unfortunately no sample of stars in the literature which meets them all (see the suggestions for future work in the conclusion).

Code *et al.* derive the effective temperatures of 32 stars via interferometric angular diameters and observed flux distributions. Model atmospheres have been used only to correct these angular diameters for the effects of limb darkening and to extend the flux distributions shortward of 110 nm. Since we are interested only in the cooler stars, the dependence of our results on model atmospheres is further reduced because the short wavelength flux from cool stars is negligible. For example, the flux shortward of 110nm from stars with T_e<~12500K is less than 1 per-cent of the total flux.

Trigonometric parallaxes are available for a subset of 13 of these stars, allowing radii to be determined. Code (1975) estimates the surface gravity of these stars by coupling the radii with masses derived either dynamically or by comparing the empirical luminosities and temperatures with stellar evolution models. Code notes that the gravity determinations are relatively insensitive to errors in the derived masses, because the dominant source of error comes from the radius determination which is in turn due to errors in the observed parallax.

Infrared K band photometry for ten of the stars is available either from the unpublished UKIRT bright standards list or from Fernley (1989). Where information was available from both, that from the UKIRT list was adopted. The optical photometry was taken from Code *et al.* As can be seen from the two-colour diagram of figure 4, this is not an ideal sample of stars, since none of the stars fall within the range where the colour to effective temperature relation is gravity insensitive. Also, none of the stars have temperatures comparable to globular cluster main sequence or giant branch stars, or except for BS2943, with any but the bluest of horizontal branch stars.

The question of an accurate composition is more difficult. Five of the stars have values of [Fe/H] listed in the catalogue of Cayrel de Strobel *et al.* (1992), however the entry for BS7557 (HD187642, α Aql) is erroneously that of α Aqr. The metallicities of the

Figure 3(a): (V-K) vs T_e from the [A/H]=0 Kurucz models.

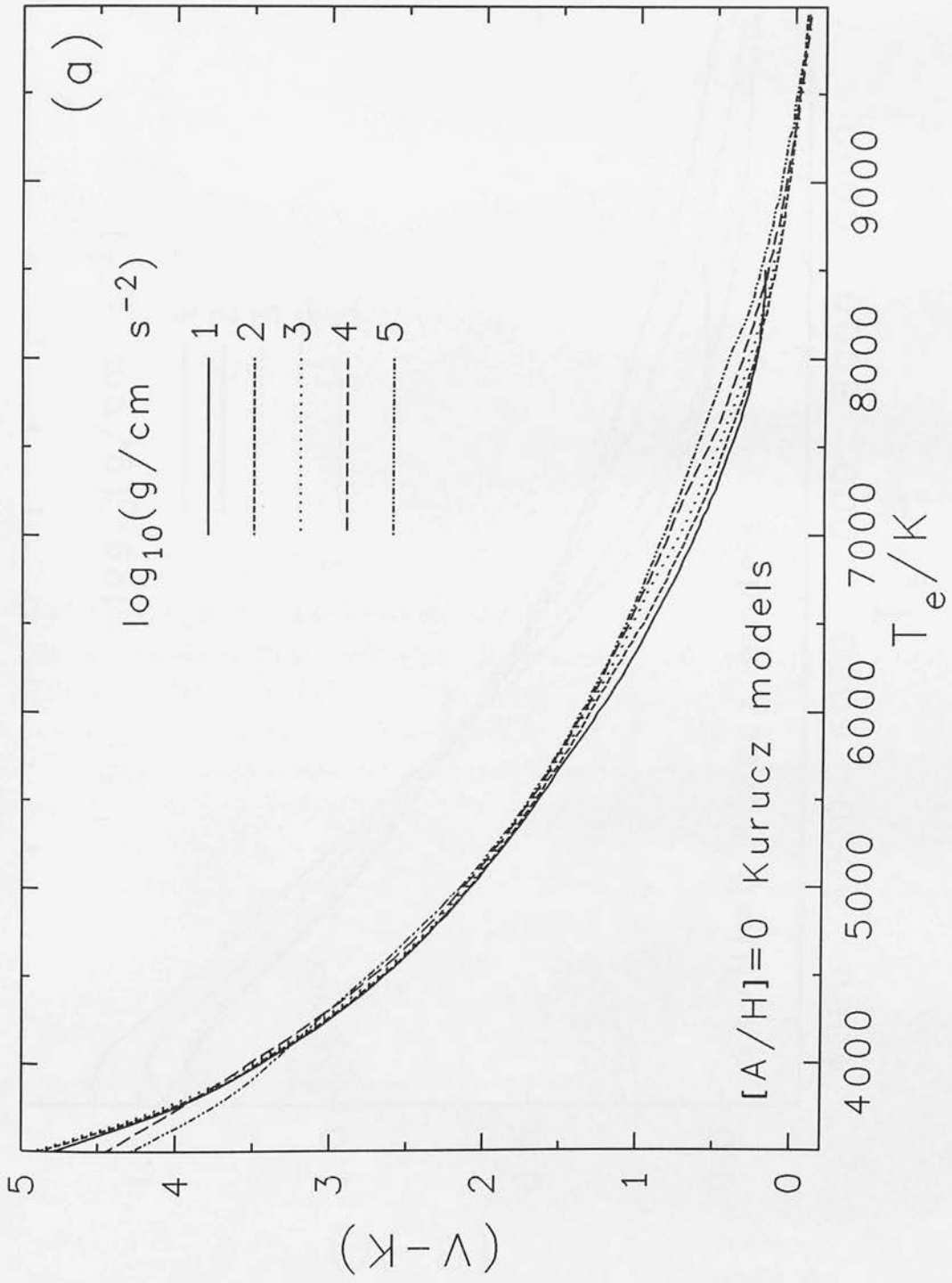

Figure 3(b): (B-V) vs T_e from the [A/H]=0 Kurucz models.

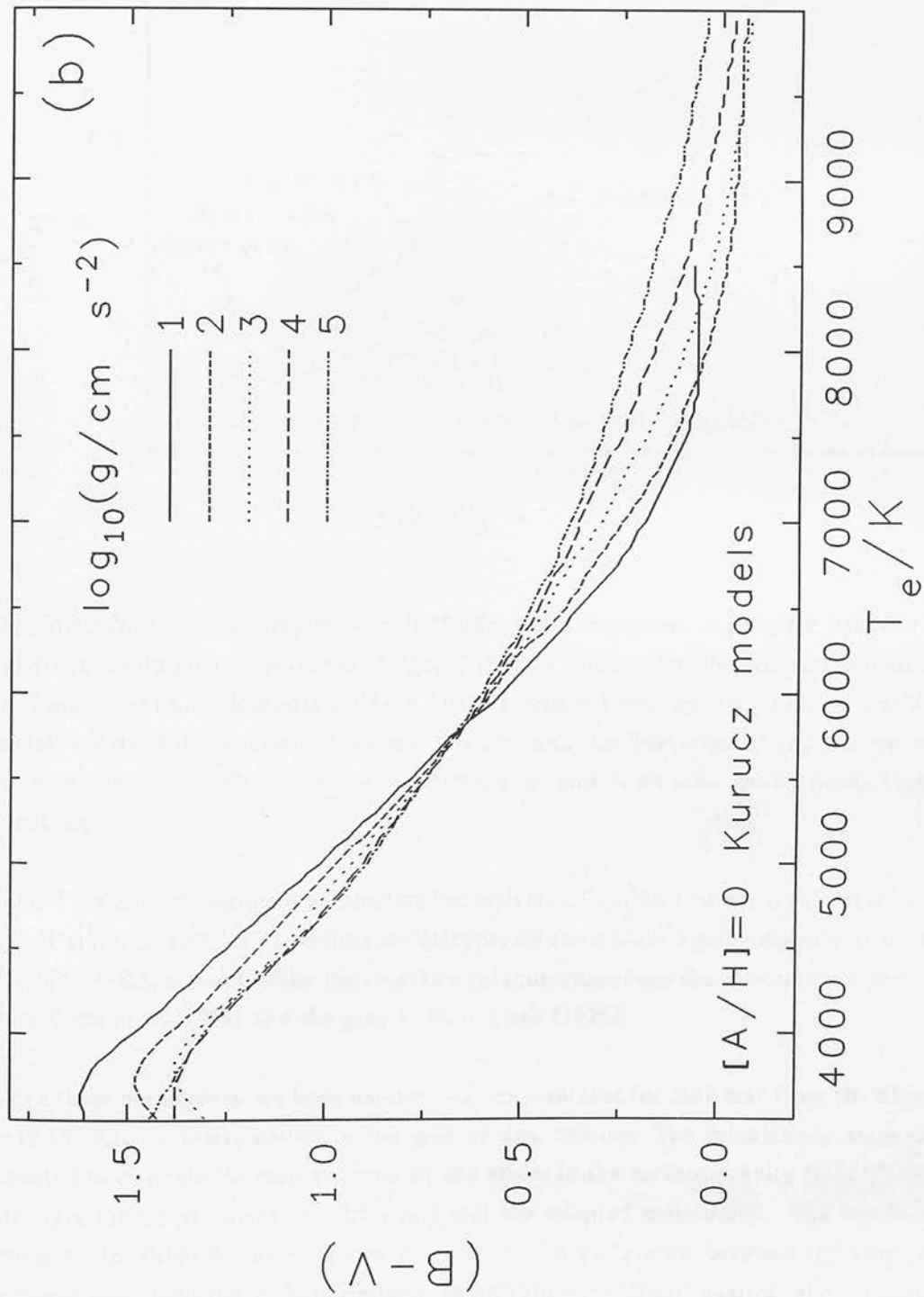

Figure 4: The two-colour diagram of the sample of ten stars with empirical temperatures, accurate trigonometric parallaxes and optical & infrared photometry.

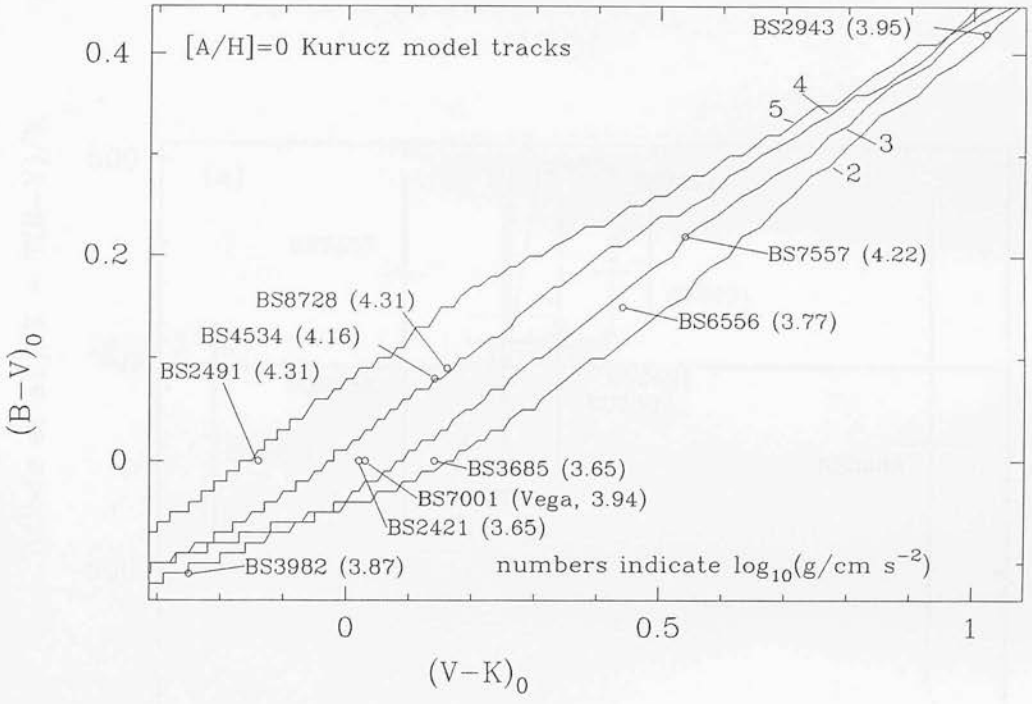

remaining four stars are reproduced in Table 4; unfortunately the scatter between the individual evaluations is extremely large. The final column lists the adopted metallicity. For BS7001 we have adopted [Fe/H]=-0.5 to be consistent with the metallicity of our Vega model. Metallicity determinations are not available for the other stars, and we have assumed [Fe/H]=0. This is rather unsatisfactory, and is an area which needs further attention.

Table 5 presents the adopted parameters for each star. Column 1 identifies the star by the BS/HR number, column 2 lists the spectral type, columns 3 and 4 give respectively the $(B-V)_0$ and $(V-K)_0$ colours, while the final two columns reproduce the effective temperature from Code *et al.* (1976) and the gravity from Code (1975).

Using these parameters, we have determined temperatures for each star from $(B-V)_0$ and from $(V-K)_0$ by interpolation in the grid of new colours. The calculations were then repeated to estimate the errors caused by the errors in the surface gravity from Table 5, and by a metallicity error of ±0.5 dex about the adopted metallicity. The results are presented in Table 6, and in figure 5 we show the difference between the empirical temperatures and the colour-derived temperatures plotted against the empirical temperatures.

The first important point to note from figure 5 is the size of the error bars, which are

Figure 5: The difference between the colour derived temperatures and the empirical temperatures of Code *et al.* The colour derived temperatures are from (a) (B-V), and (b) (V-K).

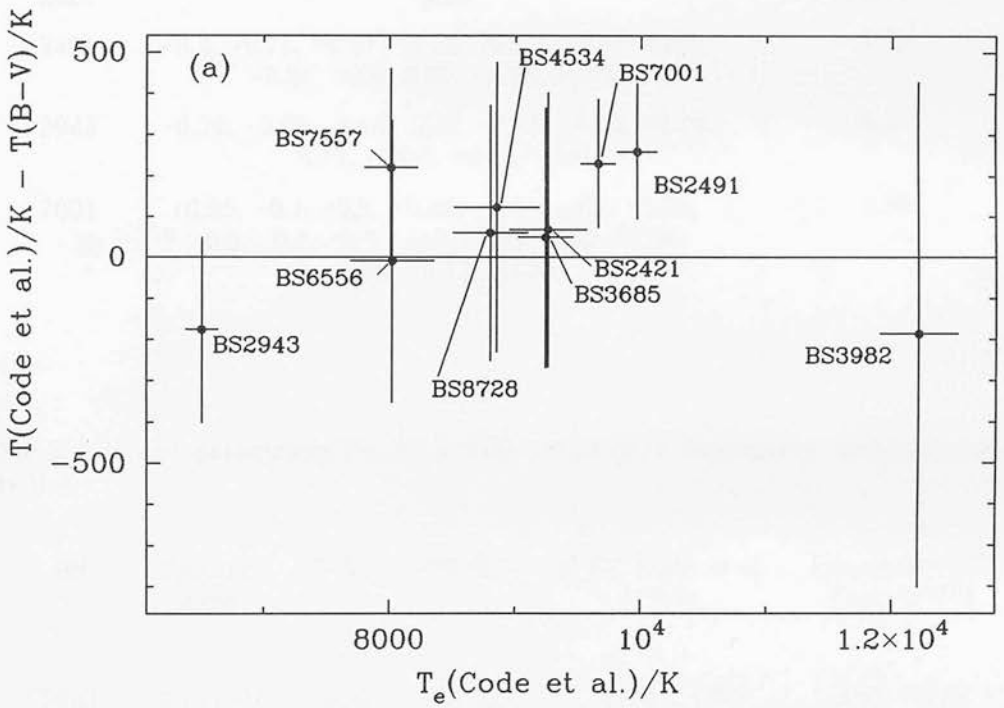

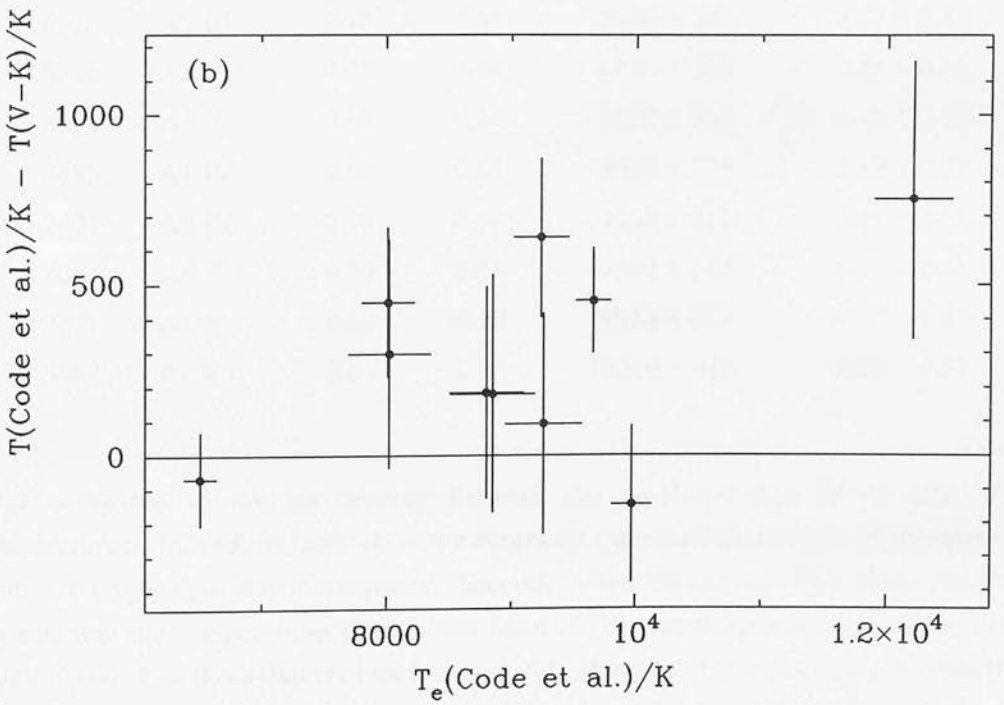

Table 4: Metallicity determinations of four of the Code *et al.* stars.

Star (BS)	[Fe/H] Cayrel de Strobel *et al.*	Adopted [Fe/H]
2421	-0.05	-0.05
2491	+0.4, +0.71, +0.87, +0.36, +0.80, +0.82, +0.70, +0.81, +0.4, 0.00, +0.60, +0.26	0.56
2943	-0.29, +0.03, +0.07, 0.00, +0.22, -0.40, +0.74, -0.15, +0.02, +0.04, +0.01	0.03
7001	+0.05, -0.1, +0.2, +0.06, -0.25, -0.1, +0.02, -0.3, -0.1, -0.9, -0.5, -1.36, 0.00, -0.58, -0.55, -0.73, -0.72	-0.50

Table 5: Adopted parameters for stars with empirically determined temperatures and gravities.

BS	Spectral type	$(B-V)_0$	$(V-K)_0$	T_e/K Code *et al.* (1976)	$\log_{10}(g/cm\ s^{-2})$ Code (1975)
2943	F5 IV-V	0.42	1.02	6510 ± 130	3.95 ± 0.04
7557	A7 IV,V	0.22	0.54	8010 ± 210	4.22 ± 0.08
6556	A5 III	0.15	0.44	8020 ± 330	3.77 ± 0.13
8728	A3 V	0.09	0.16	8800 ± 300	4.31 ± 0.10
4534	A3 V	0.08	0.14	8850 ± 340	4.16 ± 0.12
3685	A1 IV	0.00	0.14	9240 ± 220	3.65 ± 0.31
2421	A0 IV	0.00	0.02	9260 ± 310	3.65 ± 0.17
7001	A0 V	0.00	0.03	9660 ± 140	3.94 ± 0.08
2491	A1 V	0.00	-0.14	9970 ± 160	4.31 ± 0.04
3982	B7 V	-0.11	-0.25	12210 ± 310	3.87 ± 0.22

large compared to the discrepancy between the empirical and (B-V) and (V-K) temperatures. Indeed, in most cases the errors on the empirically derived temperatures alone are larger than this discrepancy. Second, when we consider the whole sample, it appears that the temperatures determined from (B-V) match the empirical temperatures much better than those determined from (V-K). If we limit our attention to those three stars with metallicity determinations, neglecting Vega which is discrepant on both plots, then we conclude the reverse. However, while these data represent the state-of-the-art

Table 6: Temperatures and errors derived from the colours of the Code *et al.* program stars using the new Kurucz model grid.

BS	T(B-V)/K	σT(B-V) [Fe/H]±0.5	σT(B-V) log(g)±σ	T(V-K)/K	σT(V-K) [Fe/H]±0.5	σT(V-K) log(g)±σ
2943	6686	185	4	6579	-47	2
7557	7790	114	28	7562	-59	17
6556	8029	75	63	7723	-54	19
8728	8740	54	69	8617	-79	15
3685	9191	-2	229	8602	-71	38
4534	8727	58	79	8670	-79	18
7001	9430	-14	71	9207	-65	9
2421	9192	-2	126	9168	-92	14
2491	9711	-21	36	10116	-169	2
3982	12397	-468	254	11460	-268	-11

as far as model atmosphere independent temperatures are concerned, they do not have the accuracy, and form such a pitifully small sample that any conclusions drawn from them should be applied with caution, especially to temperature ranges outwith the one defined by this sample.

Considering the advantages gained by use of the longer wavelength baseline and remembering that (V-K) is not expected to suffer from temperature dependent normalisation problems, we tentatively adopt the temperature scale determined from (V-K).

6 COMPARISON WITH OTHER COLOUR-TEMPERATURE RELATIONS

In this section we compare the (V-K) vs effective temperature relations derived from the new Kurucz models with existing relations.

In their Table 4, Peterson & Carney (1979) list (V-K) colours and effective temperatures for 48 metal-poor dwarf stars. The effective temperatures were determined by comparing scanner data with ATLAS6 models with the ratio of mixing length to pressure scale height set to 1, and are quoted as being accurate to ±80K. Some of these effective temperatures have been amended by Carney (1983).

We show in figure 6(a) the (V-K) colours of 38 of these stars plotted against scanner effective temperature. The data have been divided into four metallicity bins with

Figure 6: (V-K) vs scanner temperatures. Also showing ATLAS9 colour vs T_e relations for (a) $\log_{10}$(g/cm s^{-2})=4, $-2 \leq$[A/H]≤ 0, and (b) [A/H]=-1, $\log_{10}$(g/cm s^{-2})=3 & 5.

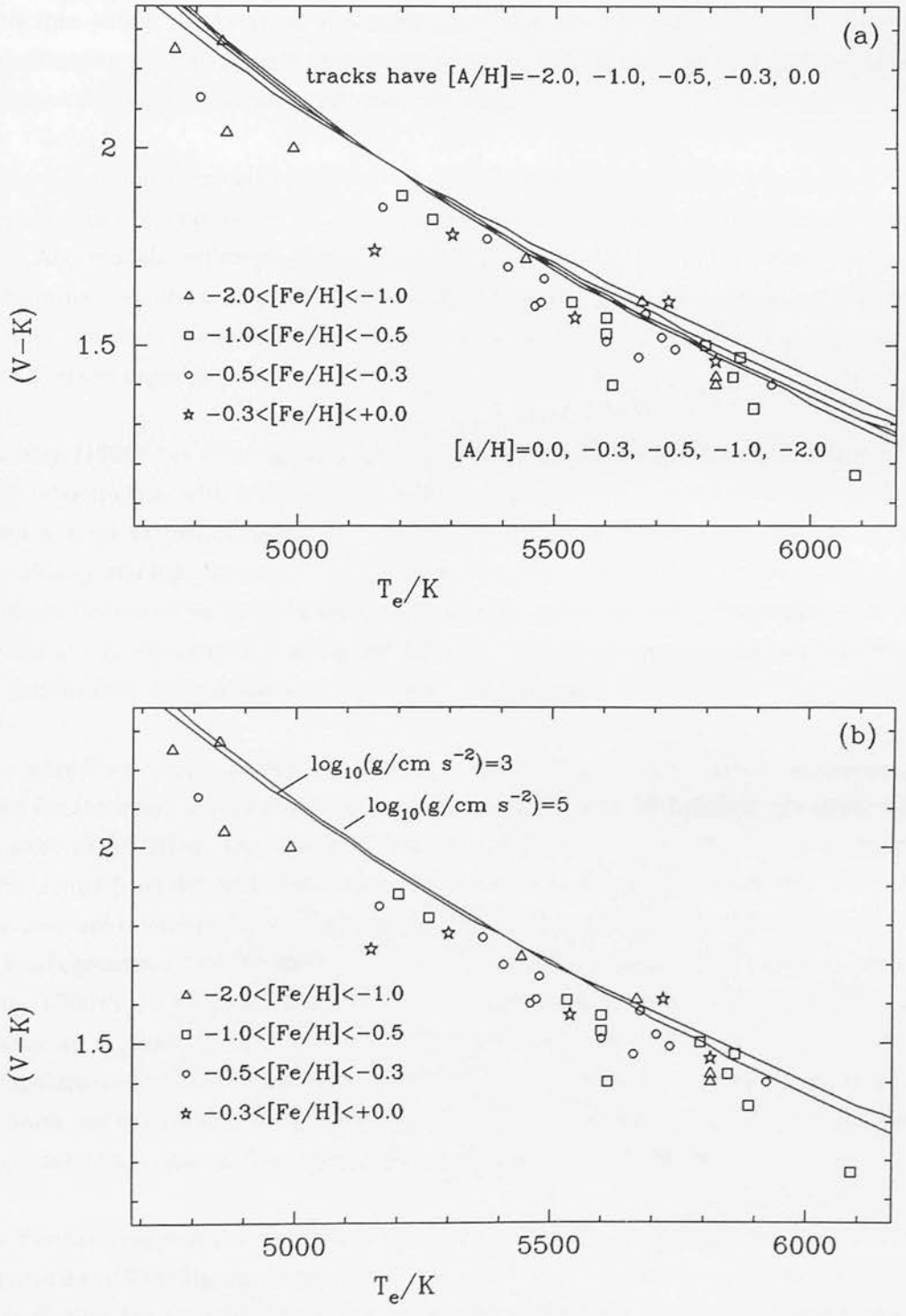

$-2.0<[Fe/H]<-1.0$, $-1.0<[Fe/H]<-0.5$, $-0.5<[Fe/H]\leq-0.3$ and $-0.3<[Fe/H]<+0.0$ on the basis of the values of $\delta(U-B)_{0.6}$ also given in Table 4 of Peterson & Carney. We have converted $\delta(U-B)_{0.6}$ to [Fe/H] using the relation given by Carney (1979) which is reproduced in equation 2 of Chapter 2. Superimposed on figure 6(a) are the new Kurucz model tracks with $\log_{10}(g/cm\ s^{-2})=4.0$ and values of [A/H] which bracket the metallicity bins into which the Peterson & Carney data have been placed. Note that there is no stratification with metallicity evident amongst the data in the four metallicity bins, even between the most metal poor and metal rich bins.

It is evident that at any given colour the new ATLAS9 models predict temperatures which are systematically hotter by ~130K than those which were assigned on the basis of the old ATLAS6 models, although the scatter in the data makes the exact offset difficult to determine. To show that this comparison is insensitive to the surface gravity of the dwarfs, we show in figure 6(b) the same data but with the $[A/H]=-1.0$, $\log_{10}(g/cm\ s^{-2})=3$ and 5 tracks superimposed.

Fernley (1989) has determined a (V-K) vs temperature calibration, also based on the ATLAS6 models, with $5500\leq T_e/K\leq10000$, $2\leq\log_{10}(g/cm\ s^{-2})\leq4$ and $-2\leq[A/H]\leq0$. He used a semi-empirical approach, where the (V-K) vs temperature relation of solar metallicity and $\log_{10}(g/cm\ s^{-2})=4$ was forced to agree with the best fit line drawn by eye through the colour vs temperature data of 42 main-sequence stars. The majority of these temperatures were determined via the infrared flux method, and so Fernley's calibration is tied into the calibrations of other model atmospheres.

In figure 7 we reproduce Fernley's figure 2, showing the (V-K) vs effective temperature data for the main-sequence stars in his Table 1(a), his best-fit line through them, which is also his $[A/H]=0$, $\log_{10}(g/cm\ s^{-2})=4$ track by default, and the actual relation he determined from the ATLAS6 models. We also plot on this figure the (V-K) vs effective temperature relation which we have determined from the ATLAS9 models. Clearly there is good agreement between the ATLAS6 and ATLAS9 relations, except in the temperature range $6700<T_e/K<7400$ where the ATLAS9 relation predicts temperatures which are ~60K hotter at a given (V-K), and in the range $8200<T_e/K<10000$ where the ATLAS9 temperatures are 90 to 120 K hotter. The discrepancy between Fernley's semi-empirical relation and our relation for $T_e>$~8000K is about the same size as the errors on the main-sequence temperatures. The agreement is excellent for $T_e<$~7000K.

To further compare our (V-K) vs T_e relation with that of Fernley, we reproduce in figures 8 and 9 his figures 3(a) and (b). In figure 8(a) we show the colour and temperature information for main-sequence and luminosity class I and III stars. Superimposed are Fernley's semi-empirical solar metallicity (V-K) vs effective temperature relations with $2\leq\log_{10}(g/cm\ s^{-2})\leq4$. Figure 8(b) is analogous, but shows our ATLAS9 colour vs

Figure 7: Effective temperature data from Fernley (1989). Also shown are Fernley's [A/H]=0, $\log_{10}$(g/cm s^{-2})=4 track, his ATLAS6 (V-K) vs T_e relation, and our ATLAS9 relation.

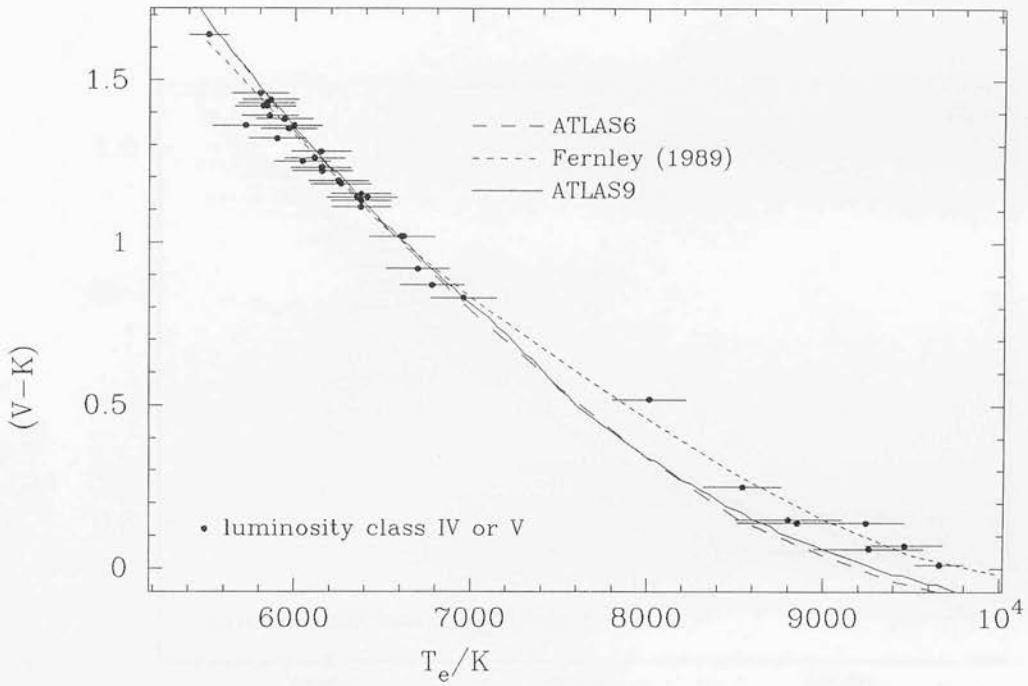

temperature relations of the same metallicity and gravity. The excellent agreement between the two calibrations at low temperatures is retained. In figure 9(a) we show the colour vs temperature information for the main-sequence and metal-poor dwarfs, together with Fernley's $\log_{10}$(g/cm s^{-2})=4 tracks with $-2 \leq$[A/H]≤ 0. Once again, figure 9(b) is similar but shows the ATLAS9 results. At a given (V-K), the colour vs temperature relations over the whole metallicity range are in excellent agreement for $T_e > 6200$K while Fernley's temperatures become increasingly lower with decreasing temperature. The new relations also exhibit a realistic variation with metallicity and gravity, as do those of Fernley, in that at a given effective temperature, lower metallicity and lower gravity stars are redder and bluer respectively.

7 CONCLUSION

We have calculated a new grid of (B-V) and (V-K) colours from ATLAS9 spectral energy distributions supplied to us by Kurucz, with 2 km s^{-1} and covering $0 \leq \log_{10}$(g/cm s^{-2})≤ 5, $-5 \leq$[Fe/H]$\leq +1$, $3500 \leq T_e/K \leq 50000$. The model colour were normalised by assuming that a Vega model with 0 km s^{-1} microturbulent velocity, T_e=9400K, $\log_{10}$(g/cm s^{-2})=3.90 and [A/H]=-0.5 has (B-V)=(V-K)=0.

Figure 8: (a) Fernley's figure 3(a) showing temperatures and colours for various luminosity classes, and his (V-K) vs T_e relations for [A/H]=0 and various gravities. (b) Similar but showing the ATLAS9 relations.

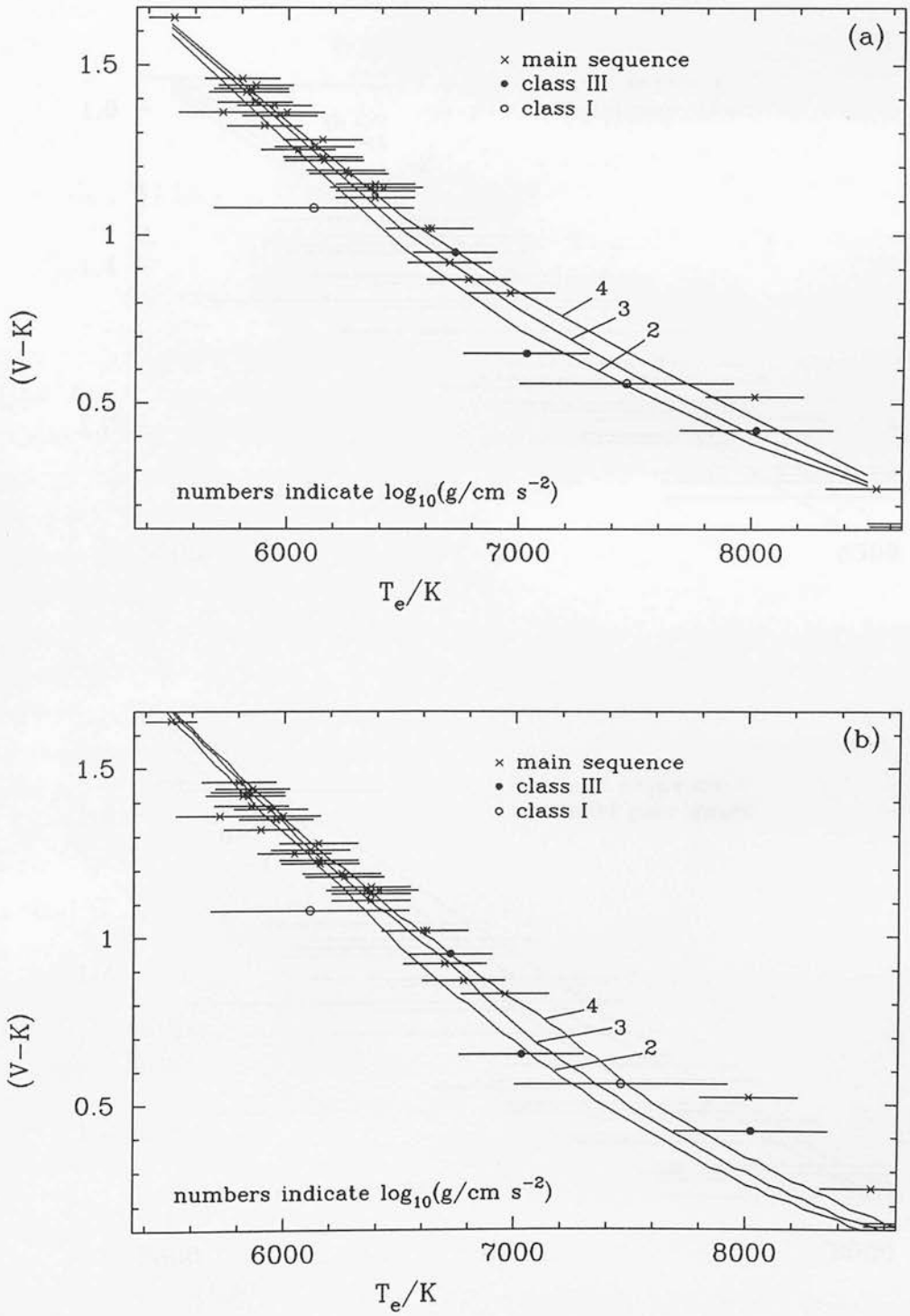

Figure 9: (a) Fernley's figure 3(b) showing data of metal rich & poor dwarfs, and his (V-K) vs T_e relations with $\log_{10}(g/cm\ s^{-2})=4$ and various metallicities. (b) The ATLAS9 relations.

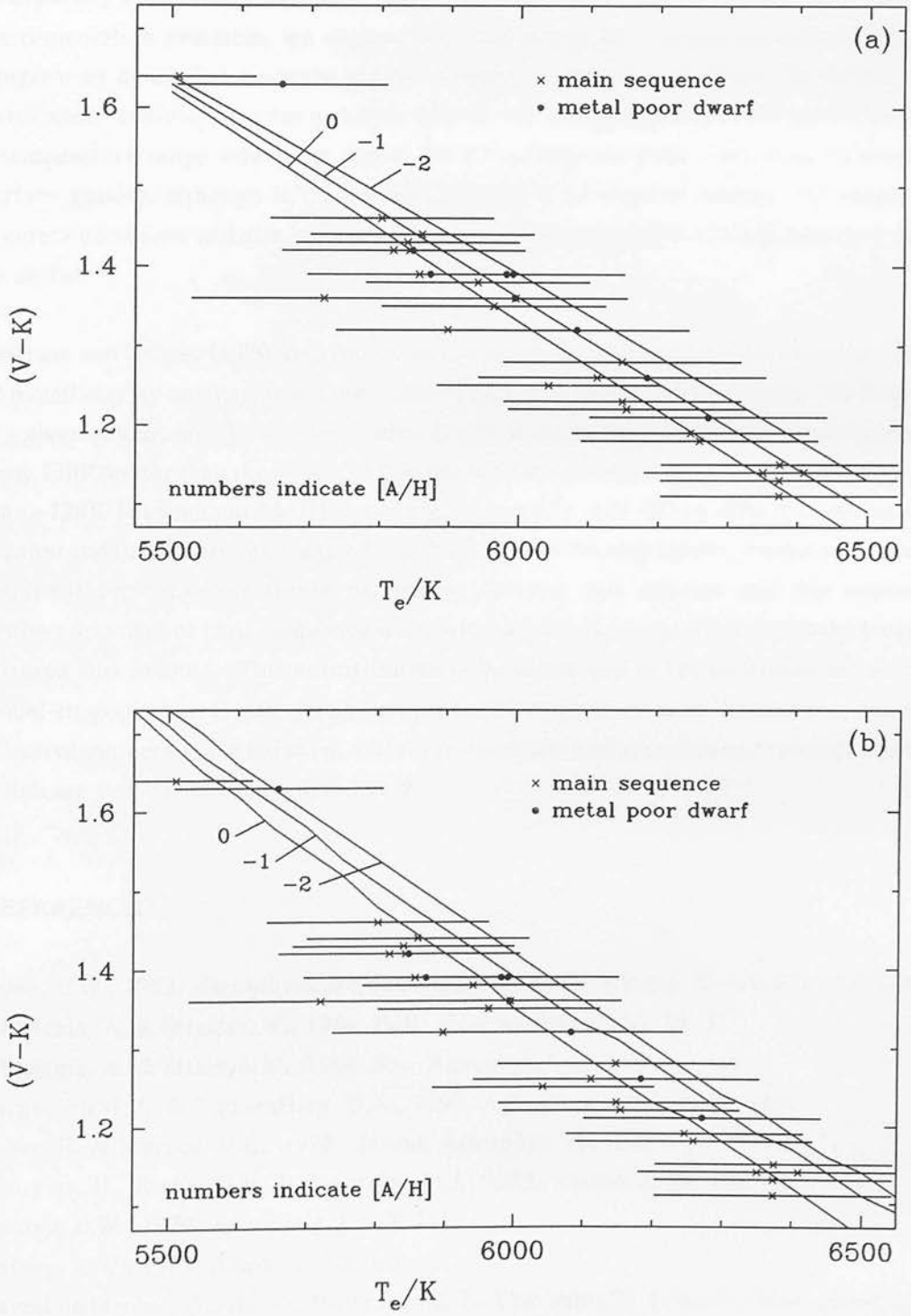

We have attempted to use empirical temperatures of field stars, which were determined, almost independently of model atmospheres, from interferometric angular diameters and observed flux distributions, to check the temperature normalisation of the models. Although the temperatures determined from both (B-V) and (V-K) colours reproduce the empirical temperatures within the errors, the sample is too small and the errors too large to draw any firm conclusions about this. With large telescopes and ever more sensitive instrumentation available, we suggest that this would be a propitious time to begin a program to determine accurate angular diameters, flux distributions, photometry and particularly compositions for a sample of cool main-sequence stars. We have identified a temperature range where the model (V-K) colours are most insensitive to errors in surface gravity, although if the normalisation is to be checked outside this range then accurate parallaxes will also be needed, so overlap with the HIPPARCOS catalogue would be useful.

Peterson and Carney (1979) determine the temperatures of 48 dwarf stars covering a range of metallicity by comparing scanner information with the ATLAS6 models. We find that at a given colour, our (V-K) vs effective temperature relation would lead to temperatures some 130K hotter than those assigned by the ATLAS6 models. We find differences of less than ~120K between our [A/H]=0 and $\log_{10}(g/cm\ s^{-2})=4$ (V-K) vs effective temperature relation and that determined, again from ATLAS6, by Fernley (1989). However, his semi-empirical normalisation forces agreement between this relation and the colour vs temperature data of main-sequence stars, with temperatures determined mostly from the infrared flux method. This normalisation is therefore tied to the normalisation of other model atmospheres. It also leads to some complicated differences between our colour vs effective temperature relations at various metallicities and gravities and those of Fernley, which are summarised in figures 7 to 9.

REFERENCES

Allen, C.W., 1963. *Astrophysical Quantities.* The Athlone Press, University of London.

Ažusienis, A. & Straižys, V., 1966. *Bull. Vilnius Observatory* **18,** 3.

Ažusienis, A. & Straižys, V., 1969. *Sov. Astron. A.J.* **13,** 316.

Bergbusch, P.A. & VandenBerg, D.A., 1992. *Astrophys. J. Suppl.* **81,** 163.

Buser, R. & Kurucz, R.L., 1978. *Astron. Astrophys.* **70,** 555.

Campins, H., Rieke, G.H. & Lebofsky, M.J., 1985. *Astron. J.* **90,** 896.

Carney, B.W., 1979. *Astrophys. J.* **233,** 211.

Carney, B.W., 1983. *Astron. J.* **88,** 623.

Cayrel de Strobel, G., Hauck, B., François, P., Thévenin, F., Friel, E., Mermilliod, M. & Borde, S., 1992. *Astron. Astrophys. Suppl.* **95,** 273.

Clements, G.L. & Neff, J.S., 1979. *Astron. Astrophys.* **75,** 193.

Code, A.D., 1975. *Dudley Observatory Reports* **9**, 221.

Code, A.D., Davis, J., Bless, R.C. & Hanbury Brown, R., 1976. *Astrophys. J.* **203**, 417.

Fernley, J.A., 1989. *Mon. Not. Roy. astr. Soc.* **239**, 905.

Hayes, D.S., 1985. In International Astronomical Union Symposium 111, *Calibration of Fundamental Stellar Quantities*, D.S. Hayes, L.E. Pasinetti & A.G. Davis Philip, editors. Page 225.

Hayes, D.S. & Latham, D.W., 1975. *Astrophys. J.* **197**, 593.

Johnson, H.L., 1966. *Ann. Rev. Astron. Astrophys.* **4**, 193.

Johnson, H.L. & Morgan, W.W., 1953. *Astrophys. J.* **117**, 313.

Jørgensen, U.G., Jensen, P. & Sørensen, G.O., 1993. Preprint. To appear in Poster-proceedings of the International Astronomical Union colloquium 146. P. Thejll & U.G. Jørgensen, editors. Copenhagen University.

Kurucz, R.L., 1979. *Astrophys. J. Suppl.* **40**, 1.

Kurucz, R.L., 1991. in *Precision Photometry,* A.G. Davis Philip, A.R. Upgren & K.A. Janes, editors. L. Davis Press. Page 27.

Kurucz, R.L., 1992. *Rev. Mexicana Astron. Astrof.* **23**, 181.

Peterson, R.C. & Carney, B.W., 1979. *Astrophys. J.* **231**, 762.

Traub, W.A. & Stier, M.I., 1976. *Appl. Optics* **15**, 364.

Strom, S.E. & Kurucz, R.L., 1966. *J. Quant. spectrosc. Radiat. Transfer* **6**, 591.

Valley, S.L., 1966. in *Handbook of Geophysics and Space Environments*, editor S.L. Valley, McGraw-Hill, chapter 7.

VandenBerg, D.A., 1992. *Astrophys. J.* **391**, 685.

VandenBerg, D.A. & Poll, H.E., 1989. *Astron. J.* **98**, 1451.

Chapter 4

A Re-evaluation of Cluster Ages in the Light of "New" Models

" In the beginning the universe was created. This has made a lot of people very angry, and been widely regarded as a bad move."
- The Hitch-hikers Guide to the Galaxy.

ABSTRACT

New models have been obtained by transforming the Bergbusch & VandenBerg theoretical isochrones to V, (V-K) and V, (B-V) using the Kurucz model atmosphere results discussed in the previous chapter. In this sense, these results are unique; for the first time it is possible to use just one grid of up-to-date model atmosphere results over the entire range of temperature, gravity and abundance.

We highlight the differences between the new models and the original Bergbusch & VandenBerg (1992) and Bell (1992) colours, taking the [Fe/H]=-0.78 models as an example. We find that a major difference occurs on the lower main-sequences with (V-K)>~2.8 or (B-V)>~0.8, where the new main sequence becomes systematically fainter. Since this disagreement manifests itself in the regions of the main sequence where convection is important, we suggest differences between the convective treatment in the MARCS and ATLAS9 model atmospheres are to blame.

We re-examine the ages of the four globular clusters M13, M30, 47 Tuc and NGC6752 by comparing the new isochrones directly to the V_0, $(V-K)_0$ and V_0, $(B-V)_0$ colour-magnitude diagrams, constraining the theoretical main-sequence to match the observed main-sequence by subdwarf fits. This effectively removes any systematic uncertainty in the model magnitudes due to uncertainties in the bolometric corrections.

We also find that the new subgiant branches are anomalously blue compared to the observed subgiant branches; the original subgiant branches fit the data well. A comparison of the NGC6752, 47 Tuc and M30 data and the new isochrones in the two-colour plane suggests that this is caused by (possibly convection related) mismatches

between the temperature to (B-V) and to (V-K) relations.

Giving maximum weight to ensuring that the models fit the observed upper main sequence well, and that the observed horizontal branches are not anomalously placed with respect to the zero-age horizontal branches, we derive ages of ~14 Gyr for each cluster. The specific ages derived are presented in Table 6. Had we placed greater weight on the fit of the subgiant branches, we would have derived much older ages, in the case of M30 the age would have been ~18 Gyr.

1 NEW MODELS

VandenBerg has made available to us in machine readable form the Bergbusch & VandenBerg (1992) theoretical isochrones, which have been converted to V, (V-K) and V, (B-V) by Longmore, using our Kurucz model atmosphere results detailed in Chapter 3. The rationale behind this conversion was to use the very latest model atmosphere results to produce isochrones in the observational plane, in particular V, (V-K), which were hopefully free of the colour-shift problems found in previous models, both optical and infrared. For brevity we shall refer to these as new models, although this is strictly a misnomer. The Bergbusch & VandenBerg (1992) models will sometimes be referred to as the 'original' models.

These results are unique, in the sense that, for the first time the transformation from theoretical to observational parameters is possible over the entire temperature, gravity and abundance range with just one set of model atmosphere results. It has not been necessary to go through the contortions described by VandenBerg (1991), and summarised in Chapter 2, to produce the V and (B-V) values of the original Bergbusch & VandenBerg isochrones. Nor has it been necessary to 'tag on' the giant branches, as did Straniero & Chieffi (1991).

The preliminary results are very encouraging. In figure 1 we show the V, (B-V) colour-magnitude diagram of M3. The data are taken from Stetson & Harris (1988) while the fiducial is from Paez *et al.* (1990). M3 is well known to suffer from minimal reddening, with E[B-V]=0.00 to 0.01 [see references in Paez *et al.*]. We have therefore plotted the data and the fiducial without a reddening correction.

Also shown on this figure are the new 12, 14 and 16 Gyr isochrones with [Fe/H]=-1.66, which is the appropriate metallicity for comparison with M3 [Zinn (1985)]. The models have been shifted in magnitude only, until the main-sequence turn-off and subgiant branches matched; this required a shift of ΔV=14.93 magnitudes. As we shall see later, the bolometric corrections used in the new models are probably too negative by ~0.08

Figure 1: The V, (B-V) colour-magnitude diagram of M3 with data from Stetson & Harris and the fiducial from Paez *et al.* The new models with [Fe/H]=-1.66 are also shown. The reddening to M3 is E[B-V]=0.00 to 0.01.

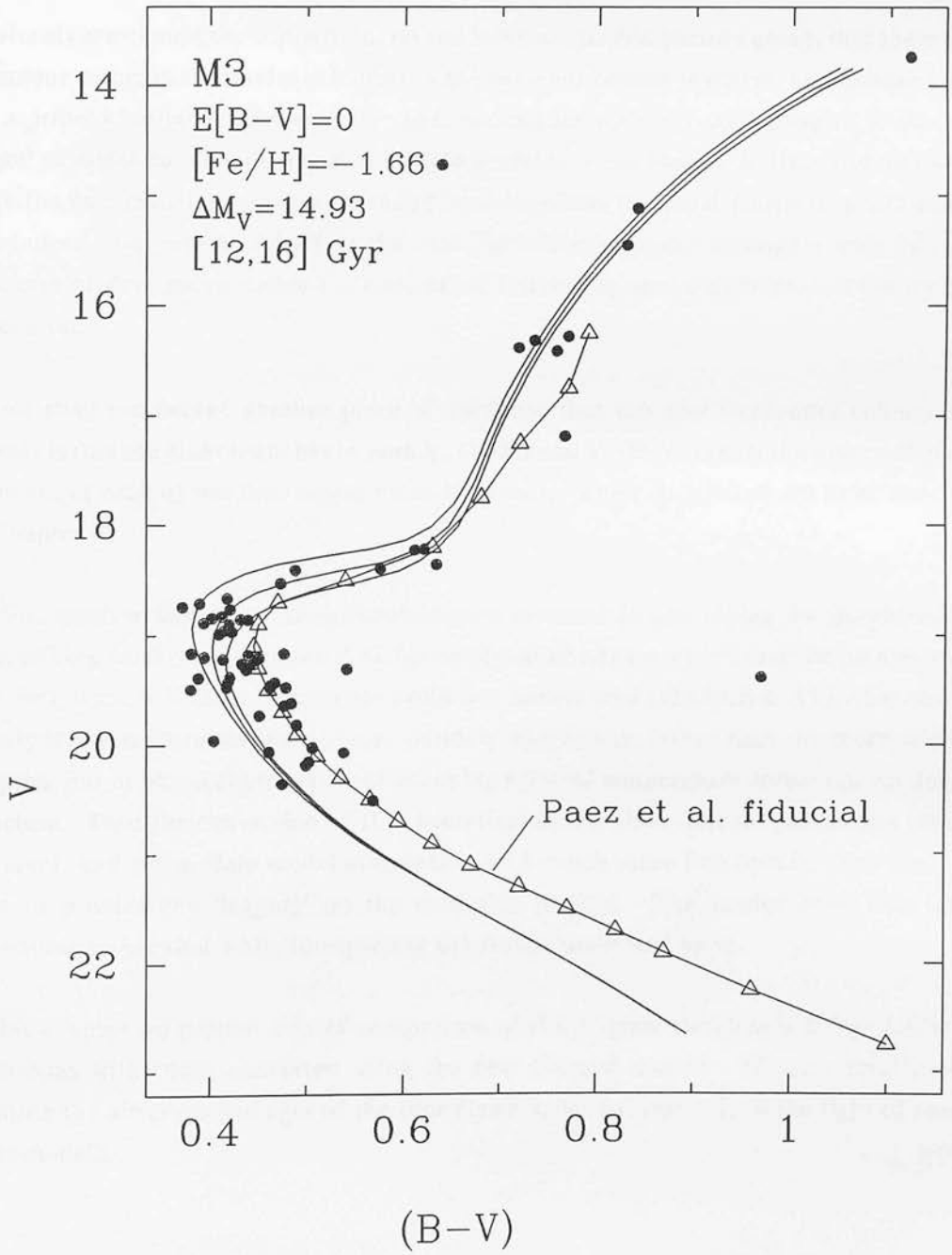

magnitudes, making the models too faint by that amount. The isochrones have thus been corrected to a distance modulus of ~15 magnitudes.

Note that the isochrones pass through the turn-off and agree well with the subgiant-branch data, without recourse to any colour-shifts; the very low reddening of M3 means that any colour shifts found would *have* to be due to errors in the model colours.

Obviously we cannot say for certain, on the basis of this comparison alone, that there are no colour errors in the model colours; the M3 subgiant branch is sparse, and neither have we *a priori* knowledge of the cluster age, making the turn-off something of a 'moving target' to match to. There may also be colour errors in the Stetson & Harris photometry since the Paez fiducial passes to the red of the bulk of the Stetson & Harris turn-off data - or, indeed, vice-versa. The fact that the Paez fiducial passes through a well defined sequence of data points below the turn-off is interesting, and clearly more work on M3 is required.

As we shall see below, another piece of evidence that the new isochrones colours are correct is that the giant branches in *both* V, (V-K) *and* V, (B-V) match the observed giant branches of each of our four clusters simultaneously, which was found not to be the case in Chapter 2.

On the negative side, there is an inconsistency involved in combining the Bergbusch & VandenBerg isochrones with the ATLAS9 model atmospheres which must be pointed out. The Bergbusch & VandenBerg stellar evolution models used (MARCS & ATLAS6) model atmosphere results to set the surface boundary conditions, rather than the more widely adopted, but unphysical procedure of assuming a scaled temperature versus optical depth structure. Thus the conversion of the theoretical to the observational parameters uses a different, and up-to-date model atmosphere with much more line opacity than the one used to provide the 'lagging' on the evolution models. The reader *must* bear this inconsistency in mind while interpreting the results presented here.

In this chapter we present a brief comparison of the original Bergbusch & VandenBerg isochrones with those converted using the new Kurucz models. We also briefly re-examine the distances and ages of the four clusters, as in Chapter 2, in the light of these 'new' models.

2 COMPARISON OF THE ORIGINAL AND NEW ISOCHRONES

The purpose of this section is to briefly highlight the differences between the old and new models, both in V, (V-K) and V, (B-V), which should be borne in mind in the next section in which we derive ages from the new models.

In figure 2 we show the V, (V-K) Bergbusch & VandenBerg 12 and 18 Gyr isochrones with [Fe/H]=-0.78 and [O/Fe]=0.39, taken from Bell (1992). These have been matched to the new isochrones around the turn-off region, to highlight differences in the overall shapes. The match required the original models to be shifted by 0.06 magnitudes to the blue and 0.16 magnitudes fainter. This colour shift is half of the value which Bell suggested should be applied to his (V-K) colours; if the colours of the new models can be trusted, then the implication is that Bell has overestimated the colour correction. This would act to reduce the ages predicted from his models with the too-large correction. Conversely, if Bell were right, then the new model colours require a blueward shift of ~0.06 magnitudes, which would act to increase the ages derived from them. We must, however, bear in mind Bell's comment that no linear colour transformation exists to correct his model (V-K) colours, and that the 0.12 magnitude shift is only a compromise, based partly on fits of the isochrones to our preliminary, unpublished 47 Tuc field F3 data.

Note that the main sequences agree well until $(V-K)>\sim2.8$, whereupon the new main sequence is systematically fainter. The structures of the stars in this region of the main sequence change from radiative-convective ($M_V<\sim9.6$) to fully convective ($M_V>\sim9.6$), which suggests that this difference is caused by differences in mixing length to pressure scale height ratios between the MARCS and ATLAS9 model atmospheres.

In figure 3 we compare the new 12 and 18 Gyr isochrones to the original isochrones of the same age including Bell's suggested 0.12 magnitude blueward shift. The main sequences still match well, but now the new red giant and subgiant branches lie completely to the red of the originals. In order to obtain a consistent fit from the new models, one would need to adopt a lower abundance for a cluster whose main-sequence and giant branch were well fit by the original models.

Figure 4 shows the V, (B-V) models superimposed without colour or magnitude corrections, since the original V, (B-V) isochrones are not known to need a colour correction. Now only the main sequences with $(B-V)<\sim0.8$ match well. The entire subgiant and giant branches of the new models are to the red of the originals. One must allow both colour and magnitude shifts to resolve the discrepancy, as shown in figure 5, where the original models are shifted to the red by 0.04 magnitudes and fainter by 0.18 magnitudes. In that case the subgiant branches do not match.

Figure 2: The new and original 12 & 18 Gyr [Fe/H]=-0.78 [O/Fe]=0.39 V, (V-K) isochrones, matched around the turn-off, to highlight differences in the main-sequence and giant branches.

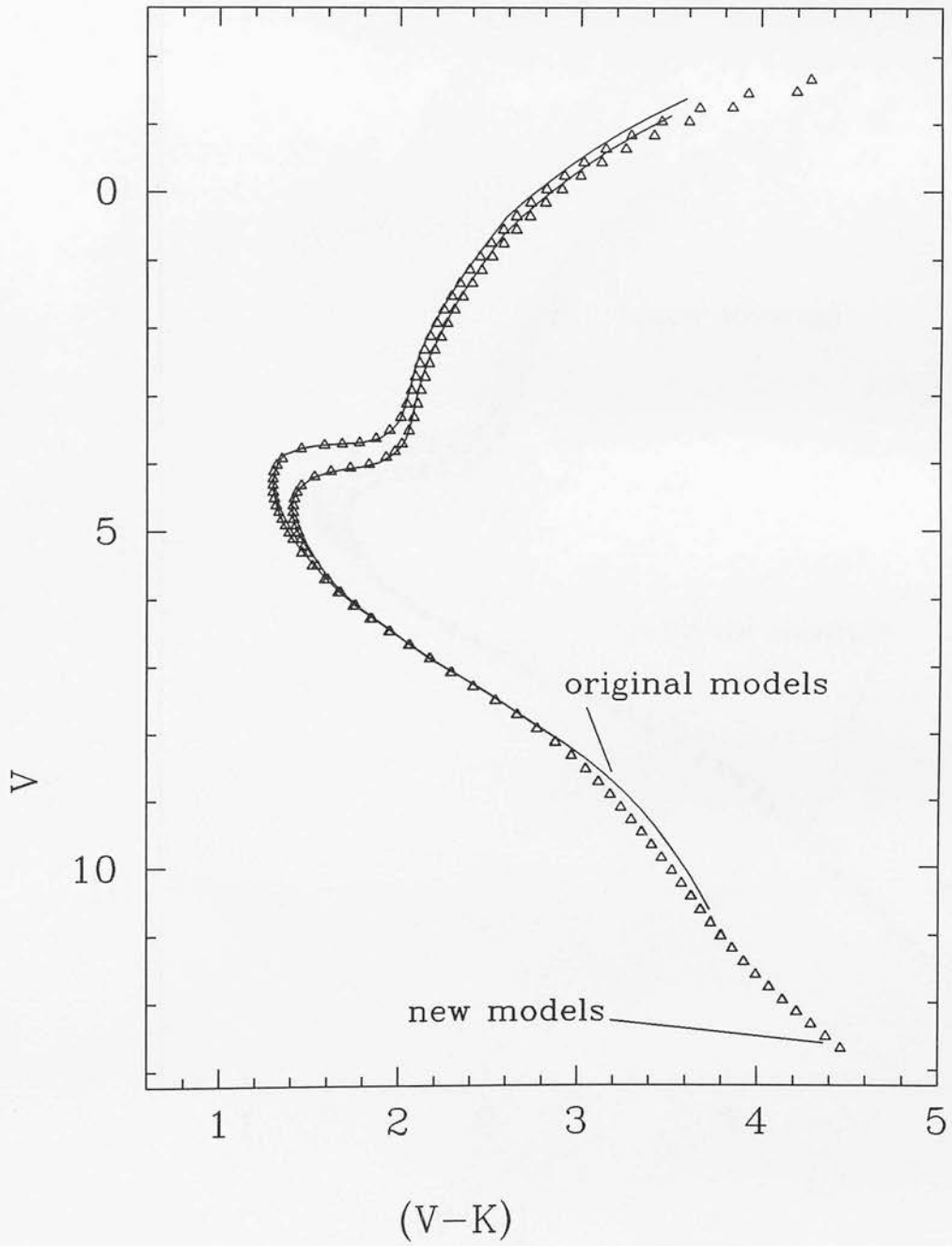

Figure 3: As figure 2, but showing the original models shifted to the blue by 0.12 magnitudes, as used to derive ages in Chapter 2. This comparison highlights the differences in cluster ages which would be derived from the original and new models.

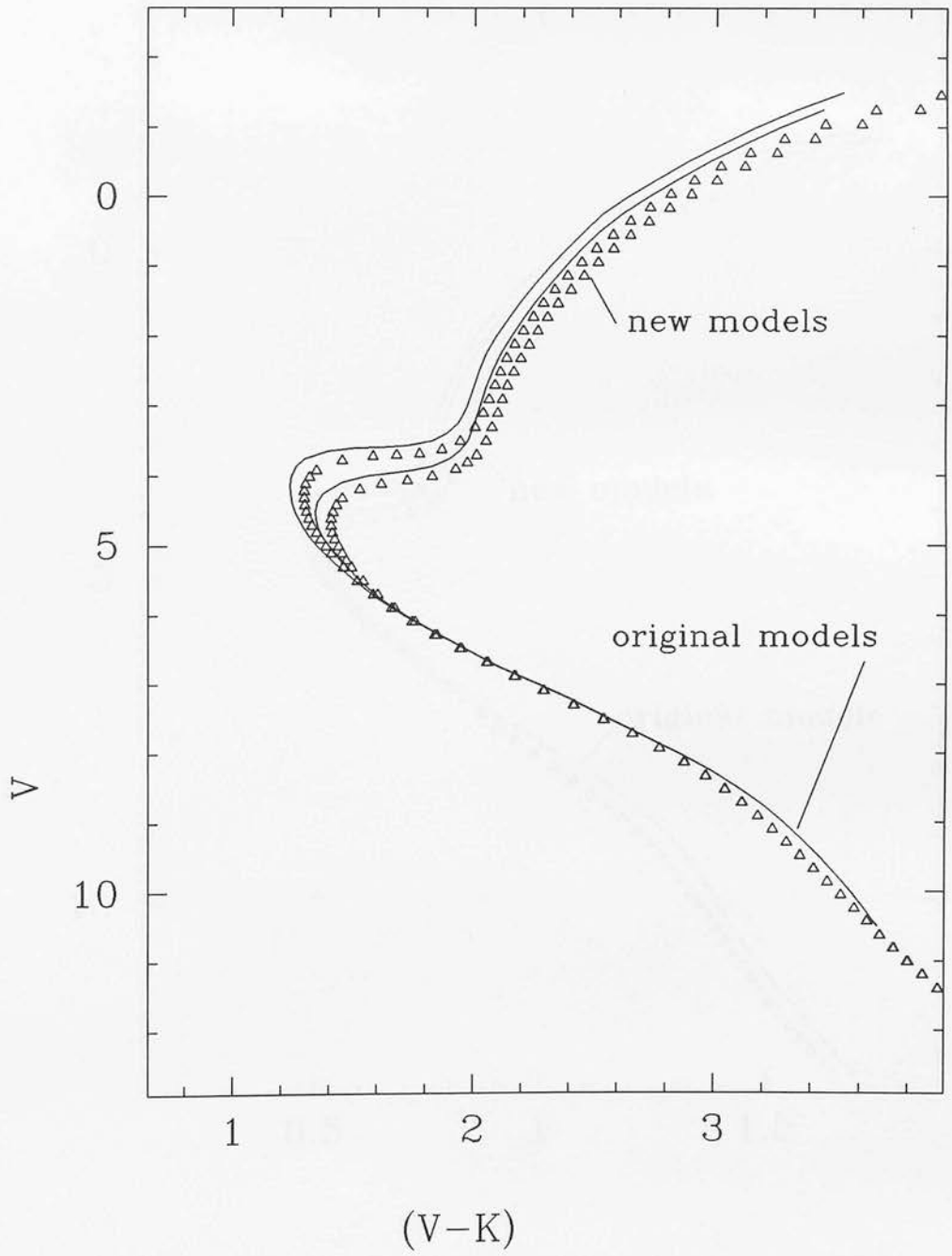

Figure 4: The new and original 12 & 18 Gyr [Fe/H]=-0.78 [O/Fe]=0.39 V, (B-V) isochrones. This comparison again highlights the expected differences in cluster ages derived from the old and new models.

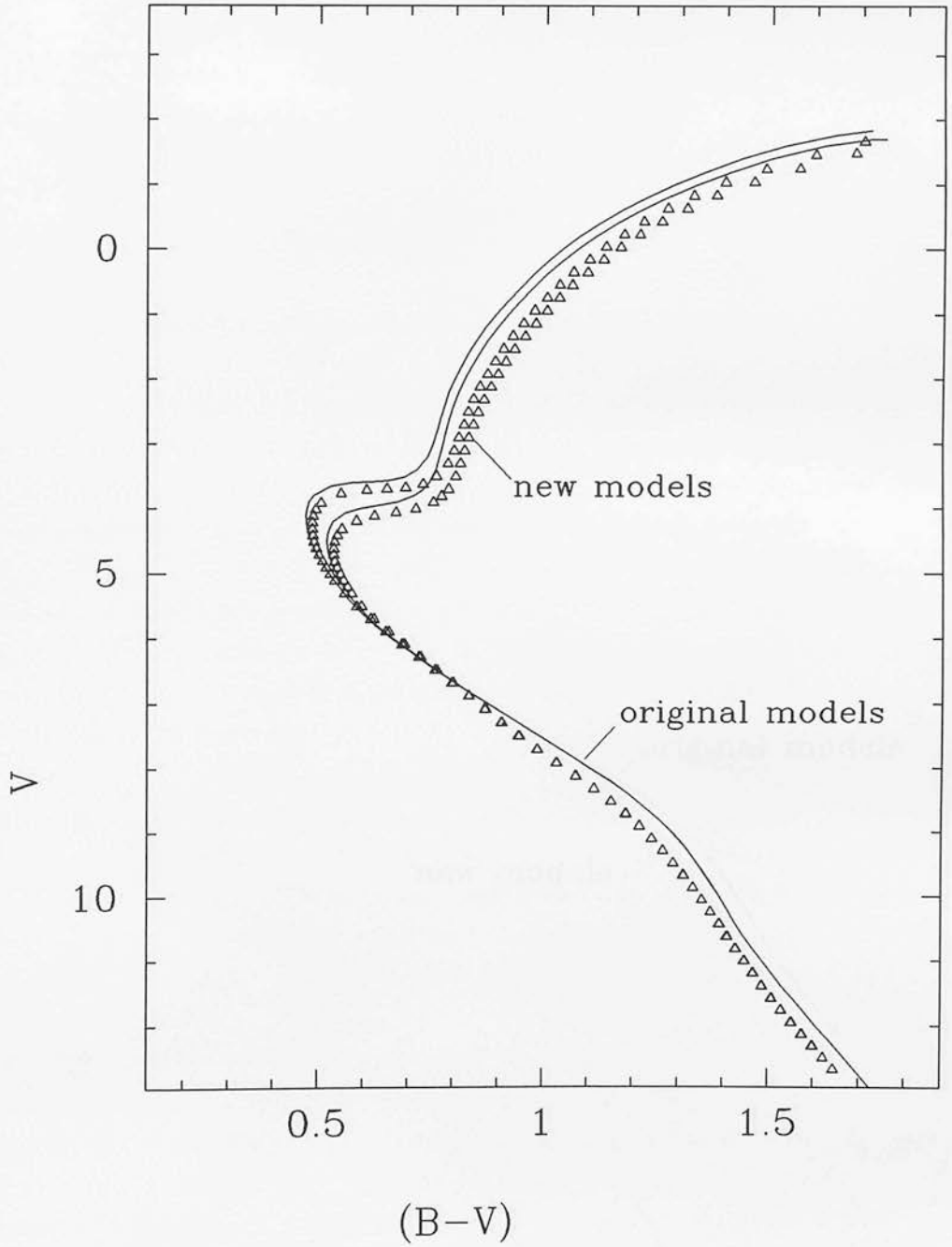

Figure 5: As figure 4, but with the original models shifted to the red by 0.04 magnitudes and fainter by 0.18 magnitudes, to match produce the best simultaneous fit to the upper giant branch and main-sequence.

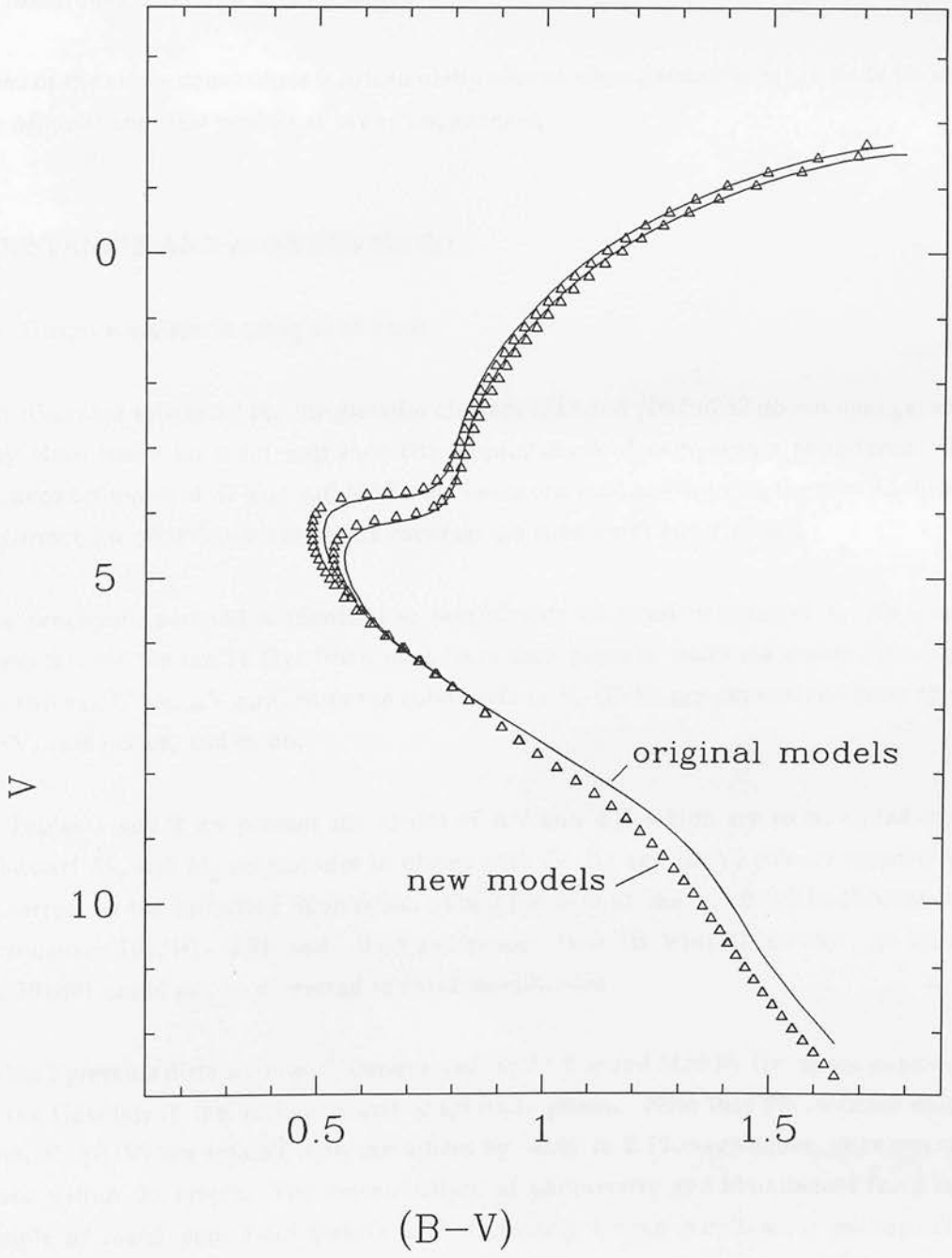

Note that a comparison of the main-sequence turn-offs in figures 3 and 4 provides evidence that a shift in the original isochrone V, (V-K) colours, such as was suggested by Bell (1992) *is* necessary. The difference in ages derived for a cluster from the two sets of V, (V-K) isochrones - including the 0.12 magnitude correction to the original (V-K) colours - is in the same sense as the difference in ages derived from the two sets of V, (B-V) isochrones, although slightly larger.

None of the above conclusions is substantially altered when comparisons are made between the original and new models at lower abundances.

3 DISTANCES AND AGES REVISITED

3.1 Distance estimates using subdwarfs

The distances estimated for the globular clusters M13 and NGC6752 do not change, since they were based on main-sequence fits to subdwarfs of comparable abundance. The distance estimates of 47 Tuc and M30 must be determined again, using the new isochrones to correct for abundance variations between the subdwarfs and clusters.

The procedure adopted is identical to that already outlined in Chapter 2. As a brief reminder, we use the 16 Gyr isochrones from each plane to make the correction. Thus, the values of, say, ΔV applied to the subdwarfs in V, (B-V) are determined from the V, (B-V) isochrones, and so on.

In Tables 1 and 2 we present the values of ΔV and ΔK which are to be added to the subdwarf M_V and M_K magnitudes in planes with (V-K) and (B-V) colours respectively, to correct to the indicated abundance. The turn-offs of the V, (B-V) isochrones with abundances [Fe/H]=-0.78 and -0.65 are redder than (B-V)=1.42 so that, as before, HD201891 could not be corrected to these metallicities.

Table 3 presents distance moduli determined for 47 Tuc and M30 by fitting the subdwarfs to the fiducials in the various colour-magnitude planes. Note that the distance moduli from K, (B-V) are smaller than the others by ~0.07 to 0.12 magnitudes, although they agree within the errors. The determination of photometry and abundances for a large sample of metal-poor field dwarfs with accurately known parallaxes - perhaps from HIPPARCOS - should be given the utmost priority.

Table 4 summarises the distance moduli determined for the four globular clusters without Lutz-Kelker corrections. The adopted distance modulus of 47 Tuc is that determined

Table 1: Corrections to be added to the subdwarf magnitudes in the V, (V-K) and K, (V-K) colour-magnitude planes.

Star	[Fe/H]=-2.26	[Fe/H]=-0.65	[Fe/H]=-0.78
	ΔV	ΔV & ΔK	ΔV & ΔK
HD25329	0.29	-0.43	-0.35
HD103095	0.18	-0.37	-0.31
HD134439	0.18	-0.37	-0.31
HD134440	0.29	-0.42	-0.36
HD201891	0.16	-0.58	-0.42
BD+66°268	0.02	-0.47	-0.40

Table 2: Corrections to be added to the subdwarf magnitudes in the V, (B-V) and K, (B-V) colour-magnitude planes.

Star	[Fe/H]=-2.26	[Fe/H]=-0.65		[Fe/H]=-0.78	
	ΔV	ΔV	ΔK	ΔV	ΔK
HD25329	0.30	-0.54	-0.45	-0.45	-0.38
HD103095	0.34	-0.55	-0.45	-0.45	-0.35
HD134439	0.34	-0.54	-0.45	-0.45	-0.31
HD134440	0.30	-0.53	-0.45	-0.44	-0.37
HD201891	0.40	-	-	-	-
BD+66°268	0.13	-0.86	-0.50	-0.74	-0.40

from V_0, $(V-K)_0$ only.

3.2 Absolute ages from the isochrones

In this section we use the distances derived in section 3.1 above to overlay the isochrones on the V_0, $(V-K)_0$ and V_0, $(B-V)_0$ colour-magnitude diagrams of the four globular clusters, from which we derive absolute ages. As usual, the isochrone absolute magnitude scale has been corrected to that of the subdwarfs without Lutz-Kelker corrections; the results of fitting the isochrone main-sequences to the subdwarfs are presented in Table

Table 3: Distance moduli from least squares fits of subdwarfs to fiducials. Numbers in parentheses indicate the number of subdwarfs used in the fits.

Plane	True distance modulus from fiducials	
	No Lutz-Kelker corrections	Full Lutz-Kelker corrections
47 Tuc [Fe/H]=-0.78 [O/Fe]=0.39		
V_0, $(V-K)_0$	13.20±0.11 (6)	13.32±0.11 (6)
K_0, $(V-K)_0$	13.20±0.12 (6)	13.33±0.12 (6)
V_0, $(B-V)_0$	13.23±0.14 (5)	13.33±0.10 (5)
K_0, $(B-V)_0$	13.11±0.19 (5)	13.21±0.15 (5)
Hesser *et al.* V_0, $(B-V)_0$	13.19±0.15 (5)	13.29±0.11 (5)
47 Tuc [Fe/H]=-0.65 [O/Fe]=0.30		
V_0, $(V-K)_0$	13.28±0.12 (6)	13.41±0.14 (6)
K_0, $(V-K)_0$	13.28±0.14 (6)	13.41±0.15 (6)
V_0, $(B-V)_0$	13.33±0.14 (5)	13.43±0.09 (5)
K_0, $(B-V)_0$	13.21±0.18 (5)	13.31±0.14 (5)
Hesser *et al.* V_0, $(B-V)_0$	13.29±0.14 (5)	13.39±0.10 (5)
M30 E[B-V]=0.07 [Fe/H]=-2.26 [O/Fe]=0.75		
Richer *et al.* V_0, $(B-V)_0$	14.47±0.12 (4)	14.61±0.15 (4)
M30 E[B-V]=0.03 [Fe/H]=-2.26 [O/Fe]=0.75		
Richer *et al.* V_0, $(B-V)_0$	14.45±0.16 (6)	14.58±0.15 (6)

Table 4: Adopted distance moduli of four globular clusters without Lutz-Kelker corrections.

Cluster	True distance modulus without Lutz-Kelker corrections	
M13	14.27	
NGC6752	13.03	
47 Tuc	13.28	[Fe/H]=-0.65
	13.20	[Fe/H]=-0.78
M30	14.47	E[B-V]=0.07
	14.45	E[B-V]=0.03

5. Note that the isochrones appear to be systematically too faint by ~0.07 magnitudes compared to the absolute magnitude scale of the subdwarfs, although the V, (B-V) isochrones with [Fe/H]=-1.48 are fainter still by ~0.04 magnitudes - a small discrepancy compared to the r.m.s. fitting error. In Chapter 3, when we derived the bolometric corrections with respect to the V filter from the Kurucz ATLAS9 models, we found a model solar bolometric correction of $BC_{\odot}$=-0.20 magnitudes, while the commonly adopted value is $BC_{\odot}$=-0.12 [see VandenBerg & Bell (1985) and references therein]. The solar-abundance models are thus ostensibly too faint by ~0.08 magnitudes; the above fitting of the isochrones to the subdwarfs confirms this and shows that it is constant within the abundance range -2.26<[Fe/H]<-0.65. We are unable to say if the discrepancy is also independent of surface gravity.

3.2.1 Comparison of isochrones and M13 colour-magnitude data

Figures 6 and 7 show the V_0, $(V-K)_0$ and V_0, $(B-V)_0$ colour-magnitude diagrams of M13, the latter with the full optical dataset of Richer & Fahlman (1986). The new isochrones of abundance [Fe/H]=-1.48 are overlaid upon these figures, corrected to a distance modulus of 14.27 magnitudes and including the correction from Table 5.

Consider first figure 6. Although the data are rather sparse, the isochrones fit both the main-sequence and the giant branch well. An age of (14.5±2.5) Gyr is suggested by the V_0, $(V-K)_0$ data. Now consider figure 7. Generally, the fit to the data is good, with two notable exceptions. First, the theoretical main-sequence is systematically fainter than the

Table 5: True 'distance moduli' of the 16 Gyr isochrones from main-sequence fits to the subdwarfs corrected to the same abundance. Numbers in parentheses indicate the number of subdwarfs used in the fits.

Isochrone	'distance modulus' from subdwarfs	
	No Lutz-Kelker corrections	Full Lutz-Kelker corrections
	[Fe/H]=-0.65 [O/Fe]=0.30	
V, (V-K)	0.06±0.11 (6)	0.19±0.08 (6)
V, (B-V)	0.07±0.15 (5)	0.17±0.12 (5)
	[Fe/H]=-0.78 [O/Fe]=0.39	
V, (V-K)	0.06±0.10 (6)	0.19±0.07 (6)
V, (B-V)	0.07±0.15 (5)	0.17±0.12 (5)
	[Fe/H]=-1.48 [O/Fe]=0.60	
V, (V-K)	0.07±0.09 (5)	0.19±0.06 (5)
V, (B-V)	0.11±0.14 (5)	0.23±0.13 (5)
	[Fe/H]=-2.26 [O/Fe]=0.75	
V, (V-K)	0.06±0.09 (6)	0.18±0.07 (6)
V, (B-V)	0.07±0.14 (6)	0.20±0.13 (6)

observed main-sequence for $(B-V)_0 > \sim 0.9$. Second, although the theoretical giant branch fits the brighter giants well, the giants with $V_0 < 12.5$ appear to the blue of the theoretical sequences. This is also seen in the subgiants, although these conclusions are based on only three points each, and so should be treated with caution, lest we be misled by small-number statistics. The main-sequence data up to the turn-off suggest an age for M13 of (13±2) Gyr while the three points which define the sweep between the turn-off and the base of the subgiant branch suggest an age of (15±1) Gyr. We therefore adopt a weighted average absolute age from these models of (14.4±1.6) Gyr.

Figure 6: The V_0, $(V-K)_0$ colour-magnitude diagram of M13 with the new isochrones overlaid.

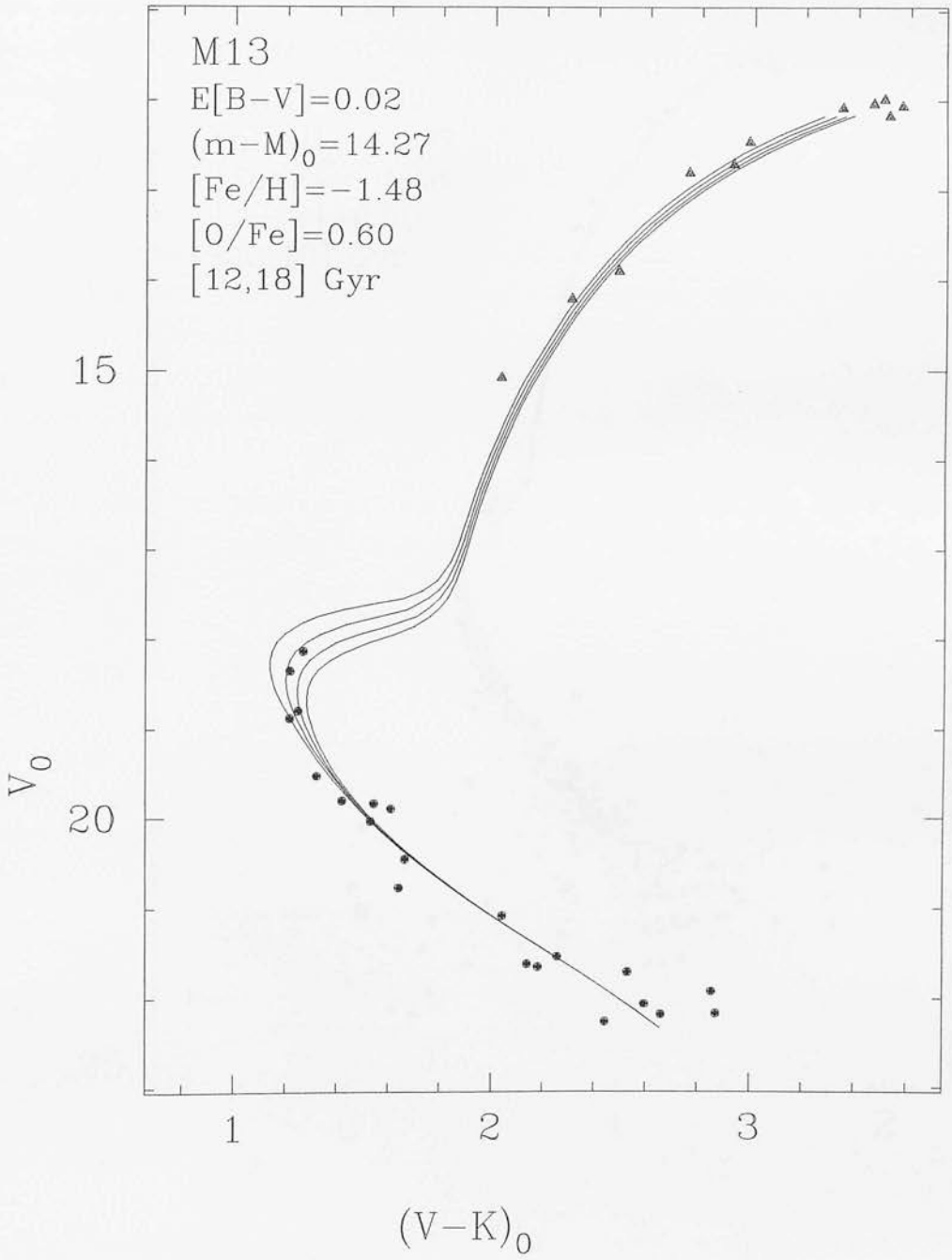

Figure 7: The V_0, $(B-V)_0$ colour-magnitude diagram of M13 with the new isochrones overlaid.

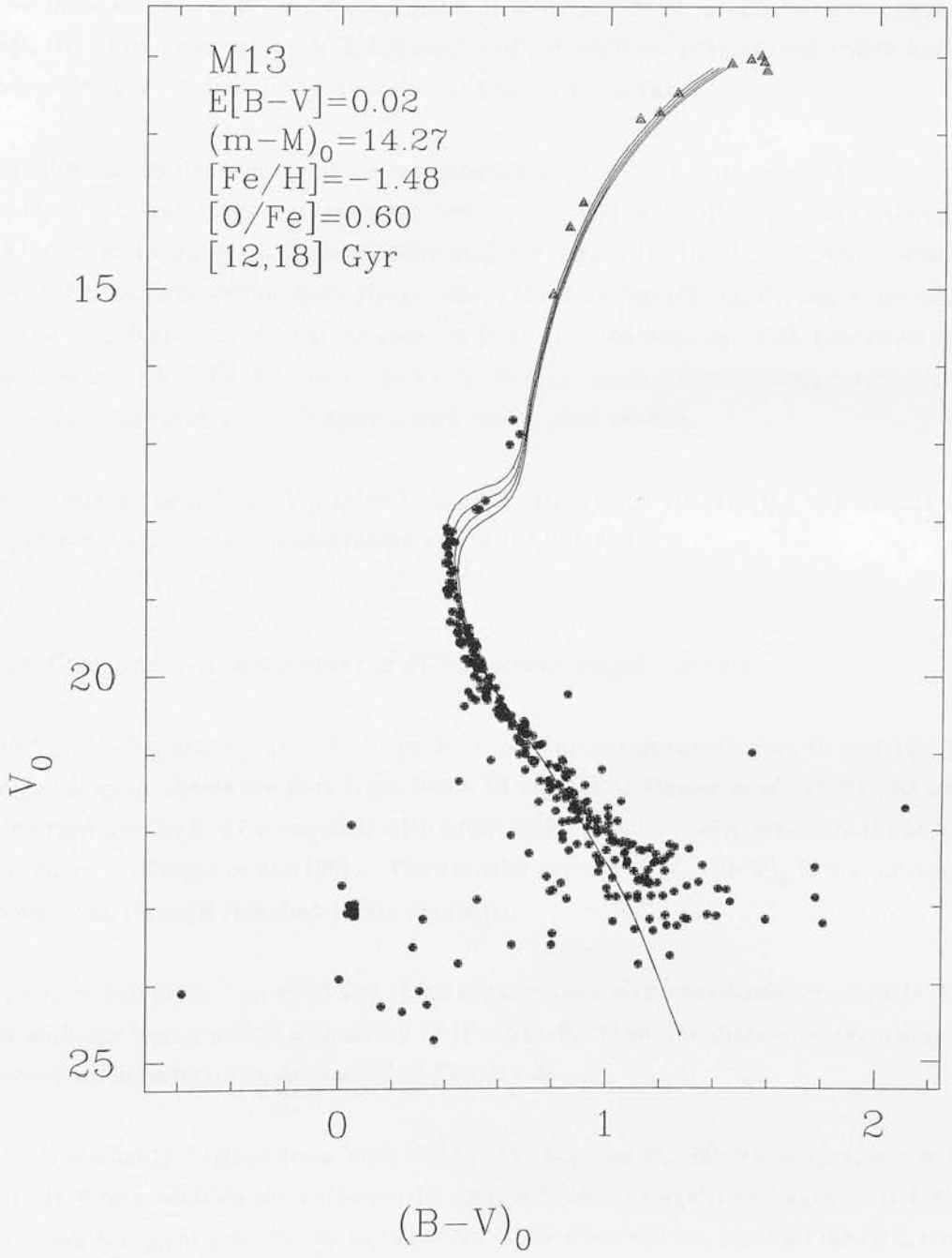

3.2.2 Comparison of isochrones and NGC6752 colour-magnitude data

Figures 8 and 9 show the V_0, $(V-K)_0$ and V_0, $(B-V)_0$ colour-magnitude diagrams of NGC6752, with the isochrones corrected to a distance modulus of 13.03 magnitudes. The full optical dataset from Penny & Dickens (1986) is shown, as is their fiducial. On figure 9 we show the zero-age horizontal branch of Dorman (1992), which was also converted to V, (B-V) by us using the ATLAS9 results of the previous chapter, and which has also been corrected brightward by the relevant amount from Table 5.

Note the excellent agreement of the theoretical and observed lower main-sequences in the V_0, $(V-K)_0$ colour-magnitude diagram, compared to that in V_0, $(B-V)_0$, where once again, the theoretical sequence is systematically too faint redward of $(B-V)_0$=0.9. Otherwise, the models fit the data well on both planes except for the subgiant branch where the models are too red. Note also, as was the case for M13, that the observed and theoretical giant branches in *both* V, (V-K) and V, (B-V) match well - such a simultaneous match was not found for these clusters in Chapter 2 with the original models.

We determine ages from V_0, $(V-K)_0$ and V_0, $(B-V)_0$ of (15±2) Gyr and (13±2) Gyr respectively, and we adopt an average age of (14.0±1.4) Gyr.

3.2.3 Comparison of isochrones and 47 Tuc colour-magnitude data

The V_0, $(V-K)_0$ and V_0, $(B-V)_0$ diagrams of 47 Tuc are shown figures 10 and 11. The optical diagram shows the data from fields F1 and F3 of Hesser *et al.* (1987), the latter being restricted to V>17.2, together with additional photometry of giants from the sources referenced by Frogel *et al.* (1981). The fiducial marked in V_0, $(B-V)_0$ is that drawn by Hesser *et al.* through their composite diagram.

In parts (a) and (b) of figures 10 and 11 we show models with abundances of [Fe/H]=-0.65 and with the 'compromise' abundance of [Fe/H]=-0.78 [see the discussion regarding α-element enhancements in section 2.7 of Chapter 2].

It is immediately obvious from both the V_0, $(V-K)_0$ and V_0, $(B-V)_0$ diagrams that the [Fe/H]=-0.65 models do not reproduce the observed colour-magnitude diagrams well, with the theoretical giant branches being to the red of the observations, and that the fit is much worse than found in Chapter 2 from the original models of the same abundance. On the other hand, the [Fe/H]=-0.78 models provide a much better fit. This is to be expected, since we have already seen that the effect of the ATLAS9 models has been to make the new giant branches somewhat redder than the originals, as would be expected from models

Figure 8: The V_0, $(V-K)_0$ colour-magnitude diagram of NGC6752 with the new isochrones overlaid.

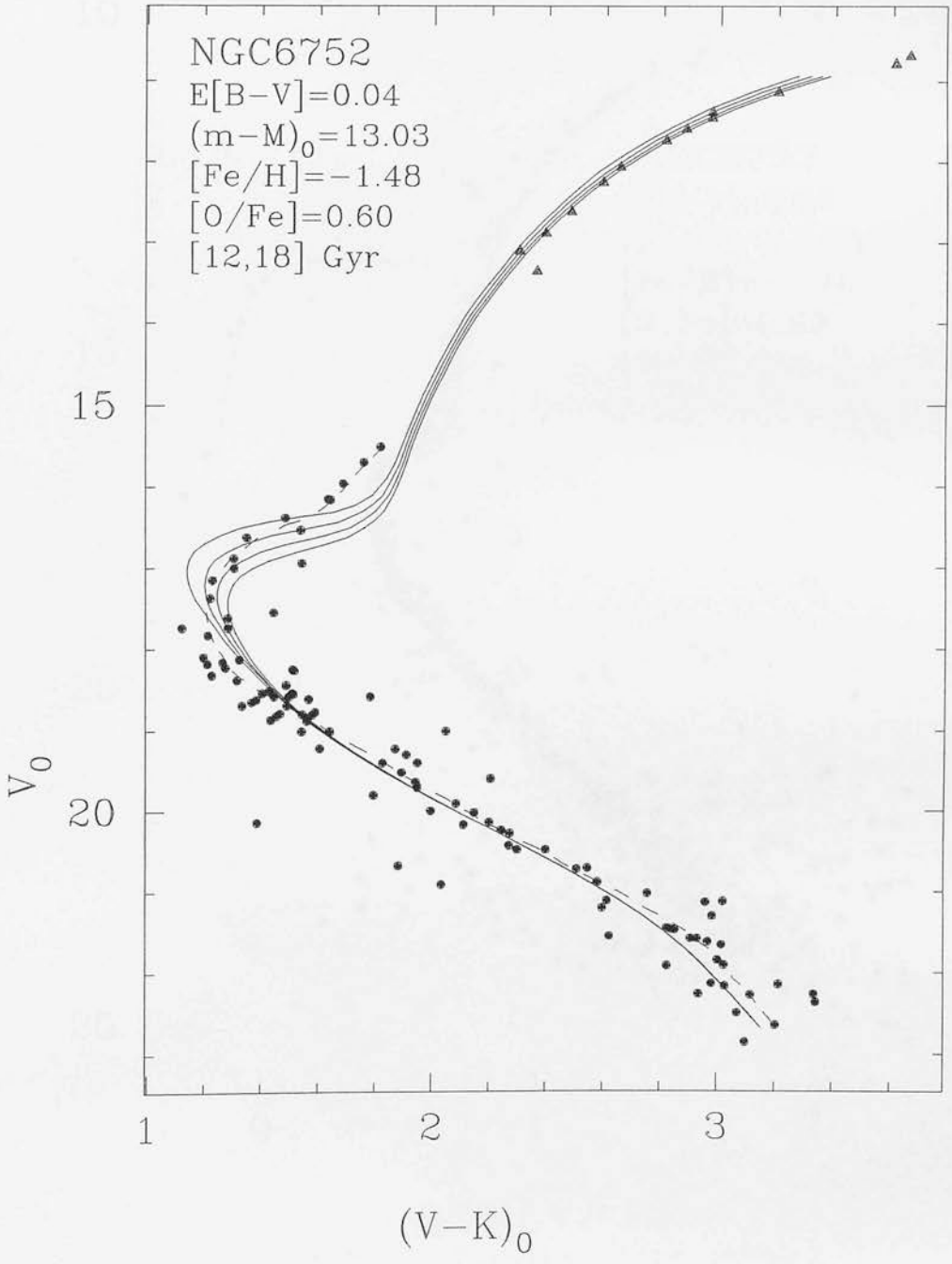

Figure 9: The V_0, $(B-V)_0$ colour-magnitude diagram of NGC6752 with the new isochrones overlaid.

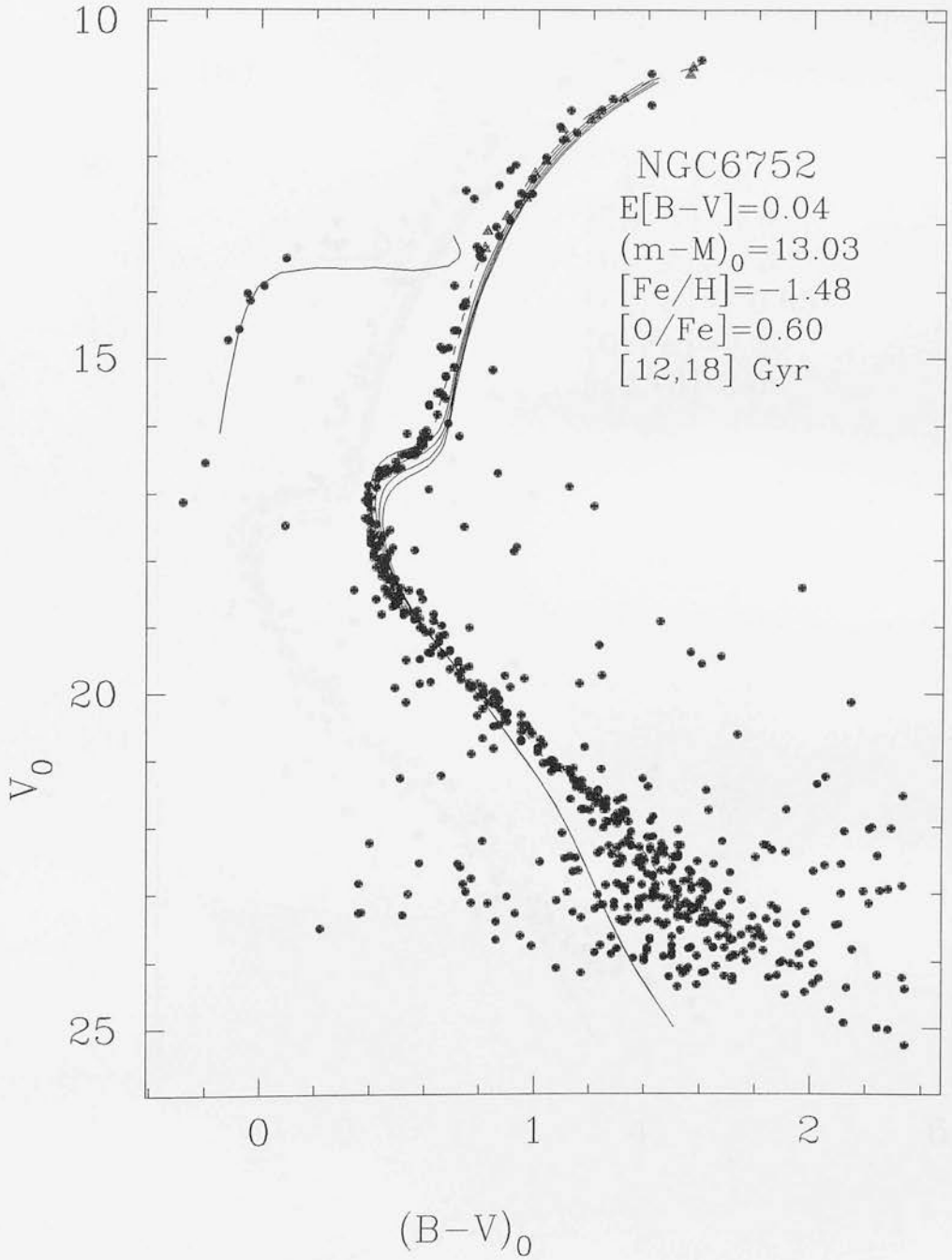

Figure 10(a): The V_0, $(V-K)_0$ colour-magnitude diagram of 47 Tuc with the new [Fe/H]=-0.65 [O/Fe]=0.30 isochrones overlaid.

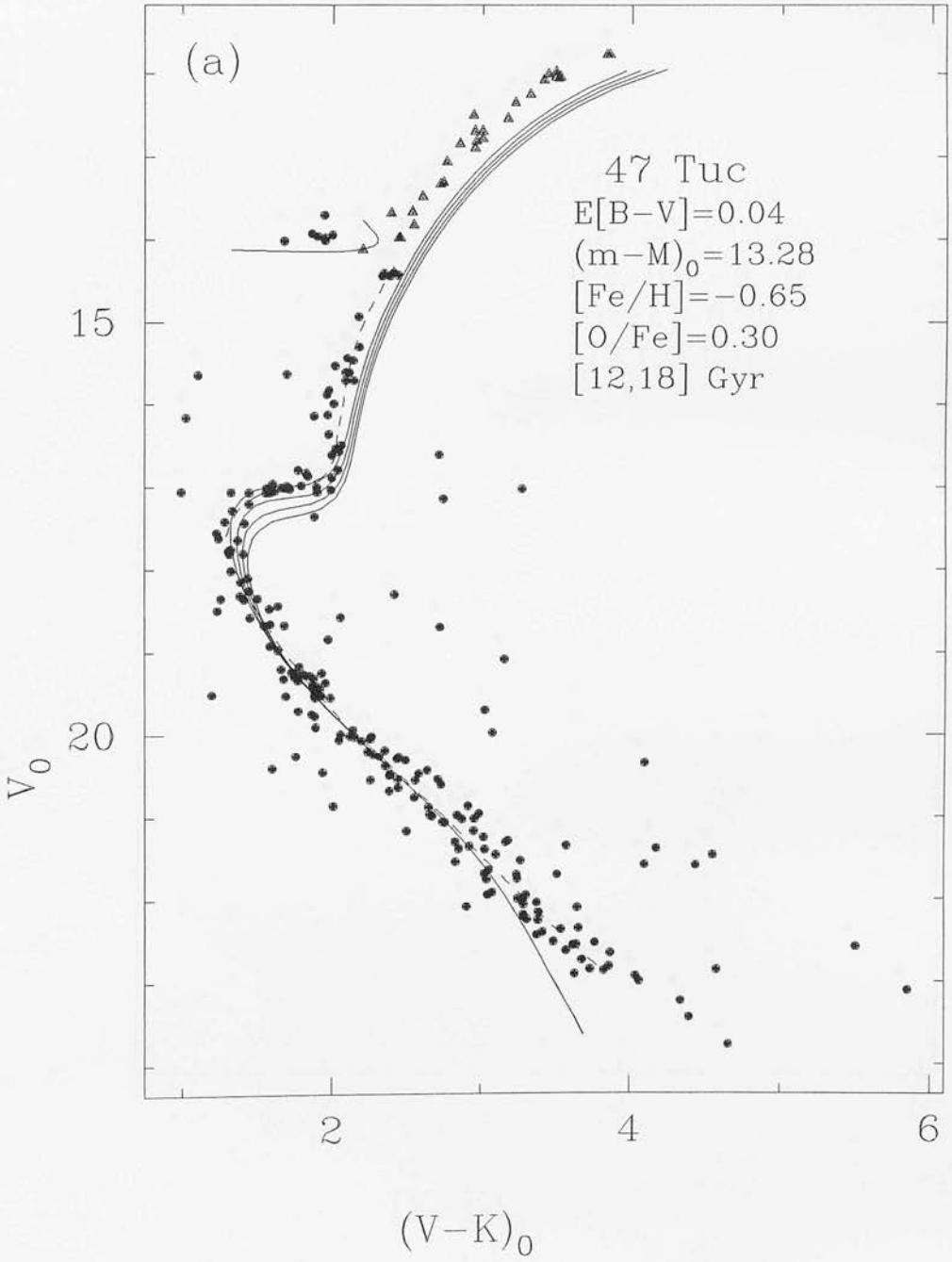

Figure 10(b): As (a) but with the new [Fe/H]=-0.78 [O/Fe]=0.39 isochrones overlaid.

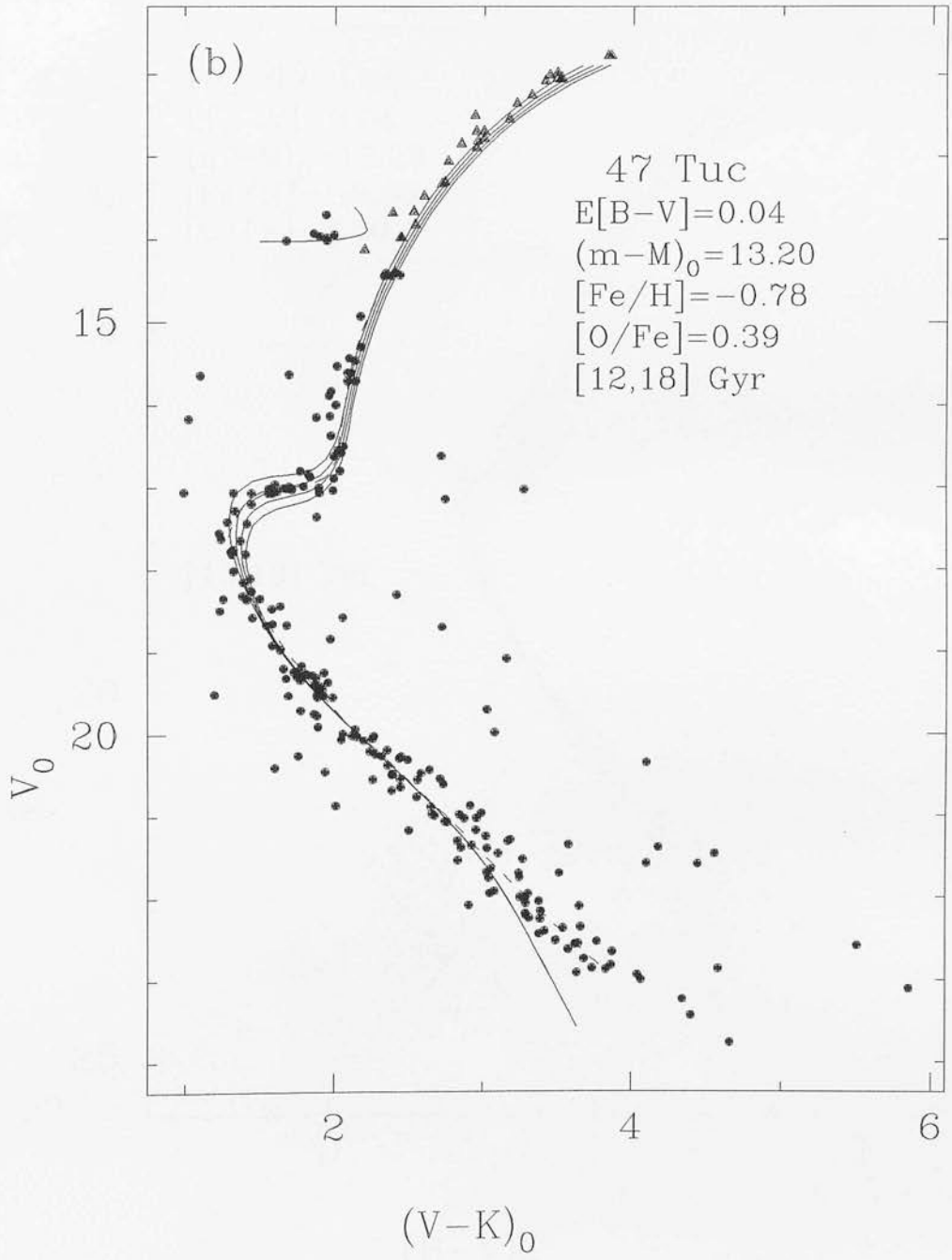

Figure 11(a): The V_0, $(B-V)_0$ colour-magnitude diagram of 47 Tuc with the new [Fe/H]=-0.65 [O/Fe]=0.30 isochrones overlaid.

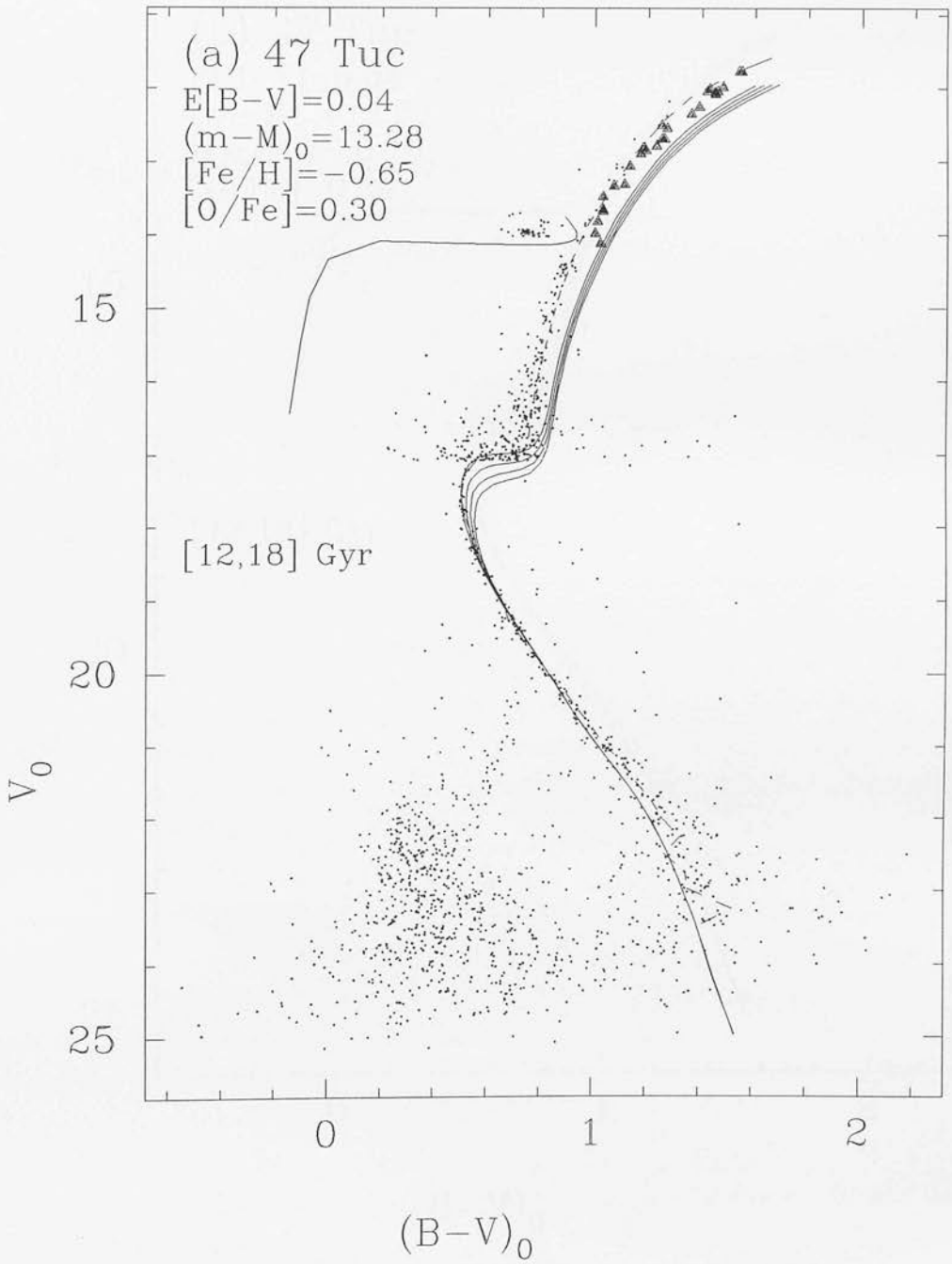

Figure 11(b): As (a) but with the new [Fe/H]=-0.78 [O/Fe]=0.39 isochrones overlaid.

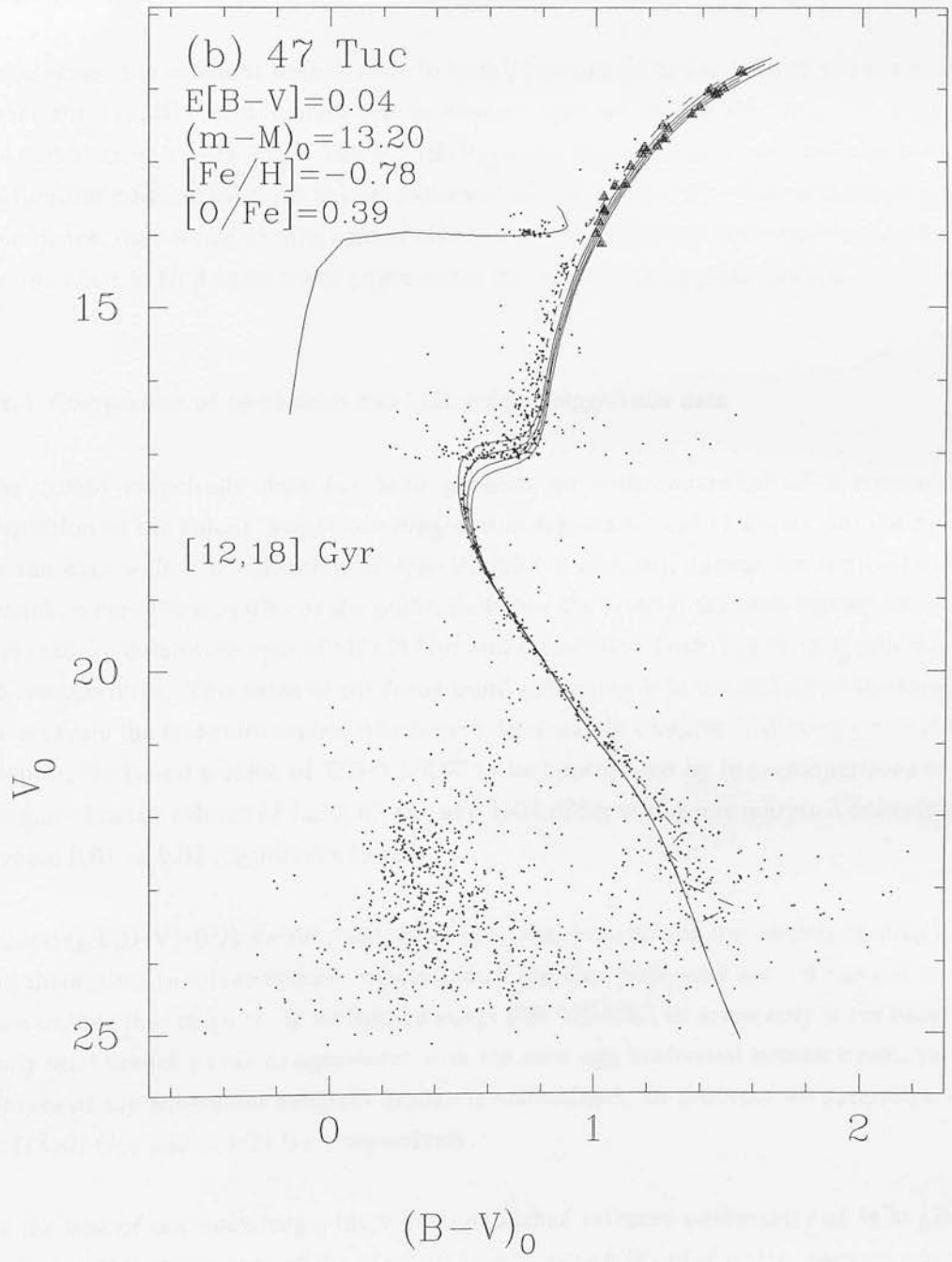

containing extra opacity.

As we have already pointed out in Chapter 2, there is a mismatch of 0.02 to 0.04 magnitudes in (B-V) between the field F3 giants and those from Frogel *et al.*. The [Fe/H]=-0.78 model giant branch agrees with the latter, indicating that slightly more metal-poor models may be more appropriate.

Once again, the subgiant branch stars in both diagrams lie to the blue of the isochrones. From the [Fe/H]=-0.78 models we determine ages of (14±2) Gyr [V_0, $(V-K)_0$] and (14.0±0.5) Gyr [V_0, $(B-V)_0$]. The V_0, $(B-V)_0$ main-sequence is so well defined that it is difficult to place an error on the age estimate! If instead [Fe/H]=-0.65 is the appropriate abundance, then we determine ages of (12±2) Gyr and (12.0±0.5) Gyr respectively, but we are then left to find some other explanation for the ill-fitting giant branch.

3.2.4 Comparison of isochrones and M30 colour-magnitude data

The colour-magnitude data for M30 presents us with somewhat of a conundrum. Inspection of the colour-magnitude diagrams in figures 12 and 13 shows that the models fit the data well if a reddening of E[B-V]=0.03 is adopted, except for the horizontal-branch, where the majority of the points lie below the level of the zero-age sequence. In this case we determine ages of (18±2) Gyr and (16±2) Gyr from V_0, $(V-K)_0$ and V_0, $(B-V)_0$ respectively. This value of the foreground reddening is in the middle of the range of values from the recent literature, which were discussed in Chapter 2, although later in that chapter, we found a value of E[B-V]=0.07 to be appropriate by intercomparisons of the subgiant branch colours of M30, 47 Tuc and NGC6752, with some marginal evidence for a value 0.01 to 0.02 magnitudes lower.

Adopting E[B-V]=0.03 would mean, however, that alone among the clusters studied here, the theoretical subgiant branch colours match the data well, and are not too red as was seen in the other clusters. If we instead adopt E[B-V]=0.07, then not only is the observed horizontal branch in better agreement with the zero-age horizontal branch track, but the picture of the anomalous subgiant branch is maintained. In this case we determine ages of (14±2) Gyr and (13±2) Gyr respectively.

To the best of our knowledge, there is no published infrared photometry of M30 giants, and optically photometry of the giants is sparse, which is unfortunate, because we thus have insufficient evidence to select between the above two ages.

We tentatively adopt an age for M30 of (13.5±1.4) Gyr, which is based on the better match of the observed and theoretical horizontal branches when the higher reddening is applied,

Figure 12(a): The V_0, $(V-K)_0$ colour-magnitude diagram of M30. A reddening correction of E[B-V]=0.07 has been introduced.

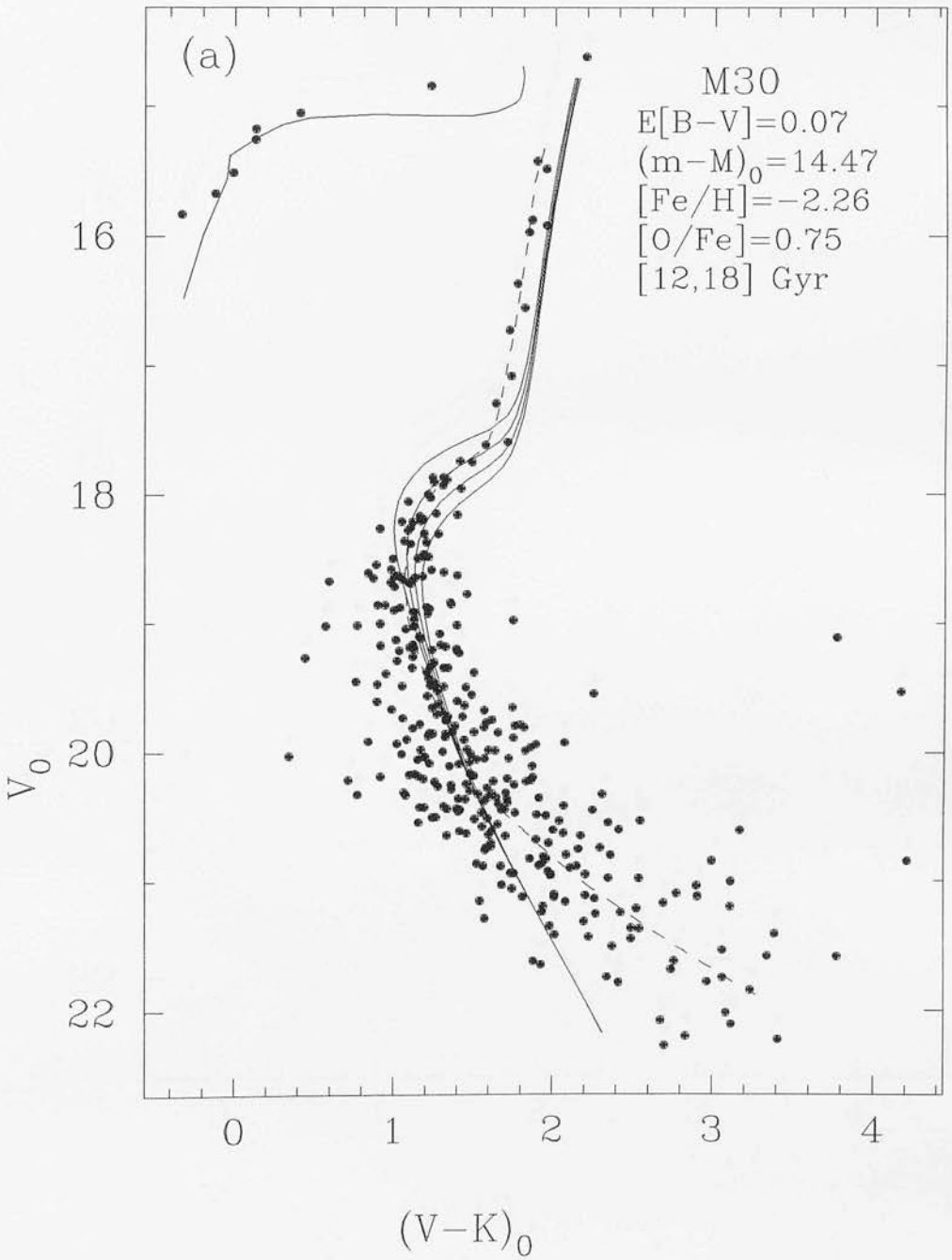

Figure 12(b): As (a) but with a reddening correction of E[B-V]=0.03.

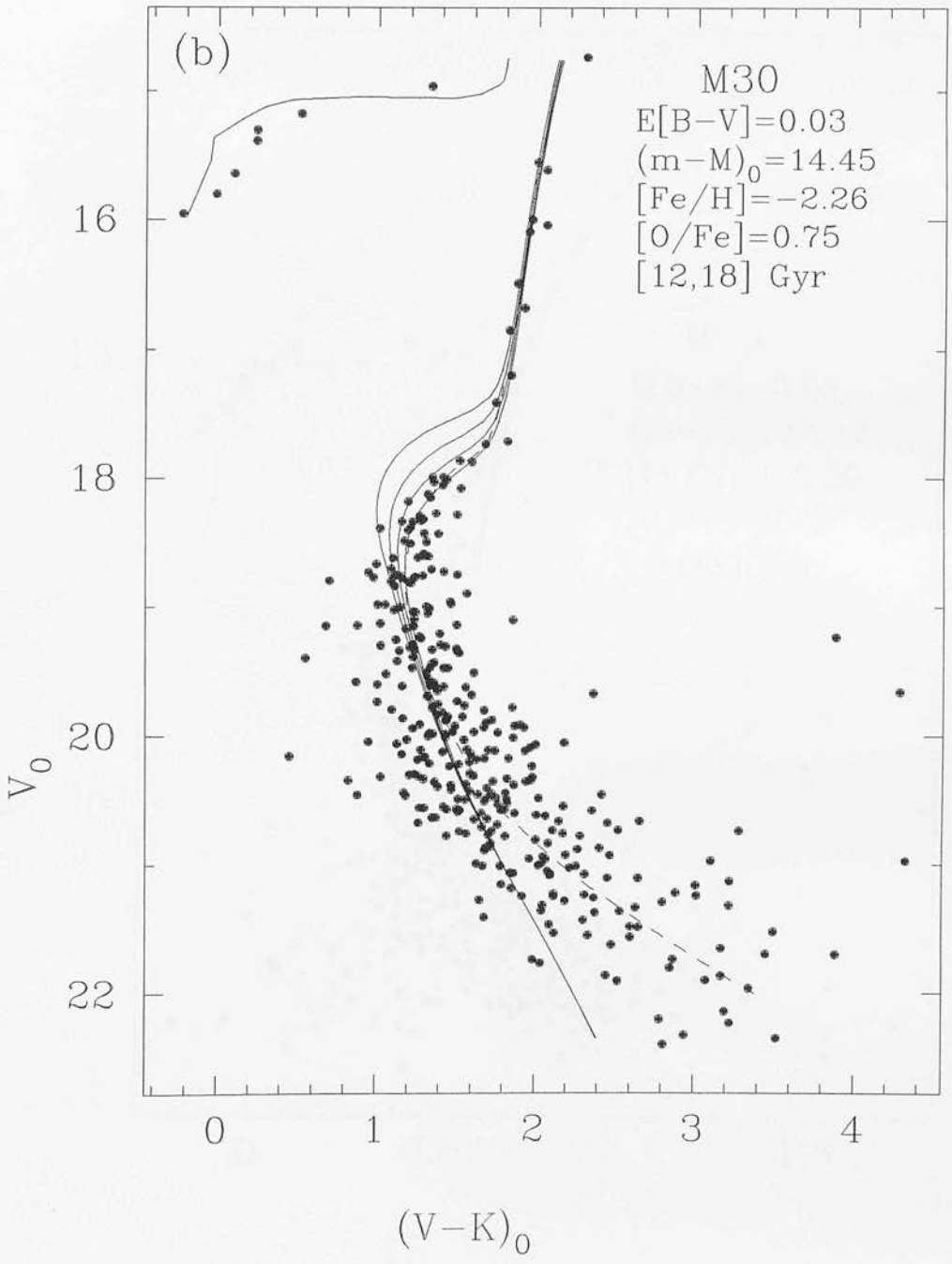

Figure 13(a): The V_0, $(B-V)_0$ colour-magnitude diagram of M30. A reddening correction of E[B-V]=0.07 has been introduced.

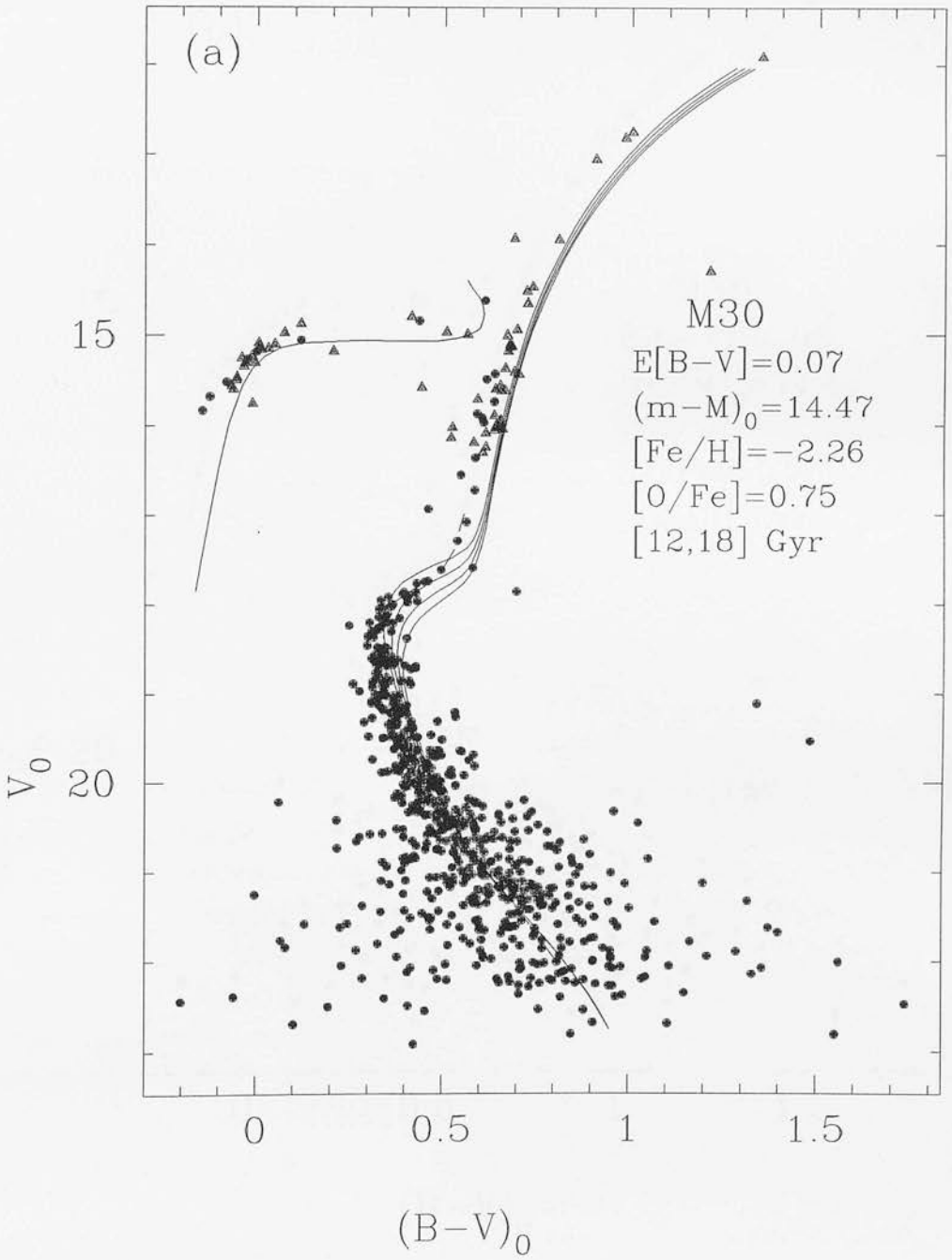

Figure 13(b): As (a) but with a reddening correction of E[B-V]=0.03.

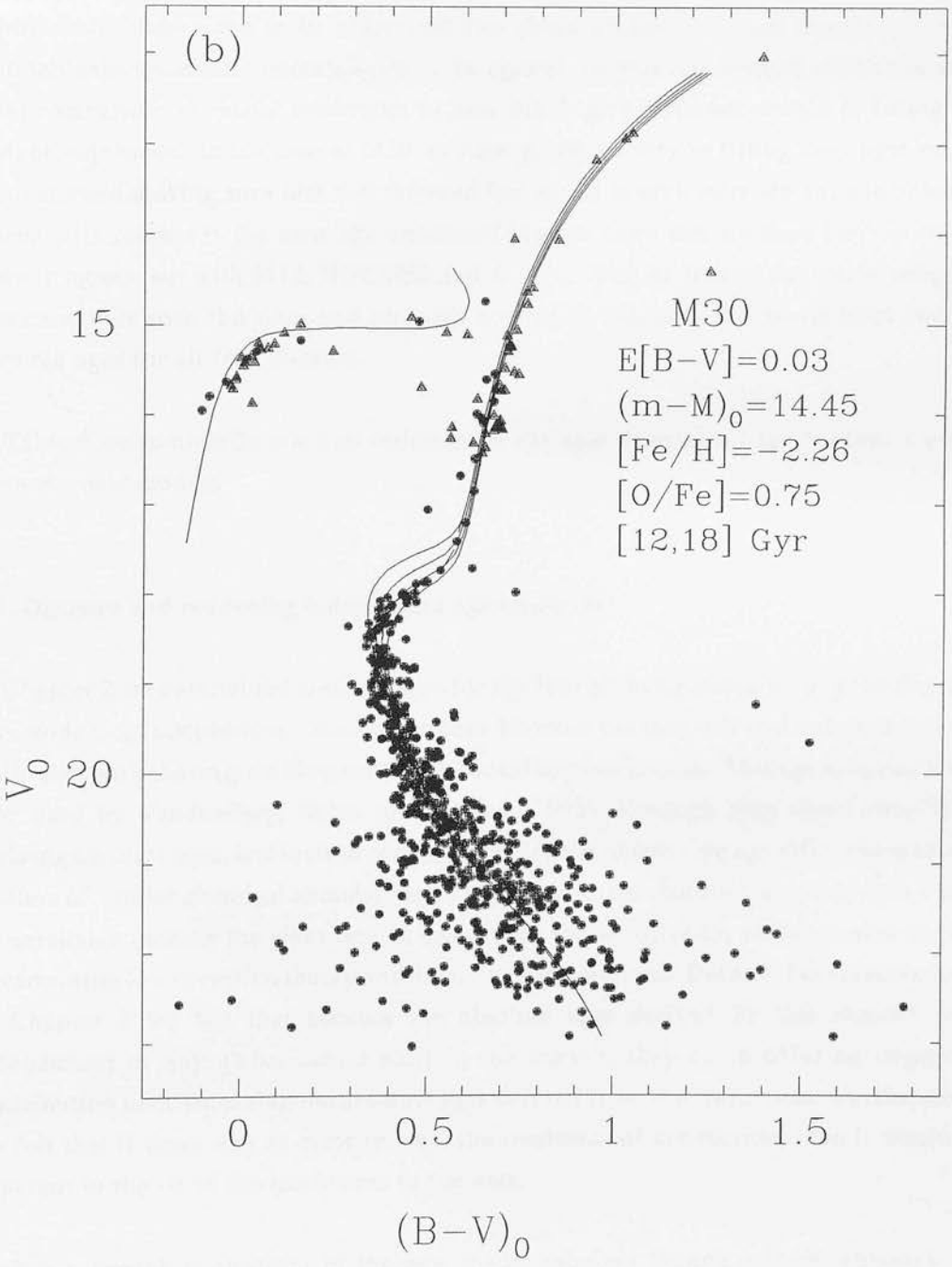

and on the fact that this also maintains the picture of the anomalous theoretical subgiant branch, which was consistently too red compared to the M13, 47 Tuc and NGC6752 data. However, until photometry of M30 giants becomes available, there is also reason to adopt an age ~4 Gyr older.

From a cosmological point of view, this is a huge difference, since the age of the universe is obviously constrained to be older than the oldest object in it; this example of M30 highlights the systematic uncertainties in the ages of the globular clusters which can arise from comparison of model isochrones to data which give different weight to fitting the various sequences. In the case of M30 we have given priority to fitting the upper main-sequence and making sure that the observed horizontal branch stars are not anomalously placed with respect to the zero-age horizontal branch; from this we have derived an age more in agreement with M13, NGC6752 and 47 Tuc. Had we trusted the model subgiant branches more than the giant and zero-age horizontal branches, we would have derived very old ages for all four clusters.

In Table 6 we summarise our best estimates of the ages determined for the four clusters from the new models.

3.3 Distance and reddening independent age estimates

In Chapter 2 we determined absolute ages for the four globular clusters using the distance and reddening independent colour difference between the turn-off and subgiant branch, calibrated with the original Bergbusch & VandenBerg isochrones. This age diagnostic was first used by VandenBerg, Bolte, and Stetson (1990), although they shied away from deriving absolute ages, and instead confined themselves to deriving age differences among clusters of similar chemical abundances. They commented that such absolute ages would be unreliable because the giant branch colours are too sensitive to, amongst other things, uncertainties in convection theory and colour transformations. Despite these reservations, in Chapter 2 we felt that because the absolute ages derived by this method were independent of any global colour shift in the models, they could offer an important contribution to constraining the absolute ages derived from the isochrones. Furthermore, we felt that if there was an error in, say, the treatment of convection, then it would be apparent in the fit of the isochrones to the data.

Such a mismatch is apparent in the new model subgiant branch colours, although the source remains to be determined. It is therefore important to consider consequences for age determinations from this method, whether absolute or relative. The first step in a complete answer to this question would be to find the source of the discrepancy between theory and observations. This will require the model builders to calculate the isochrones

Table 6: Ages determined from comparison of the new models to V_0, $(V-K)_0$ and V_0, $(B-V)_0$ colour-magnitude diagrams.

Cluster	age/Gyr	Parameters
M13	14.4±1.6	canonical
NGC6752	14.0±1.4	canonical
47 Tuc	14.0±0.5	[Fe/H]=-0.78
M30	13.5±1.4	E[B-V]=0.07

using the Kurucz models consistently throughout. It may be that the discrepancies, both on the subgiant branch and on the main sequence [in V, (B-V)] are a consequence of having used disparate model atmospheres to calculate these isochrones and convert the theoretical results to the observational plane.

If the discrepancies persist then this perhaps indicates some lacking or poorly understood physics in the models. Remember that in subgiant branch stars, energy generation comes from hydrogen burning in a shell surrounding a hydrogen-exhausted core, and this shell becomes thinner as the star ages along the subgiant branch. The Bergbusch & VandenBerg computations model this with Lagrangian code; it is not until the giant-branch phase that the shell becomes thin enough to warrant non-Lagrangian treatment. At some stage, close to the level of the horizontal-branch, this shell passes through a composition discontinuity left by the deepest penetration of the convective envelope. This is thought to be the origin of the 'clump' of stars observed on many subgiant branches; the clumps in M71 and 47 Tuc were used by Dixon (1992) to determine relative reddenings, distances and chemical abundances between these clusters. The unphysical modelling of convection could therefore be one source of the problem, as could variations in the microturbulent velocity, which is another poorly understood parameter.

In figures 14 and 15 we show plots of $\Delta(V-K)$ and $\Delta(B-V)$ versus age determined from the new and original Bergbusch & VandenBerg models with abundances [Fe/H]=-2.26 and -0.78. As was clear from the colour-magnitude diagrams, at [Fe/H]=-2.26 the models predict much larger values of $\Delta(V-K)$ and $\Delta(B-V)$ for a given age. In the region of 14 Gyr, calibration of $\Delta(V-K)$ and $\Delta(B-V)$ by the new models would lead to ages older by ~1 Gyr; the smaller change in $\Delta(B-V)$ between the two sets of models is made up for by the shallower gradient of $\Delta(B-V)$ with age. At [Fe/H]=-0.78, the increase of $\Delta(B-V)$, at a fixed age, when using the new models is devastating; values of $\Delta(B-V)$ which gave an age of ~12 Gyr when calibrated by the old models, now give an age of ~18 Gyr.

Figure 14: The (V-K) and (B-V) colour differences between the main-sequence turn-off and the subgiant branch versus age, calculated from the new and original Bergbusch & VandenBerg [Fe/H]=-2.26 [O/Fe]=0.75 isochrones.

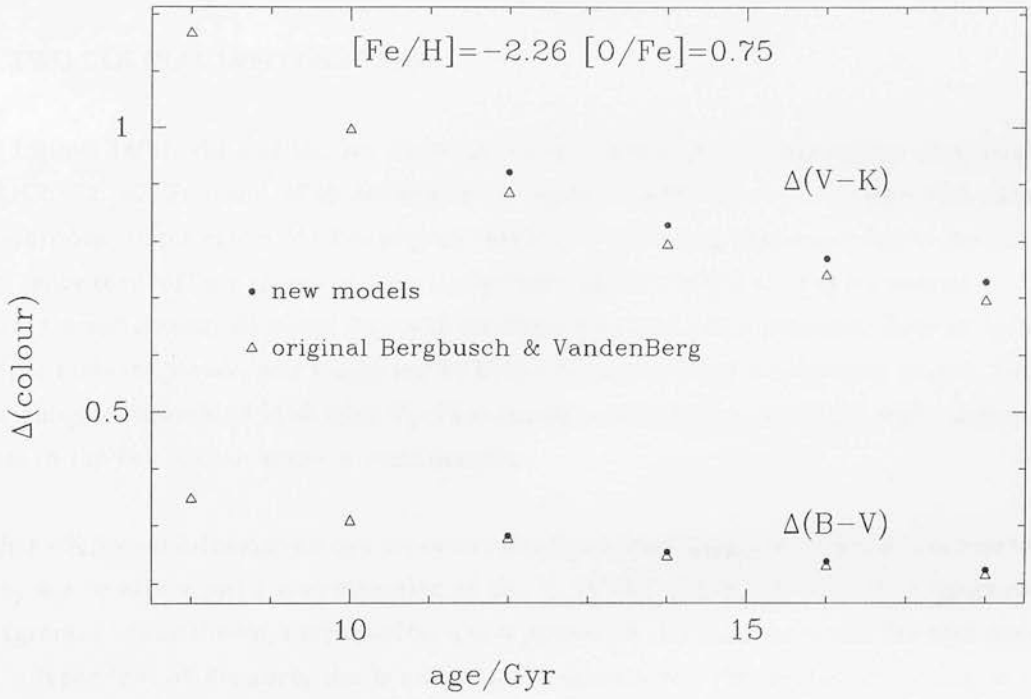

Figure 15: The (V-K) and (B-V) colour differences between the main-sequence turn-off and the subgiant branch versus age, calculated from the new and original Bergbusch & VandenBerg [Fe/H]=-0.78 [O/Fe]=0.39 isochrones.

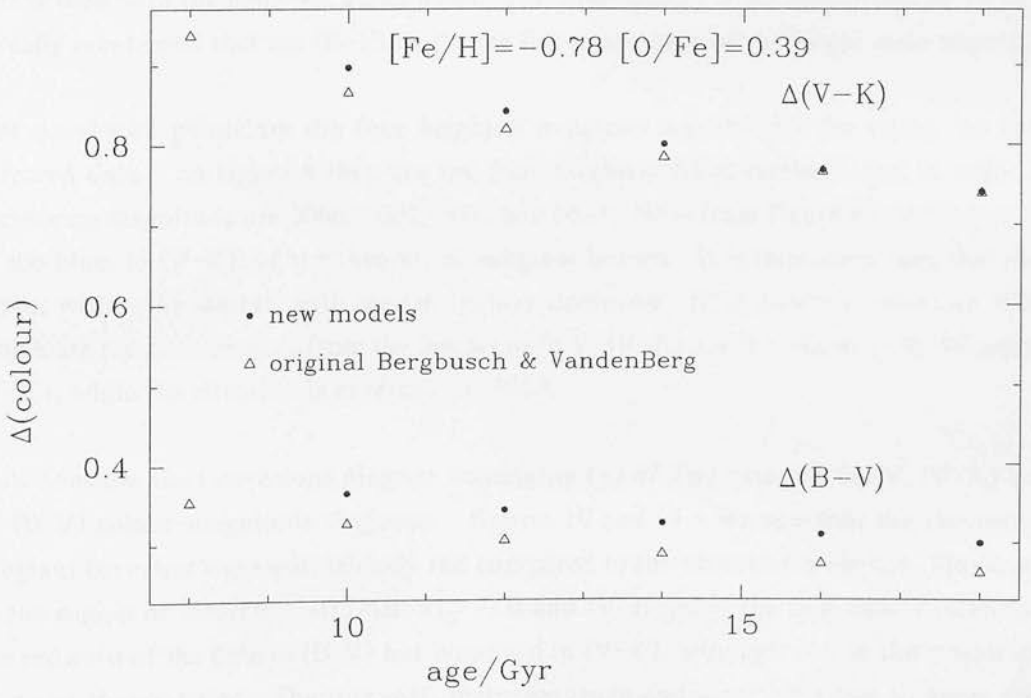

We therefore do not feel able to use this method in an absolute sense, to further constrain the ages determined directly from the isochrones.

4 TWO COLOUR INFORMATION

In figures 16(a), (b) and (c), we show the (V-K) versus (B-V) two-colour diagrams of NGC6752, 47 Tuc and M30 respectively, together with the new 14 Gyr two-colour isochrones. In the case of 47 Tuc [figure 16(b)], our data from above and below the main-sequence turn-off are shown as separate symbols, as are the giants. The horizontal branch stars are not shown, although they also lie along the tight linear sequence defined by the upper main-sequence, and would not be easily distinguishable if they were shown. Only the subgiant branch of M30 with $V_0<18$ is shown, since the scatter of the main-sequence data in the two-colour plane is considerable.

What additional information can we determine from these diagrams? While it is true that they are in effect just a concatenation of the V, (V-K) and V, (B-V) colour-magnitude diagrams already shown, they do offer a comparison of the isochrones and the data which is independent of distance, the bolometric corrections and the method of fitting to the data, which in this thesis has been via the subdwarfs.

Consider first figure 16(a), which shows the comparison of the 14 Gyr [Fe/H]=1.48 two-colour isochrone with the NGC6752 data. The main sequence data with $(V-K)_0>\sim2.8$ tend to agree much better with the locus of the theoretical giant-branch, or are bluer than it, rather than with the main-sequence locus. This discrepancy is not surprising, as we have already mentioned that the (B-V) isochrone lies to the blue of the lower main sequence.

The numbered points are the four brightest subgiant-branch stars for which we have infrared data - on figure 8 they are the four brightest filled circles - and in order of increasing magnitude are 3006, 5002, 5003 and 5004. Note from figure 8 that they all lie to the blue, in (V-K), of the theoretical subgiant branch. It is thus surprising that they agree, within the scatter, with the two-colour isochrone. Note also that 3006 and 5002, which are the most deviant from the isochrone in V, (V-K) are the closest in (B-V) versus (V-K), while the situation is reversed for 5004.

Now consider the two-colour diagram containing the 47 Tuc data. In the V, (V-K) and V, (B-V) colour-magnitude diagrams - figures 10 and 11 - we saw that the theoretical subgiant branches were anomalously red compared to the observed branches. However, in the region of interest - $\sim0.7<(B-V)_0<\sim1.0$ and $(V-K)_0\sim2$ - the two-colour isochrone lies redward of the data in (B-V) but blueward in (V-K), although within the scatter the data and theory agree. The turn-off, main-sequence and giant branches all agree well

Figure 16: The $(B-V)_0$ versus $(V-K)_0$ two-colour diagrams of (a) NGC6752 and (b) 47 Tuc.

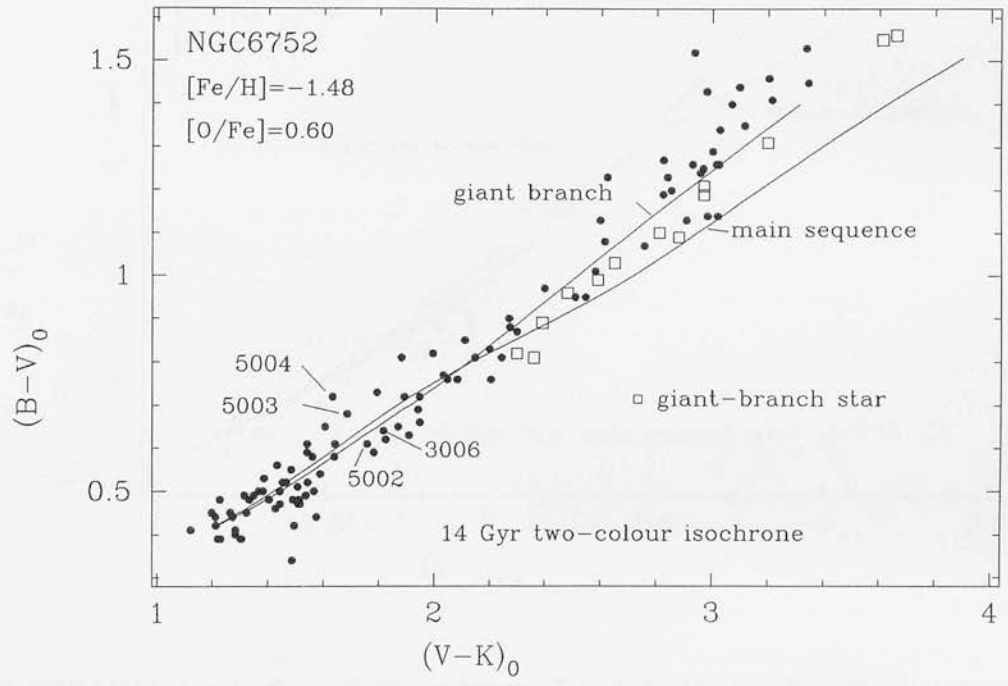

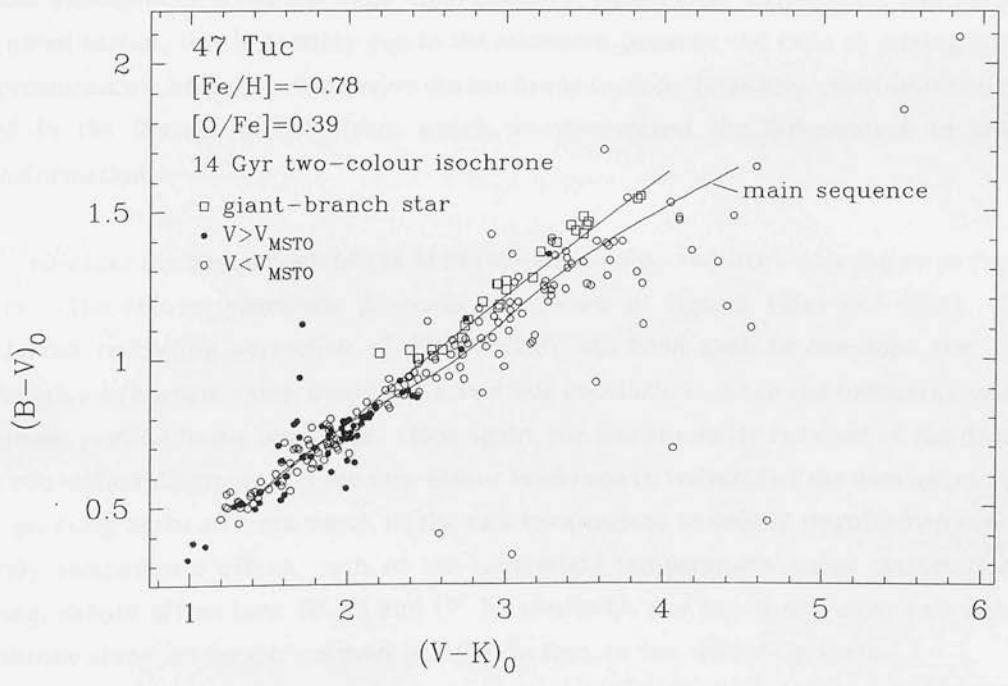

Figure 16(c): The $(B-V)_0$ versus $(V-K)_0$ two-colour diagram of M30, showing only those subgiant branch data with $V_0<18$.

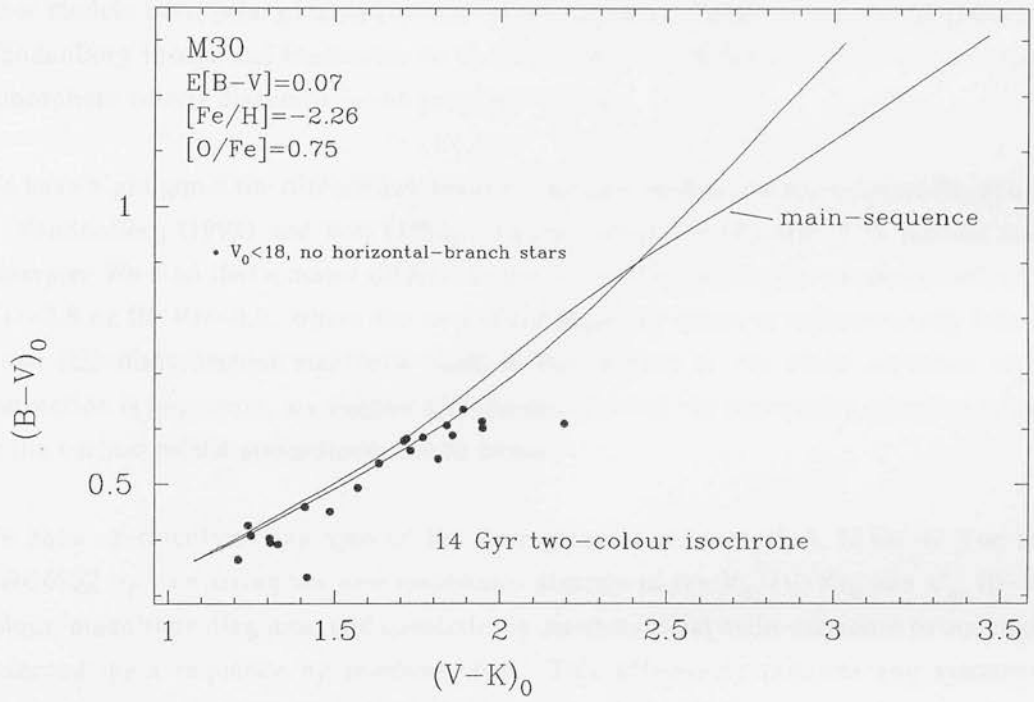

with their respective portions of the isochrone. This suggests that there is a discrepancy, in the subgiant-branch region, between the (V-K) and (B-V) colours predicted from the model atmospheres given the same input chemical abundance, temperature and gravity. As noted earlier, this is possibly due to the mismatch between the ratio of mixing length to pressure scale height used to derive the isochrone surface-boundary conditions and that used in the Kurucz models from which we determined the temperature to colour transformation.

Now consider the comparison of the M30 two-colour data and isochrone shown in figure 16(c). The colour-magnitude diagrams are shown in figures 12(a) and 13(a). Our preferred reddening correction of E[B-V]=0.07 has been used to deredden the data, although an alternate value would not affect our conclusions, since the reddening vector is almost parallel to the isochrone. Once again, the isochrones lie redward of the data in the two-colour diagrams, but the two-colour isochrone is redward of the data only in (B-V), pointing again to a mismatch in the two temperature to colour transformations. A purely temperature effect, such as the theoretical temperatures being systematically wrong, should affect both (B-V) and (V-K) similarly, and act to move the two-colour isochrone along it's length - almost parallel, in fact, to the reddening vector.

5 CONCLUSIONS

New models have been obtained which were created by transforming the Bergbusch & VandenBerg theoretical isochrones to V, (V-K) and V, (B-V) using the Kurucz model atmosphere results discussed in the previous chapter.

We have highlighted the differences between the new models and the original Bergbusch & VandenBerg (1992) and Bell (1992) colours, taking the [Fe/H]=-0.78 models as an example. We find that a major difference occurs on the lower main-sequences with (V-K)>~2.8 or (B-V)>~0.8, where the new main sequence becomes systematically fainter. Since this disagreement manifests itself in the regions of the main sequence where convection is important, we suggest differences between the convective parameters used in the various model atmospheres are to blame.

We have re-calculated the ages of the four globular clusters M13, M30, 47 Tuc and NGC6752 by comparing the new isochrones directly to the V_0, $(V-K)_0$ and V_0, $(B-V)_0$ colour-magnitude diagrams, and constraining the theoretical main-sequence to match the observed main-sequence by subdwarf fits. This effectively removes any systematic uncertainty in the model magnitudes due to uncertainties in the bolometric corrections. We find that new subgiant branches are anomalously blue compared to the observed subgiant branches; the original theoretical subgiant branches fit the data well. A comparison of the NGC6752, 47 Tuc and M30 data and the new isochrones in the two-colour plane suggests that this is caused by (possibly convection related) mismatches between the temperature to (B-V) and to (V-K) relations.

Giving maximum weight to ensuring that the models fit the observed upper main sequence well, and that the observed horizontal branch is not anomalously placed with respect to the zero-age horizontal branch, we derive ages of ~14 Gyr for each cluster. Had we placed greater weight on the fit of the subgiant branches, we would have derived much older ages, in the case of M30 the age would have been ~18 Gyr.

Discussion of the implications of these cluster ages to the galactic formation scenario is given next in the conclusion to this thesis.

REFERENCES

Bell, R.A., 1992. *Mon. Not. Roy. astr. Soc.* **257**, 423.
Bergbusch, P.A. & VandenBerg, D.A., 1992. *Astrophys. J. Suppl.* **81**, 163.
Dixon, R.I., 1992. Ph.D. thesis, University of Edinburgh.
Frogel, J.A., Persson, S.E. & Cohen, J.G., 1981. *Astrophys. J.* **246**, 842.

Hesser, J.E., Harris, W.E., VandenBerg, D.A., Allwright, J.W.B., Shott, P. & Stetson, P.B., 1987. *Publs astr. Soc. Pacif.* **99,** 739.

Paez, E., Straniero, O. & Martinez Roger, C., 1990. *Astrophys. J. Suppl.* **84,** 481.

Penny, A.J. & Dickens, R.J., 1986. *Mon. Not. Roy. astr. Soc.* **220,** 845.

Richer, H.B. & Fahlman, G.G., 1986. *Astrophys. J.* **304,** 273.

Stetson, P.B. & Harris, W.E., 1988. *Astron. J.* **96,** 909.

Straniero, O. & Chieffi, A., 1991. *Astrophys. J. Suppl.* **76,** 525.

VandenBerg, D.A., 1991. *Astrophys. J.* **391,** 685.

VandenBerg, D.A. & Bell, R.A., 1985. *Astrophys. J. Suppl.* **58,** 561.

VandenBerg, D.A., Bolte, M. & Stetson, P.B., 1990. *Astron. J.* **100,** 445.

Zinn, R., 1985. *Astrophys. J.* **293,** 424.

Conclusion

The Age and Formation of the Galaxy

" There is a theory which states that if ever anyone discovers exactly what the Universe is for and why it is here, it will instantly disappear and be replaced by something even more bizarre and inexplicable. There is another theory which states that this has already happened. " - The Hitch-hikers Guide to the Galaxy

1 THE CLUSTER-GALAXY CONNECTION

It is appropriate at this point to give a brief reminder of the *raison d'être* of the previous four chapters.

One of the most promising routes to the formation of a quantitative model of the processes and timescales involved in transforming pre-galactic, primordial material into the galaxy as we know it today is to study the 'fossil record'.

One such component of the fossil record is, of course, the globular cluster system. As a simple starting point, one might expect that observations of globular clusters would yield the following information:

- The age of the oldest cluster would set the time when recognisable structures first formed - it would give, in effect, the age of the galaxy.

- The age of the oldest cluster can be used to set a lower limit to the age of the universe, thus placing observational constraints on cosmological models.

- Clusters which are shown to be associated with the various components of the galaxy - nuclear bulge, halo, disk and so forth - could trace the chronology of formation of these components.

- The age spread amongst the clusters associated with any particular component of the galaxy would show how long that component took to form.

- An intercomparison of the chemical composition of the clusters would allow limits to be set on the chemical composition and homogeneity of the primordial material from which the galaxy formed. This is provided that the composition has not changed in the meantime due to nucleosynthesis within the component stars.

- An analysis of the mass function of cluster stars would allow conclusions to be drawn about early star formation within the galaxy. Unfortunately, dynamical effects have to be modelled in order to change the observed mass function into the initial mass function.

- An analysis of cluster orbits would give an idea of the dynamics of the gas from which they originally formed. Care is needed because this involves extrapolating back over the entire life of the galaxy, to when the dynamical processes are likely to have been very different than those observed today.

This section deals with the use of the globular cluster system to trace the formation history of the galaxy.

1.1 The current picture

The picture currently emerging from studies of the galactic globular cluster system is of a much more complicated and chaotic galaxy formation process than was envisioned by early models such as that of Eggen, Lynden-Bell & Sandage (1962). In that model, the galaxy formed from a single, large protogalaxy in a rapid collapse on timescales short compared to the timescales involved in circular orbits at the radius of first star formation. The basic ideas of the Eggen *et al.* model, reiterated recently by Sandage (1993), that the galaxy condensed from a larger volume, and that the initial collapse was rapid, are almost certainly part of, but not the whole story.

Van den Bergh (1993) identifies three distinct populations within the galactic globular cluster fossil record, to which he assigns labels α, β and γ, based on the positions of clusters in the horizontal-branch type versus abundance diagram. Considering only those clusters with abundances in the range $-2<[Fe/H]<-1$, population β is defined to be those clusters which lie close to the 'isochrone' placed through the positions of clusters within the solar galactocentric radius, assumed to be 8.5 kpc. Population α consists of those clusters in the same abundance range which lie away from this 'isochrone'. The third, strongly centrally concentrated population consists of clusters with $[Fe/H]>-0.8$, which van den Berg prefers to describe as a nuclear population with Population I kinematics rather than the heretofore more common 'thick disk' system.

Table 1: A brief summary of the properties of α, β and γ population clusters found by Van den Bergh (1993). R_h is the galactic radius containing half of all clusters.

α-clusters	β-clusters	γ-clusters
No concentration on the galactic centre	Moderate concentration on the galactic centre	Strong concentration on the galactic centre
R_h=12 kpc	R_h=5 kpc	R_h<~4 kpc
On average α-clusters are more metal rich than β-clusters		
Predominantly Oosterhoff class I	Both Oosterhoff I and II in roughly equal proportions	
Most frequently found in retrograde motion	Most frequently found in prograde or intermediate motion	
Large fraction have plunging orbits	Large fraction have circular orbits	
Age dispersions of a few Gyr	Essentially coeval, with age dispersions of <~1 Gyr	

A brief summary of the properties of α, β and γ clusters is given in Table 1.

As attested to by the galactocentric radii containing half the numbers of clusters, R_h, which are given in Table 1, and as can also be seen from van den Berg's figure 6, α-clusters are mostly found with galactocentric radii greater than the solar galactocentric radius, while population β consists mostly of those clusters with smaller galactocentric radii.

The inner halo, β-clusters are found to be essentially coeval, within the limits set by the observations, with age dispersions of <~1 Gyr. Conversely, the outer halo α-clusters, which are on average younger and more metal rich than the inner halo clusters, have age dispersions of a few Gyr. Implicit in these conclusions is, of course, the identification of

age variations as the 'second parameter', that is, the parameter which, after metal abundance, has the greatest effect on horizontal branch morphology. This identification is still controversial.

Lee (1992) notes that an analysis of the abundance distribution of RR Lyrae variable stars in the galactic bulge suggests that this age versus galactocentric radius relation continues to the galactic centre, and that the oldest bulge stars are thus older by ~1 to 1.5 Gyr than the oldest halo population.

The evidence presented by Lee and by van den Bergh favours the 'bottom-up' scenario of galaxy formation. Lee favours the scenario, outlined by Larson (1990), with a centrally concentrated system of many gas-rich protogalactic clouds such as was envisioned by Searle & Zinn (1978). The frequent and violent collisions and mergers between clouds in the centre of the system would lead to early star and cluster formation, but would also quickly destroy the clouds thereby halting the process and producing the small age dispersions observed. The process would, on the other hand, proceed more slowly, and for longer, in the more sparse outer halo. Van den Berg, on the other hand, favours a scenario where the inner halo formed from a rapid, Eggen *et al.*-type collapse, while the outer halo formed as outlined above.

Van den Bergh also notes that clusters with [Fe/H]<-2 occur at all galactocentric radii and thus do not fit the pattern of the $\alpha\beta\gamma$ model. The study of such clusters obviously offers the potential for future refinement to the galaxy formation model. One would wish to know, for example, if there is a sharp division at exactly [Fe/H]=-2, if these clusters have different kinematics in any way from the $\alpha\beta\gamma$-clusters, whether they are all coeval, or are significantly older - or younger - than clusters which do fit into the $\alpha\beta\gamma$ classification.

1.2 The classification of M13, M30, NGC6752 and 47 Tuc

According to Table 1 of van den Berg (1993), both M13 and NGC6752 fall into class β, the coeval inner-halo clusters, while M30, with [Fe/H]<-2, is one of the clusters that do not fit the $\alpha\beta\gamma$ classification.

It is not immediately obvious into which class 47 Tuc should be placed, although it *is* clear that we must be cautious about assigning a classification to 47 Tuc based on the metallicity alone. Since the individual elemental abundances are decoupled, it is not even clear what [Fe/H] means in this case. If it is taken, at face value, to mean the logarithmic iron-to-hydrogen ratio with respect to the sun then following the discussion in Chapter 2, [Fe/H]~-1. In this case 47 Tuc could be placed into either the α or β classes depending

on the position in the horizontal-branch type versus [Fe/H] diagram. If on the other hand, [Fe/H] is taken to be the single parameter which best describes the chemical abundance, even though these are non-scaled-solar, then it should be set at the same value as the best-fitting isochrones. As we saw in Chapters 2 and 4, this parameter is model-dependent, but is more metal rich than [Fe/H]=-1, excluding 47 Tuc from classes α and β.

We therefore also need to know about the kinematics of 47 Tuc, and in particular if it belongs to the 'thick disk' population.

Armandroff (1989) tabulates for 47 Tuc an abundance of [Fe/H]=-0.71, the apparent visual magnitude of the horizontal branch V_{HB}=14.06, reddening E[B-V]=0.04, distance above the galactic plane Z=-3.0 kpc and projected distance from the Galactic centre in the plane r=6.7 kpc. This latter was calculated from the horizontal-branch magnitude and the theoretical horizontal branch absolute magnitude versus [Fe/H] relation of Lee *et al.* (1987), which is reproduced in equation 1, and assuming a solar galactocentric radius of 8 kpc.

$$M_V(HB) = 0.2[Fe/H] + 0.92 \qquad (1)$$

Armandroff notes that there is not a perfect division between disk and halo clusters at [Fe/H]=-0.8, and that in particular the gap in the |Z| versus r diagram - see his figure 1 - between the three metal-rich clusters with the largest values of |Z| and the rest might indicate that these clusters are not part of the disk system. He also notes that the gap could be caused by small number statistic, observational errors or both. The three clusters are 47 Tuc, NGC6356 and Pal 11.

However, he proceeds to demonstrate in section V that these clusters have kinematics which are indistinguishable from the rest of the disk-cluster sample, which would not be expected if they were from the metal-rich end of the halo-cluster population. See in particular his figure 6.

On the basis of the kinematics and, to a lesser extent, chemical abundance, 47 Tuc should be accorded γ-cluster status.

1.3 Constraints on the galactic age

In Table 2 we present a summary of the ages and distances derived for M13, M30, NGC6752 and 47 Tuc from Chapters 2 and 4. Note that although our age derivations in

Table 2: A summary of (a) the ages and (b) the distances of M13, M30, NGC6752 and 47 Tuc derived in Chapters 2 and 4. R_{GC} is the galactocentric distance calculated as described in the text.

(a)

Cluster	age/Gyr		Best comparison age[1]
	Chapter 2	Chapter 4	
M30	14.9±2.3	13.5±1.4	13
M13	14.1±1.4	14.4±1.6	13
NGC6752	13.6±1.1	14.0±1.4	13
47 Tuc	14.6±1.5	14.0±0.5	13.5

[1]The ages derived by Richer, Fahlman & VandenBerg (1988) for M30, by Richer & Fahlman (1986) for M13, by Penny & Dickens (1986) for NGC6752 and by Hesser *et al.* (1987) for 47 Tuc are respectively 14, 16, 16 and 13.5 Gyr, from isochrones with oxygen enhancements of [O/Fe]=0.5, 0, 0 and 0.3 respectively. These ages have been reduced by 7.5%, 18%, 18% and 0% to correct to the oxygen enhancements used by us, following the suggestion by VandenBerg (1985) that a 0.5 dex increase in [O/Fe] in the isochrones reduces ages by ~15%, and these new ages are given as the 'best comparison ages' above.

(b)

Cluster	Class	distance/kpc		R_{GC}
		Chapter 2	Chapter 4	
M30	-	8.1	7.8	7.4
M13	β	7.1	7.1	8.7
NGC6752	β	4.0	4.0	5.7
47 Tuc	γ	4.4	4.4	7.8

Chapters 2 and 4 were from Bergbusch & VandenBerg isochrones converted to the observational planes using different model atmospheres, the conclusions we derive will not depend upon which set of ages is adopted, since the two agree within the internal errors. Only in the case of M30 is there a variation of more than 0.4 Gyr between the ages, which is not surprising given the quality of the photometry around the turn-off.

We also present in Table 2 revised galactocentric distances R_{GC} of each cluster, calculated using the distances in column 5, the equatorial coordinates of the clusters given by Sawyer-Hogg (1973), the (1950) equatorial coordinates of the galactic centre: $\alpha_{GC}=17^h42.4^m$, $\delta_{GC}=-28°55'$ from Fredrick (1989) and assuming a solar galactocentric radius of 8.5 kpc. The equation giving the angle between the cluster and the galactic centre is reproduced in equation 2 from Duffet-Smith (1988), which can be substituted into equation 3 to yield the distance.

$$\cos\theta = \sin(\delta_{cluster})\sin(\delta_{GC}) + \cos(\delta_{cluster})\cos(\delta_{GC})\cos(\alpha_{cluster} - \alpha_{GC}) \qquad (2)$$

$$R_{GC} = \sqrt{R_{\odot}^2 + d^2 - 2R_{\odot}d\cos\theta} \qquad (3)$$

In each case, the galactocentric distances are in good agreement with those tabulated by van den Berg. All the clusters are in the inner halo, with the exception of M13 whose galactocentric radius places it slightly outside the assumed solar galactocentric radius.

Our first general comment is that it is not possible, with the results presented in this thesis, to distinguish between the two galactic formation scenarios outlined above, or others which have not been discussed [see for example Berman & Suchkov (1991)]. Taken at face value, these results could be used to support either a rapid Eggen *at al.*-type formation scenario which would require a small age dispersion between *all* clusters, or the more chaotic scenario favoured by Lee, which would require a chronology similar to that presented in his figure 6. More work, including deriving ages for many α-clusters and clusters in the galactic bulge, will need to be performed before this question is settled. Indeed, the derivation of accurate ages for metal-poor bulge clusters, which are expected to have formed *in situ* in the bulge [Harris (1990)] also offers the possibility of a direct observational attack on the second parameter problem; if they are not 1 to 1.5 Gyr older than the oldest halo clusters, then age as the second parameter can be ruled out. This in turn would have consequences for the galactic formation chronology of Lee (1992) who assumes that age is the second parameter. The ages will be best determined via infrared observations, since the optical extinction to many of these bulge clusters is $>\sim 1$ magnitude.

We shall discuss our results in the context of the chaotic galactic formation scenario outlined by Larson (1990), Lee (1992), and van den Berg (1993). It should be borne in mind, though, that the internal errors on our age determinations do not preclude variations in age between our clusters of ~2 Gyr.

Adopting the ages from column 2 of Table 2, we first note that the two inner halo β-clusters in our sample, M13 and NGC6752, are essentially coeval. This suggests that

recognisable structure existed within the inner halo of the galaxy at least as long ago as (14.1±1.4) Gyr. An estimate of the duration of the inner-halo formation is unfortunately precluded by the size of the errors. We note that this also lends some support to one necessary condition of the hypothesis that age is *a* second parameter - two clusters which do not exhibit the second parameter effect are essentially coeval.

We can conclude from the age and chemical abundance of 47 Tuc that protostellar material significantly enriched in heavy elements either co-existed with metal-poor protostellar material, or that the enrichment occurred over a period of ~2 Gyr. We also conclude that the galactic disk began to form within ~2 Gyr of the inner halo.

M30 does not fit into the $\alpha\beta\gamma$ classification scheme, since it is one of the clusters with [Fe/H]<-2 that van den Berg notes are found at all galactocentric radii. He suggests that such clusters formed in gas-rich subsystems - which he terms 'ancestral objects' - that subsequently merged into the galaxy or protogalaxy. Examination of the data in van den Berg's Table 1 shows some evidence for this; of the clusters with [Fe/H]<-2, excluding the two clusters with orbits that have been classified but are uncertain, three clusters have plunging orbits while only one has a circular orbit. Unfortunately, six clusters have unknown orbits, which could change the statistics completely if it were found that they all had circular orbits, say. From the age of M30 presented in column 2 of Table 2 we conclude that recognisable structure had formed in these outlying subsystems within ~2 Gyr of the formation of structure in the disk and inner halo.

1.4 A potential 'fly in the ointment' ?

Lee's (1992) chronology of the formation of the galaxy is based on two crucial relations for the galactic globular cluster system, namely the mean age versus metallicity relation, and the mean age versus galactocentric distance relation.

Mean age versus metallicity relation

Lee derives this relation by coupling the synthetic relation between [Fe/H] and the mean absolute visual magnitude of cluster RR Lyrae stars [equation 4 reproduced from Lee, 1990] with the fact that *in the mean* the V magnitude difference between the horizontal branch and the turn-off is constant and adopting a suitable calibration of the latter with age. For further details see the description in section 2 of Buonanno, Corsi & Fusi Pecci (1989). Note that care must be exercised here, since equation 4 refers to the *mean* level

$$\langle M_V(RR) \rangle = 0.19[Fe/H] + 0.97 \qquad (4)$$

of the RR Lyrae stars, and thus the horizontal branch, which will be brighter than the zero-age horizontal branch due to evolution.

The age versus metallicity relation derived from the value of $dM_V(HB)/d[Fe/H]$ in equation 4 predicts age variation of ~3 to 4 Gyr over the abundance range of the galactic globular cluster system, with the metal-rich clusters being younger. However, $dM_V(HB)/d[Fe/H]$ is probably *the* single most controversial parameter in the subject, and while the low value of ~0.2 agrees with the latest results from Baade-Wesselink analysis of field RR Lyrae stars, it is approximately half the value found by Sandage from analysis of his 'period shift effect' [see papers by Sandage, 1981, 1982, 1990, 1993, Sandage & Cacciari, 1990, Catelan, 1992 and references therein]. For an excellent review, and the possible reconciliation of the $M_V(HB)$ versus [Fe/H] relations found by various authors, see Carney, Storm & Jones (1992).

Mean age versus galactocentric distance relation

The horizontal-branch models are used to produce isochrones in the horizontal-branch type versus [Fe/H] plane. These are then used to investigate the radial variation of cluster ages, with the result - already outline above - that the inner-halo clusters are essentially coeval, the outer-halo clusters have age dispersions of several Gyr, and the bulge is older than the oldest halo objects by ~1 to 1.5 Gyr.

Both the mean age versus metallicity relation and the mean age versus galactocentric distance relation have been derived from models which do not assume an oxygen enhancement. In particular, the consequence of the oxygen enhancements assumed in the Bergbusch & VandenBerg isochrones is that the more metal-poor clusters have become much younger, as is illustrated by the discussion in the footnote to Table 2(a), such that there appears to be no correlation of age with metallicity.

In figure 1 we plot the ages of M13, M30, NGC6752 and 47 Tuc, derived by us, against the value of [Fe/H] of the isochrones used to derive the age. An age difference of a few Gyr such as that predicted by the horizontal-branch models is not inconsistent with the data. However, if future work confirms that these clusters are coeval, and reduces the error bars to the extent that an age difference of a few Gyr cannot exist, this would undermine the galactic formation scenario outline by Lee.

This renders crucial a concerted observational attack on the true variation of oxygen and other α-element abundances with [Fe/H] for population II stars, and a subsequent re-examination of the horizontal-branch models.

Figure 1: The age versus metallicity relation, with ages derived from (a) the original Bergbusch & VandenBerg models in Chapter 2, and (b) the new models in Chapter 4. The mean age is shown as a horizontal line across each figure.

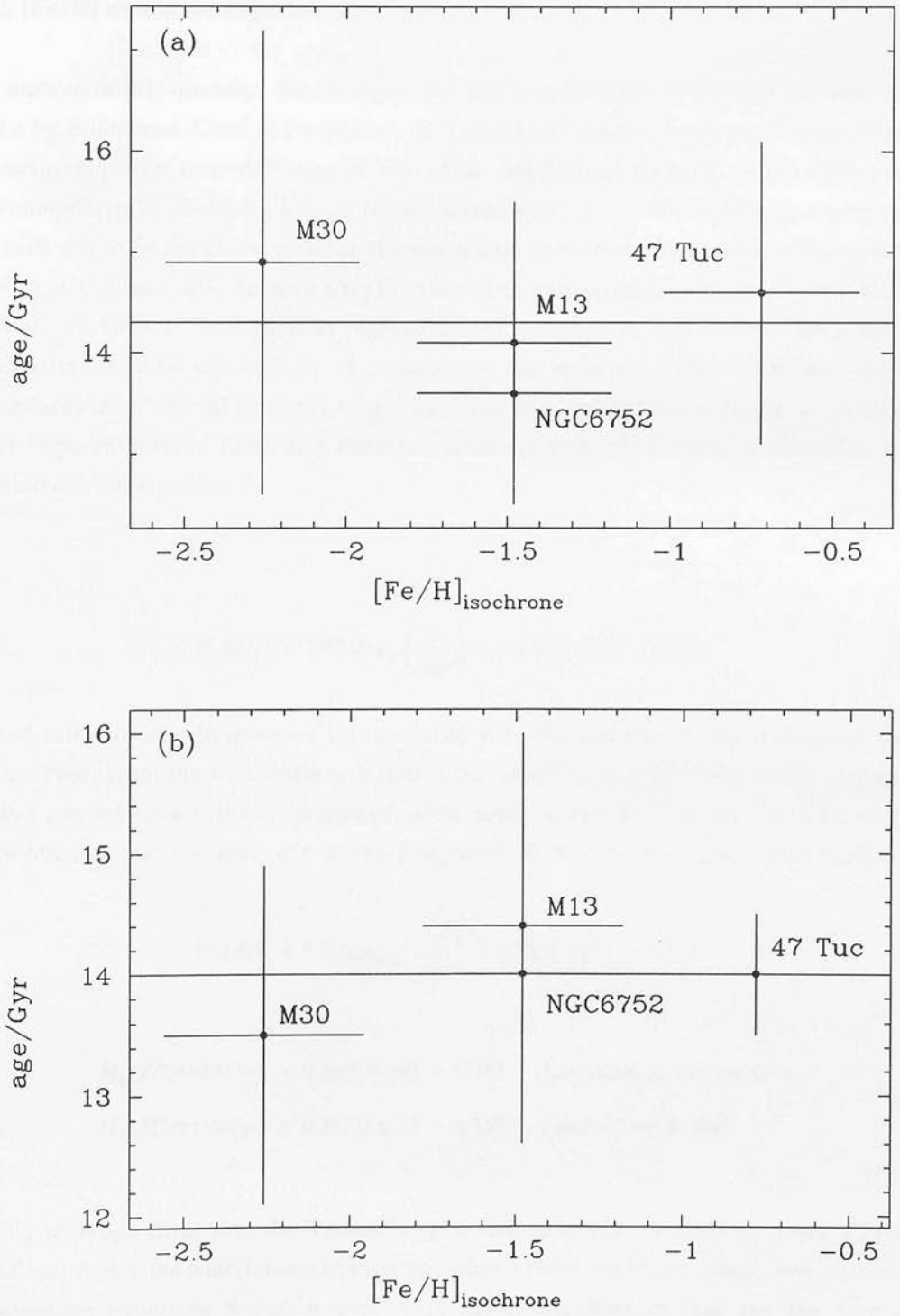

1.5 Consequences of coevolution for the M_V(HB) versus [Fe/H] relation

If the functionality of the oxygen enhancement assumed for the Bergbusch & VandenBerg isochrones is found to be applicable to globular cluster stars, what variation of M_V(HB) with [Fe/H] should we expect?

An answer to this question can be found by working backwards through the derivation given by Buonanno, Corsi & Fusi Pecci. In Table 3 we present the absolute magnitude of the main-sequence turn-off as a function of [Fe/H] derived from the original Bergbusch & VandenBerg V, (B-V) 12, 14 and 16 Gyr isochrones. As is conventional we have taken the turn-off to be the bluest point on the isochrone, and where the isochrone has a vertical section at the turn-off we have simply taken the average magnitude along that vertical section. A bilinear least squares regression was performed, and the resulting best-fit relation is given by equation 5. A measure of the accuracy with which this equation reproduces the observed turn-off magnitudes can be gleaned by examining the residuals, given in parentheses in Table 3, in the sense measured turn-off magnitude minus the value predicted from equation 5.

$$M_V(TO) = 2.401\log_{10}\left(\frac{\tau}{Gyr}\right) + 0.265[Fe/H] + 1.723 \qquad (5)$$

It is of some interest to compare this equation with the one derived by Buonanno, Corsi & Fusi Pecci from the VandenBerg & Bell (1985) isochrones, and given by their equation 4. For convenience this is reproduced, after some rearrangement, in equation 6. It is quite obvious that the turn-off of the Bergbusch & VandenBerg isochrones varies less

$$M_V(TO) = 2.703\log_{10}\left(\frac{\tau}{Gyr}\right) + 0.351[Fe/H] + 1.378 \qquad (6)$$

$$\begin{aligned} M_V(TO,\tau=15Gyr) &= 0.265[Fe/H] + 4.547 \quad \textit{Bergbusch \& VandenBerg} \\ M_V(TO,\tau=15Gyr) &= 0.351[Fe/H] + 4.557 \quad \textit{VandenBerg \& Bell} \end{aligned} \qquad (7)$$

rapidly with age than does the VandenBerg & Bell turn-off. Since Buonanno, Corsi & Fusi Pecci derive the coefficients in their equation 4 from the 15 Gyr isochrone, equations 7 reproduce equations 5 and 6 with τ=15 Gyr. At least at this age the turn-off magnitudes differ by ΔM_V(TO)=0.086[Fe/H]+0.01 in the sense VandenBerg & Bell minus Bergbusch & VandenBerg.

Table 3: The main-sequence turn-off absolute magnitude from the original Bergbusch & VandenBerg V, (B-V) isochrones. Numbers in parentheses are the residual values from equation 5 in the sense measured value minus equation 5 value.

[Fe/H]	M_V(TO)		
	12 Gyr	14 Gyr	16 Gyr
-0.65	4.15 (0.01)	4.30 (0.00)	4.45 (0.01)
-0.78	4.10 (-0.01)	4.25 (-0.02)	4.40 (-0.01)
-1.26	4.00 (0.02)	4.15 (0.01)	4.30 (0.02)
-1.48	3.95 (0.03)	4.05 (-0.03)	4.20 (-0.02)
-2.03	3.75 (-0.03)	3.95 (0.01)	4.10 (0.02)
-2.26	3.70 (-0.02)	3.90 (0.02)	4.00 (-0.02)

We now use the fact that Buonanno, Corsi & Fusi Pecci find the mean magnitude difference between the turn-off and the zero-age horizontal-branch at the RR Lyrae gap to be a constant, viz:

$$\Delta V_{TO}^{ZAHB} = 3.55 \pm 0.09 \qquad (8)$$

to derive the absolute magnitude of the zero-age horizontal branch as a function of age and [Fe/H]:

$$M_V(ZAHB) = 2.401 \log_{10}\left(\frac{\tau}{Gyr}\right) + 0.265[Fe/H] - 1.827 \qquad (9)$$

which for constant age implies $dM_V(ZAHB)/d[Fe/H]=0.265$. Equation 4 from Carney, Storm & Jones (1992), which is also reproduced here in equation 10 for convenience, suggests that the gradient of 0.265 should be reduced by 0.05 if comparison is to be made

$$\langle V(HB) \rangle = V(ZAHB) - 0.05[Fe/H] - 0.20 \qquad (10)$$

with the mean level of the horizontal branch, such as $\langle M_V(RR) \rangle$ calculated by Lee and reproduced in equation 4. This value of $dM_V(ZAHB)/d[Fe/H] \sim 0.22$ resulting from the oxygen enhanced isochrones, and assuming no dependence of cluster age with [Fe/H], is still in excellent agreement with the Baade-Wesselink results.

It is interesting to subdivide the clusters from which Buonanno, Corsi & Fusi Pecci derive the turn-off to horizontal-branch magnitude difference (their Table 3) and look at the values solely on the basis of $\alpha\beta\gamma$ class. In Table 4 we present such a determination, where

the results presented in the class 'other' are for the clusters with [Fe/H]<-2 in Table 1 of van den Bergh (1993), although it is probably not correct to include these in a single class just because they fail to fall into any other class. In particular, the value of the turn-off to horizontal-branch magnitude difference for M30 is 3.53±0.14, in excellent agreement with the mean value from equation 8.

Clearly there is a difference, with the α-clusters having a significantly smaller turn-off to horizontal-branch V magnitude difference than either the β or γ-clusters. The values for the β and γ-clusters are in very good agreement with the average presented in equation 8.

We have also performed linear regressions to look for correlations of the turn-off to horizontal-branch V magnitude difference with [Fe/H], the latter again being taken from van den Bergh. Since there are errors on both the metallicity and the magnitude difference, we have adopted the usual method and taken the bisector of the x-on-y and y-on-x regression lines to be the best fit line through the data. Only for the 'other' clusters was a significant correlation found, while the correlation was marginal for the α-clusters, as can be seen from equations 11.

$$\begin{aligned} \Delta V_{TO}^{ZAHB} &= (-0.43\pm0.38)[Fe/H] + (2.84\pm2.36) \quad \alpha\text{-clusters} \\ \Delta V_{TO}^{ZAHB} &= (-2.09\pm0.74)[Fe/H] - (0.96\pm1.40) \quad others \end{aligned} \tag{11}$$

However, a much larger sample size is needed before either the zero-point or the coefficient of [Fe/H] can be usefully altered in equation 9 on the basis of the $\alpha\beta\gamma$ classification.

Equation 9 allows us to calculate the absolute magnitudes of the (zero-age) horizontal branches of the four clusters with which this thesis is concerned, given their ages and chemical compositions. These can then be compared with the values derived from the apparent magnitudes of the (zero-age) horizontal branches and the distance moduli from subdwarf fitting. Such a comparison is presented in Table 5.

The second column of this table presents the absolute visual magnitude of the zero-age horizontal branch determined for each cluster from equation 9. The corrections from Table 22 of Chapter 2, which bring the absolute magnitudes of the isochrones onto the system defined by the subdwarfs have also been introduced, which is why the magnitudes in column 2 depend upon the Lutz-Kelker corrections, and so differ between parts (a) and (b) of the table. Since equation 9 was derived from the original Bergbusch & VandenBerg isochrones, the appropriate ages to choose are those derived from these isochrones in

Table 4: The mean V magnitude difference between the horizontal branch and turn off with clusters grouped into classes α, β or γ. The 'other' class consists of those clusters with [Fe/H]<-2 which van den Bergh notes do not fit the αβγ classification scheme.

Class	Sample size	ΔV_{TO}^{ZAHB}	standard deviation
α	4	3.46±0.06	0.05
β	6	3.60±0.06	0.04
γ	1	3.65±0.18	-
others	3	3.49±0.08	0.07

Chapter 2.

We have taken the apparent visual magnitudes of the zero-age horizontal branches from Buonanno, Corsi & Fusi Pecci. Since none of the four clusters has a horizontal branch which is populated on both sides of the RR Lyrae gap, they derive M_V(ZAHB) by superimposing colour-magnitude diagrams of clusters with well-populated horizontal branches. As can be seen from inspection of parts (a) and (b) of Table 5, the absolute magnitudes of the zero-age horizontal branch derived from the apparent visual magnitudes and the subdwarf distance moduli agree with those calculated from equation 9, whether Lutz-Kelker corrections are included or not, lending support to the predicted horizontal branch magnitude versus metallicity relation presented in equation 9.

1.6 Further constraints on the M13 distance via the horizontal branch - the RR Lyrae $\log_{10}$(period) versus mean K magnitude relation

The discovery of a relation between the fundamental pulsation period of an RR Lyrae variable star and the mean K(2.2μm) magnitude [Longmore, Fernley & Jameson (1986)] together with the calibration of such a relation [Longmore *et al.* (1990), Cacciari, Clementini & Fernley (1992), see also Carney, Storm & Jones (1992)] has offered an exciting opportunity to use these stars as standard candles in the determination of globular cluster distances. Indeed, in the latter paper, Longmore & co-workers presented determinations of the relation in 8 clusters, namely M3, M4, M5, M15, M107, NGC3201, NGC5466 and ω Cen.

Two of the clusters in particular - M3 and ω Cen - have extremely well determined relations, defined by ~8 observations star^{-1} of 49 and 28 variables. In each case the scatter from the best fit relation is only ~0.03 magnitudes, and there is no evidence that this is caused by other than observational error [see Buckley, Longmore & Dixon (1992)]. The observed gradients of the relation also agree within the errors, with the value of $M_K(RR) \propto -2.22 \log_{10}(P/\text{days})$ expected theoretically. Thus by reference to a fixed period, taken by Longmore *et al.* as $\log_{10}(P/\text{days}) = -0.3$, extremely accurate distances can be derived from this relation.

Other advantages of the method are:

- The RR Lyrae mean K magnitudes can be determined almost independently of extinction, since $A_K \sim 0.1 A_V$.

- Based on the scatter about the known relation, which is ~0.03 magnitudes, distances can be determined with much less uncertainty than is introduced by the Lutz-Kelker corrections, for example. Examination of Table 5 of Longmore *et al.* shows that the distance moduli determined from the relation agree well with the distances to M5 and M15 from subdwarfs without Lutz-Kelker corrections.

- The $\log_{10}(P/\text{days})$ versus mean K relation of ω Cen is extremely tight, even though the variables exhibit a large metallicity range, leading to the conclusion that the relation is insensitive to metallicity.

- The $\log_{10}(P/\text{days})$ versus mean K relation is expected, theoretically, to be insensitive to the evolutionary status of the variables. This is seen in figure 4 of Buckley, Longmore & Dixon, which shows a synthetic $\log_{10}(P/\text{days})$ versus mean K relation generated from the horizontal branch models of Lee & Demarque (1990). This figure shows that evolution is expected to affect distances derived from the relation by less than ~10% [see also the discussion following Buckley *et al.*]. There is some observational support for this, as can be seen by plotting the V height above the zero-age horizontal branch of M3 variables against residuals from the $\log_{10}(P/\text{days})$ versus mean K relation. Such a plot can be found in figure 3 of Buckley *et al.* While evolution has carried the variables 0.05 to 0.15 magnitudes above the zero-age horizontal branch in V, they are only ~0.05 K magnitudes bright of the $\log_{10}(P/\text{days})$ versus mean K relation.

As a preliminary study, we have obtained observations of the three known RR Lyrae stars in M13, via the United Kingdom Infrared Telescope service program. Since RR Lyrae lightcurves are more sinusoidal and have smaller amplitudes in the infrared than their

Table 5: Comparison between the absolute horizontal-branch magnitudes derived from equation 9 with those from the distance moduli derived in Chapter 2 with (a) no Lutz-Kelker corrections, and (b) full Lutz-Kelker corrections.

(a) No Lutz-Kelker corrections

Cluster	M_V(ZAHB) equation 9	V_{ZAHB} Buonanno *et al.*	$(m-M)_0$	M_V(ZAHB)
M30	0.42	15.20±0.10	14.54±0.11	0.44±0.15
M13	0.54	14.95±0.15	14.27±0.15	0.62±0.21
NGC6752	0.50	13.75±0.15	13.02±0.12	0.61±0.19
47 Tuc	0.83	14.10±0.15	13.19±0.13	0.79±0.20

(b) Full Lutz-Kelker corrections

Cluster	M_V(ZAHB) equation 9	V_{ZAHB} Buonanno *et al.*	$(m-M)_0$	M_V(ZAHB)
M30	0.29	15.20±0.10	14.68±0.12	0.30±0.16
M13	0.42	14.95±0.15	14.44±0.15	0.49±0.21
NGC6752	0.38	13.75±0.15	13.14±0.16	0.49±0.22
47 Tuc	0.72	14.10±0.15	13.30±0.11	0.68±0.19

optical counterparts, an accurate mean K magnitude can be determined from just two observations separated by half a pulsation period - or, indeed, any odd number of half pulsation periods, making this type of preliminary study easily amenable to service mode observing.

The two variables V5 and V9, which are short period c-type first overtone pulsators, form a close pair with a separation of ~2.5 arcseconds. We therefore obtained IRCAM images at 0.3 arcseconds pixel^{-1} scale separated by half of the pulsation period. The observations of the other variable V8, which is an a-type fundamental mode variable, were separated by 9.5 periods.

Weather conditions were non-photometric during some of the observing, which necessitated the use of non-variable stars on each frame to provide the calibrations. For

this reason, and because the mean magnitude is derived from only two phases in each case, these results must remain preliminary until more observations can be made.

Table 6(a) summarises the parameters of the variables and presents the mean K magnitudes determined from these observations. The periods are taken from Pike & Meston (1977). We also present the absolute K magnitudes determined from the calibrated $\log_{10}$(period) versus mean K magnitude relation given by Longmore (1993) and reproduced in equation 12. P_f denotes the fundamental pulsation period; for the c-type variables which pulsate in the first overtone, the pulsation period has been 'fundamentalised' by adding 0.127 to $\log_{10}$(period) [Iben, 1974].

$$M_K = -2.38\log_{10}\left(\frac{P_f}{days}\right) + 0.04[Fe/H] - 0.88 \qquad (12)$$

In Table 6(b) we compare this value of M_K with the values calculated from the apparent mean K magnitudes and the subdwarf-determined distances both with and without Lutz-Kelker corrections. The final column tabulates the distance modulus derived from the apparent mean magnitudes and the absolute magnitudes from equation 12. It is immediately obvious that only for the a-type V8 is there good agreement between the absolute magnitudes from equation 12 and from the subdwarf distance, at least without Lutz-Kelker corrections. The c-type variables are more than 10% brighter than is predicted by the subdwarfs without Lutz-Kelker corrections, and the discrepancy is increased if we adopt full Lutz-Kelker corrections. On the other hand, if we use the distance of $(m-M)_0$=14.07 derived for M13 by Leonard, Richer & Fahlman (1992) from velocity dispersion measurements, there would be much better agreement between the predicted and observed values of M_K for the c-types.

It is well known that these variables are peculiar, with periods and colours at the extreme ends of the ranges encountered in other clusters. See references within Richer & Fahlman (1986) and see also Sandage (1970), although the more recent optical photometry of Pike & Meston apparently resolves the problem of the anomalous magnitude of one of the variables mentioned therein. The period distribution of RR Lyrae stars in globular clusters can be found in figure 2 of Sawyer-Hogg (1973).

One explanation for the peculiarity could be that these variables are evolved, rather than zero-age, RR Lyrae stars. However, one would expect from figure 4 of Buckley *et al.* that evolution would cause the a-type variable to deviate most from the $\log_{10}$(period) versus mean K relation, rather than the c-type, contrary to our findings here. We know, however, what the visual level of the zero-age horizontal branch should be in M13, since we calculated it from equation 9 and it is tabulated in Table 5. We found that with no

Table 6: The mean K magnitudes of the M13 RR Lyrae variables and the distances determined from the $\log_{10}$(period) versus mean K magnitude relation. M_V in (c) is from $\langle V\rangle - \langle K\rangle$ in (a) and M_K in (b).

(a)

Variable	Type	Period/days	$\langle K\rangle$	$\langle V\rangle - \langle K\rangle$	M_K equation 12
V5	c	0.3817240	13.869	0.81	-0.243
V8	a	0.7503750	13.613	1.30	-0.639
V9	c	0.3926066	13.876	0.90	-0.272

(b)

Variable	M_K			$(m-M)_0$
	equation 12	Subdwarfs without Lutz-Kelker corrections	Subdwarfs with Full Lutz-Kelker corrections	
V5	-0.243	-0.408	-0.578	14.104
V8	-0.639	-0.665	-0.835	14.245
V9	-0.272	-0.402	-0.572	14.140

(c)

Variable	M_V	
	No Lutz-Kelker corrections	Full Lutz-Kelker corrections
V5	0.402	0.232
V8	0.635	0.465
V9	0.498	0.328

Lutz-Kelker corrections $M_V(ZAHB)=0.54$ while this becomes 0.42 with full Lutz-Kelker corrections. The observed values of M_V for each variable are given in Table 6(c), and were calculated from the $<V>-<K>$ colours in Table 6(a) and the subdwarf-determined values of M_K in Table 6(b). Note that in the case of no Lutz-Kelker corrections, only the c-type V9 is near to the zero-age horizontal branch - in fact ~0.04 magnitudes above - while the other c-type is ~0.14 magnitudes brighter than the zero-age level. The a-type V8 is actually *fainter* than the zero-age level, which is unphysical. With full Lutz-Kelker corrections it is V8 that is close to the zero-age level while the c-types are much brighter, as expected from figure 4 of Buckley *et al.*

Clearly, further study of these variables and the possible effects of evolution on the $\log_{10}$(period) versus mean K magnitude relation is called for.

2 SUGGESTIONS FOR FUTURE WORK

2.1 Serendipitous discoveries

An object has been discovered, which appears on all four of the infrared mosaics of NGC6752 field 5 but is not visible on the optical finding chart of Penny & Dickens (1986). This object is marked on the finding charts in Appendix A and labelled MO1 (mysterious object number 1!). Such very red objects are interesting as they may be potential brown-dwarf candidates. The K and K' magnitudes determined for MO1 are reported in Table 7, as are the weights used to combine the photometry from these four nights. The difference of ~0.11 to 0.12 magnitudes between the K magnitudes from the 5/6 May 1991 and the other nights is slightly larger than the scatter expected from figure 3(b) of Chapter 1.

Following our previous methodology we determine $<K>=16.315$ using the weights from Table 7, although without a V magnitude it is impossible to include the result from 17/18 April 1992. The weighted combined error of ±0.02 magnitudes is probably too low, given that the unweighted standard deviation is ±0.05 magnitudes.

It is difficult to place limits on the colour of this object. The faintest object photometered by Penny & Dickens in field 5 has V=19, although the frame goes deeper. Thus only the modest limit that $(V-K)>\sim2.7$ can be set. From $<K>-K'=-0.228$ and the calibration of (K-K') with (H-K) given by Wainscoat & Cowie, used in Chapter 1 to set the K' magnitudes of the standards, we find that $(H-K)\sim1$. The calibration of (K-K') with (H-K) should probably not be used for $(H-K)>\sim0.4$ though.

When comparing our NGC6752 field 3 observations with the measurements by Penny &

Table 7: Photometry of MO1 from the NGC6752 field 5 mosaics.

UT Date	Magnitude	Weight
4/5 May 1991	K = 16.350±0.035	4
5/6 May 1991	K = 16.230±0.025	2
16/17 April 1992	K = 16.343±0.035	1
17/18 April 1992	K' = 16.543±0.025	2

Dickens, we found that their star number 25 [V=17.25, (B-V)=-0.24] has no matching counterpart on our infrared mosaic. In figure 2 we show a plot of DAOPHOT error versus K' magnitude from the 19/20 April field 3 mosaic which should contain star 25. The limiting K' magnitude, after filtering to remove objects with too large errors for their magnitudes, is K'~18.4. From this we are able to set the limit that (V-K')<-1.15. This star is obviously one of the two very blue stars which are at the level of the turn-off in figure 3 of Penny & Dickens, and bluer than the group of stars which define the horizontal branch.

A systematic search for other anomalous objects in all the fields for which we have infrared images is currently underway.

2.2 Other suggestions

Some other suggestions which have already been mentioned during the course of this thesis are briefly reiterated here.

- Accurate photometry, chemical compositions and parallaxes for a large sample of metal-poor field dwarf stars for matching with globular cluster main-sequences

- Accurate abundance determinations for globular clusters stars, in particular for oxygen and the other α-process elements

- Interferometric angular diameters, parallaxes and flux distributions of field stars covering a range of chemical abundances, and with sufficient accuracy to check the normalisation of model atmosphere temperature scales (see Chapter 3)

Figure 2: DAOPHOT error versus K' magnitude of data from the 19/20 April 1992 NGC6752 field 3 mosaic which should contain star 25.

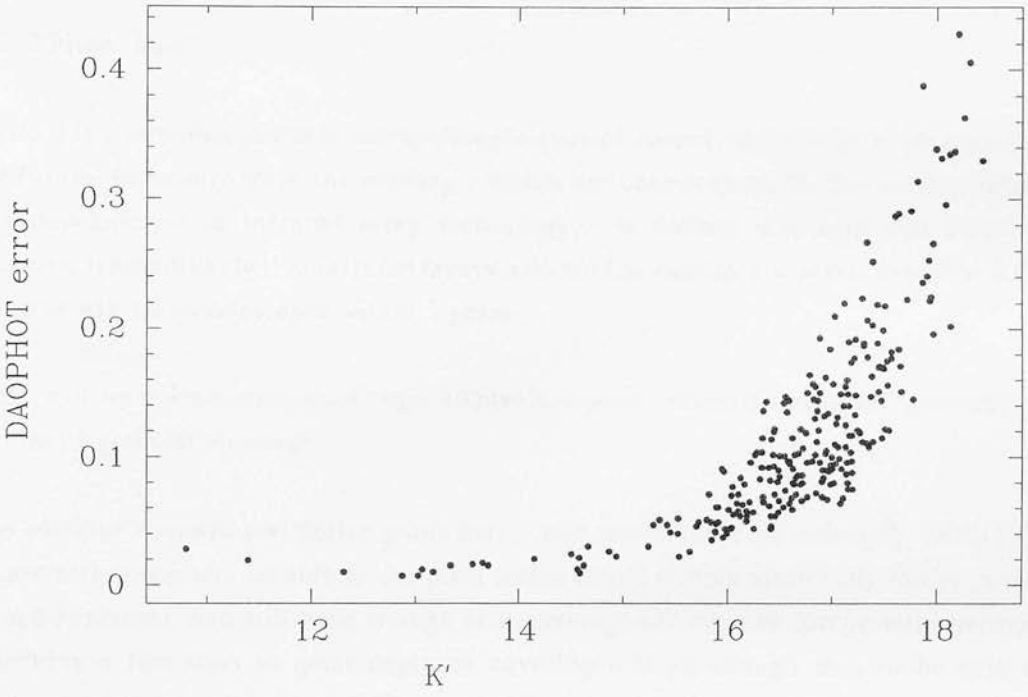

Other suggestions, more specific to this thesis are outlined below.

- The optical CCD frames used by Penny & Dickens in their optical CCD study of NGC6752 contain many more images than were photometered, particularly in field 3. A re-reduction of this data to extract all the photometric information and match it with our infrared data would be useful.

- More infrared data of NGC6752 stars should be obtained to ensure that the problem with the detector which produced the striping effect in some of our data, and our efforts to remove the stripes, have not seriously affected the photometric results.

- An independent check on the photometric zero-points applied to our photometry should be obtained. Mighell & Harrison, who made some of the 47 Tuc observations used in this thesis have also obtained aperture photometry of stars in each field, although to the best of our knowledge this has not yet been reduced.

- In a similar vein, accurate V photometry of many of the IRIS infrared standards is not yet available, meaning that the transformation from K' to K as a function of (V-K') used in Chapter 1 was derived from only 5 standard stars. This transformation should be re-examined, using standards covering a large range of

colours.

2.3 Whither now?

While it is always dangerous to extrapolate the pace of current technological advance into the future, especially when the military - which has been responsible for much research and development in infrared array technology - is feeling post cold-war financial pressure, it seems likely that infrared arrays with similar numbers of pixels to optical CCD cameras will be on telescopes within 5 years.

What will be the advantages of, say, 1024x1024 pixel infrared arrays for photometric studies of globular clusters?

The obvious answers are 'better photometry' and 'more time for science'! With 1024 square arrays one will be able to use pixel scales which sample more fully stellar point-spread functions, and still have enough area coverage not have to compromise between observing a few stars to great depth or covering a large enough area to be sure of photometering enough stars to define - to a lesser depth - the principle sequences of the colour-magnitude diagram. The necessity for mosaicing will be removed, and with it the uncertainties both in the relative zero-points between mosaics and those caused by seeing variations. Producing mosaics from infrared array data is a time-consuming task, and removing the necessity to do this will provide more time for science.

It will then be possible to easily achieve equivalent photometric accuracy to current optical studies. This is needed to realise the many advantages of the long wavelength baseline of (V-K), such as the derivation of more accurate ages, distances and reddenings. These improvements in accuracy are vitally important when looking for, say, the age differences of 1 to 1.5 Gyr between halo and bulge clusters which would confirm or refute age as the second parameter.

The increase in integration time per star will allow photometry to be extended much further down the main sequence, possibly as far as the hydrogen-burning limit in the closest clusters. That limit has important consequences for stellar theory by defining the lower mass limit for stars.

Are there brown dwarfs in globular clusters? The answer to this also needs deep infrared photometry.

The large area will enable deep main-sequence luminosity functions to be derived, which as we said in the introduction, is the first step to the mass function and hence to an

understanding of low-mass star formation in the early universe.

The possibility of future exciting science in the field of globular cluster studies seems assured.

REFERENCES

Armandroff, T.E., 1989. Astron. J. **97,** 375.

Berman, B.G. & Suchkov, A.A., 1991. *Astrophys. Space Sci.* **184,** 169.

Buckley, D.R.V., Longmore, A.J. & Dixon, R.I., 1992. In *New Results on Standard Candles.* F. Caputo, editor. *Mem. Soc. Astron. Ital.* **63,** 433.

Buonanno, R., Corsi, C.E. & Fusi Pecci, F., 1989. *Astron. Astrophys.* **216,** 80.

Cacciari, C., Clementini, G. & Fernley, J.A., 1992. *Astrophys. J.* **396,** 219.

Carney, B.W., Storm, J. & Jones, R.V., 1992. *Astrophys. J.* **386,** 663.

Catelan, M., 1992. *Astron. Astrophys.* **261,** 457.

Duffet-Smith, P., 1988. In *Practical Astronomy with your Calculator* (third edition). Cambridge University Press. Page 51.

Eggen, O.J., Lynden-Bell, D. & Sandage, A., 1962. *Astrophys. J.* **136,** 748.

Fernley, J.A., 1992. In *New Results on Standard Candles.* F. Caputo, editor. *Mem. Soc. Astron. Ital.* **63,** 453.

Fredrick, L.W., 1989. In *A Physicist's Desk Reference.* Physics Vade Mecum (second edition). H.L. Anderson, editor in chief. American Institute of Physics, New York. Section 3.03.

Harris, W.E., 1990. In *Proceedings of the ESO/CTIO Workshop on Bulges of Galaxies.* ESO Conference and Workshop Proceedings Number 35. B.J. Jarvis and D.M. Terndrup, editors. Page 153.

Hesser, J.E., Harris, W.E., VandenBerg, D.A., Allwright, J.W.B., Shott, P. & Stetson, P.B., 1987. *Publs astr. Soc. Pacif.* **99,** 739.

Iben, I., 1974. *Ann. Rev. Astron. Astrophys.* **12,** 215.

Larson, R.B., 1990. *Publs astr. Soc. Pacif.* **102,** 709.

Lee, Y-W. & Demarque, P., 1990. *Astrophys. J. Suppl.* **73,** 709.

Lee, Y-W., Demarque, P. & Zinn, R., 1987. In *The Second Conference on Faint Blue Stars.* International Astronomical Union Colloquium Number 95. A.G.D. Philip, D.S. Hayes and J.W. Liebert, editors. Page 137.

Lee, Y-W., 1990. *Astrophys. J.* **363,** 159.

Lee, Y-W., 1992. *Publs astr. Soc. Pacif.* **104,** 798.

Leonard, P.J.T., Richer, H.B. & Fahlman, G.G., 1992. *Astron. J.* **104,** 2104.

Longmore, A.J., Dixon, R.I. & Buckley, D.R.V., 1990. In *Confrontation Between Stellar Pulsation and Evolution.* Astronomical Society of the Pacific Conference Series,

volume 11. C. Cacciari and G. Clementini, editors. Page 36.

Longmore, A.J., Dixon, R.I., Skillen, I., Jameson, R.F. & Fernley, J.A., 1990. *Mon. Not. Roy. astr. Soc.* **247,** 684.

Longmore, A.J., Fernley, J.A. & Jameson, R.F., 1986. *Mon. Not. Roy. astr. Soc.* **220,** 279.

Longmore, A.J., 1993. Astronomical Society of the Pacific Conference Series, in press.

Penny, A.J. & Dickens, R.J., 1986. *Mon. Not. Roy. astr. Soc.* **220,** 845.

Pike, C.D. & Meston, C.J., 1977. *Mon. Not. Roy. astr. Soc.* **180,** 613.

Richer, H.B. & Fahlman, G.G., 1986. *Astrophys. J.* **304,** 273.

Richer, H.B., Fahlman, G.G. & VandenBerg, D.A., 1988. *Astrophys. J.* **329,**

Sandage, A., 1970. *Astrophys. J.* **162,** 841.

Sandage, A., 1981. *Astrophys. J.* **248,** 161.

Sandage, A., 1982. *Astrophys. J.* **252,** 553.

Sandage, A., 1990. *Astrophys. J.* **350,** 631.

Sandage, A., 1993. *Astron J.* **106,** 719.

Sandage, A. & Cacciari, C., 1990. *Astrophys. J.* **350,** 645.

Sawyer-Hogg, H., 1973. The Third Catalogue of Variable Stars in Globular Clusters. *Publs David Dunlop Obs.* **3,** number 6.

Searle, L. & Zinn, R., 1978. *Astrophys. J.* **225,** 357.

VandenBerg, D.A., 1985. In *ESO Workshop on the Production and Distribution of CNO Elements.* I.J. Danziger, F. Matteucci and K. Kjär, editors. page 73.

VandenBerg, D.A. & Bell, R.A., 1985. *Astrophys. J. Suppl.* **58,** 561.

van den Berg, S., 1993. *Astrophys. J.* **411,** 178.

Appendix A

Finding Charts

In this appendix we present finding charts for each of the fields with infrared photometry. A rough scale is marked on each. In two cases these finding charts are of images which did not produce the photometry presented in this thesis. The NGC6752 field 3 image was split into two to take account of seeing variations. The Western extension of the 47 Tuc field F1 position 2 K' mosaic from 19/20 September 1991 was non-photometric, and was discarded.

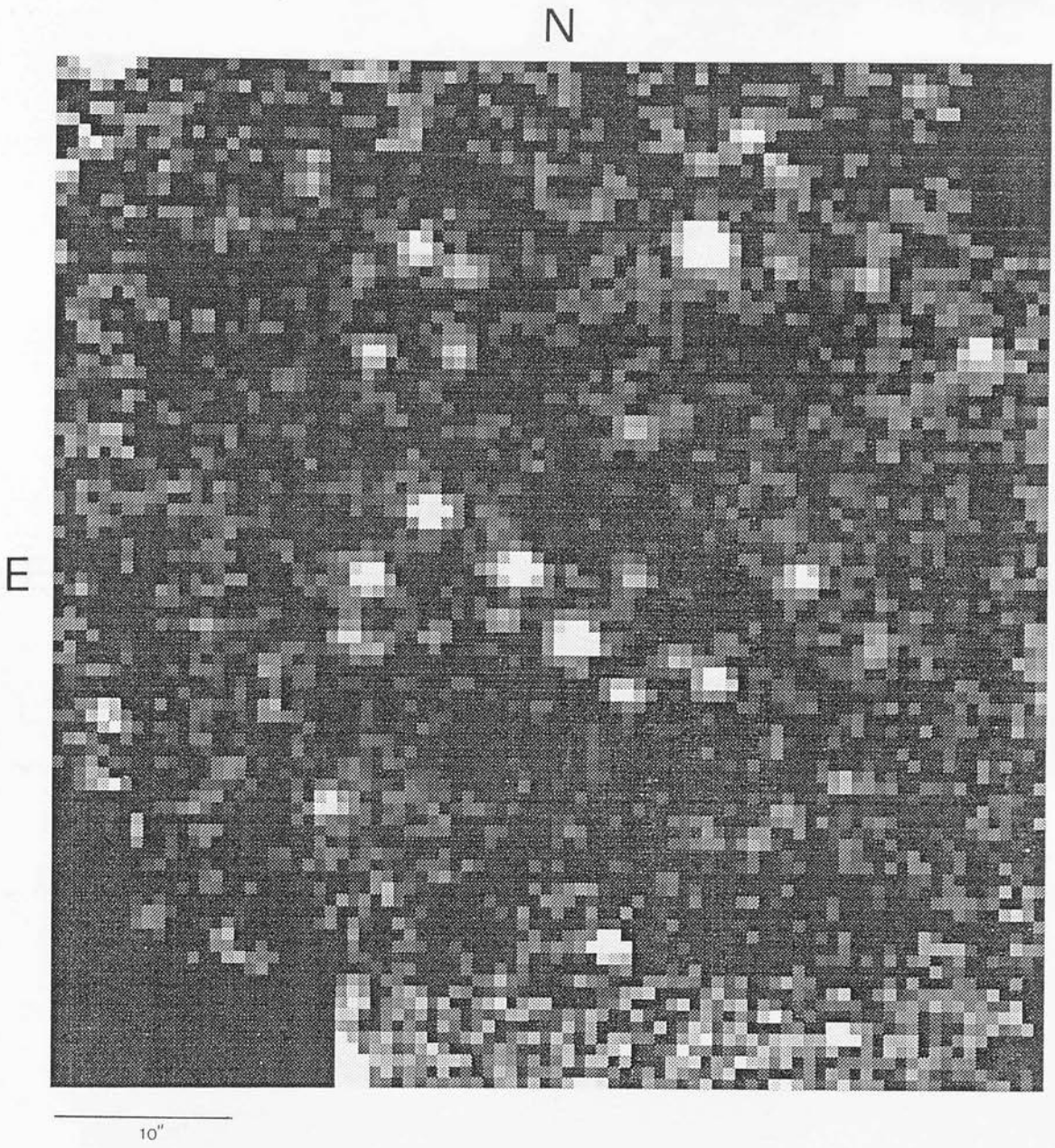

M13 - 10/11 June 1990

N

E

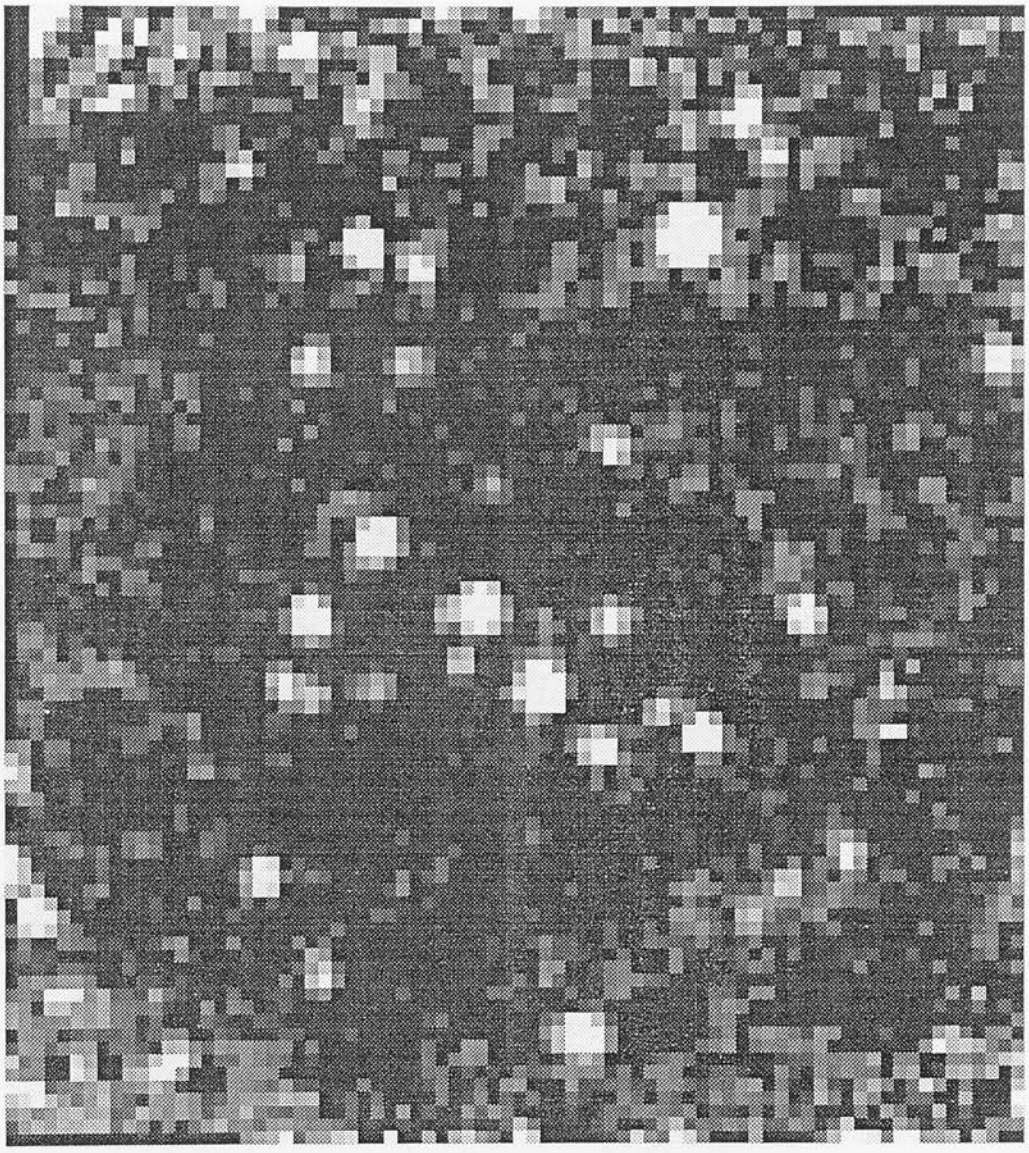

10″

M13 - 16/17 JUNE 1990

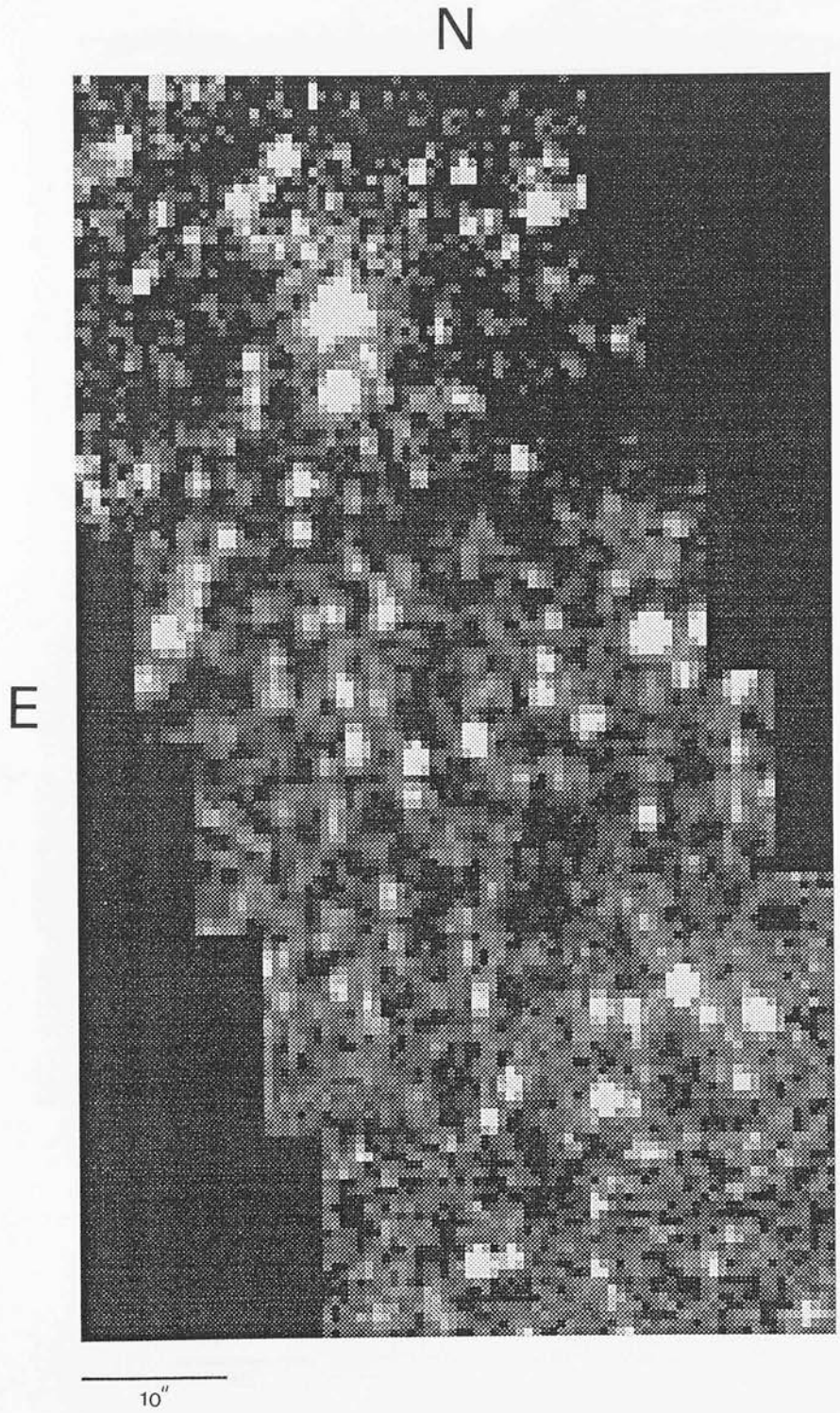

M30 - 10/11 June 1990

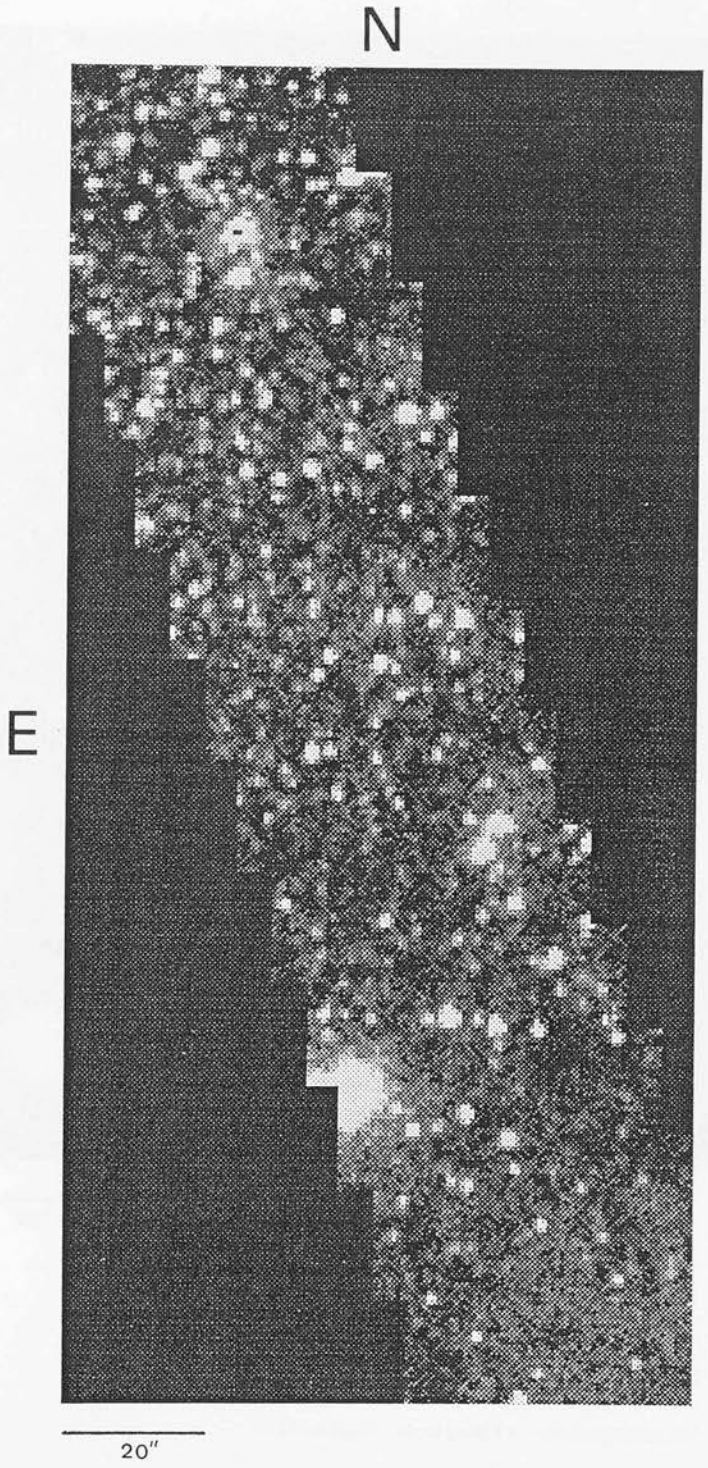

M30 - 16/17 June 1990

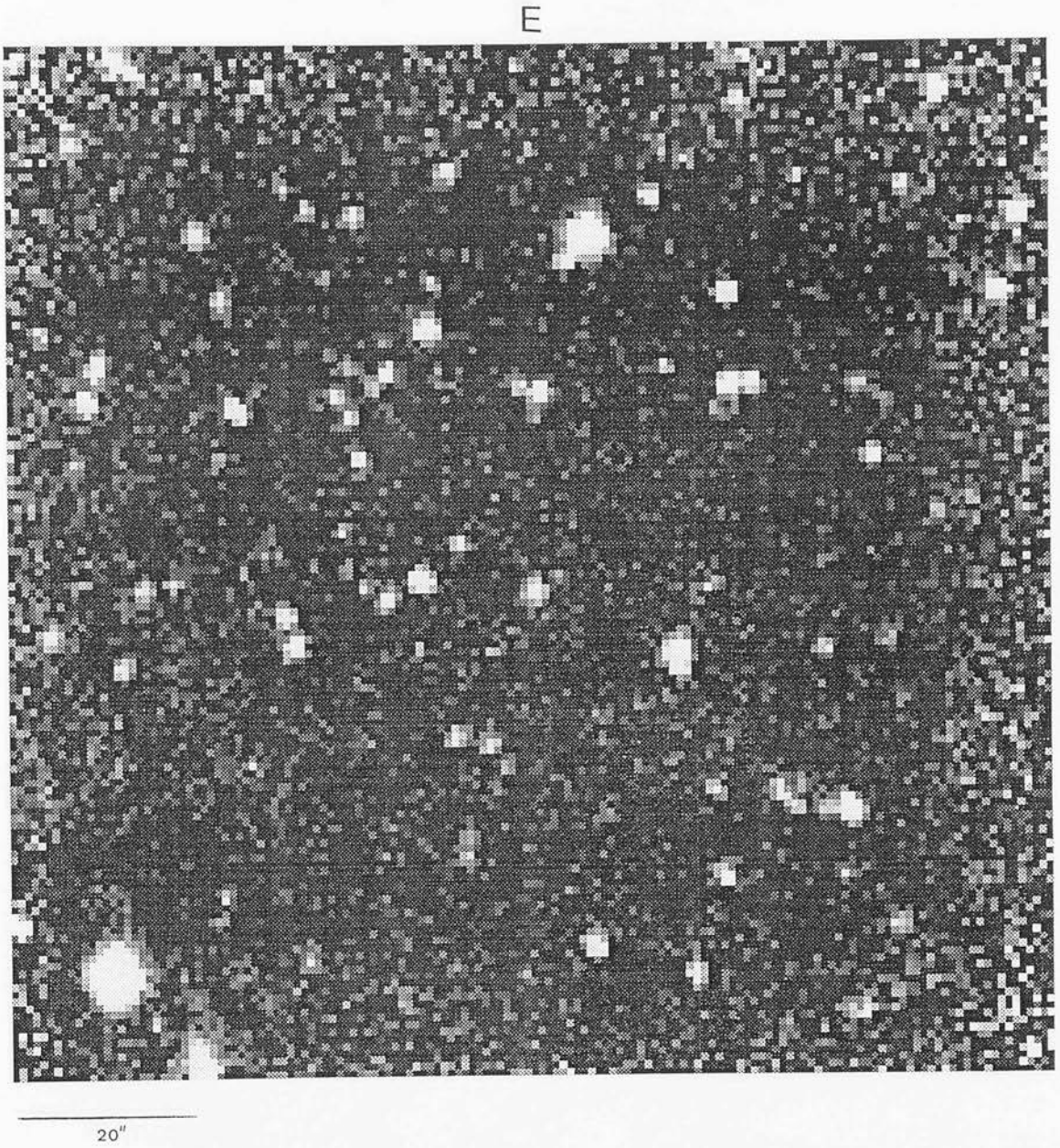

47 Tuc Field F1 central position K' - 19/20 September 1991

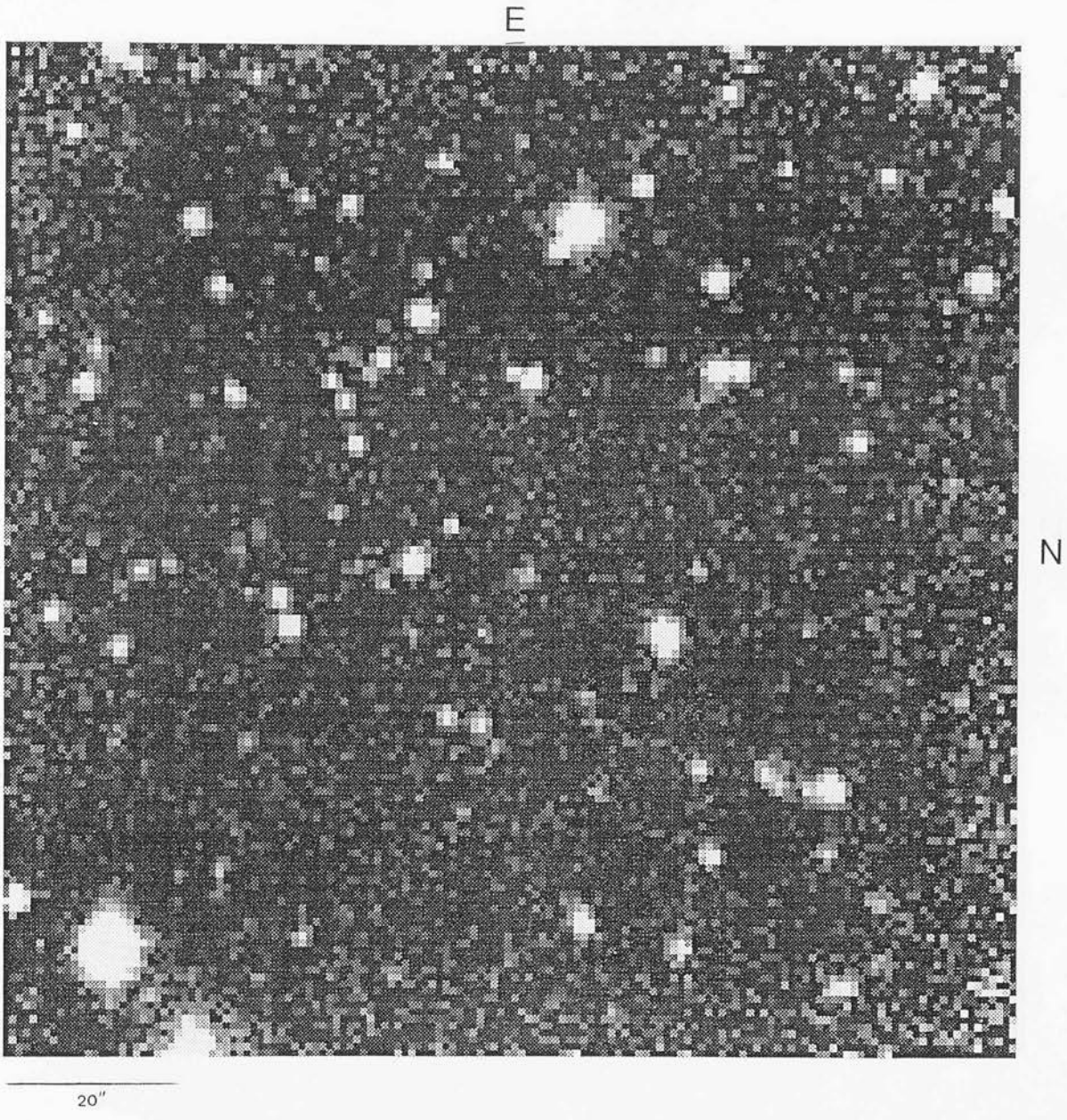

47 Tuc Field F1 central position J - 19/20 September 1991

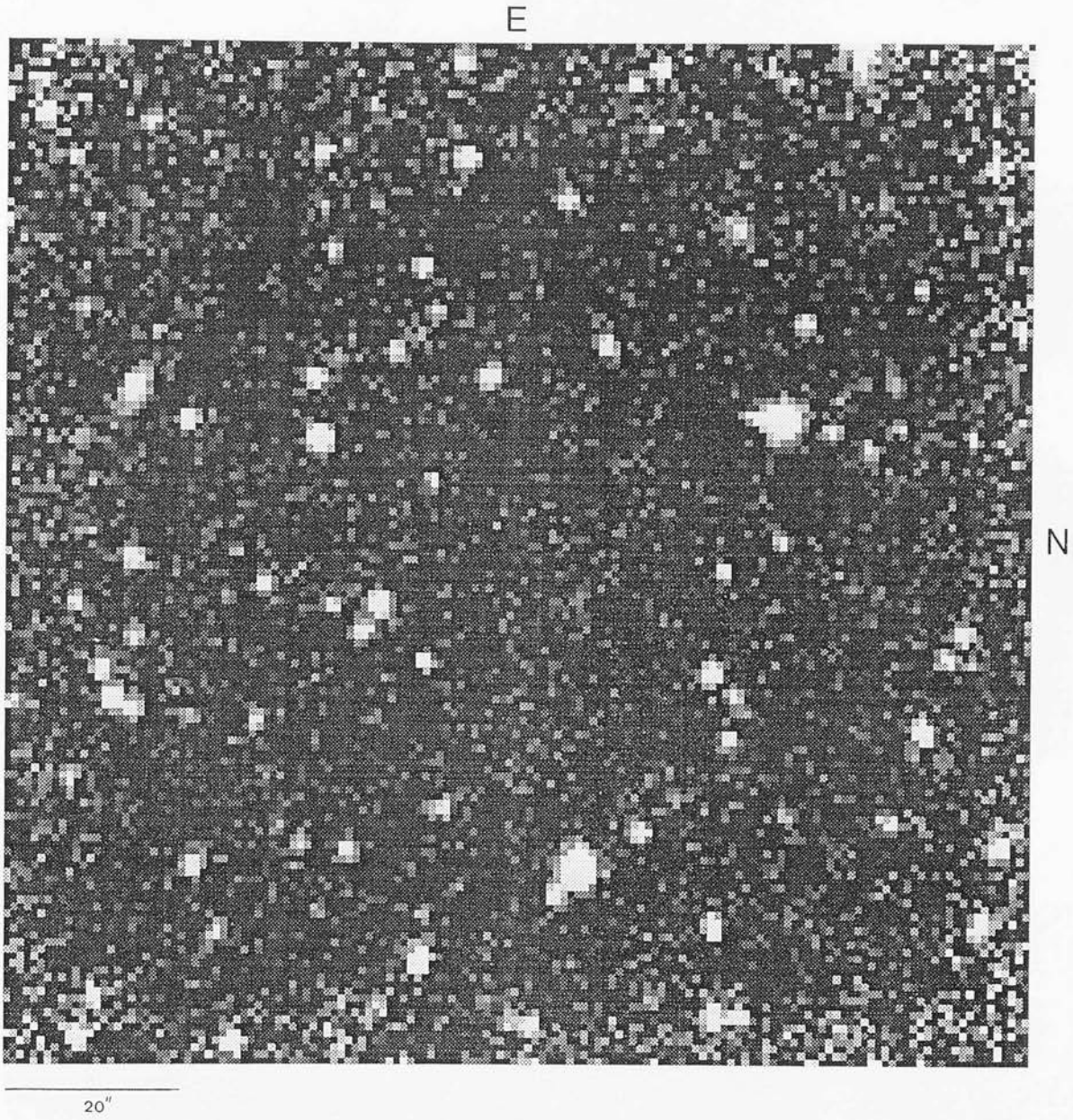

47 Tuc Field F1 position 1 K' - 20/21 September 1991

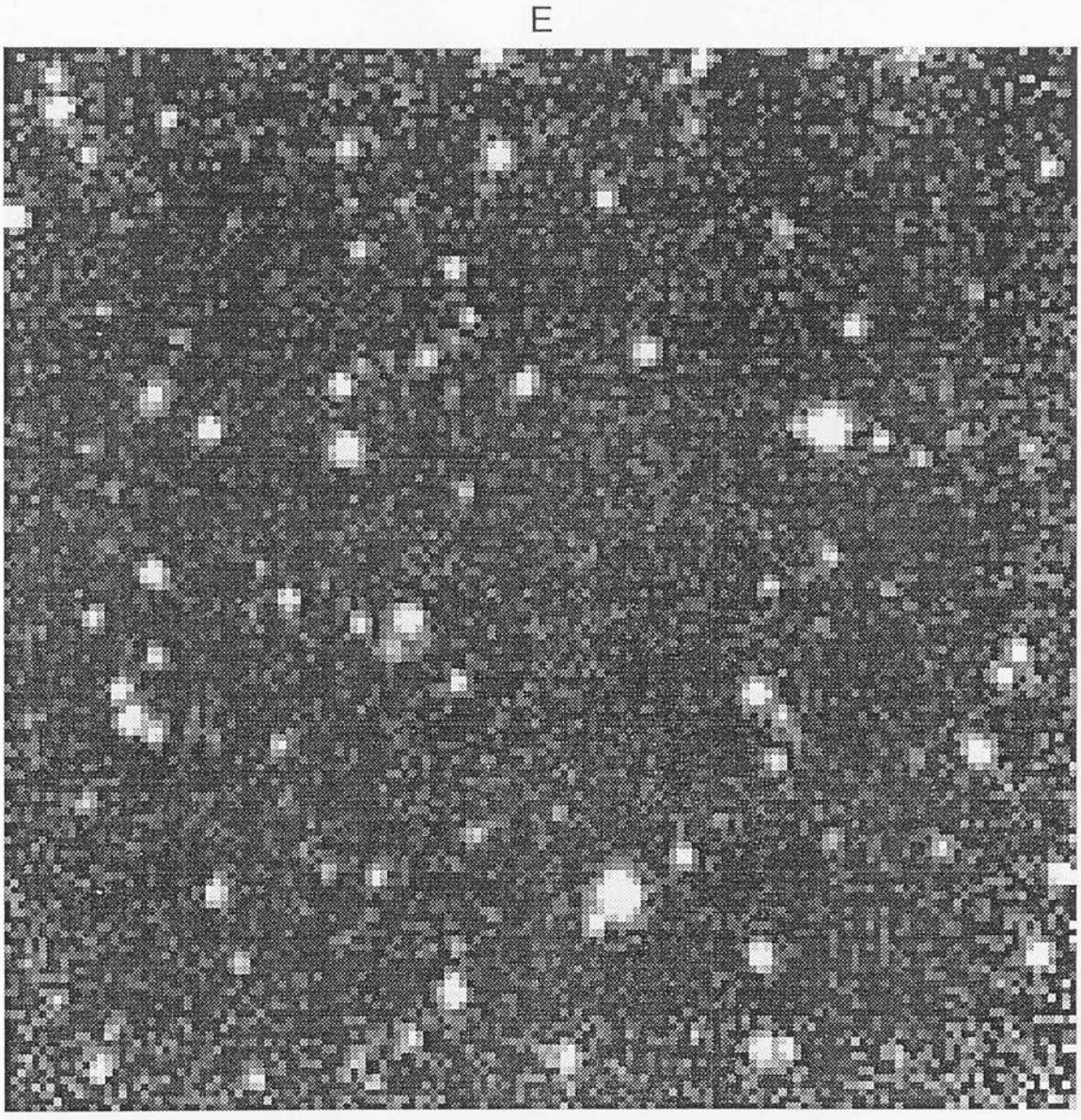

47 Tuc Field F1 position 1 J - 20/21 September 1991

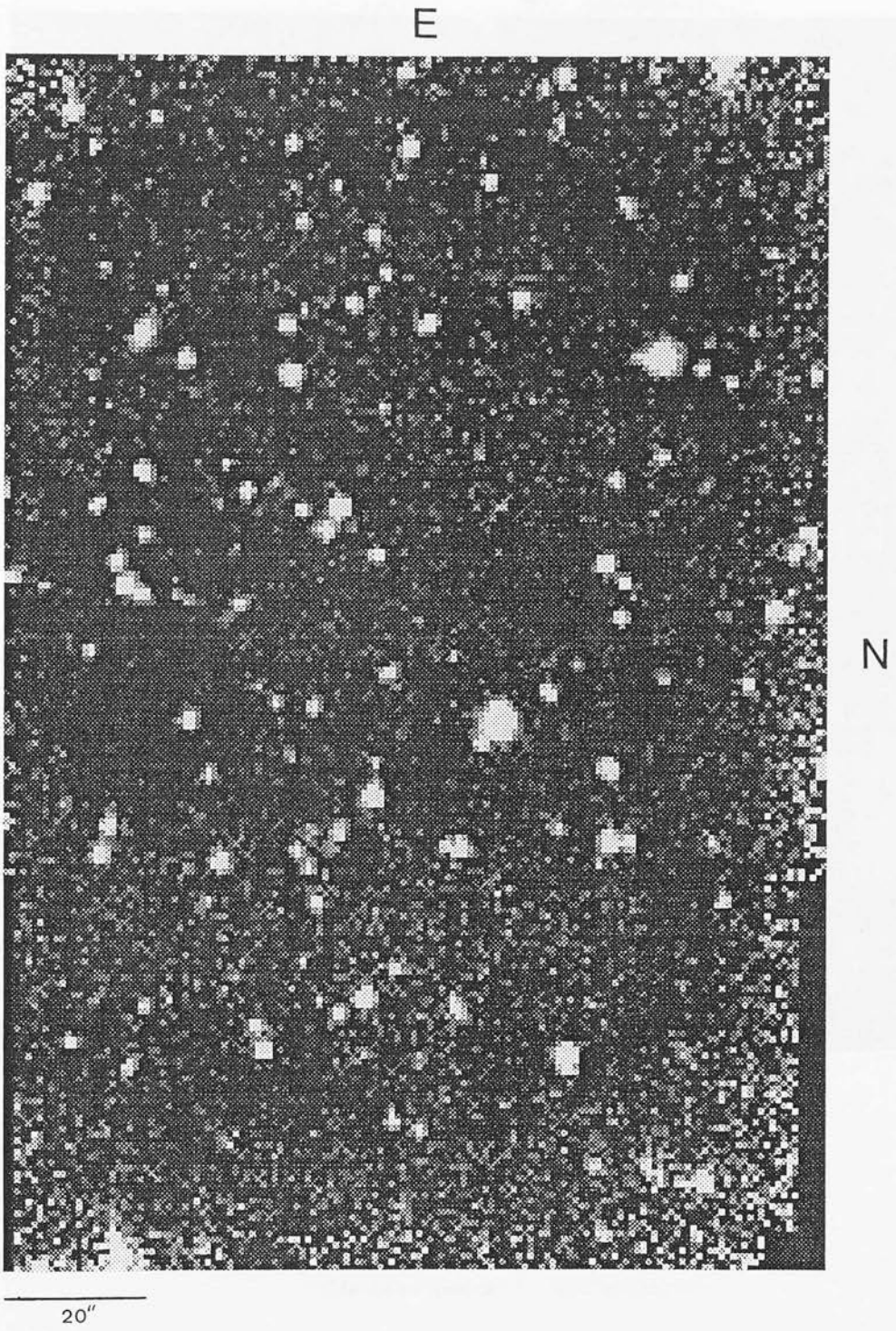

47 Tuc Field F1 position 2 K' - 19/ 20 September 1991

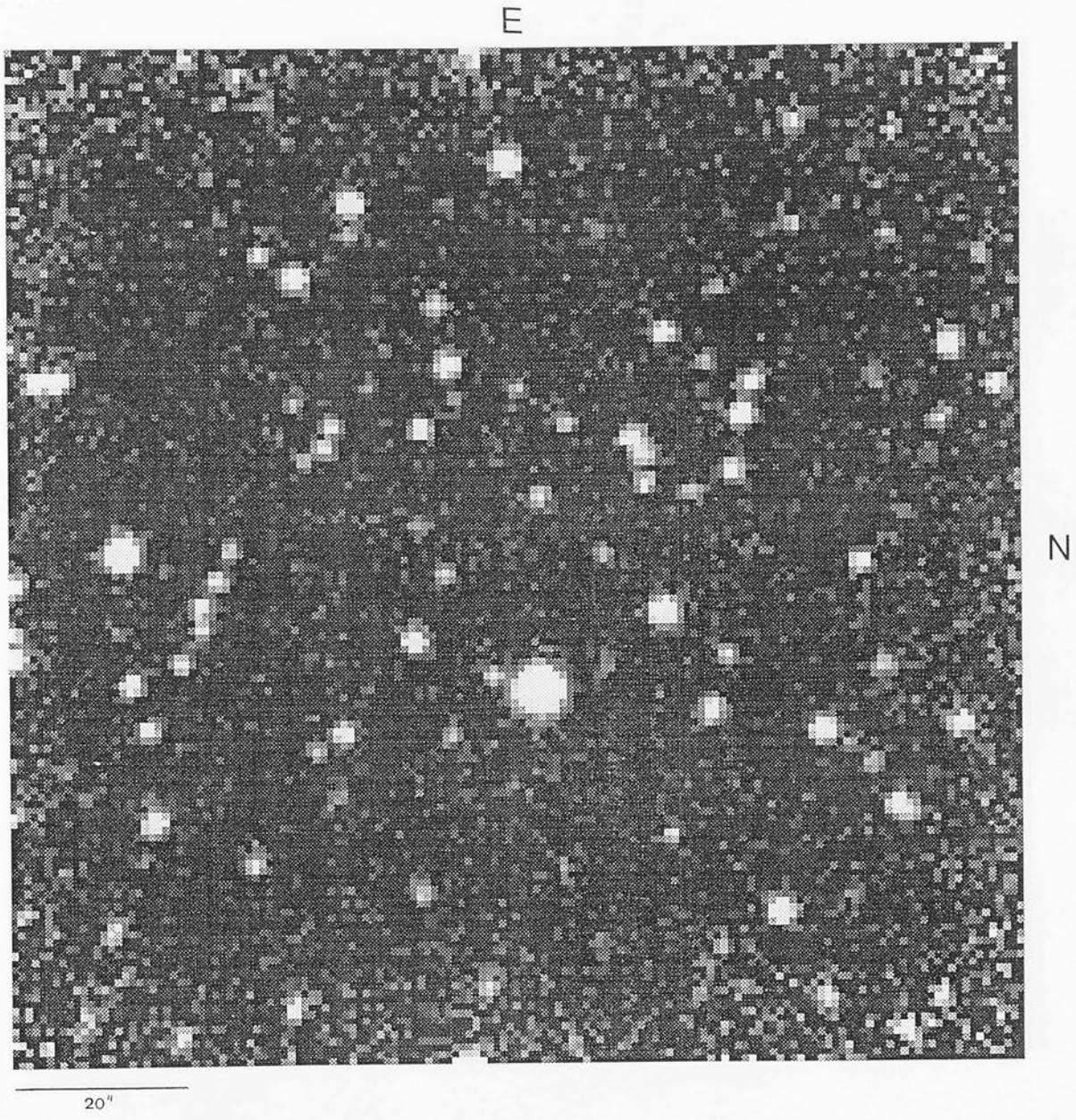

47 Tuc Field F1 position 3 K' - 19/20 September 1991

47 Tuc Field F1 position 3 J - 20/21 September 1991

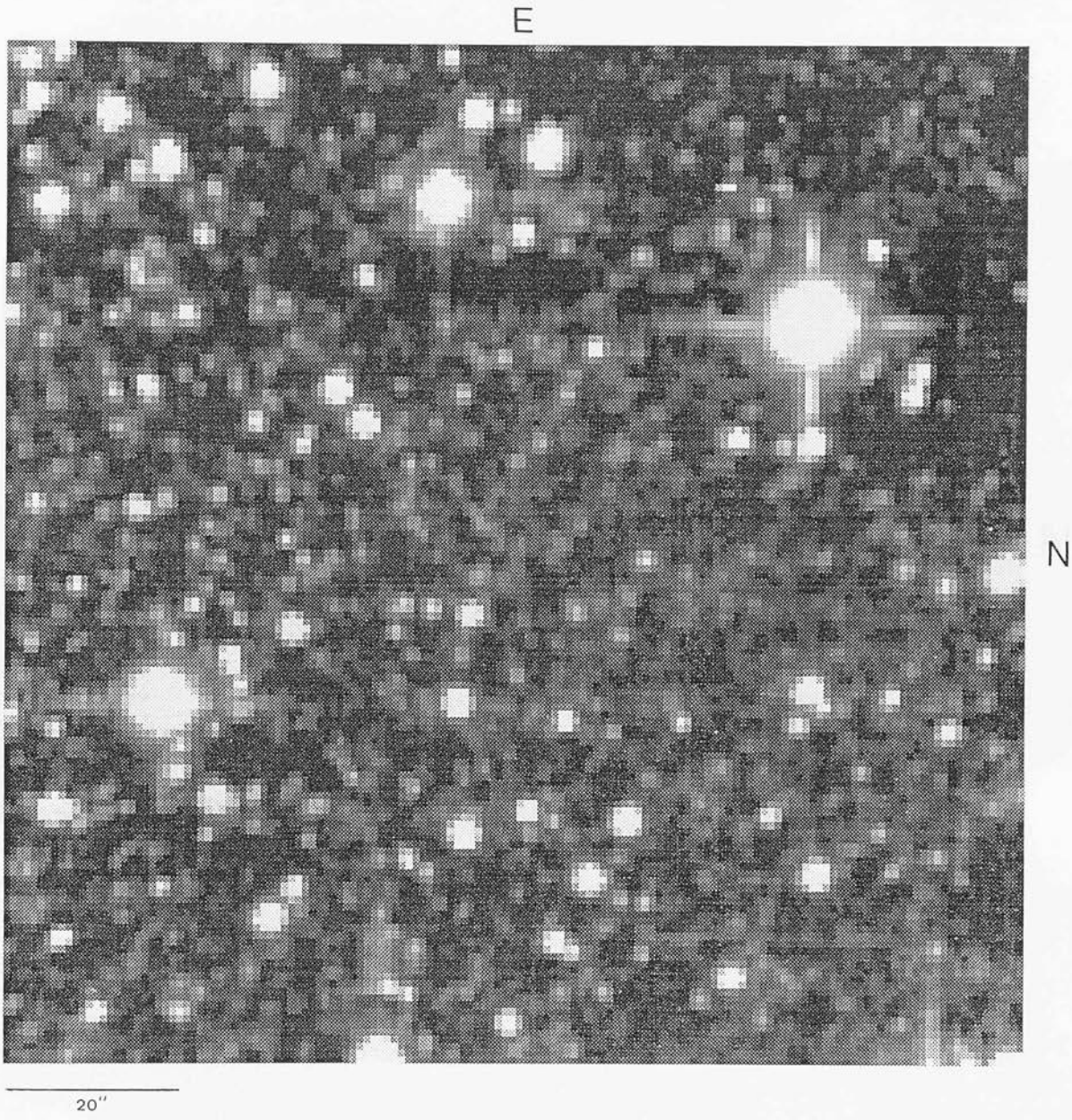

47 Tuc Field F3 K - 3/4 February 1991

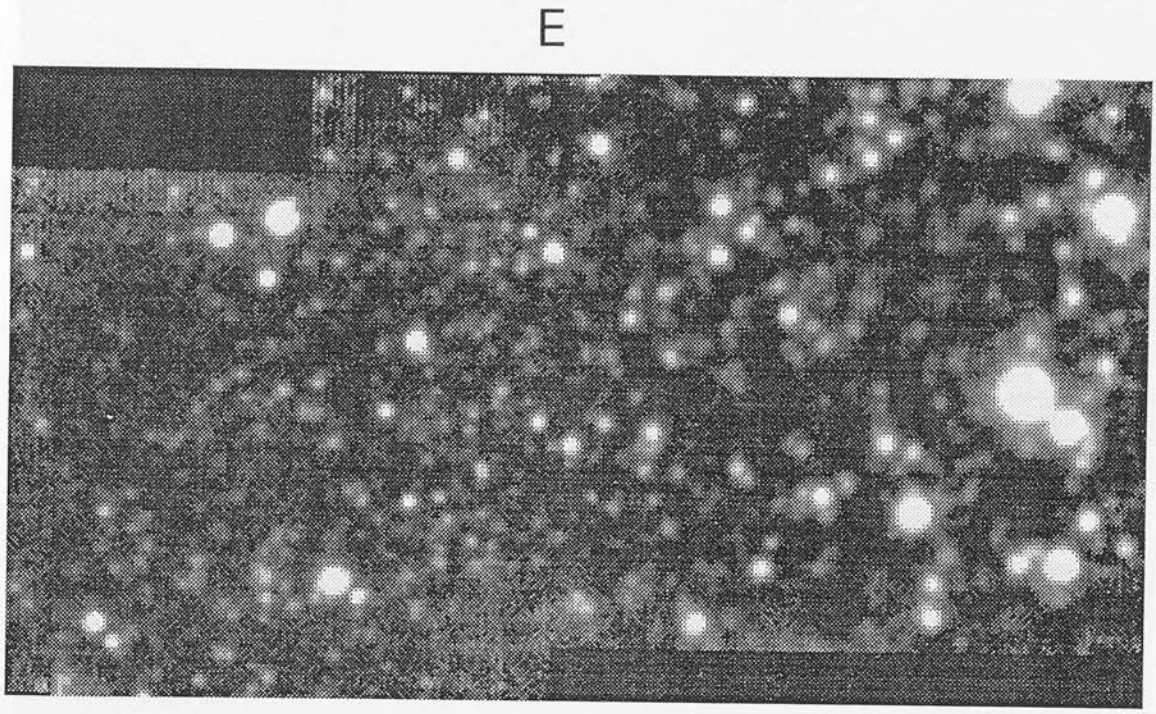

NGC6752 Field 3 K' - 19/20 April 1992

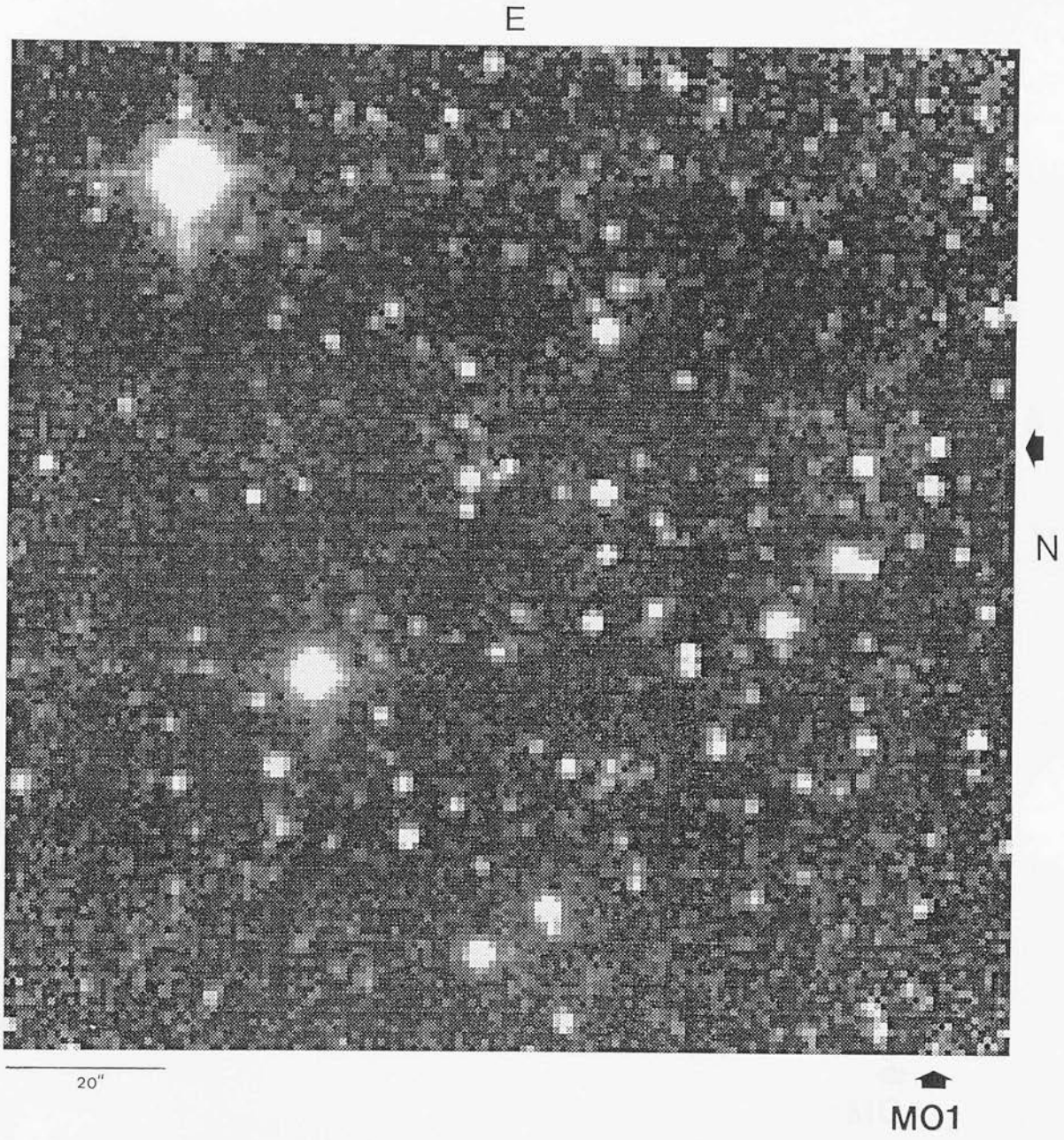

NGC6752 Field 5 K - 4/5 May 1991

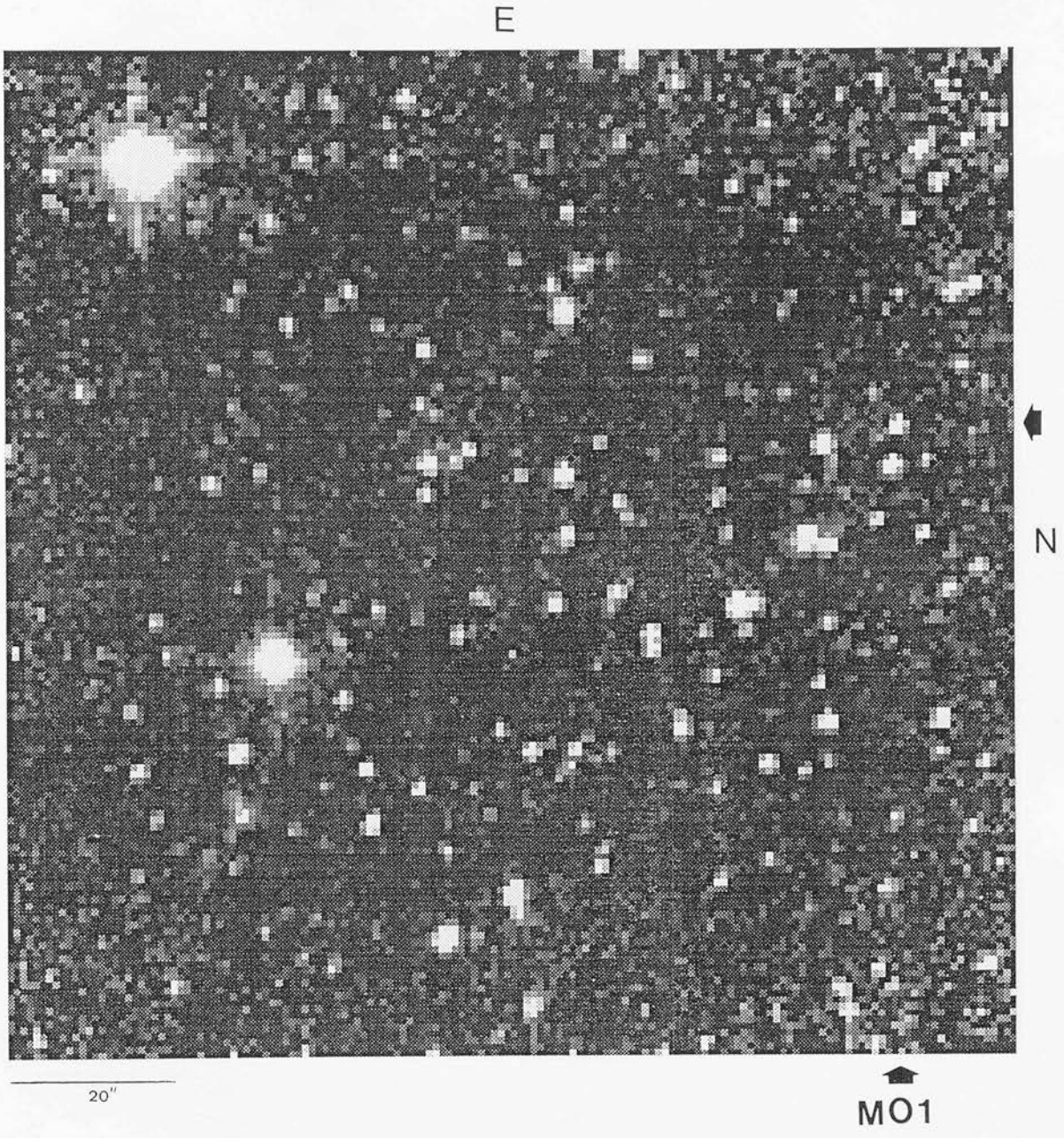

NGC6752 Field 5 K - 5/6 May 1991

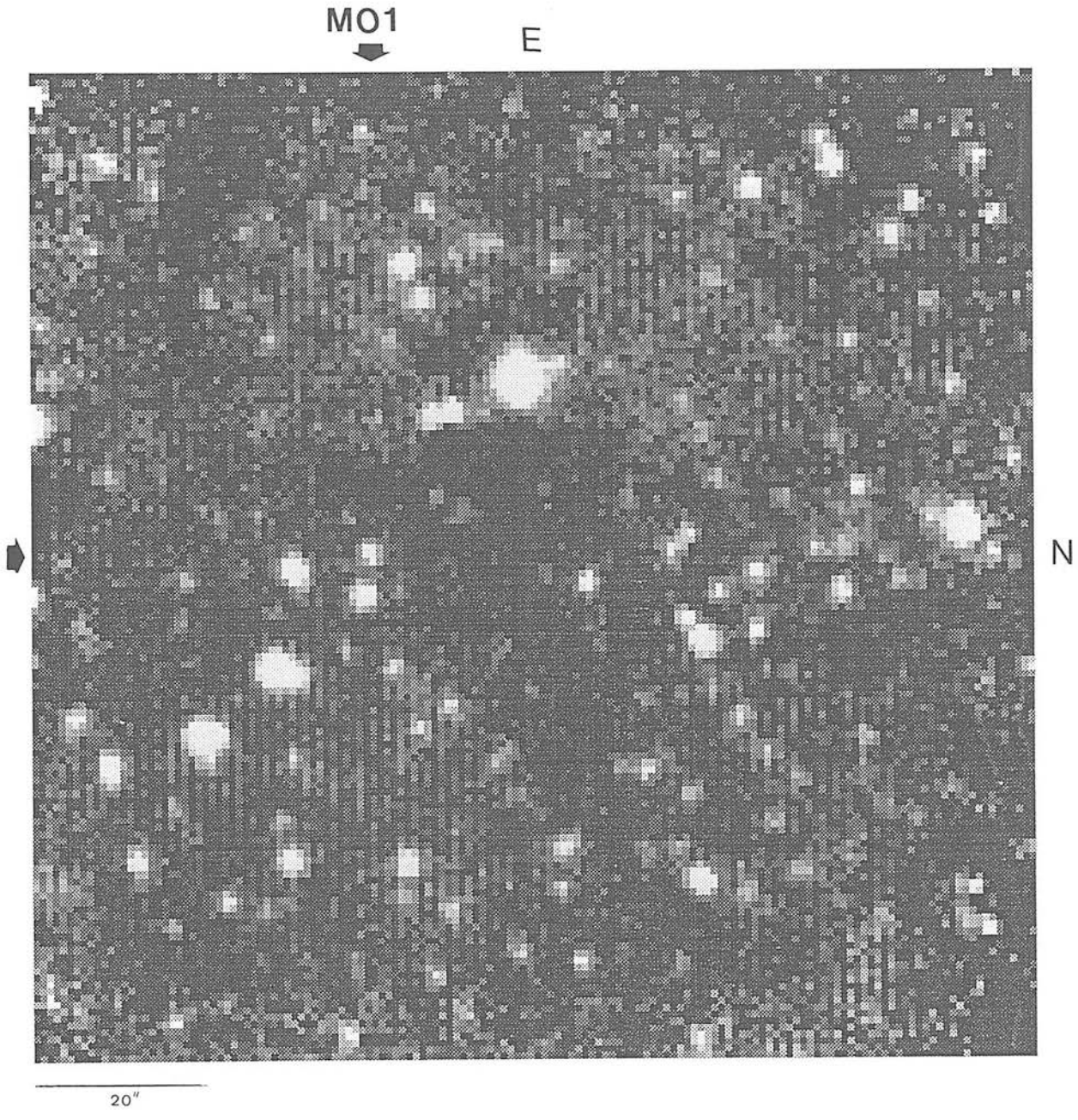

NGC6752 Field 5 K - 16/17 April 1992

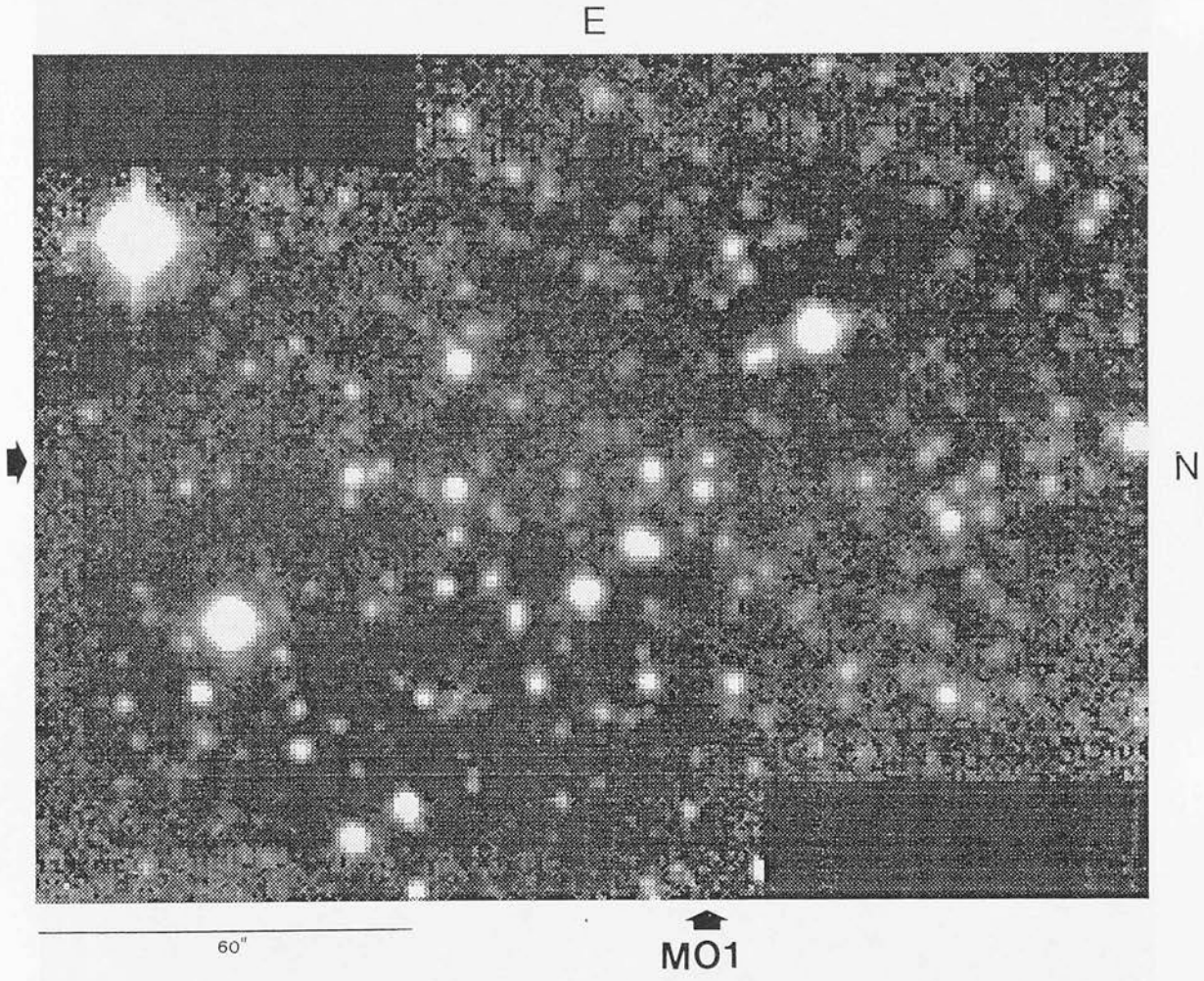

NGC6752 Field 5 K' - 17/18 April 1992

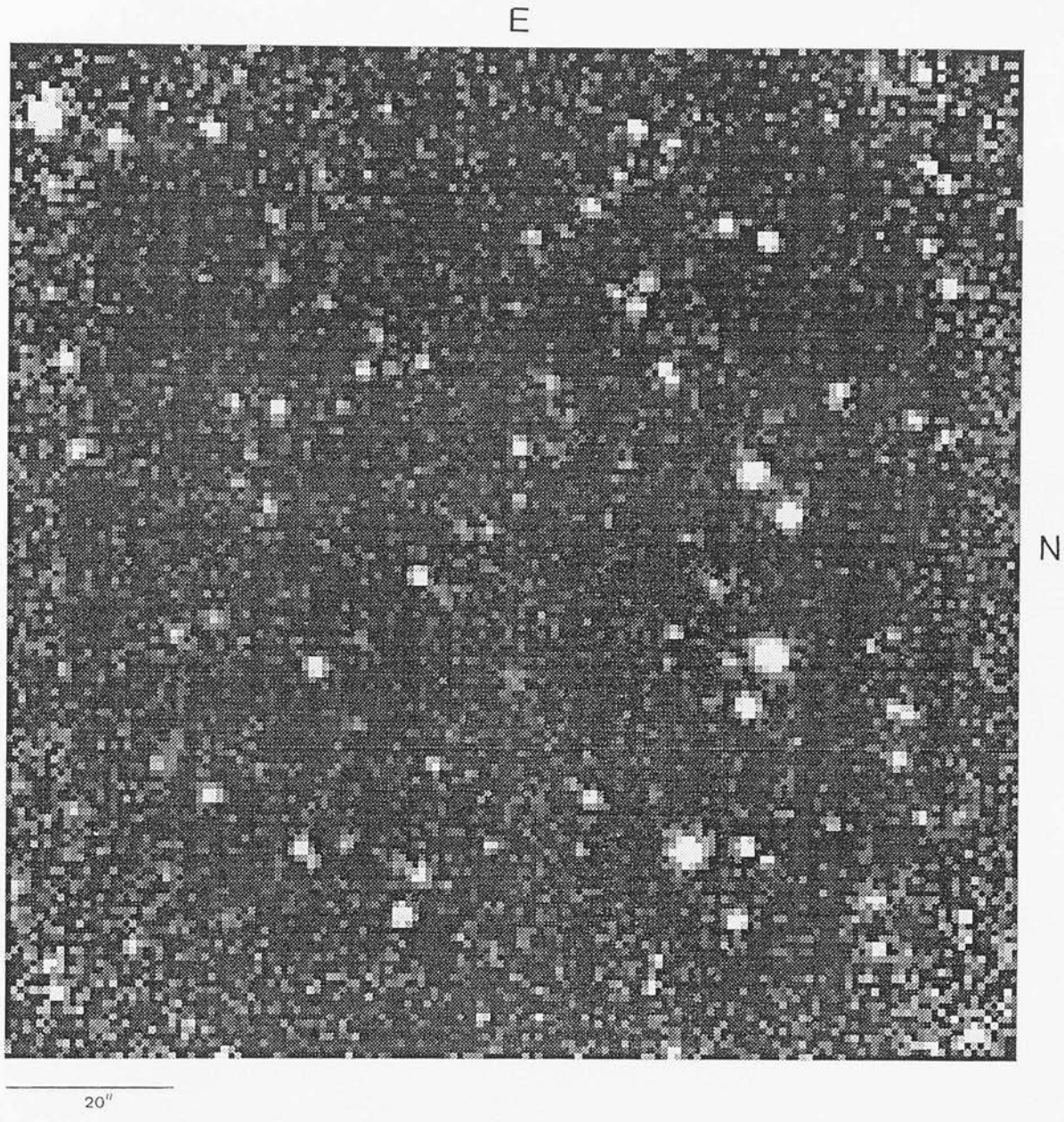

NGC6752 Field 8 K - 4/5 May 1991

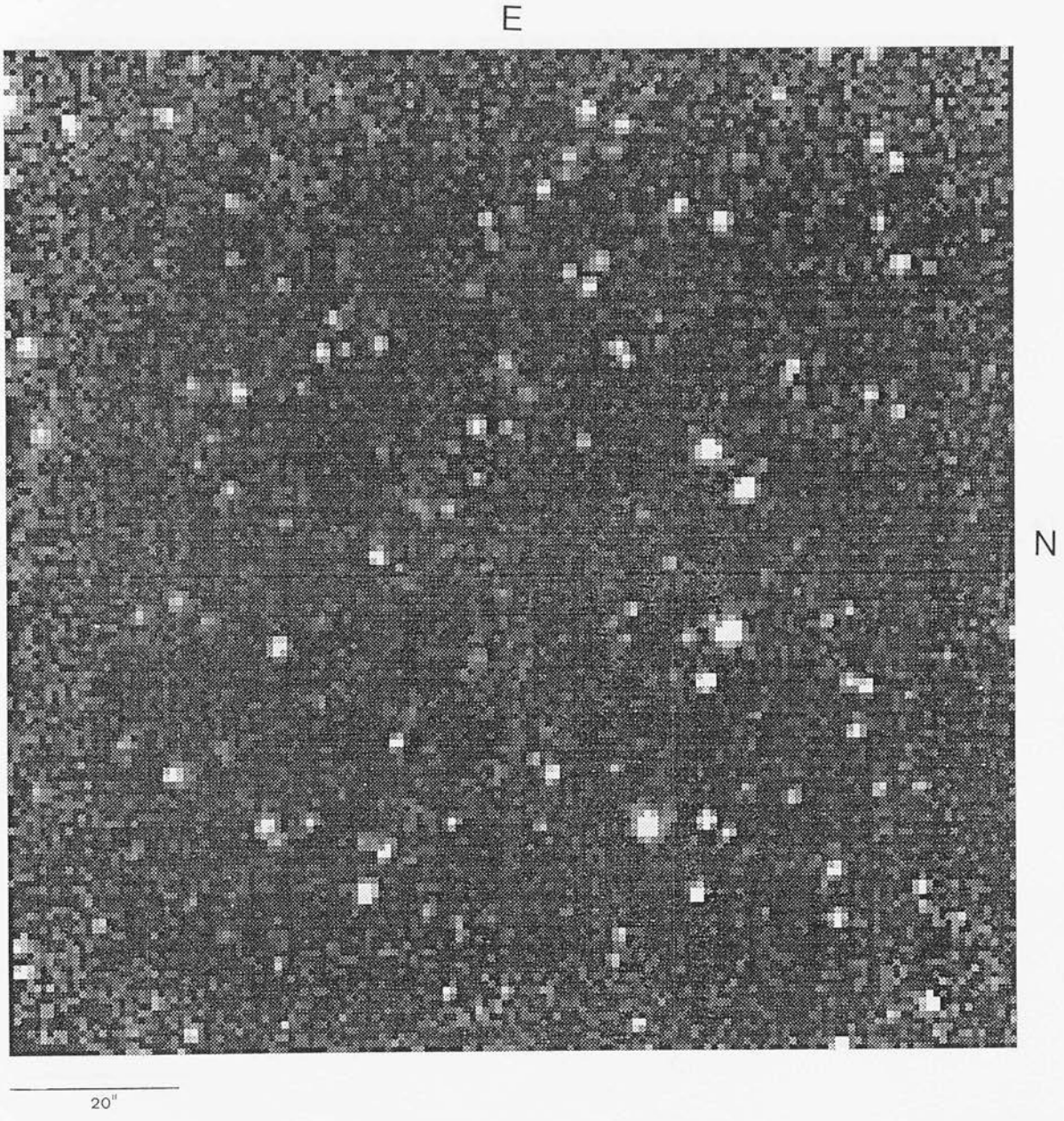

NGC6752 Field 8 K - 5/6 May 1991

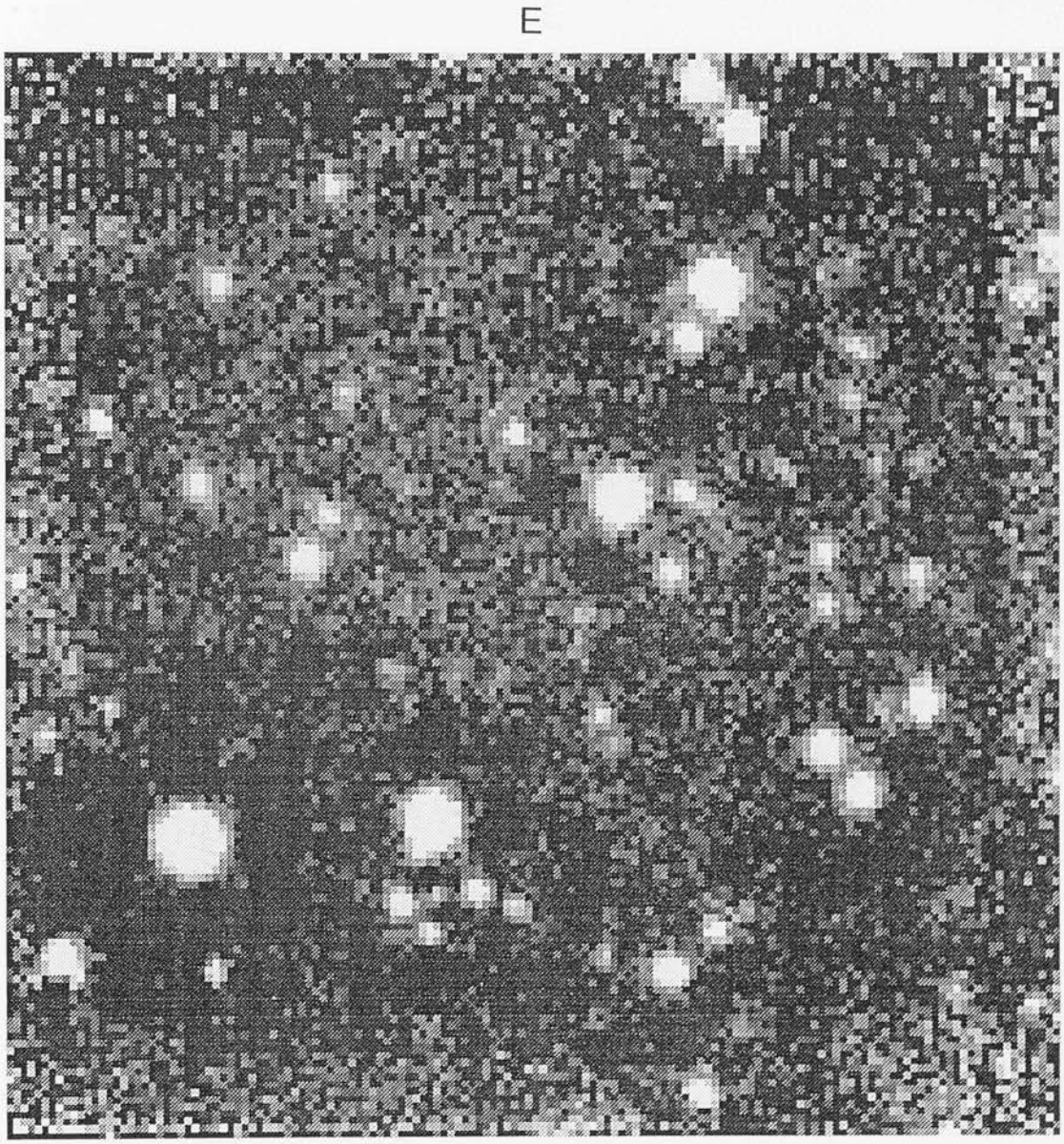

NGC6752 Field 8 K - 16/17 April 1992

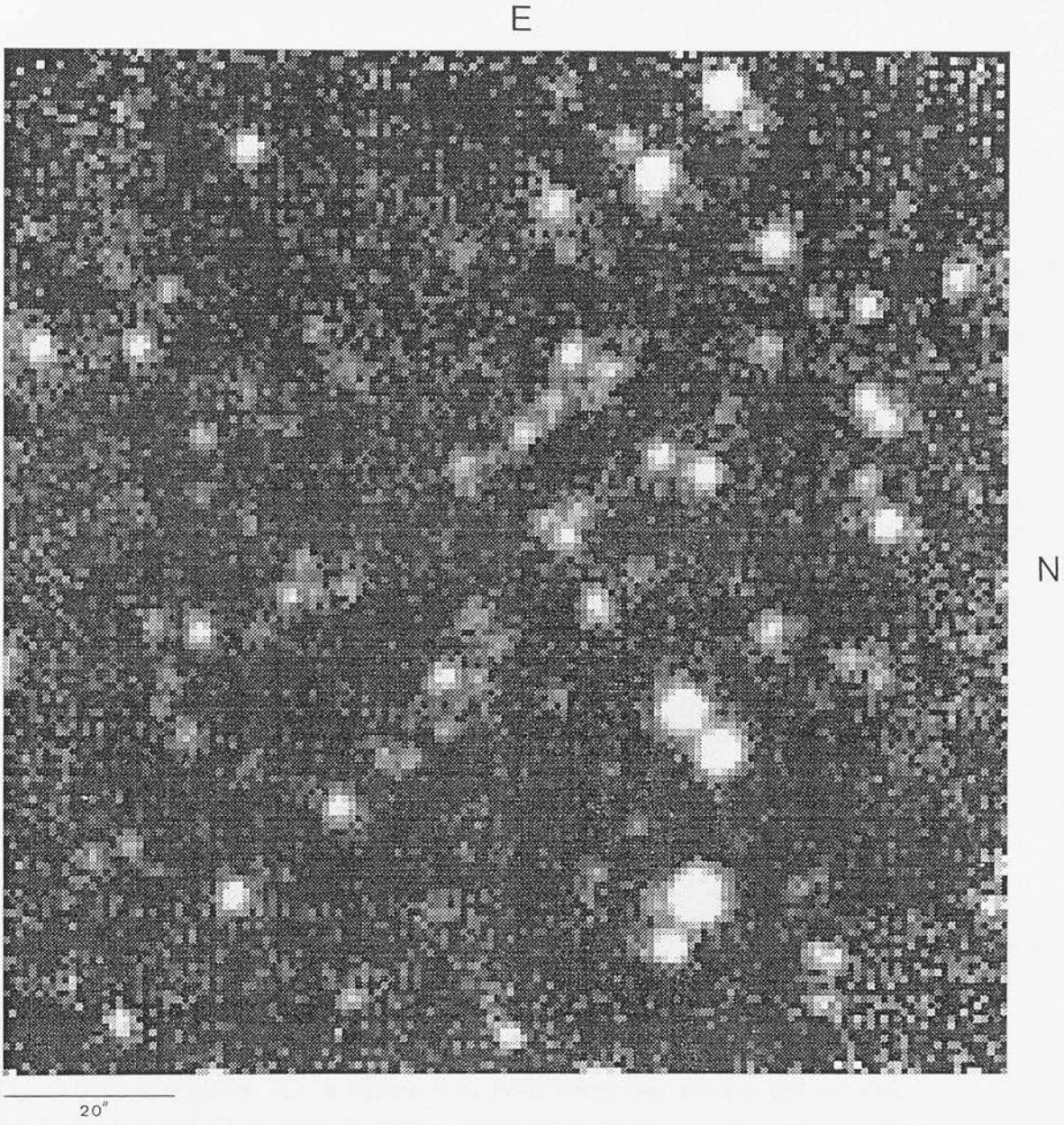

NGC6752 Field 8 K' - 19/20 April 1992

Appendix B

Publications List

Refereed

Buckley, D.R.V. & Longmore, A.J., 1992. *Mon. Not. Roy. astr. Soc.* **257**, 731.
The distance to M13 via a subdwarf fit in the optical-infrared colour-magnitude plane.

non-refereed

Longmore, A.J., Dixon, R.I. & Buckley, D.R.V., 1990. In *Confrontation Between Stellar Pulsation and Evolution.* C. Cacciari and G. Clementini, editors. Astronomical Society of the Pacific Conference Series, volume 11. Page 36.
How infrared observations of RR Lyrae stars enhance their usefulness in distance and pulsation studies.

Buckley, D.R.V. & Longmore, A.J., 1991. *UKIRT and JCMT newsletter* 1, 29.
Photometry of main-sequence globular cluster stars with IRCAM.

Buckley, D.R.V., Longmore, A.J. & Dixon, R.I., 1992. *Mem. Soc. Astron. Ital.* **63**, 433.
The RR Lyrae log(period) vs mean K magnitude relation: intrinsic scatter, applications and remaining uncertainties.

Buckley, D.R.V. & Longmore, A.J., 1992. *Newsletter on Analysis of Astronomical Spectra (CCP7 Newsletter)* **17**, 26.
Globular cluster infrared photometry as observational tests of ATLAS9 model atmosphere results.

Appendix C

A Query

A query has been raised which warrants further discussion. The reader might question whether the poor agreement seen between the V, (V-K) isochrones and the NGC6752 & M13 colour-magnitude diagrams [Chapter 2 figures 10 and 12] compared to the good agreement of the purely optical isochrones and data for these same clusters [figures 11 and 13] might be caused by systematic zero-point differences between our infrared photometry and that of the giants. Potential zero-point errors of ~0.1 magnitudes - which is roughly the size of the discrepancy - are evident in comparisons of the infrared photometry of stars in the overlapping regions of NGC6752 fields 3 and 5 [Chapter 1 figures 3(a) and (b)]. If such zero-point discrepancies were found and removed, this would also remove the simultaneous good agreement of both the V, (V-K) and the V, (B-V) colour-magnitude diagrams of NGC6752 & M13 with the 'new' isochrones [Chapter 4 figures 6 to 9].

We do not believe that zero-point errors in our photometry are responsible for these discrepancies for two reasons. First, as we have already pointed out, the systematic differences seen in Chapter 1 figures 3(a) and (b) are between the photometry of individual fields, and the discrepancy will have been reduced when the photometry from the individual fields was combined by taking a weighted average. Second, a zero-point error in the same sense and of roughly the same size as that seen in the NGC6752 photometry would have to have been introduced independently into the M13 photometry, which is unlikely since those observations were made at a different site with a different instrument to the NGC6752 photometry, and have systematic uncertainties of $<\sim 0.05$ magnitudes [figure 1 of Buckley & Longmore (1992) *Mon. Not. Roy. astr. Soc.* **257**, 731].

However, we reiterate the comment made in section 2.2 of the Conclusion [suggestions for future work] that an independent check of our photometric zero-points should be obtained. We also suggest that photometry of NGC6752 and M13 subgiant-branch stars should be obtained to provide some overlap between the giants and our turn-off region in the V, (V-K) colour-magnitude diagram. This will not only allow any zero-point offsets between the two to be found, but will also be necessary for further study of the discrepancy between the observed and theoretical subgiant branches found in Chapter 4.